CNIC-01266
CNDC-0022
INDC(CPR)-044 / L

CNIC-01266
CNDC-0022
INDC(CPR)-044/L

COMMUNICATION OF NUCLEAR DATA PROGRESS

No.19 (1998)

China Nuclear Data Center

China Nuclear Information Centre

Atomic Energy Press

Beijing, June, 1998

EDITORIAL NOTE

This is the 19th issue of *Communication of Nuclear Data Progress* (CNDP), in which the achievements in nuclear data field for the last year in China are carried. It includes the measurements of neutron activation cross sections on some nuclides, excitation functions of some reactions induced by charge particle and double differential cross section of $^{40}Ca(n,\alpha)$ reaction; theoretical calculations of $Zr(n,\gamma)$ cross section, photonuclear reaction data, excitation function on some nuclides and direct inelastic scattering cross section and angular distribution of Pu isotopes; the evaluation of Ni isotope complete neutron nuclear data, some reference fission yield, activation cross sections and decay data; benchmark testing of CENDL–2.1 and its applications. Also the activities in nuclear data field are summarized.

The editors hope that our readers and colleagues will not spare their comments, in order to improve this publication.

Please write to Drs. Liu Tingjin and Zhuang Youxiang
Mailing Address: China Nuclear Data Center
China Institute of Atomic Energy
P.O.Box 275 (41), Beijing 102413
People's Republic of China
Telephone: 86-10-69357729 or 69357830
Telex: 222373 IAE CN
Facsimile: 86-10-6935 7008
E-mail: cndc @ mipsa.ciae.ac.cn

EDITORIAL BOARD

CONTENTS

I EXPERIMENTAL MEASUREMENT

Measurement of Double Differential Cross Sections for $^{40}Ca(n,\alpha)^{37}Ar$ Reaction at 5.0 and 6.0 MeV

Zhang Guohui Tang Guoyou Chen Jinxiang Shi Zhaomin
(Institute of Heavy Ion Physics, Peking University, Beijing 100871, China)

Yu. M. Gledenov G. Khuukhenkhuu M. Sedysheva
(Joint Institute for Nuclear Research, Dubna 141908, Russia)

Chen Zemin Chen Yingtang Zhang Xuemei
(Department of Physics, Tsinghua University, Beijing 100084, China)

Introduction

Calcium is one of the most important structural materials. The abundance of ^{40}Ca in natural calcium is 96.94%, so $^{40}Ca(n,\alpha)$ data are very important in nuclear engineering. As we know, experimental data for $^{40}Ca(n,\alpha)$ reaction are scarce and there are large differences among them. Although ^{40}Ca is a double magic nucleus, theoretical calculation of $^{40}Ca(n,\alpha)$ data is difficult to fit experimental ones. Reliable data are needed for the study of reaction mechanism.

A gridded ionization chamber (GIC) was used in experiment because it has such characteristics as simple structure, high geometrical efficiency for charged particle detection and being capable of energy-angle determination and particle selection[1]. The cross section, angular distribution, energy spectrum and double differential cross section data can be derived at the same time.

1 Experiment

1.1 Setup

The twin GIC was constructed in Dubna, Russia[2]. There is a sample changer,

with five sample positions. The electrodes area is 19×19 cm^2. In our experiment, the distances from cathode to grid, grid to anode, and anode to shield were 4.5, 2.2 and 1.1 cm, respectively. The voltages for anode, cathode and grid were 1400, −1600 and 0 Volt. The chamber was filled by Kr and 2.78% CO_2 as the working gas in the pressure of 1.2 atm*.

CaF_2 was chosen as the sample material, because it can be found easily and contamination from the (n,α) reactions of fluorine and other calcium isotopes to ^{40}Ca is very little. Two CaF_2 samples with 4.50 cm in diameter were used, one was in forward and another in backward direction. They were evaporated on tungsten backings in a vacuum chamber and then attached to the cathode of the GIC. Their thicknesses are given in Table 1. The samples were so thin that different groups of alphas in energy spectra could be separated. Two tungsten backing films without samples were placed inside the GIC for background measurement.

The experiment was performed at the 4.5 MV Van de Graaff accelerator of the Institute of Heavy Ion Physics, Peking University. Monoenergetic neutrons were produced by D(d,n) reaction with a deuteron gas target of 2.0 cm long and 2.7 atm in pressure separated from the vacuum system by a 5 μm Mo foil. The energy of the deuterons were 2.39 and 3.25 MeV for 5.0 and 6.0 MeV neutrons, and the beam current was about 2 μA during experiment. The GIC was placed at 0° to the beam line, and the distance from the cathode of the GIC to the center of the neutron source was 37.9 cm. The energy resolution for 6.0 MeV neutrons was determined about 0.2 MeV by TOF technique.

To reduce the background, a collimator made of copper and iron, with 12 cm in thickness was placed in front of the deuteron gas target.

A BF_3 long counter and a stilbene crystal detector were used as relative neutron flux monitors. A ^{238}U sample was placed inside the GIC. The absolute neutron flux was determined via $^{238}U(n,f)$ reaction by counting the fission fragments. The weight and the area of the ^{238}U sample were 1.066 mg and 2.0 cm^2.

The positions of the samples are shown in Table1.

Table 1 Sample position during experiment

	Forward	Backward
1	α-source	α-source
2	^6LiF	^6LiF
3	CaF_2: 220 μg/cm²	CaF_2: 272 μg/cm²
4	W	W
5		^{238}U

* 1 atm = 101 325 Pa

1.2 Procedure

Firstly, compound α-source and $^{6}Li(n_{th},t)^{4}He$ reaction were used for energy calibration[2]. To derive thermal neutrons, paraffin board was placed between the collimator and chamber.

After energy calibration, the sample changer was turned to CaF_2 samples for effective event plus background measurement. The measuring time for event plus background was about 20 hours and that for background was about 10 hours.

After effective event plus background and background measurement, energy calibration was also performed to check the system stability.

Using $^{238}U(n,f)$ reaction, the absolute neutron flux calibration was carried out. The bombarding time was about 8 hours. The cross sections of $^{238}U(n,f)$ reaction were taken from ENDF/B-6 library.

2 Results

The cross sections for total α, α_0, and $\alpha_{1,2}$ are showed in Fig.1, 2 and 3. α_1 and α_2 couldn't be separated because the corresponding energy levels of ^{37}Ar are very close. It can be seen that the total α cross section at 5.0 MeV is almost the same as that 6.0 MeV. Other results of experiment or evaluation are also illustrated in the

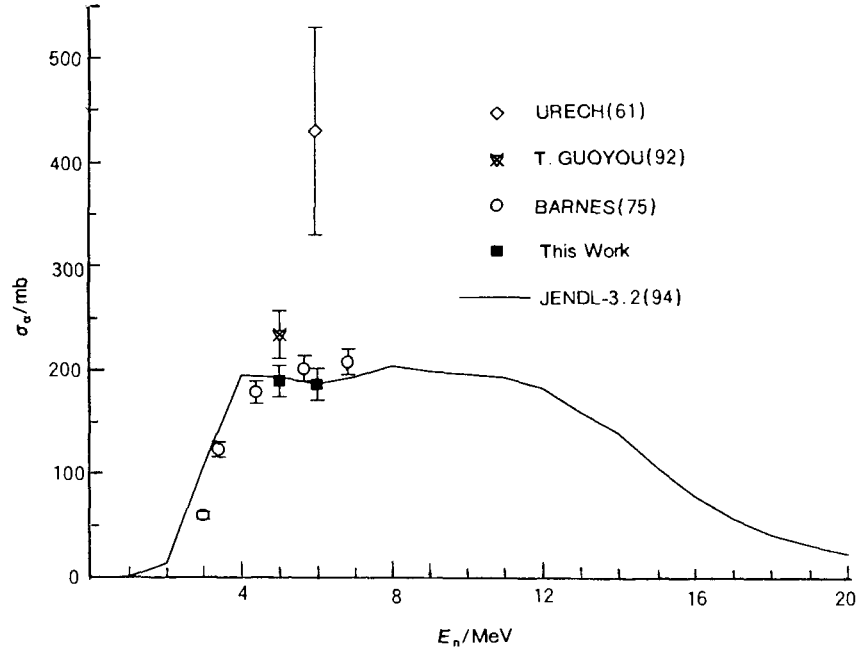

Fig.1 (n,α) cross section for ^{40}Ca

figure for comparison[3~9]. Our result of α cross section well-confirmed JENDL-3.2 data. Figs.2 and 3 show that from 5.0 MeV to 6.0 MeV, $\sigma_{\alpha 0}$ decreases and $\sigma_{\alpha 1,2}$ increases.

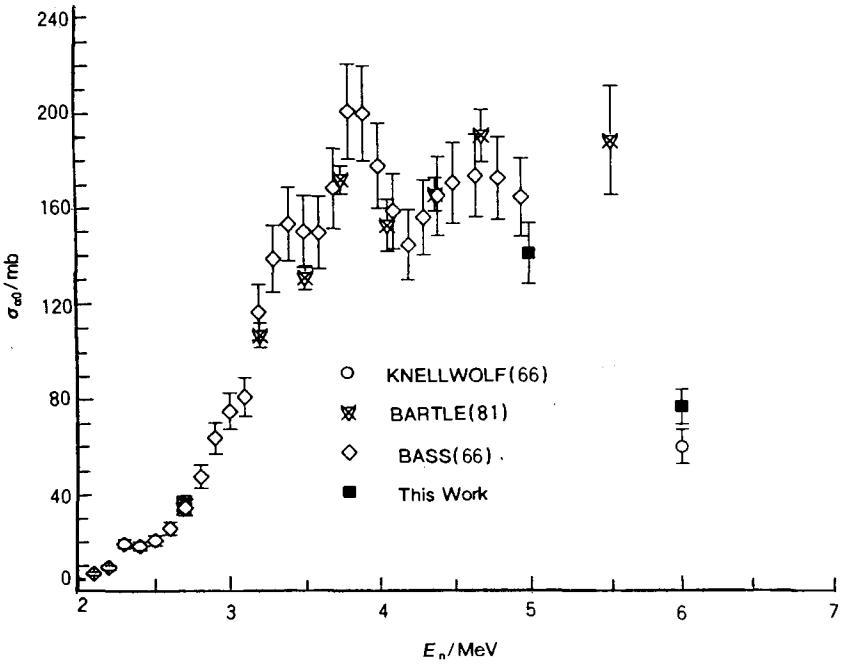

Fig.2 (n,α_0) cross section for ^{40}Ca

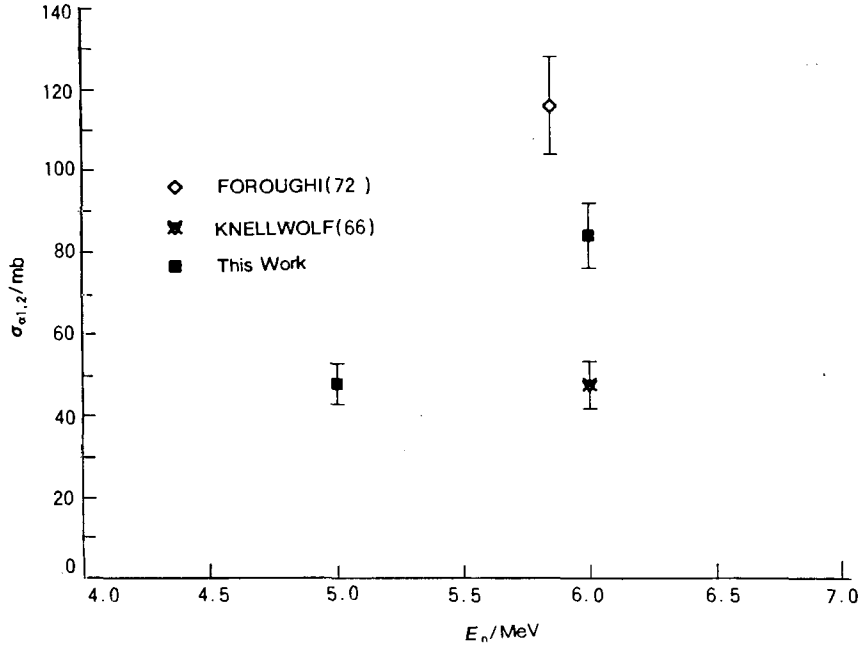

Fig.3 (n,$\alpha_{1,2}$) cross section for ^{40}Ca

Figs. 4 and 5 are the α double differential cross sections for E_n = 5.0 MeV and 6.0 MeV, cosθ = 0.95. From 5.0 to 6.0 MeV, the ratio of $\alpha_{1,2}$ to α_0 increases. For double differential cross section data, only Cavallaro's data can be found[10], and they are also included in Fig.4.

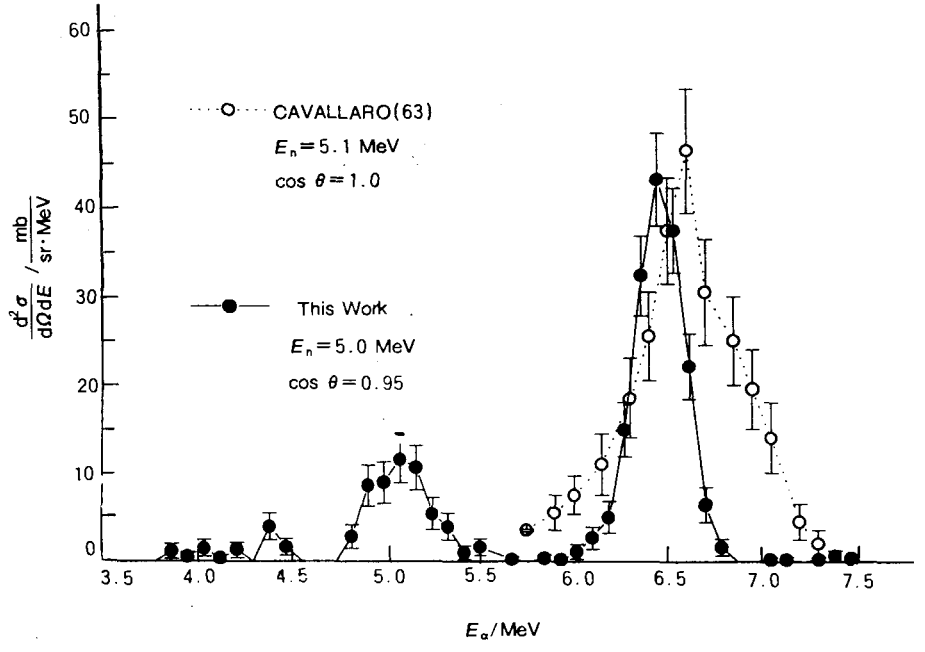

Fig. 4 Double differential cross section of $^{40}Ca(n,\alpha)^{37}Ar$
E_n = 5.0 MeV, cosθ = 0.95

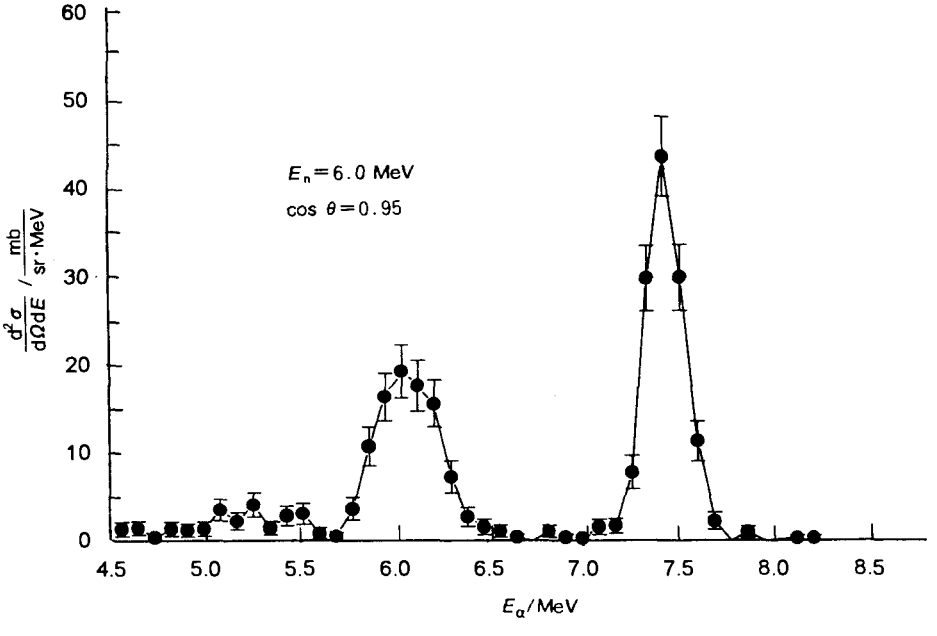

Fig. 5 Double differential cross section of $^{40}Ca(n,\alpha)^{37}Ar$
E_n = 6.0 MeV, cosθ = 0.95

Since the area of the CaF_2 sample was not the same as that of the ^{238}U sample, their average neutron flux densities were not the same. Neutron flux density non-uniformity correction was made to derive the neutron flux through CaF_2 sample from that through ^{238}U sample. The correction of event loss due to the geometrical efficiency of the GIC and the thickness of the sample was also performed.

Error analysis for cross section is listed in Table 2.

Table 2 Principal source of error for cross sections

Source of uncertainty	Relative errors / %
$^{238}U(n,f)$ cross section	2.0~3.5
interference from other calcium isotopes	< 1.0
statistics for fission counts	2.5
statistics for α counts	2.0~5.0
background subtraction	2.0~3.0
nuclear number of ^{238}U	3.0
nuclear number of ^{40}Ca	0.5
total α cross section	< 8.0

3 Conclusion

From the experiment, these conclusions for $^{40}Ca(n,\alpha)^{37}Ar$ reaction can be drawn:
(1). At 5.0 MeV and 6.0 MeV, total α cross sections are almost the same;
(2). At 5.0 MeV the cross section for α_0 is much bigger than that for $\alpha_{1,2}$, but at 6.0 MeV the cross section for α_0 is almost the same as that for $\alpha_{1,2}$.

The authors thank the China National Nuclear Corporation for the financial support and appreciate the crew of 4.5 MV Van de Graaff accelerator at Peking University for their cooperation. They also indebted to Prof. Xia Songjiang from the Technical Physics Department, Peking University for the help on the data acquisition system.

References

[1] C. Budtz-Jφrgensen et al., Nucl. Instr. and Meth., A258, 209(1987)
[2] Tang Guoyou et al., INDC(CPR)-043/L (1997)
[3] J. W. Barnes et al., EXFOR Data No. 10476002
[4] S. Urech et al., EXFOR Data No. 21245002
[5] T. Guoyou et al., EXFOR Data No. 32609002
[6] T. Knellwolf et al., EXFOR Data No. 21247005 and 21247006
[7] C. M. Bartle et al., EXFOR Data No. 10447002
[8] R. Bass et al., EXFOR Data No. 21275002
[9] F. Foroughi et al., EXFOR Data No. 20832003
[10] S. Cavlllaro et al., EXFOR Data No. 21259003

Cross Section Measurement in Neutron Energy Range of 6 ~ 12 MeV

Zhao Wenrong Lu Hanlin Yu Weixiang Han Xiaogang Huang Xiaolong
(Department of Nuclear Physics, CIAE, P. O. Box 275, Beijing 102413)

Introduction

The cross section measurements in neutron energy range from 6 to 12 MeV for the reactions with low threshold are very important to obtain a whole excitation function and to make datum eveluation. But in this energy range, purely monoenergitic neutron source is not available, which make the measured data very few. And there is a serious effect of low energy neutrons on the activation cross section measurement. The correction for the effect of the low energy neutrons are not sufficient for some available data, which cause the published data largely discrepant.

In present work, the cross sections for 14 reactions were measured in the energy range of 6 ~ 12 MeV and the corrections for the influence of the low energy neutrons are considered very carefully.

1 Source of the Low Energy Neutrons

Usually a deuteron gas target is employed to produce the neutrons in the energy range of 6 to 12 MeV through D(d,n)^{3}He reaction. In this condition, the low energy neutrons come from:

a. D-d low energy neutrons from self building solid D target formed in both entrance window and the beam stop of gas target due to irradiation of deuteron beam.

b. When E_d is higher than 4.45 MeV, a continuous distribution of breakup neutrons from D(d,pn)D reaction can not be avoided.

c. The low energy neutrons are produced through charged particle interaction with the target structure materials.

d. The scattering of primary neutrons.

These four kinds of low energy neutrons form a continuous distribution spectrum. The intensity of some of them depend on incident E_d, and detected angle, while some of them rely on irradiated distance of sample, irradiated time, focused situation of the deuteron beam etc. Due to the influence of the low energy neutrons

on the activation cross section measurements for the reactions with low threshold is very serious, one of the key questions for getting reliable results is how to deduct the influence of the low energy neutrons reasonably.

2 Deducted Method for the Low Energy Neutrons

a. The influence of a and c kinds of the low energy neutrons mentioned in section 2 can be subtracted by irradiated the samples under gas in and gas out conditions. The effect of b and d kinds is deducted using the neutron spectra of gas in and gas out runs, at the same distance with the sample irradiation.

b. In some case, to finish gas out run is very difficult, for example, in the long-lived nuclide measurement. Therefore the investigated reaction is measured relative to a monitor reaction, which has nearly the same threshold and the similar excitation function shape with the investigated one. In this way, the influence of the low energy neutrons can be subtracted very well. Or a group of monitors are selected with different threshold and irradiated with the investigated reaction together. And a relationship between the neutron flux and the threshold can be obtained. The neutron flux for the investigated reaction will be got using the relationship according to its threshold. The effect of the low energy neutron can be subtracted essentially, using this method.

3 Cross Section Measurement for 14 Reactions

The cross sections for $^{46}Ti(n,p)^{46}Sc$, $^{47}Ti(n,p)^{47}Sc$, $^{54}Fe(n,p)^{54}Mn$, $^{54}Fe(n,\alpha)^{51}Cr$, $^{58}Ni(n,d+np+pn)^{57}Co$, $^{59}Co(n,p)^{59}Fe$, $^{60}Ni(n,p)^{60}Co$, $^{62}Ni(n,\alpha)^{59}Fe$, $^{64}Zn(n,p)^{64}Cu$, $^{63}Cu(n,\alpha)^{60}Co$, $^{85}Rb(n,2n)^{84m+g}Rb$, $^{93}Nb(n,2n)^{92m}Nb$, $^{140}Ce(n,2n)^{139}Ce$ and $^{181}Ta(n,2n)^{180m}Ta$ reactions were measured in the neutron energy range from 6 to 11.4 MeV, using activation method. The samples were irradiated in the 0-degree direction with neutrons produced via the $D(d,n)^3He$ reaction on a D_2 gas target, at the tandem accelerator.

The neutron flux density was determined by a group of monitor reactions, with different threshold. The influence of the low energy neutrons are subtracted using the methods mentioned in section 3. The radioactivities of each investigated product and monitor reactions were determined via Ge(Li) detector gamma-ray spectrometer. The decay characteristics of products are summarized in Table 1. Table 2 lists the measured cross sections. Among them, $^{58}Ni(n,d+np+pn)^{57}Co$, $^{85}Rb(n,2n)^{84m+g}Rb$, $^{140}Ce(n,2n)^{139}Ce$, and $^{181}Ta(n,2n)^{180m}Ta$ reactions were measured for the first time. The principal sources of errors include efficiency of Ge(Li) detector, neutron

flux determination, peak area of gamma ray, sample weight, and etc. Combining those errors in quatric, the total error for each cross section value was obtained.

Table 1 Relevant parameters of the products

Reaction	$T_{1/2}$	E_γ / keV	I_γ / %	Abundance / %
$^{46}Ti(n,p)^{46}Sc$	83.83d	889.25	99.984	7.93
$^{47}Ti(n,p)^{47}Sc$	3.341d	159.38	68	7.3
$^{54}Fe(n,p)^{54}Mn$	312.12d	834.826	99.975	5.9
$^{54}Fe(n,\alpha)^{51}Cr$	27.702d	320.084	9.83	5.9
$^{58}Ni(n,d+np+pn)^{57}Co$	271.8d	122.061	85.5	68.077
$^{60}Ni(n,p)^{60}Co$	5.271y	1173.237	99.9	26.23
$^{62}Ni(n,\alpha)^{59}Fe$	44.496d	1099.25	56.5	3.634
$^{63}Cu(n,\alpha)^{60}Co$	5.271y	1173.237	99.9	69.1
$^{64}Zn(n,p)^{64}Cu$	12.701h	1345.78	0.48	48.89
$^{85}Rb(n,2n)^{84m+g}Rb$	32.87d	881.69	67.9	72.15
$^{93}Nb(n,2n)^{92m}Nb$	10.15d	934. 53	99.0	100
$^{140}Ce(n,2n)^{139}Ce$	137.2d	165.853	79.9	88.48
$^{181}Ta(n,2n)^{180m}Ta$	8.152h	93.331	4.27	99.988
$^{59}Co(n,p)^{59}Fe$	44.496d	1099.25	56.5	100

Table 2 The cross section (in mb) for 14 reactions

Reaction	E_n / MeV							
	6.00±0.17	7.07±0.19	8.40±0.58	9.40±0.46	10.40±0.33	10.6±0.27	11.40±0.35	11.6±0.24
$^{46}Ti(n,p)^{46}Sc$	152.1±9.1	208.1±11.2	248.9±12.9	249.1±12.9	273.4±13.8		293.7±14.7	
$^{47}Ti(n,p)^{47}Sc$	76.6±3.7	87.6±4.0	106.2±5.0	114.1±5.9	125.7±6.3		120.8±6.3	
$^{54}Fe(n,\alpha)^{51}Cr$	12.4±0.8	18.1±1.3	37.1±1.6	44.1±2.3	60.3±3.0		63.9±3.2	
$^{54}Fe(n,p)^{54}Mn$	500.0±28.3	537.2±30.4	502.9±21.7	530.2±25.9	530.5±25.7		506.5±24.8	
$^{58}Ni(n,d+np+pn)^{57}Co$				0.37±0.02	42.1±1.8		175.0±7.7	
$^{59}Co(n,p)^{59}Fe$	19.1±1.1	22.1±1.2	30.6±1.6	35.7±1.9	49.2±2.6		53.4±2.8	
$^{60}Ni(n,p)^{60}Co$	28.0±2.8	76.5±4.1	89.1±6.6	105.5±5.3	126.0±6.5		161.8±8.5	
$^{62}Ni(n,\alpha)^{59}Fe$			4.9±0.3	7.1±0.4	9.7±0.5		15.5±0.8	
$^{63}Cu(n,\alpha)^{60}Co$	9.0±0.8	19.5±1.9	24.7±1.7	29.1±2.1	40.4±2.2		47.7±2.5	
$^{64}Zn(n,p)^{64}Cu$			234.9±12.0	251.3±13.8	249.0±13.3		242.8±12.3	
$^{85}Rb(n,2n)^{84m+g}Rb$						3.1±1.4		202.1±9.3
$^{93}Nb(n,2n)^{92m}Nb$					215.4±10.3	238.1±11.4	337.3±16.2	350.3±16.8
$^{140}Ce(n,2n)^{139}Ce$						505.7±22.5		898.4±41.2
$^{181}Ta(n,2n)^{180m}Ta$			264.3±10.6	706.7±3.3	1008.9±45.0		1190.9±56.0	

Cross Section for $^{176}Hf(n,2n)^{175}Hf$ Reaction

Lu Hanlin Zhao Wenrong Yu Weixiang Han Xiaogang
(Department of Physics, CIAE, P.O.Box 275(49), Beijing 102413)

Abstract

Measurements of neutron cross section of $^{176}Hf(n,2n)^{175}Hf$ are reported. In the experiment, the $D(d,n)^3He$ and $T(d,n)^4He$ reactions were served as the neutron sources, in neutron energy ranged of 10 ~ 12 MeV, about 14 MeV and 18 MeV. The neutron flux was monitored with the $^{93}Nb(n,2n)^{92m}Nb$ reaction and BF_3 long counter or ^{238}U fission chamber. Details of this experiment were described and the results were compared with ENDF/B-6, JEF-2, JENDL-3, ADL-3 and the data from literature.

Introduction

This particular material is chosen for measurement because it is commonly used for the ITER design, the evaluated values of this cross-sections are chaotic and contradictory, moreover, all available data are concentrated on 14 MeV. The new measurements are performed in order to confirm the excitation function shape.

1 Experimental Details

The neutron irradiation was performed at the HI-13 tandem accelerator, Cockcroft Walton accelerator in CIAE and the 4.5 MV Van-de-Graff accelerator of Beijing University. $D(d,n)^3He$ and $T(d,n)^4He$ reactions were used as the neutron source. All experiments were made relatively to the $^{93}Nb(n,2n)^{92m}Nb$ reaction. Natural hafnium samples (higher than 99% purity) 10 mm in diameter and 1 g in weight, were irradiated at distance of 3 ~ 10 cm from neutron source. Each hafnium foil was sandwiched between two niobium foils. The neutron flux was determined by measuring the monitor foils. BF_3 long counter and ^{238}U fission chamber were used during the irradiation for the correction of neutron flux fluctuation.

The radioactivities were measured with a calibrated Ge(Li) γ-detector by counting the full energy peaks of the 343.4 keV γ-ray emitted in the decay of ^{175}Hf. The measurement was done at a distance of 18 cm between sample and detector so that the coincidence summing was avoided. At the same time self-absorption was

measured to correct the loosing of the 343.4 keV γ-ray in samples. The decay data of radioactive nuclei are given in Table 1.

Table 1 Decay data of radioactivity nuclei

Nuclide	$T_{1/2}$ / d	E_γ / keV	P_γ / %	Abundance / %
^{92m}Nb	10.15±0.02	934.3	99.0±0.3	100
^{175}Hf	70±2	343.4	84±3	5.206

2 Result

The experimental cross sections for ^{176}Hf(n,2n)^{175}Hf reaction are summarized in Table 2. They are plotted in Fig.1, compared with the evaluations of ENDF/B-6, JEF-2, JENDL-3, and ADL-3. There is basically agreement between present data and other data within uncertainties around 14 MeV. All data concentrate on 14 MeV except ours. At low energy, the deviation between ADL-3 and ENDF/B-6 is about 100%, our data around 11 MeV are between the evaluations of JEF-2 and ADL-3. At 18 MeV, the main correction of our data was the effect of ^{177}Hf(n,3n)^{175}Hf reaction which threshold is 14.6 MeV. The values of UNF, JENDL-3 and ADL-3 of ^{177}Hf(n,3n)^{175}Hf which were very closed, were used for this correction. The evaluated values based on our experimental data are given.

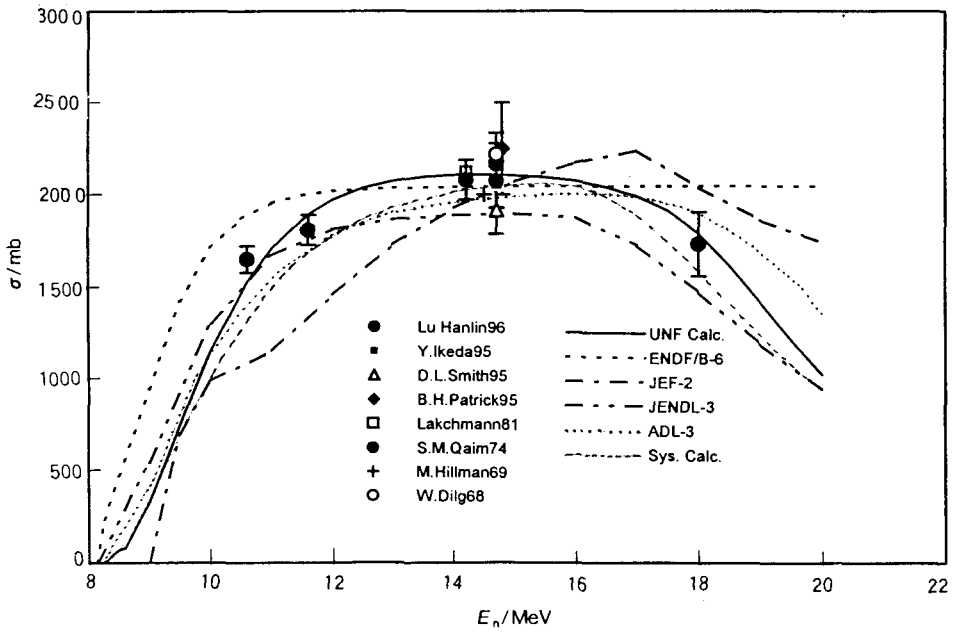

Fig.1 The comparison of the cross sections for ^{176}Hf(n,2n)^{175}Hf reaction

Table 2 $^{176}Hf(n,2n)^{175}Hf$ cross section

Time	Author	E_n / MeV	σ / mb	Monitor	σ / mb** 14.7 MeV	σ / mb***	Weight
	CIAE	10.6	1648±71				
		11.6	1807±81				
1996		14.2	2081±108	$^{93}Nb(n,2n)$	2102		2
		14.7	2166±112*		2166		2
		18.0	4239±250*			1730±173#	
1995	Y. Ikeda	14.7	2057±128*	$^{93}Nb(n,2n)$	2057		2
1995	D. L. Smith	14.7	1915±130*	$^{58}Ni(n,p)$	1915		1
1995	B. H. Patrick	14.8	2250±250*	$^{27}Al(n,\alpha)$	2245		1
1981	Lakchmann	14.2	2124		2145		1
1974	S. M. Qaim	14.7	2076±150*	$^{27}Al(n,\alpha)$	2076	1940	1
1969	M. Hillman	14.5	2000±100	$^{27}Al(n,\alpha)$	2008	2011	1
1968	W. Dilg	14.7	2220±115*	$^{27}Al(n,\alpha)$	2220	2332	1
14.7 MeV: mathematical average nine experimental data					2102±137		
weighted average nine experimental data					2104±119		
average of the data for CIAE and Y.Ikeda					2108#±55		

* Including the cross section of $^{177}Hf(n,3n)^{175}Hf$ reaction.

\# Calculated with the UNF program, excluding the disturbance of the $^{177}Hf(n,2n)^{175}Hf$ reaction.

** Corresponding cross section values at 14.7 MeV.

*** Cross section after the σ_0 and I_γ correction.

Measurement of Neutron Capture Cross Section for ^{71}Ga

Shi Zhaomin Chen Jinxiang Zhang Guohui Tang Guoyou
(Institute of Heavy Ion Physics, Peking University, Beijing 100871)

Lu Hanlin Huang Xiaolong
(China Institute of Atomic Energy, P. O. Box 275(3), Beijing 102431)

The excitation curve for $^{71}Ga(n,\gamma)^{72}Ga$ reaction has been measured from 0.2 to 2.0 MeV by different authors[1~5]. All of these measured cross sections are not in very good agreement with each other. To clarify the discrepancy it is necessary to measure the cross sections for $^{71}Ga(n,\gamma)^{72}Ga$ reaction again.

In present work, the cross sections for $^{71}Ga(n,\gamma)^{72}Ga$ reaction were measured with activation technique at neutron energies of 0.31, 0.51, 1.05 and 1.58 MeV. The cross sections of $^{197}Au(n,\gamma)^{198}Au$ reaction were used as reference for neutron fluence measurement. The values of $^{197}Au(n,\gamma)^{198}Au$ cross sections were taken from ENDF/B -6.

The experiments were carried out at the 4.5 MV Van de Graaff accelerator of the Institute of Heavy Ion Physics, Peking University. The monoenergetic neutrons were produced via the $T(p,n)^3He$ reaction on a solid T-Ti target. The Ga samples made of natural oxide Gallium powder were pressed into disks of 20 mm in diameter and 0.1 mm in thickness. The gold disks with 20 mm in diameter and 1 mm in thickness were used as neutron monitors. Each sample was sandwiched between two gold disks. Then it was packed in a 0.5 mm thick cadmium case. During Irradiation, the samples were placed in 0° direction relative to the incident proton beam at a distance of about 1.5 cm from the target. The proton beam currents were generally 10 ~ 12 μA and the duration of irradiation was 20 ~ 24 h. The fluctuation of neutron fluence was monitored with a BF_3 long counter at 0° placed at a distance of 300 cm from neutron source. The integral count rate of the long counter per 10 minutes was recorded continuously by microcomputer multiscalar for calculating the correction of the neutron flnence fluctuation.

After irradiation, the activities from residual nuclei were measured with a HPGe γ-detector. The detector was calibrated with standard gamma sources in the energy range of 0.1 ~ 1.5 MeV. The relevant decay data of ^{72}Ga and ^{198}Au are listed in Table 1. After the corrections for the detector efficiency, cascade effect, γ-intensity, fluctuation of neutron fluence and γ-ray self absorption in the samples, the cross sections of $^{71}Ga(n,\gamma)^{72}Ga$ reaction were calculated by well known activation equation. The cross sections measured for the $^{71}Ga(n,\gamma)^{72}Ga$ reaction and the $^{197}Au(n,\gamma)^{198}Au$ reaction taken from ENDF/B-6 are listed in Table 2. The principal contributions of errors and their magnitudes are given in Table 3.

Table 1 Decay data of radioactive products

Resid. nucl.	$T_{1/2}$ / h	E_γ / keV	I_γ / %
^{72}Ga	13.95	834.03	95.63
^{198}Au	64.704	411.8	95.57

Table 2 Measured results of cross sections (in mb)

E_n / MeV	$^{71}Ga(n,\gamma)^{72}Ga$	$^{197}Au(n,\gamma)^{198}Au$
0.31±0.02	33.4±1.5	199.9±5.9
0.51±0.03	22.1±1.1	129.7±4.5
1.05±0.03	12.4±0.7	78.8±3.5
1.58±0.04	7.7±0.4	6.8±0.3

The measured cross sections of the present work are plotted in Fig.1 along with the literature values[1~5] and JENDL-3 evaluation. It can be seen from Fig.1 that our results are close to JENDL-3 evaluation. The cross section values of Johnsrud[1] are systematically smaller than JENDL-3, since the normalized cross section he used

Table 3 Principal sources of errors

Source of uncertainty	Relative errors / %
Reference cross section	3 ~ 4.5
γ-counting statistics for ^{72}Ga	0.3 ~ 0.5
γ-counting statistics for ^{198}Au	0.6 ~ 0.8
γ-detection efficiency for ^{72}Ga	1.5
γ-detection efficiency for ^{198}Au	1.5
Correction of self absorption for ^{72}Ga	1.5
Correction of self absorption for ^{198}Au	1.0
Correction of cascade effect for ^{72}Ga	1.0
^{72}Ga sample weight	0.5
^{197}Au sample weight	0.1

was smaller than latest recommendation. In the energy range of 0.2 ~ 0.4 MeV, the data of Dorbenko[3] are considerably higher than JENDL-3.

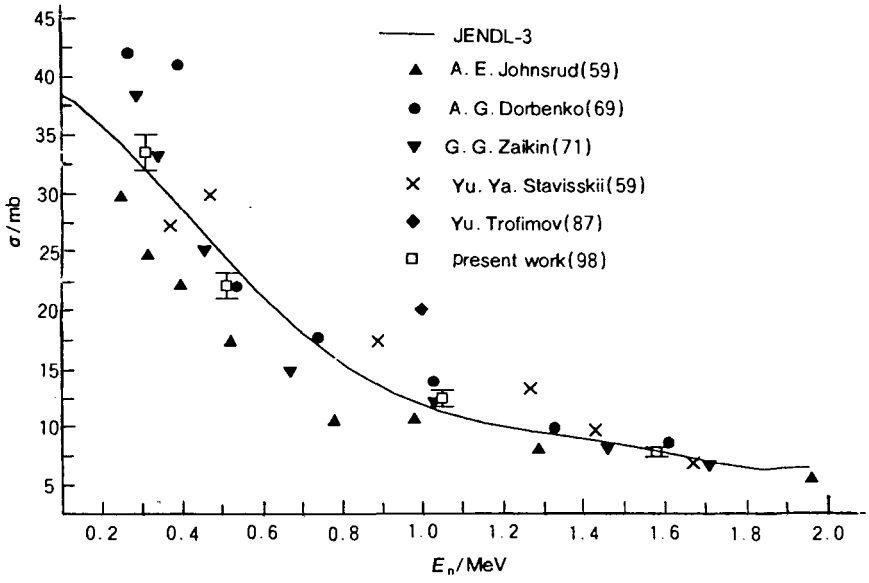

Fig.1 The cross sections of ^{71}Ga(n,γ)^{72}Ga reaction

The authors are indebted to CNDC for its financial support. In addition, acknowledgment is also made to the crew of the 4.5 MV Van de Graaff accelerator at Peking University for numerous irradiation.

References

[1] E. Johnsrud et al., Phys. Rev., 16, 927(1959)
[2] Yu. Ya. Stavissikii et al., Atomnaya Energiya, 7, 259(1959)

[3] A. G. Dovbenko et al., Atomnaya Energiya, 26, 67(1969)
[4] G. G. Zaikin et al., Ukrainskij Fizichnij Zhurnal,16, 1205(1971)
[5] Yu. N. Trofimov, 1st International Conference on Neutron Physics, Keiv, Vol.3, 331(1987)

CN9901224

Measurement of the Cross Sections for the $^{175}Lu(n,2n)^{174m,g}Lu$ Reaction

Yu Weixiang Zhao Wenrong Lu Hanlin Han Xiaogang
(Department of Nuclear Physics, CIAE, P. O. Box 275, Beijing 102413)

Introduction

The $^{175}Lu(n,2n)^{174m,g}Lu$ reaction is an important indicator. There are 10 sets of measured data since 1960 (total 58 experimental values). Most of the data are finished at 14 MeV with 20% ~ 30% discrepancy. So we measured the cross section by activation method in neutron energies of 14 MeV and 10 ~ 12 MeV.

1 Experiment

The measurement is carried out at the Cockcroft-Walton and HI-13 Tandem accelerator of CIAE for 14 MeV and 10 ~ 12 MeV neutrons. The $T(d,n)^4He$ and $D(d,n)^3He$ reactions are used as the neutron sources. Two kinds of samples (pressed Lu_2O_3 powder and natural metal Lu with 20 mm in diameter) are used in the experiment. The natural metal Nb of thin disk is used as neutron flux monitor. Lu sample is sandwiched with two Nb films. But for 10 ~ 12 MeV neutron energies, a group of monitors with different threshold were used to get rid of the effect of D-d low energy neutrons in the measurements with D-d neutron sources and get the correct neutron flux. The distance between the sample and the target is about 1 ~ 1.5 cm. The half-life is 142±2 d for ^{174m}Lu and 3.31±0.01 y for ^{174g}Lu. The activities of the samples are measured with Ge(Li) detectors by the off-line collection and analysis using computer system. The measured γ peaks in the experiment are 67(7.25±0.22), 177(0.470±0.019), 273(0.550±0.024), 992(0.546±0.021) and 1242 keV (5.14±0.13).

2 Results

The results are shown in Table 1 with reference cross sections of $^{93}Nb(n,2n)^{92m}Nb$ reaction and in Fig.1. The evaluation function by Lu Hanlin and Huang Xiaolong and the data measured by other laboratories are also plotted in Fig.1.

Table 1 The cross sections of $^{175}Lu(n,2n)^{174m,g}Lu$ reactions in mb

Sample	E_n / MeV	m	g	m+g	Nb
Lu	14.47	567±28	1276±51	1843±79	459±5
	14.47	576±28	1311±53	1887±81	459±5
	14.44	554±28	1269±51	1823±79	459±5
	14.80	559±28	1207±48	1766±76	459±5
	14.80	553±28	1213±48	1766±76	459±5
	11.50	464±25	1146±58	1610±83	
	10.50	403±28	1000±42	1403±71	
Lu_2O_3	13.50	528	1216	1744±122	449±7
	14.00	551	1282	1833±128	457±5
	14.60	576	1257	1833±128	459±5
	15.00	590	1205	1795±125	458±6

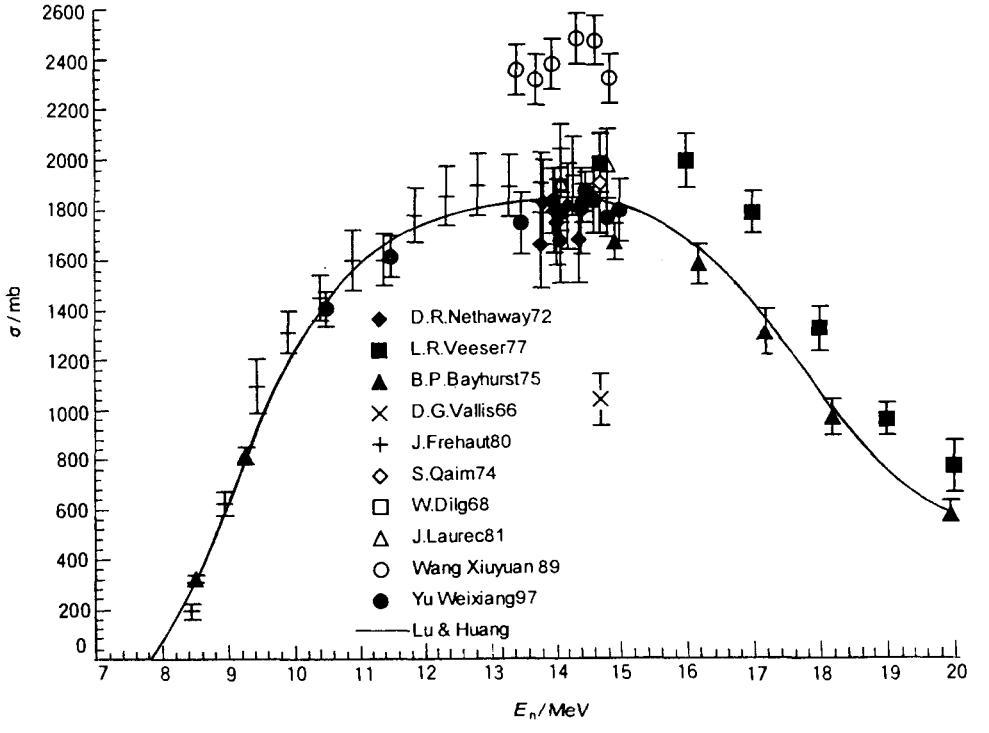

Fig. 1 The cross sections of $^{175}Lu(n,2n)^{174m+g}Lu$ reaction

At the beginning the results of ^{174g}Lu, which are calculated from the activities, measured at different time are in disagreement with each other. We found that it is

due to incorrect intensity of 1242 keV γ-ray. When the intensity is 5.14%, the measurements at different time are in agreement very well.

Due to the effect of the impurity of the sample, the results of the Lu_2O_3 samples are about 5.4% less than that of the natural metal Lu. The first is very closed with the results of Nethway and Qaim who used same sample. So we only use the relative values of the Lu_2O_3 samples.

The main uncertainties come from the error of reference cross section, efficiency of Ge(Li) detector, γ-absorption in sample, statistics of γ peak area and intensities of γ-rays.

CN9901225

Excitation Functions of Reactions from d+Ti, d+Mo, p+Ti and p+Mo

Zhao Wenrong Yu Weixiang Han Xiaogang Lu Hanlin
(Department of Nuclear Physics, CIAE, P. O. Box 275, Beijing 102413)

Introduction

The excitation functions for the reactions induced by proton or deuteron beam are very important for the evaluation of nuclear reaction, which is quite useful in nuclear technology applications. Some of them can be used to derive the thick-target yield, and this characteristic is significant for medicine isotope production.

However, the published data for proton or deuteron beam bombarding natural metal Ti and Mo are very few. In present work, the excitation functions for the products of ^{48}V from p+Ti and d+Ti and of $^{95m,g}Tc$, ^{96g}Tc and ^{99}Mo from p+Mo, and d+Mo were studied.

1 Experiment Procedure

The excitation functions were measured by the conventional stacked foil method. The technique used is essentially the same as described in earlier publications[1,2]. Here only some salient features relevant to the present measurements are described. The experiments were carried out at the HI-13 tandem

accelerator of CIAE in the energy range from threshold to 22 MeV. The incident particle beam adjusted to about 4 mm in diameter was focused on the center of the samples, and determined by a Faraday cup and ORTEC mode 439 digital current integrator. Typical beam currents were about 200 nA, and total collected charge was about 1200 μC.

Three stacks were irradiated with different primary energy for each reaction, and a considerable energy overlap was obtained in the measurements with various stacks. The metallic foils of Ti and Mo were rolled and machined into the shape of 22 mm in diameter and 6 to 20 mg/cm^2 in thickness. In general, a stack consisted of 4 to 6 foils and several Al foils used as energy degraders. One V foil was placed in front of each stack to monitor the intensity of incident beam. The energy on each foil of Ti, Mo, and Al was calculated using the knowledge of C. F. Willimson[3].

Table 1 Decay characteristics of products

reaction	product	Q / MeV	half-life	E_γ / keV	I_γ / %
^{47}Ti(d,n)	^{48}V	4.61	15.976d	983.5	99.99
^{48}Ti(d,2n)		−7.02			
^{47}Ti(p,γ)		6.832			
^{48}Ti(p,n)	^{48}V	−4.795			
^{49}Ti(p,2n)		−12.937			
^{94}Mo(d,n)		2.63			
^{95}Mo(d,2n)	^{95m}Tc	−4.74	61d	835.1	27.9
^{96}Mo(d,3n)		−13.96		582.1	31.4
^{94}Mo(p,γ)		4.892			
^{95}Mo(p,n)	^{95m}Tc	−2.473			
^{96}Mo(p,2n)		−11.627			
^{97}Mo(p,3n)		−18.446			
^{94}Mo(d,n)		2.67			
^{95}Mo(d,2n)	^{95g}Tc	−4.70	20.0h	765.8	94
^{96}Mo(d,3n)		−13.89			
^{94}Mo(p,γ)		4.855			
^{95}Mo(p,n)	^{95g}Tc	−2.512			
^{96}Mo(p,2n)		−11.666			
^{97}Mo(p,3n)		−18.487			
^{94}Mo(d,γ)		10.542			
^{95}Mo(d,n)	^{96g}Tc	3.18	4.28d	849.9	98
^{96}Mo(d,2n)		−5.98			
^{97}Mo(d,3n)		−12.80			
^{95}Mo(p,γ)		5.399			
^{96}Mo(p,n)	^{96g}Tc	−3.715			
^{97}Mo(p,2n)		−10.576			
^{98}Mo(p,3n)		−19.218			
^{98}Mo(d,p)	^{99}Mo	3.70	2.7477d	739.5	12.14
^{100}Mo(d,dn)		−8.292			
^{100}Mo(d,p2n)		−10.514			
^{100}Mo(p,pn)	^{99}Mo	−8.29			
^{100}Mo(p,d)		−6.066			

The activities of the γ rays for each product were measured by γ ray spectrometry using Ge(Li) detector coupled to 919 analyzer and 486 computer. The decay properties of the relevant products are given in Table 1.

2 Result

Since the natural metal Ti and Mo were used as the samples, the investigated product nuclides were produced through two to four reactions, with different threshold. Therefore, the isotope abundance of Ti and Mo elements was not considered in the calculations of the cross sections. That is, the present results are element cross sections for these products. The detail information for the products can be found in Table 1. Some γ rays are produced by two or three products, such as 765.789 keV γ-ray is formed through ^{95g}Tc, and ^{95g}Nb ($T_{1/2}$ = 34.97 d), while 849.9 keV γ-ray is produced by ^{94g}Tc ($T_{1/2}$ = 4.883 h), ^{96g}Tc and ^{96}Nb ($T_{1/2}$ = 23.35 h) nuclides. In order to get the activities for ^{95g}Tc and ^{96g}Tc products, it is needed to measure them for many times and deduce the interference according to their half-lives. In Table 2 are listed the excitation functions leading to the formations of ^{48}V, ^{95m,g}Tc, ^{96g}Tc and ^{99}Mo.

The dominant uncertainties include 1.5% for the efficiency calibration, 2% ~ 3.5% for weight and uniformity of sample, 1% ~ 2% for activity determination, 1.5% for intensity of incident beam measurement, 0.4% ~ 4% for statistics, 1.5% for correction of product nuclide recoil, and 3% ~ 4% for influence of detection position (only for ^{95m}Tc from d+Mo). The total uncertainty is about 3.5% ~ 7%.

Table 2 The products cross sections (in mb) of ^{48}V, ^{95m,g}Tc, ^{96g}Tc, ^{99}Mo

E_d / MeV	^{95m}Tc	^{95g}Tc	^{96g}Tc	^{99}Mo	E_d / MeV	^{48}V
21.64± 0.19	233.0 ±12.4	138.6 ±6.2	153.2 ± 6.6	28.3 ± 1.3	21.74 ± 0.09	314.2 ± 11.5
20.31± 0.19	236.8 ±12.6	135.9 ±6.1	162.7 ± 7.0	26.2 ± 1.3	20.60 ± 0.11	336.9 ± 12.3
18.86± 0.26	234.9 ±12.5	129.3 ±5.8	175.0 ± 7.5	33.4 ± 1.6	19.38 ± 0.13	352.8 ± 12 9
17.32±0.22	231.6 ±12.4	126.4 ±5.7	186.9 ± 8.0	37.5 ± 1.7	18.13 ± 0.10	364.6 ± 13.4
16.50±0.31	227.3 ±12.8	122.8 ±5.5	191.1 ± 8.2	38.8 ± 1.9	16.85 ± 0.10	354.7 ± 13.0
15.64±0.32	227.5 ±13.6	115.5 ±5.2	184.7 ± 7.9	40.9 ± 2.0	16.70 ± 0.10	361.2 ± 13.2
14.78±0.23	217.8 ±11.3	109.4 ±5.0	175.9 ± 7.5	42.1 ± 1.9	15.34 ± 0.10	340.6 ± 12.5
12.97±0.28	224.4 ±12.9	101.3 ±4.6	156.9 ± 6.7	47.2 ± 2.1	13.86 ± 0.13	311.4 ± 12.1
11.87±0.39	234.7 ±14.0	92.9 ±4.2	142.0 ± 6.1	50.3 ± 2.1	12.23 ± 0.13	259.5 ± 9.5
10.94±0.30	232.3 ±14.0	87.7 ±4.0	131.6 ± 5.8	54.7 ± 2.6	12.19 ± 0.12	263.8 ± 9.7
9.46±0.43	215.6 ±14.0	72.1 ±3.2	103.4 ± 4.4	56.1 ± 2.7	10.46 ± 0.13	170.7 ± 6.2
6.49±0.58	92.7 ± 6.5	25.4 ±1.8	29.3 ± 1.3	40.9 ± 2.2	10.35 ± 0.20	163.8 ± 6.0
					8.11 ± 0.27	34.7 ± 1.3
					6.48 ± 0.31	25.5 ± 0.9
					4.47 ± 0.41	20.3 ± 0.8

E_p / MeV	^{95m}Tc	^{95g}Tc	^{96g}Tc	^{99}Mo	E_p / MeV	^{48}V
21.85 ± 0.07	42.2 ±1.7	114.8 ±4.7	115.2 ±4.7	12.9 ±0.6	21.86 ±0.05	71.4 ±3.2
21.16 ± 0.10	50.9 ±2.1	131.2 ±5.4	124.1 ±5.1	15.7 ±0.7	21.23 ±0.04	75.0 ±3.5
20.42 ± 0.09	51.4 ±2.2	126.1 ±5.3	118.5 ±5.0	14.1 ±0.7	20.60 ±0.05	81.7 ±3.8
19.69 ± 0.08	52.3 ±2.2	117.4 ±4.9	119.2 ±5.2	12.7 ±0.7	19.93 ±0.06	90.4 ±4.2
18.93 ± 0.09	52.9 ±2.3	112.1 ±4.8	118.2 ±5.2	9.7 ±0.5	19.24 ±0.06	105.6 ±4.9
18.16 ± 0.09	56.3 ±2.8	117.0 ±5.3	129.8 ±6.5	10.8 ±0.6	18.54 ±0.06	122.1 ±5.8
16.78 ± 0.10	52.5 ±2.2	104 2 ±4.3	113.6 ±4.8	6.8 ±0.4	16.85 ±0.07	182.0 ±8.2
15.90 ± 0.13	51.8 ±2.2	102.0 ±4.2	117.3 ±5.0	5.4 ±0.3	16.06 ±0.07	232.5 ±10.8
14.99 ± 0.09	51.3 ±2.2	98.8 ±4.1	123.8 ±5.4	3.8 ±0.3	15.22 ±0.08	298.3 ±13.9
14.07 ± 0.11	50.2 ±2.2	99.7 ±4.2	140.3 ±6.3		14.36 ±0.07	371.4 ±18.6
13.09 ± 0.11	45.0 ±2.0	94.6 ±4.1	161.3 ±6.4		13.46 ±0.08	409.3 ±20.9
12.22 ± 0.13	38.2 ±1.6	76.9 ±3.2	171.8 ±7.2		12.52 ±0.06	415.3 ±21.0
12.03 ± 0.14	35.4 ±1.8	72.3 ±3.6	163.6 ±9.0		12.28 ±0.07	415.4 ±23.0
11.07 ± 0.15	34.0 ±1.5	68.8 ±2.6	133.8 ±5.8		11.26 ±0.09	382.4 ±19.0
9.81 ± 0.17	31.6 ±1.4	59.9 ±2.5	114.6 ±5.2		10.14 ±0.10	371.8 ±19.3
8.42 ± 0.18	23.2 ±1.2	47.2 ±2.0	87.5 ±4.4		8.91 ±0.11	347.2 ±18.4
6.81 ± 0.23	12.6 ±0.8	24.9 ±1.1	44.6 ±4.5		7.53 ±0.15	275.0 ±16.5

Reference

[1] Zhao Wenrong, Shen Qingbiao, Lu Hanlin, et al. Investigation of ^{89}Y(p,n)^{89}Zr, ^{89}Y(p,2n)^{88}Zr, and ^{89}Y(p,pn)^{88}Y reactions up to 22 MeV. Chinese J. of Nucl. Phys, 1992, 14(1), 7

[2] Zhao Wenrong, Lu Hanlin, Yu Weixiang, et al. Cross Section Measurement for ^{51}V(d,2n)^{51}Cr Reaction, Chinese J. of Nucl. Phys, 1992, 14(4), 309

[3] C. F. Williamson, J. P. Baijot, J. Picard. Table of range and stopping power of chemical elements for charged particles of energy 0.5 to 500 MeV. 1966, report CEA–R 3042

CN9901226

Excitation Functions for the Reactions Ti(α,x)^{51}Cr and Ti(α,x)^{48}Cr

Peng Xiufeng He Fuqing Long Xianguan

(Institute of Nuclear Science and Technology, Sichuan Union Univ., Chengdu)

Introduction

The excitation function measurement of charged-particle-induced nuclear reaction is an useful subject for reasons of both basic knowledge and technological progress. It is important in such fields as production of radio-isotopes with an accelerator, charged-particle activation analysis, thin-layer activation for study of wear and erosion in a metal and research of nuclear reaction mechanism, etc.

The products ^{51}Cr and ^{48}Cr from $Ti(\alpha,x)^{51}Cr$ and $Ti(\alpha,x)^{48}Cr$ reactions are important radioisotopes for medical application because of their suitable half-life (27.72 d and 22.56 h, respectively) and low energy photon emission (320 keV, 308 keV for ^{51}Cr and ^{48}Cr, respectively)[1~4]. In addition, ^{51}Cr is a standard gamma ray source in the efficiency calibration of gamma detector. Up to now some measured data on the excitation functions of α-particle impact of titanium have been published[5~9], and there are some discrepancies among those data. In present work we measured those excitation functions by using a high resolution HPGe detector in the energy range from threshold to 26.4 MeV. A theoretical calculation using the exciton model was performed.

1 Experimental

Excitation functions were measured by the conventional stacked-foil technique. A natural titanium plate of 99.9% purity was rolled down to foil with thicknesses from 1 to 2 mg/cm^2. Each titanium foil was covered by two aluminum foils with 1.2 and 5 mg/cm^2 thickness to prevent the loss of activity owing to atom recoil. Target thickness was determined in all case by weight and area measurement, and a balance with a precision of 10^{-5} g was used.

The stack was irradiated by using the external α-particle beam with 26.8 MeV. It was placed inside a Faraday cup in conjunction with an exact ORTEC model 439 digital current integrator having a digitized output accuracy of 0.2% of reading from 100 nA to 10 mA. The beam intensity was kept at about 300 nA and the total charge amounted to 2700 μC. During irradiation the stack was cooled continuously by a liquid nitrogen finger.

About 15 h after the stop of irradiation the ^{51}Cr and ^{48}Cr γ-ray activities of irradiated samples were counted. A low background activity chamber having a counting level of 2.5 cps in the energy range from 23 to 1595 keV and an ORTEC GEM–30190 HPGe detector with an energy resolution of 1.95 keV for 1332 keV photons of ^{60}Co were employed for gamma spectrum measurement. A multichannel system based on the IBM PC/XT computer were adopted for the data collection and subsequent analysis. The efficiency and energy calibration of the detector system have been carried out with a set of standard sources, ^{57}Co, ^{152}Eu and ^{137}Cs, uncertainty of which are 3%. The photopeaks of 320 and 308 keV were selected to identify ^{51}Cr and ^{48}Cr, respectively.

2 Results and Discussion

In Table 1 some main decay data of the nuclear reaction products were given.

Table 1 Decay data of the product nuclides

Nuclide	Reaction	Half-life	E_γ / keV	I_γ / %
^{51}Cr	Ti(α,x)^{51}Cr	27.704d	320.084	9.92
^{48}Cr	Ti(α,x)^{48}Cr	21.56h	308.24	100

Table 2 Experimental cross section values and errors (10^{-27} cm^2)

E_α / MeV	Ti(α,x)^{48}Cr	Ti(α,x)^{51}Cr
26.4±0.6	1.4±0.08	47.8±2.6
24.8±0.6	1.2±0.07	55.1±2.9
23.2±0.6	1.0±0.05	73.8±3.6
21.5±0.6	0.7±0.04	92.7±4.4
19.7±0.6	0.7±0.04	161.1±7.1
17.8±0.6	0.2±0.01	240.3±10.5
15.9±0.6		347.5±15.2
13.7±0.7		497.0±21.8
11.3±0.7		389.1±17.2
8.5±0.8		219.6±9.6
4.7±1.1		8.0±0.4

The energies of incoming and outgoing α-particles at each target foil were determined by calculating the energy degradation in each titanium and aluminum foil in the stack. The values of aluminum stopping powers were taken from Williamson et al.[10]. Since titanium is not listed in those Tables, therefore we calculated the energy degradation for this element by using our own program, which is based on the formulae given by Ziegler[11] for fitting stopping powers. The decay effect during irradiation was considered (See Ref. [12]). The main sources of uncertainty comes from the target inhomogeneity (3%), the detector efficiency (about 3%) and the statistical errors of photopeak counting, which are from 0.8% to 3.8%; the total error is estimated to be less than 6%. The uncertainty in the projectile energy contains two factors: (1) the energy spread of the inherent beam as well as (2) the energy loss inside those foils themselves. The energies are presented in Table 2. Fig.1 shows the excitation functions. For comparison, the excitation functions published by other authors are also given. In Fig.1 the solid lines represent the calculated results by using the statistical theory including preequilibrium emission. The details have published elsewhere[13].

Fig.1(a) shows that in the energy range from 8 to 12 MeV namely from the threshold of reaction ^{48}Ti(α,n)^{51}Cr to that of reaction ^{49}Ti(α,2n)^{51}Cr, our results are in agreement with the results of Vonach et al.[8] and Morton et al.[9] within the range of errors, our results also agree with those of Iguchi et al. for the rather large energy

uncertainty of these data obtained by the stack-foil method. At the maximum of the excitation curve of Chang et al.[6], our result is up to 37% higher than that of theirs, one of the reasons may be due to no correction for the loss of activation products induced by atom recoil. In the energy range of less than 8 MeV present results are different from Vonach et al., Morton et al. and Chang et al. owing to our rather rough energy determination in this range. In the rather high range our data are higher than the calculated values owing to the contribution of reaction $^{49}Ti(\alpha,2n)^{51}Cr$, because the theoretical calculation was performed only for the reaction $^{48}Ti(\alpha,n)^{51}Cr$ without considering the contribution of reaction $^{49}Ti(\alpha,2n)^{51}Cr$.

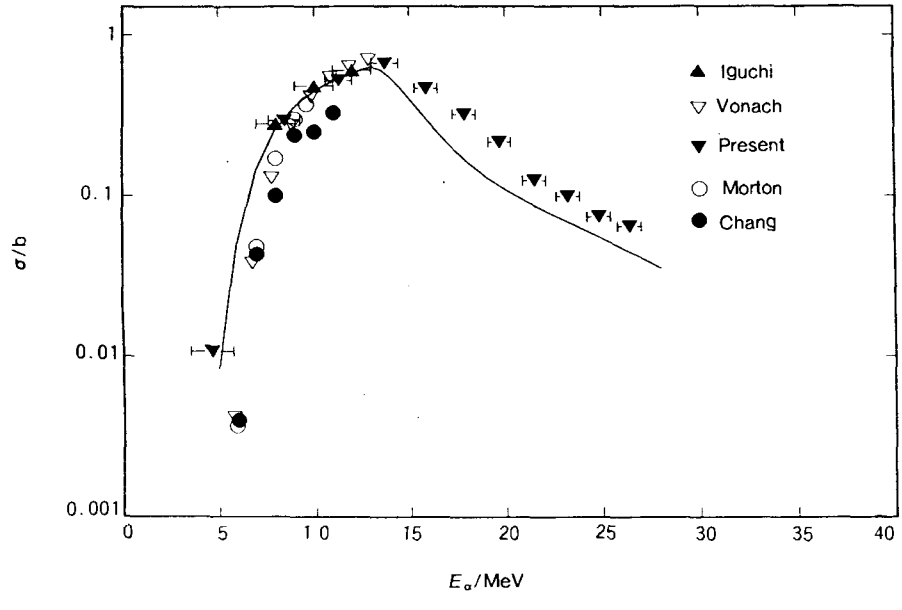

Fig. 1 Excitation functions for α+Ti reaction
(a) $^{48}Ti(\alpha,n)^{51}Cr$

We have compared our data with the results reported by Weinreich et al. (see Fig.1(b) and 1(c)). The rather large difference between two sets of data may be partially due to energy spread caused by the same stack-foil technology using in both experiments. In Fig.1(b) the theoretical excitation function in the energy range below 28 MeV was calculated with following method: the excitation functions for reactions $^{48}Ti(\alpha,n)^{51}Cr$ and $^{49}Ti(\alpha,2n)^{51}Cr$ were calculated independently, then the excitation function for reaction $Ti(\alpha,x)^{51}Cr$ was composed according to following formula:

$$\sigma(\alpha,\xi)=\varepsilon_1\sigma_1(\alpha,\nu)+\varepsilon_2\sigma_2(\alpha,2\nu)$$

Where $\sigma(\alpha,x)$ is the cross section for reaction $Ti(\alpha,x)^{51}Cr$; ε_1 and ε_2 are the abundance of ^{48}Ti and ^{49}Ti respectively; σ_1 and σ_2 are the cross sections for reactions $^{48}Ti(\alpha,n)^{51}Cr$ and $^{49}Ti(\alpha,2n)^{51}Cr$.

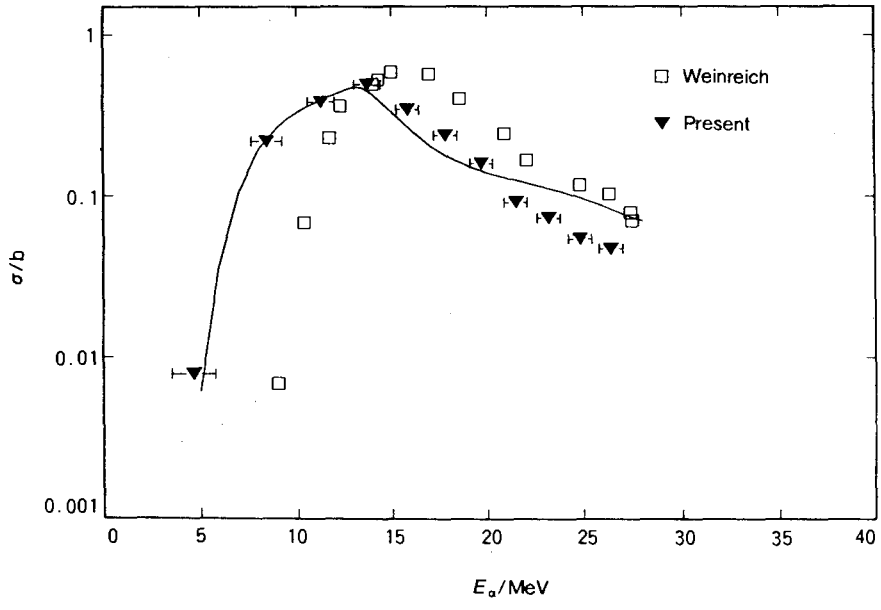

Fig. 1 Excitation functions for α+Ti reaction
(b) $Ti(\alpha,x)^{51}Cr$

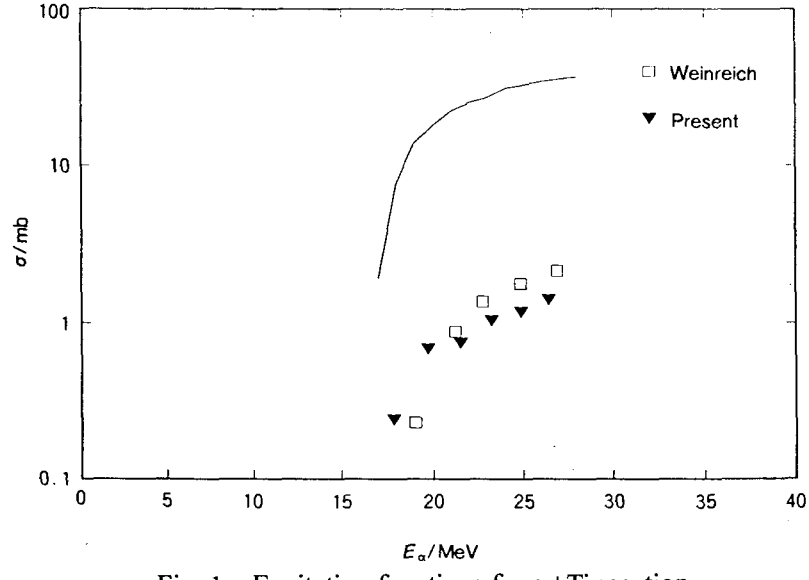

Fig. 1 Excitation functions for α+Ti reaction
(c) $Ti(\alpha,x)^{48}Cr$

Under normal conditions the cross sections for reaction $A(\alpha,\gamma)B$ are very small, so the contribution owing to the reaction $^{47}Ti(\alpha,\gamma)^{51}Cr$ can be neglected. In Fig.1(c)

our experimental values are in agreement with the measured results of Weinreich et al.

The authors would like to thank all members of the cyclotron group in our institute for their great help. The present work was supported by the China Nuclear Data center.

References

[1] S. J. Gray, K. Sterling, J. Clin. Invest. 29, 1604(1950)
[2] K. Sterling, S. J. Gray, J. Clin. Invest. 29, 1614(1950)
[3] S. J. Gray, K. Sterling, Science 112, 179(1950)
[4] C. C. Winter, W. G. Myers, J. Nucl. Med. 3, 273(1962)
[5] A. Iguchi et al., J. At. Energy Soc. Japan 2, 682(1960)
[6] C. N. Chang et al., Nucl. Inst. Meth.109, 327(1973)
[7] R. Weinreich et al., Appl. Radiat. Isot. 31, 223(1980)
[8] H. Vonach et al., Phys. Rev. C28, 2278(1983)
[9] J. Morton et al., Nucl. Phys. A537, 167(1992)
[10] C. F. Williamson et al., CEA-R3042(1966)
[11] J. F. Ziegler, Pergaman: HELIUM-Stopping Powers and Ranges In All Elements(1977)
[12] X. F. Peng et al., Nucl. Inst. Meth. B68, 145(1992)
[13] X. F. Peng et al., J. Appl. Radiat. Isot. 47, 309(1996)

II THEORETICAL CALCULATION

Neutron Radioactive Capture Cross Section Calculations of Natural Zr in the Incident Energy Region from 0.01 to 20 MeV

Liu Jianfeng Zhao Weijuan Gu Huawei Liu Xuguang
(Department of Physics, Zhengzhou University, Zhengzhou)

Liu Tingjin
(China Nuclear Data Center, CIAE)

Abstract

The neutron radiate capture cross sections of natural Zr are calculated in the neutron incident energy region from 0.01 MeV to 20 MeV. In the calculations, photon transmission coefficients of the compound statistical processes are calculated by solving the cascade gamma deexcitation processes of the compound nucleus. The nonstatistical effects of the neutron radiate captures, the radiate captures in the shape elastic scattering channels and the compound elastic scattering channels as well as the direct-semidirect captures are considered carefully in the calculated energy region. The calculated results are in better agreement with the experimental values.

Introduction

The research on neutron radiate capture is of importance in both theory and practical use. For example, it can provide the necessary parameters for the determination of the lower excited energy level characteristics and the higher excited energy level wave functions of the nucleus as well as for the tests of nuclear reaction models. Neutron radiate capture plays an important role in the calculations of the γ-production data, it provides the higher and the highest energy γ-rays in the neutrons induced nuclear reactions.

The research results of theories and experiments have shown[1,2] that when the neutron incident energy is less than 3 ~ 5 MeV, except for the nuclei with $A < 30$, which have strong nonstatistical effects, and the nuclei with $30 < A < 60$, for which

the nonstatistical effect cross section covers 10% ~ 20% of the statistical process cross section, for the nucleus with $A > 60$, unless it is or is near the neutron magic number, the major contribution to the radiate capture cross section comes from the compound statistical process. For natural Zr, the isotope ^{90}Zr possesses the neutron magic number 50 and the isotopes ^{91}Zr, ^{92}Zr, ^{94}Zr and ^{96}Zr are near the neutron magic number, therefore it can be expected that when the neutron incident energy is less than 3 ~ 5 MeV, the nonstatistical effects are still important.

In this paper, except for the compound nucleus statistical process, the nonstatistical effects, which include the radiate captures in the compound elastic scattering channels and shape elastic scattering channels below 3 ~ 5 MeV and the direct-semidirect radiate captures above 3 ~ 5 MeV, are considered reasonably. It is the purpose of this paper to investigate the contributions of the nonstatistical effects to the radiate capture cross sections for each isotope of natural Zr. In the end of the paper, some breif discussions are given.

1 Calculation Formulas

1.1 The Compound Nucleus Statistical Process

The calculation formula of the compound nucleus radiate capture cross sections given by Hauser-Feshbach statistical theory is[3]

$$\sigma_{n\gamma}^{st} = \frac{\pi}{K^2} \sum_{ljJ\pi} \frac{(2J+1)}{2(2I_0+1)} \frac{T_{lj} T_{\gamma}^{J\pi}}{T^{J\pi}} W_{lj}^{J\pi} \tag{1}$$

Where K is the wave number of the incident neutron, I_0 is the target nucleus spin, T_{lj} is neutron transmission coefficient, $T_{\gamma}^{J\pi}$ is photon transmission coefficient, $T^{J\pi}$ is the total transmission coefficient, $W_{lj}^{J\pi}$ is the width fluctuation correction factor[5]. $T_{\gamma}^{J\pi}$ is calculated by [4]

$$T_{\gamma}^{J\pi} = T_{\gamma,0}^{J\pi} = T_{\gamma\,0,0}^{J\pi} + \sum_{i=1}^{N} T_{\gamma,i}^{J\pi} S^{io} + \sum_{I'\pi'} \int_{E_c}^{E_n+B_n} T_{\gamma,I'\pi'}^{J\pi}(E') \frac{T_{\gamma\,0,0}^{I'\pi'}(E')}{T_{(E')}^{I'\pi'}} dE' \tag{2}$$

Where E_n is the neutron incident energy, B_n is the neutron binding energy, E_c is the inferior limit of the continuous region of the energy levels, S^{ij} is the gamma transition branch ratio from ith energy level to jth energy level, $i = 0$ represents the ground state, $T_{\gamma,j}^{J\pi}$ and $T_{\gamma,I'\pi'}^{J\pi}(E')$ can be calculated by the following integral

equations which describe the cascade γ deexcitations

$$\begin{cases} T_{\gamma,j}^{J\pi} = T_{\gamma 0,j}^{J\pi} + \sum_{i=j+1}^{N} T_{\gamma,j}^{J\pi} S^{ij} + \sum_{I'\pi'} \int_{E_c}^{E_n+B_n} T_{\gamma,I'\pi'}^{J\pi}(E') \frac{T_{\gamma 0,j}^{I'\pi'}(E')}{T^{I'\pi'}(E')} dE' \\ T_{\gamma,I'\pi'}^{J\pi}(E') = T_{\gamma 0,I'\pi'}^{J\pi}(E') + \sum_{I''\pi''} \int_{E'}^{E_n+B_n} T_{\gamma,I''\pi''}^{J\pi}(E'') \frac{T_{\gamma 0,E'I'\pi'}^{I''\pi''}(E'')}{T^{I''\pi''}(E'')} \rho(E'I'\pi') dE'' \end{cases} \tag{3}$$

Where $T_{\gamma 0,i}^{J\pi}$ represents the photon transmission coefficient of the primary γ transition of the J^{π} state of the compound nucleus to the *i*th discrete energy level, $T_{\gamma 0,I'\pi'}^{J\pi}(E')$ is the photon transmission coefficient of the primary γ transition of the J^{π} state of the compound nucleus to unit energy interval with spin I' parity π' and excitation energy E' of the continuous energy levels

$$T_{\gamma 0,i}^{J\pi} = \frac{1}{3\pi\hbar^2 C^2}(E_n + B_n - E_i)^2 \sigma_\alpha(E_n + B_n - E_i) H(JI_i', \pi\pi_i') \tag{4}$$

$$T_{\gamma 0,I'\pi'}^{J\pi}(E') = \frac{1}{3\pi\hbar^2 C^2}(E_n + B_n - E')^2 \sigma_\alpha(E_n + B_n - E') H(JI', \pi\pi') \tag{5}$$

Where

$$H(JI,\pi\pi') = \begin{cases} 1 & \text{if} \quad |J-1| \le I \le J+1 \quad \text{and} \quad \pi\pi' = -1 \\ 0 & \text{else} \end{cases} \tag{6}$$

and

$$\sigma_\alpha(E_\gamma) = \sum_{i=1}^{2} \frac{\sigma_{gi} E_\gamma^2 T'^2_{gi}}{(E_{gi}^2 - E_\gamma^2)^2 + E_\gamma^2 T'^2_{gi}} \tag{7}$$

is the photon absorption cross section, σ_{gi}, E_{gi} and T_{gi} are the peak cross section, the peak energy and the peak width of the giant dipole resonance, respectively, $\rho(E,J,\pi)$ represents the energy level density.

1.2 The Nonstatistical Effects

The radiate capture cross section of the nonstatistical effects can be calculated by[6~7]

$$\sigma_{n\gamma}^{non} = \sum_f \frac{2\pi m e^2 Z^2 K_\gamma^3}{3h^2 K^3 A^2} S_{dpf} \sum_{lJ} \frac{(2l+1)(2j_f+1)(2J+1)}{2I+1} \left[C_{I_{010}}^{I_f 0} W(ljl_f j_f; \frac{1}{2} 1) \right]^2 \cdot$$
$$\left\{ \left| \int r^2 U_{l_f j_f}(r) U_{lj}(r) \mathrm{d}r \right|^2 + \left| (\alpha - i\beta) \int r U_{l_f j_f}(r) h(r) U_{lj}(r) \mathrm{d}r \right|^2 + \right.$$
$$\left. 2R_e \left[\left(\int r^2 U_{l_f j_f}(r) U_{lj}(r) \mathrm{d}r \right) (\alpha + i\beta) \left(\int r U_{l_f j_f}(r) h(r) U_{lj}(r) \mathrm{d}r \right)^* \right] \right\} + \tag{8}$$
$$\sum_f \frac{2\pi m e^2 Z^2 K_\gamma^3}{3h^2 K^3 A^2} S_{dpf} \sum_{l,Jl'j'} \frac{(2l'+1)(2j_f+1)(2J+1)}{2I+1} \left[C_{I'_{010}}^{I_f 0} W(l' j' l_f j_f; \frac{1}{2} 1) \right]^2 \cdot$$
$$\left| \int r^2 U_{l_f j_f}(r) Q_{lj'}(r) \mathrm{d}r \right| \frac{T_{lj} T_{l'j'}}{T^{J\pi}}$$

Where $\sum_f$ represents the summation for the f single particle states, the first part is the capture of the shape-elastic scattering channels, which consist of the direct capture, the semidirect capture and the interference term. When the neutron incident energy is less than 3 ~ 5 MeV, only the direct capture needs to be considered, when the energy is larger than 3 ~ 5 MeV, the whole first part is important. The second part is the capture of the compound elastic scattering channels. It needs to be considered only when the neutron incident energy is less than 3 ~ 5 MeV. $S_{\alpha pf}$ represents the (d,p) reaction spectroscopic factor of fth single particle state. $U_{lj}(r)$ and $Q_{lj'}(r)$ are the wave functions of the scattering waves and are calculated in terms of the optical model. $U_{l_f j_f}(r)$ and K_γ are the eigen-function and the photon wave number of the single partial states, they are calculated in terms of the real part of the optical potential. $h(r)$ is the nucleon-phonon coupling potential. The meaning of the other symbols can be found in the references listed in this paper.

2 The Parameters and the Calculated Results

The numerical calculations for natural Zr were done in the neutron energy region from 0.01 to 20 MeV. In the calculations Becchetti-Greenless[8] optical potential was used to calculate the transmission coefficients of the neutrons and the charged particles, and the real part of this potential has been used to calculate the eigen energies and the wave functions of the single particle bound states. Gilbert-Cameron[9] formulas were used to calculate the energy level densities.

In the calculations, for each isotope, the optical potential parameters of the incident neutrons were adjusted firstly to make the calculated results of the total and elastic scattering cross sections coincide better with the experimental values. Then the optical potential parameters of charged particles and the energy level density parameters of the residual nuclei were adjusted to make the inelastic scattering cross

parameters of the residual nuclei were adjusted to make the inelastic scattering cross sections and the reaction cross sections of the (n,xγ) reactions coincide as good as possible with the experimental values. The optical potentials of the single particle bound states were adjusted to make the calculated eigen energies of the single particle bound states coincide with the experimental values. Finally the energy level density parameters of the compound nucleus and the particle-phonon coupling potential parameters in direct-semidirect capture processes were adjusted to make the calculated results of the radiate capture cross sections coincide better with the experimental values.

Table 1 shows the optical potential parameters of the incident neutrons for all isotopes. Table 2 shows the energy level density parameters and the giant dipole resonance parameters of the compound nucleus for all isotopes. The optical potential parameters for other particles and the energy level density parameters as well as the giant resonsnce parameters for other residual nuclei are not listed here in order to make the paper short.

Table 1 The optical potential parameters for the incident neutrons

	V_R	r_R	a_R	W_V	W_{SF}	r_I	a_I	V_{SO}	r_{SO}	a_{SO}
^{90}Zr	−48.98+0.32E	1.25	0.66	−0.22E+1.856	−7.15+0.25E	1.30	0.47	−5.52	1.24	0.65
^{91}Zr	−48.98+0.32E	1.25	0.73	−0.22E+2.496	−7.15+0.25E	1.30	0.47	−5.52	1.24	0.65
^{92}Zr	−48.98+0.32E	1.25	0.65	−0.22E+3.120	−7.15+0.25E	1.30	0.47	−5.52	1.24	0.65
^{94}Zr	−48.98+0.32E	1.25	0.65	−0.22E+2.496	−7.15+0.25E	1.30	0.47	−5.52	1.24	0.65
^{96}Zr	−48.98+0.32E	1.25	0.65	−0.22E+1.560	−7.15+0.25E	1.30	0.47	−5.52	1.24	0.65

Table 2 The energy level density parameters and the giant dipole resonance parameters for the compound nuclei

	Level density parameters					Giant resonance parameters		
	E_x / MeV	T / MeV	E_0 / MeV	P_N+P_Z / MeV	α / MeV^{-1}	σ_g / b	T_g / MeV	E_g / MeV
^{91}Zr	5.3484	0.9800	0.6627	1.20	9.9616	0.1840	4.50	16.58
^{92}Zr	6.0521	0.8873	0.7902	1.92	9.2721	0.2655	4.50	15.33
^{93}Zr	5.3145	0.7503	−0.5161	1.20	11.8592	0.2684	4.50	15.30
^{95}Zr	5.2805	0.7514	−0.0505	1.20	11.7723	0.2742	4.50	15.23
^{97}Zr	5.2477	0.7041	−0.1192	1.20	12.9816	0.2800	4.50	15.17

Fig. 1 shows the calculated results (the curve) and the experimental data of the total cross sections for natural Zr. It can be seen that the calculated results coincide with the experimental values better. Fig. 2 shows the ratios of the nonstatistical effect radiate capture cross sections to the compound nucleus statistical process radiate capture cross sections for each isotope. The number located near each curve represents the atomic mass number of that isotope. Fig. 3 shows the calculated results (the curve) and the experimental values of the radiate capture cross sections

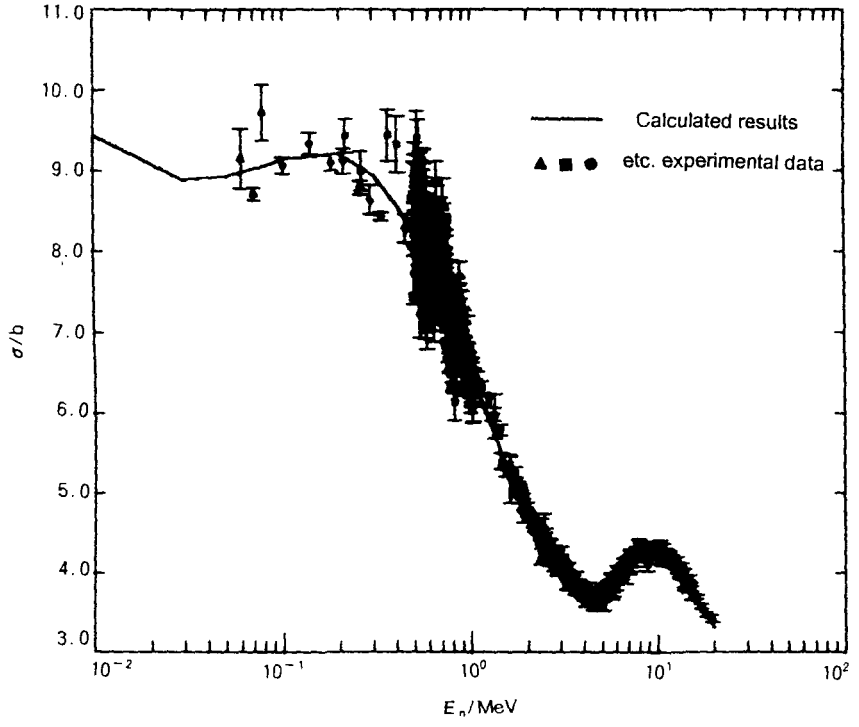

Fig.1 Calculated results and the experimental data of the total cross sections for natural Zr

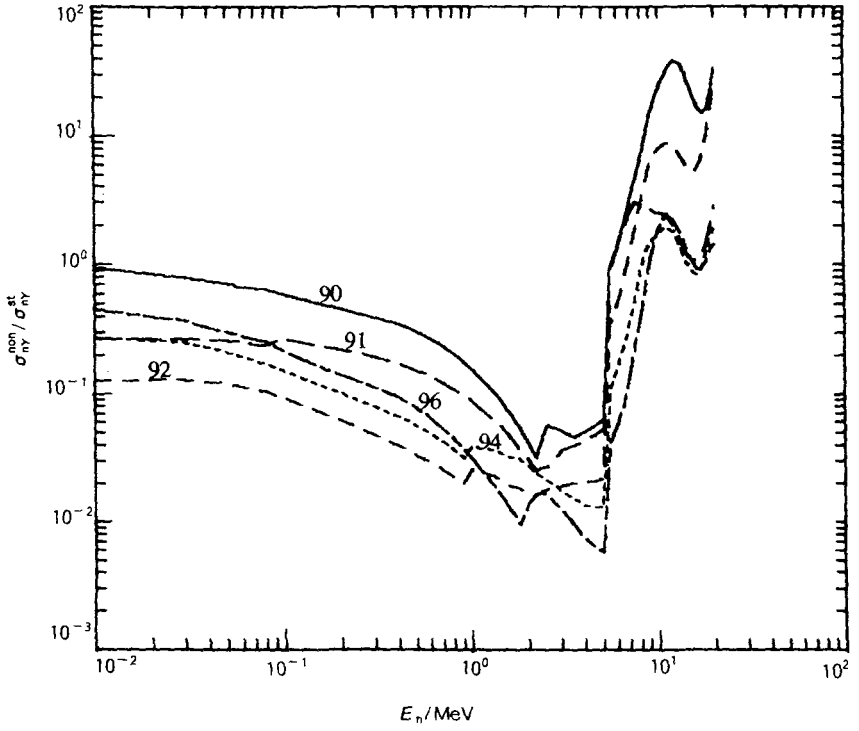

Fig.2 Ratios of the nonstatistical radiate capture cross sections to the compound nucleus radiate capture cross sections for each isotope

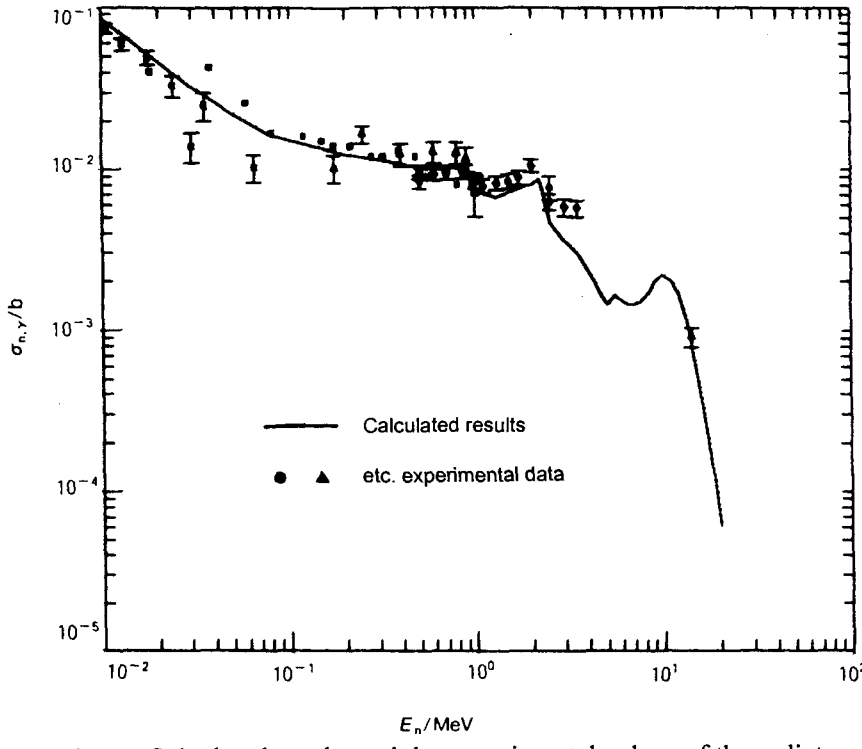

Fig.3 Calculated results and the experimental values of the radiate capture cross sections for natural Zr

for natural Zr. The experimental data of the total cross sections and the radiate capture cross sections were offered by China Nuclear Data Center.

3 Discussions

3.1 In this paper, using the compound nucleus statistical theory and considering the contributions from the nonstatistical effects in the neutron radiate capture processes, the theoretical calculations of the radiate capture reaction cross sections were in agreement with experimental data for natural Zr in the incident neutron energy region from 0.01 to 20 MeV.

3.2 From Fig. 2 It can be Seen that:

(1) When the neutron incident energies are less than 0.1 MeV, the nonstatistical effects of the neutron radiate capture are very important for all isotopes of Zr. The contributions from the nonstatistical effects are larger than 10% of the compound nucleus statistical process. Especially for ^{90}Zr, which has the neutron magic number, they are larger than 50%.

(2) When the neutron incident energies are larger than 0.1 MeV and less than 1 MeV, for ^{90}Zr and ^{91}Zr, the contributions from the nonstatistical effects are still larger than 10% of the compound statistical process. For ^{90}Zr, they are larger than 30%.

(3) When the neutron incident energies are larger than 5 MeV, for all the isotopes of Zr, the contributions from the nonstatistical effects are larger than the contributions from the compound nucleus statistical process. Especially for ^{90}Zr, near the peak value of the direct-semidirect capture, they are about 40 times as much as the ones from the compound nucleus statistical processes.

References

[1] Liu Jianfeng et al., High Energy Physics & Nuclear Physics, 4, 349(1991)
[2] Y. K. Ho et al., High Energy Physics & Nuclear Physics, 5, 265(1989)
[3] Hu Jimin et al., Nuclear Theory, Atomic Energy Press, (1987)
[4] Liu Jianfeng et al., High Energy Physics & Nuclear Physics, 6, 563(1996)
[5] Su Zongdi, High Energy Physics & Nuclear Physics, 3, 80(1979)
[6] Liu Jianfeng et al., Chinese Journal of Nuclear Physics, 1, 21(1987)
[7] Liu Jianfeng et al., Chinese Journal of Nuclear Physics, 2, 127(1992)
[8] F. D. Becchetti and G. W. Greenless, Phys. Rev., 182, 1190(1969)
[9] A. Gilbert and A. G. W. Cameron, Can. J. Phys., 43, 1446(1965)

CN9901228

Illustration on Photonuclear Data Calculation with GUNF Code

Zhang Jingshang Han Yinlu Yu Baosheng
(China Nuclear Data Center, CIAE)

Introduction

Since the main neutron libraries in the world have the up-limit incident neutron energy of 20 MeV, and the incident neutron brings binding energy into compound nucleus, the excitation energies could reach almost up to about 30 MeV, which is the up-limit of gamma-ray emitted energy. For this reason the GUNF code was developed to calculate photonuclear reaction data below incident photon energy of 30 MeV. In this incident γ-ray energy region the particle-hole excitation model was

adopted[1], while for high energies the quasideuteron model is used.

The code described herein is referred to the unified Hauser-Feshbach and exciton model with angular momentum and parity conservations. The discrete levels are also included in the calculation, this procedure could produce the reasonable shapes of outgoing particle spectra.

Since the gamma elastic scattering data are not useful in applications, we do not consider this data. In the comparison with neutron induced nuclear reactions, photonuclear reactions are the secondary nuclear reaction processes and γ production data are not calculated in this code. In this paper the illustration for some physical quantities and GUNF code are given.

1 Energy Angle Distribution

The linear momentum dependent exciton state density model has been developed[2,3]. This approach is a consistent way to obtain angular distribution of outgoing particles. In this theoretical method the leading particle is not assumed, instead a statistical population of all states compatible with energy and momentum conservation are proposed. The effect of the Fermi motion of the nucleons is included, as is the Pauli blocking by the "sea" of nucleons. In particular the angular distribution from the first preequilibrium state in a nucleon-induced reaction is identical to that obtained with the KK scattering kernel[4,5]. This method can easily obtain the explicit expression of the exciton state densities at low exciton states.

We tried to use this method to study the energy-angular distribution of the emitted particles from 1-particle and 1-hole exciton state. Based on detailed balance, the double differential emission rate for emission of a particle b with energy ε and direction Ω from (p =1, h =1) exciton state is given by[2]

$$\frac{\mathrm{d}^2\omega_{\mathrm{b}}(\varepsilon,\Omega)}{\mathrm{d}\varepsilon\ \mathrm{d}\Omega}=\frac{m\varepsilon\sigma_{\mathrm{inv}}^{\mathrm{b}}(\varepsilon)R}{2\pi^3h^3}\cdot\frac{\rho(0,1,E-\varepsilon,\vec{K}-\vec{k}_{\Omega})}{\rho(1,1,E,\vec{K})} \tag{1}$$

The $\rho(1,1,E,\vec{K})$ density requires the solution of a six dimensional integration, which can be solved analytically and expressed as

$$\rho(1p,1h,E,\vec{K})=\frac{\pi mk^2}{K}\begin{cases}k_{\mathrm{f}}^2-\left(\dfrac{mE}{K}-\dfrac{K}{2}\right)^2 & \text{if } K_{\min}<K<K_1 \text{ or } K_2<K<K_{\max}\\ 2mE & \text{if } K_1<K<K_2\\ 0 & \text{otherwise}\end{cases} \tag{2}$$

where

$$K_{\min,\max} = \sqrt{2mE + k_f^2} \mp k_f$$

$$K_{1,2} = \sqrt{2(k_f^2 - mE) \mp 2k_f\sqrt{k_f^2 - 2mE}}$$

In the case of γ-ray induced reactions $E = E_\gamma + \varepsilon_f$, and $K = E/c$, while ε_f is the Fermi energy and $\varepsilon_f = \frac{k_f^2}{2m}$. At $E_\gamma < 30$ MeV it has $K < K_{\min}$, then $\rho(1,1,E,\vec{K}) = 0$. This is caused by too weak incident momentum. If $K > K_{\min}$ it needs $E_\gamma > 1.2$ GeV. However, in this energy region the quasideuteron model should be employed. In the case of $E_\gamma < 30$ MeV the isotropic distribution is used for emitted particles.

2 Excitation Energy and Threshold Energy

Now we study the energy transportation to target from incident γ-ray. Based on the relativity the motion of the center of mass can be given by the value of $r = V_C/c$, where V_C stands for the speed of center of mass, c is the light speed. It reads

$$r = \frac{E_\gamma}{E_\gamma + Mc^2} \tag{3}$$

where E_γ is incident γ-ray energy, M is the mass of target.

Thus, the kinetic energy of the target can be given by

$$E_T = \frac{Mc^2}{\sqrt{1-r^2}} - Mc^2$$

and the excitation energy is

$$E^* = E_\gamma - E_T$$

In comparison with incident neutron, the motion of the center of mass can be given by the r_n value as follows

$$r_n = \frac{m}{m+M}\sqrt{\frac{2E_n}{mc^2}}$$

In terms of the same value of $r = r_n$ we can get the equivalent bombarded neutron energy E_n, taking $\gamma + {}^{54}Fe$ as an example, $E_\gamma = E_n$ is about 1.8 GeV.

In comparison of the neutron bombard energies, the results are shown in Table 1 with the incident γ-ray energies from 10 MeV to 3 GeV. The results indicate that at low γ-ray energies ($E_\gamma < 30$ MeV) there is only equivalent incident neutron of

several hundreds keV, while the excitation energy induced by neutron is larger than that induced by γ-ray. Based on the above analysis we can see that at low γ-ray energies ($E_\gamma < 30$ MeV) the isotropic distribution would be a good approximation for emitted particles.

Table 1 The γ value, equivalent neutron energy E_n, the kinetic energy of target E_T and excitation energies (All of energies in Table 1 are in unit MeV)

E_γ	r	E_n	E_T	E^*
10	0.00020	0.055	0.0010	9.999
20	0.00040	0.221	0.0040	19.996
30	0.00060	0.496	0.0090	29.991
40	0.00080	0.882	0.0159	39.984
50	0.00099	1.378	0.0249	49.975
60	0.00119	1.983	0.0358	59.964
80	0.00159	3.523	0.0635	79.936
100	0.00199	5.501	0.0992	99.901
200	0.00397	21.915	0.3952	199.605
300	0.00594	49.113	0.8857	299.114
400	0.00790	86.968	1.5685	398.432
500	0.00986	135.35	2.4411	497.559
600	0.01181	194.14	3.5015	596.498
800	0.01568	342.43	6.1767	793.823
1000	0.01953	530.88	9.5768	990.423
1500	0.02901	1171.5	21.140	1478.860
2000	0.03831	2043.0	36.884	1963.116
2500	0.04743	3131.9	56.576	2443.425
3000	0.05639	4425.5	80.000	2919.999

For each reaction channel the threshold energy E_{th} is given by the Q value subtracting the kinetic energy of compound nucleus caused by bombard particle. In the case of photon induced reactions the threshold energy is given by

$$E_{th} = -Q + E_T \tag{4}$$

With

$$r = \frac{E_{th}}{E_{th} + Mc^2} \tag{5}$$

This is a nonlinear equation. Since γ is a small quantity, if r^n ($n > 1$) terms are omitted, then E_{th} is obtained by

$$E_{th} = \max\left\{0, -Q\left(1 - \frac{Q}{2Mc^2}\right)\right\} \tag{6}$$

3 Summary Description of GUNF Code

GUNF code implements the Unified Hauser-Feshbach and exciton model[6,7] in an open-ended sequence of reaction chains.

Table 2 The reaction channels handled in GUNF code

1	(γ,γ)	8	(γ,2n)
2	(γ,n)	9	(γ,np)
3	(γ,p)	10	(γ,α)
4	(γ,α)	11	(γ,pn)
5	(γ,3He)	12	(γ,2p)
6	(γ,d)	13	(γ,αn)
7	(γ,t)	14	(γ,3n)

The physical quantities calculated by GUNF code are the following:

(1) Absorption cross sections, the cross sections of all reaction channels including discrete level emissions and continuum emissions. The absorption cross sections is calculated by one or two peak giant resonance model for E_1 and M_1 mode, while single peak giant resonance model for E_2 model.

(2) Outgoing particle energy spectra of each channel.

The output in ENDF/B-6 format includes the following contents as shown in Table 3.

Table 3 The contents in ENDF/B-6 output

cross section (*MF*=3)	*MT*	neutron spectrum (*MF*=6)	*MT*
(γ,abs.)	3	(γ,2n)	16
(γ,n)	4	(γ,3n)	17
(γ,2n)	16	(γ,nα)	22
(γ,^{3}n)	17	(γ,np)	28
(γ,nα)	22	(γ,n')$_c$	91
(γ,np)	28		
(γ,n')$_k$	50~90		
(γ,n')$_c$	91		
(γ,γ')	102		
(γ,p)	103		
(γ,d)	104		
(γ,t)	105		
(γ,^{3}He)	106		
(γ,α)	107		

There are 46 subroutines and 10 functions included in this code.

This code has three main functions:

(1) Adjusting the parameters of γ absorption cross section by fitting γ absorption

cross section or (γ,n) cross section.

(2) Calculating the cross sections and spectra of each reaction channel.

(3) Outputting the calculated data in ENDF/B-6 format with incident γ energy up to 30 MeV.

There are five flags included in GUNF code. The function of each flag is as following:

if "KTEST = 1" writing some medium results for physical analysis, while "KTEST = 0" does not do that.

if "KOPP = 1" outputting optical potential parameters, while "KOPP = 0" does not do that.

if "KOPD = 1" doing calculating the "T" factors, while "KOPD = 0" reading them from "GTFC.DAT" file.

if "KENDF = 1" doing ENDF/B-6 format outputting, while "KENDF = 0" does not do that.

if "KEOD = 1" outputting the threshold energies used for ENDF/B-6 format outputting, while "KEOD = 0" does not do that.

Reference

[1] E. Hayward "Photonuclear Reactions" NBS MOMOGRAPH 118 Sep 18 (1973)

[2] M. B. Chadwick, P. Oblozinsky Phys. Rev. C. 44 1740(1991) Phys. Rev. C. 46 2028(1992)

[3] M. B. Chadwick, P. Oblozinsky, P. E. Hodgson and G. Reffo Phys. Rev. C. 44 814(1991)

[4] K. Kikuchi and M. Kawai, Nuclear Matter and Nuclear reactions (North–Holland, Amsterdam, 1968) p, 44

[5] Sun Ziyang et al., Z. Phys. A. 305, 61(1982)

[6] Zhang J. S. Nucl. Sci. Eng. 114, 55 (1993)

[7] Zhang J. S. "Comprehensive Photonuclear Data Calculation: Introduction to the theory and use of GUNF code". (1997)

n+$^{238\sim242}$Pu Coupled Channel Optical Model ECIS95 Calculations

Wang Shunuan
(China Nuclear Data Center, CIAE)

It is well known that the actinide region is one of the strong nuclear deformation, neutron inelastic scattering coupled channel effects between members of the ground state rotational band have to be taken into account properly.

For the purpose of CENDL-3 actinide nuclei $^{238\sim242}$Pu calculations and evaluations, the latest coupled channel optical model calculation code ECIS95[1] is used to calculate the direct inelastic scattering cross section and angular distributions on the basis of rotation model. The additional PRE-LEG[4] and LEG[5] codes make the adopting of ECIS95[1] output file to FUNF[3] input file. The FUNF code which is designed on the basis of semi-classical multi-step nuclear reaction theory is used to calculate the whole set of neutron ($E_n \leq 20$ MeV) data in ENDF/B–6 output format.

Most of the information needed to perform ECIS95 code calculation is also needed to perform the spherical optical potential calculations. The additional information that must be furnished concerns the excited states of the target and the deformation parameters. The excitation energy, spin and parity of each of the excited states must be provided also to ECIS95 code. In the pure symmetric rotational model, all possible excited states are members of the same rotational band and more information on their structure is unnecessary. The details of ECIS95 calculations and parameters used for $^{238\sim242}$Pu are presented and discussed as the following:

1 Optical Potentials

In the calculations, the developing more realistic neutron-nucleus fissionable nuclei global optical potential within the actinide region $228 \leq A \leq 246$ for bombarding energies ranging from ~10 keV to 20 MeV recommended by D. G. Madland and P.G.Young[6] are used. In Ref.[6], the best fit spherical optical potential obtained is based primarily upon scattering data obtained from isotopes of Th, U and Pu consisting of total cross sections, elastic and inelastic angular distributions, S and P wave strength functions, and nuclear shape deformations as determined. It is then deformed, using experimentally determined nuclear deformations, and coupled-

channel calculations are performed under the assumption that the actinide nuclei are axially symmetric rotators differing from one another primarily by the features of their ground band rotational spectra. The requirements of simultaneous good fitting to the inelastic data (where it exists) as well as the elastic and total cross sections forces changes in the parameterization of the initial best fit spherical optical potential. A second series of coupled-channel calculations is then performed using the deformed modified potential. The process is repeated until satisfactory results are obtained. The iterative procedure is therefore adopted to extract the optical potentials. Initially, the regular optical model is assumed adequately to be spherical, complex, local, energy dependent and utilize Woods-Saxon form factors.

The philosophy of doing the job as mentioned above is more reasonable and realistic. As a consequence, the neutron-nucleus optical potentials for the actinide region recommended in Ref.[6] and its latest publications have been widely used in nuclear data evaluations and extrapolations and also in the present calculations for n+$^{238\sim242}$Pu inelastic angular distributions.

2 Deformations

In the present calculations, the deformations not only for the real volume and surface terms, but also for imaginary volume and surface terms, Coulomb term, real and imaginary spin-orbit terms are taken into account. The largest order in the deformations and the largest angular momentum l to be used in the multipolar expansion of the potential are taken as 4 and 8, respectively. The deformed parameters used β_λ with the static deformation of multipolarity λ = 2 and 4 are considered. The β_λ parameter values adopted for $^{238\sim242}$Pu are shown in Table 1.

Table 1 Deformed Parameters β_2 and β_4 for $^{238\sim242}$Pu

	β_2	β_4
^{238}Pu	0.12~0.20	0.02~0.07
^{239}Pu	0.12~0.22	0.02~0.07
^{240}Pu	0.12~0.20	0.02~0.07
^{241}Pu	0.12~0.22	0.02~0.07
^{242}Pu	0.12~0.218	0.02~0.046

The β_2 and β_4 values shown in Table 1 are taken from Refs.[7 ~ 9]. In Refs.[7,9], a set of coupled channel optical potential parameters for actinide nuclei in the energy range 0.001 ~ 20 MeV is proposed. This phenomenological parametrization has been extracted by runing ECIS95 code and applied to a large range of different types actinide nuclei (e-e, e-o, o-e etc) calculations, i.e. ^{232}Th, ^{233}U, ^{235}U, ^{238}U, ^{238}Pu, ^{239}Pu, ^{240}Pu, ^{241}Pu, ^{242}Pu, ^{241}Am actinide nuclei.

3 Level Schemes

The level schemes of the members of the ground state rotational band used in the present calculations for $^{238\sim242}$Pu are chosen according to the latest Nuclear Data Sheets[10] as shown in Table 2.

Table 2 Level schemes for $^{238\sim242}$Pu

	^{238}Pu		^{239}Pu		^{240}Pu		^{241}Pu		^{242}Pu	
	keV	$J\pi$	keV	$J\pi$	keV	$J\pi$	keV	$J\pi$	keV	$J\pi$
L_1	0.0	0^+	0.0	0.5^+	0.0	0^+	0.0	2.5^+	0.0	0^+
L_2	44.08	2^+	7.83	1.5^+	42.824	2^+	41.95	3.5^+	44.54	2^+
L_3	145.96	4^+	57.28	2.5^+	141.69	4^+	95.69	4.5^+	147.3	4^+
L_4	303.40	6^+	75.306	3.5^+	294.319	6^+	161.05	5.5^+	306.4	6^+
L_5	513.40	8^+	163.76	4.5^+	497.52	8^+			518.7	8^+
L_6			192.81	5.5^+					778.7	10^+

It can be seen from Table 2 that the highest ground state spin value is 2.5 for ^{240}Pu, and the highest excited state spin value of the member of the ground state rotational band is 10^+ for ^{242}Pu meeting in the present coupled channel calculations. It stands to reason that the coupled channel calculations for actinide nuclei with high ground state spin value need long computational time. The highest number of the members of the ground state rotational band is taken as 6. In actual fact, the direct inelastic scattering cross section at L_6, 778.7 keV, $J\pi = 10^+$ for ^{242}Pu is relatively small. It can be summarized from the foregoing as the following: in CENDL-3 calculations and evaluations, the $^{238\sim242}$Pu direct inelastic scattering cross sections and angular distributions for the coupling members of the ground state rotational band are carried out by ECIS95, PRECIS codes, and a set of input data file FDIR for FUNF code is finished by additional PRE-LEG and LEG Codes. A set of satisfactary results are obtained. The reasonable parameters used in the calculations are presented and specificated.

References

[1] J. Raynal, "Notes on ECIS94", CEA Scaclay Report No CEA-N-2772, 1994(unpublished)

[2] B. V. Carlson, "The Optical Model ECIS95", Workshop on Nuclear Reaction Data and Nuclear Reactors–Physics, design and Safety, 15 Apr. -17 May 1996, Miramare Trieste, Italy

[3] Zhang Jing Shang, FUNF code, CNDC,1996

[4] Sun Zheng Jun, PRE–LEG code, CNDC, 1997
[5] Wang Shu Nuan, LEG code, CNDC, 1997
[6] D. G. Madland and P. G. Young, "Neutron-Nucleus Optical Potential for the Actinide Region", International Conference on Neutron Physics and Nuclear Data for Reactors and Other Applied Purposes, 1978 Sep. 25 ~ 29, Harwell, OECD/NEA UKAEA, p.49(1978); and late on series publications
[7] Anabella Tudora, "Neutron Optical Deformed Parametrization for the Actinide Region", Abstract Book, P132, International Conference on Nuclear Data for Science and Technology, May 19 ~ 24, 1997 Trieste, Italy
[8] P. Oblozinsky, "Input Parameter Libraries", Workshop on Nuclear Reaction Data and Nuclear Reactors-Physics, design and Safety, 15 Apr. -17 May 1996, Miramare Trieste, Italy
[9] Anabella Tudora, Private Communications
[10] M. J. Martin, J. K. Tuli, "Nuclear Data Sheets", Vol. 45, 53, 59, 66, 72; "Evaluated Nuclear Structure Data File", ENSDF-May 1997

CN9901230

Calculation and Analysis of Neutron Induced Reaction on ^{185,187}Re and ^{Nat}Re

Han Yinlu Yu Baosheng
(China Nuclear Data Center, CIAE)

Zhang Zhengjun Sun Xiuquan
(Department of Physics, Northwest University, Shaanxi)

Abstract

Based on the relevant experimental data of Re and neighbor nucleus W, and the theoretical model calculations, neutron induced reaction cross sections, the energy spectrum, angular distribution, double differential cross section and γ-production data were calculated for ^{185,187,Nat}Re at incident neutron energies below 20 MeV. The calculated results were compared with experimental data.

Introduction

The cross sections of neutron induced reactions on ^{185,187,Nat}Re are important for nuclear science and technology. Because the experimental data are less, the theoretical calculation is necessary and interesting. The purpose of this work is to calculate all data of n+^{185,187,Nat}Re reactions.

In Sec.1 the theories and parameters used in the calculation are described. The calculated results and analyses are given in Sec.2. Finally, a summary is given in Sec.3.

1 Theories and Parameters

The calculation was made with the semi-classical theory code UNF[1].

First, the code APOM[2], by which the best neutron optical potential parameters can be searched automatically with fit relevant experimental total, nonelastic scattering cross sections and elastic scattering angular distributions, was used to obtain a set of optimum neutron optical potential parameters of ^{185,187,Nat}Re. Because there are no experimental data of elastic scattering angular distributions for Re, so we choose neutron elastic scattering angular distributions of W, which is neighbors nucleus of Re. A set of optimum neutron optical potential parameters of Re are obtained as follows:

$$V = 57.4563+0.1556E-0.02241E^2-24(N-Z)/A$$
$$W_S = \max\{0.0, 8.0057- 0.4181E-12.0(N-Z)/A\}$$
$$W_V = \max\{0.0, 0.06646+0.1891E-0.003214E^2\}$$
$$U_{SO} = 6.2$$
$$r_R = 1.1204, \quad r_S = 1.4095, \quad r_V = 1.6771, \quad r_{SO} = 1.1204$$
$$a_R = 0.4900, \quad a_S = 0.3970, \quad a_V = 0.9298, \quad a_{SO} = 0.4900$$

Using this set of neutron optical potential parameters, adjusting charged particle optical potential parameters and level density parameters, all cross sections of n+^{185,187,nat}Re reactions were calculated by the code UNF[1]. The direct inelastic scattering data were calculated by the code DWUCK4[3]. The exciton model parameter K was taken as 2200 MeV^3. All experimental data were taken from EXFOR library.

2 Calculated Results and Analyses

Fig.1 shows the comparison of neutron total cross section for ^{Nat}Re in energy region 0.001 ~ 20 MeV between the theoretical values (solid line) and experimental data. The calculated results are in good agreement with experimental data for energy $E_n \geq 0.5$ MeV, while for energy $E_n < 0.5$ MeV, the calculated results are in agreement with experimental data taken from Ref.[4]. The comparison for calculated results and experimental data of elastic cross sections of n+^{Nat}Re reaction is given in Fig.2.

The theoretical calculated result is reasonable. The comparison between the theoretical results and experimental data of $^{185}Re(n,\gamma)^{186}Re$, $^{187}Re(n,\gamma)^{188}Re$ and $^{Nat}Re(n,\gamma)$ reaction cross sections are given in Figs.3 to 5, respectively, The calculated values are in good agreement with experimental data for $^{185}Re(n,\gamma)^{186}Re$ and $^{187}Re(n,\gamma)^{188}Re$ reaction cross sections, but for $^{Nat}Re(n,\gamma)$ reaction cross sections, the calculated results are lower than experimental data in energy region 2 ~ 5 MeV. The cross sections of $^{187}Re(n,p)^{187}W$ and $^{187}Re(n,\alpha)^{184}Ta$ reactions are given in Figs.6 and 7, respectively. The calculated cross section values pass through the existent experimental data within error bars, respectively. The comparison of theoretical calculated results and experimental data of $^{185}Re(n,2n)^{184}Re$ and $^{187}Re(n,2n)^{186}Re$ reactions are given in Figs.8 and 9, respectively. The calculated values are in agreement with the experimental data taken from Ref.[5] for $^{185}Re(n,2n)^{184}Re$ reaction cross sections, while for $^{187}Re(n,2n)^{186}Re$ reaction cross sections, the calculated values are higher than previous experimental data, but consistent with resent measured data by Fan Tieshuan[6], the theoretical calculated results are reasonable. Figs.10 and 11 illustrate all reaction cross sections of ^{185}Re and ^{187}Re, respectively. The energy spectrum, angular distribution, double differential cross section and γ-production data were obtained at incident neutron energies below 20 MeV. Because the calculated results for many channels are in pretty agreement with existing experimental data, the predicted cross sections are reasonable.

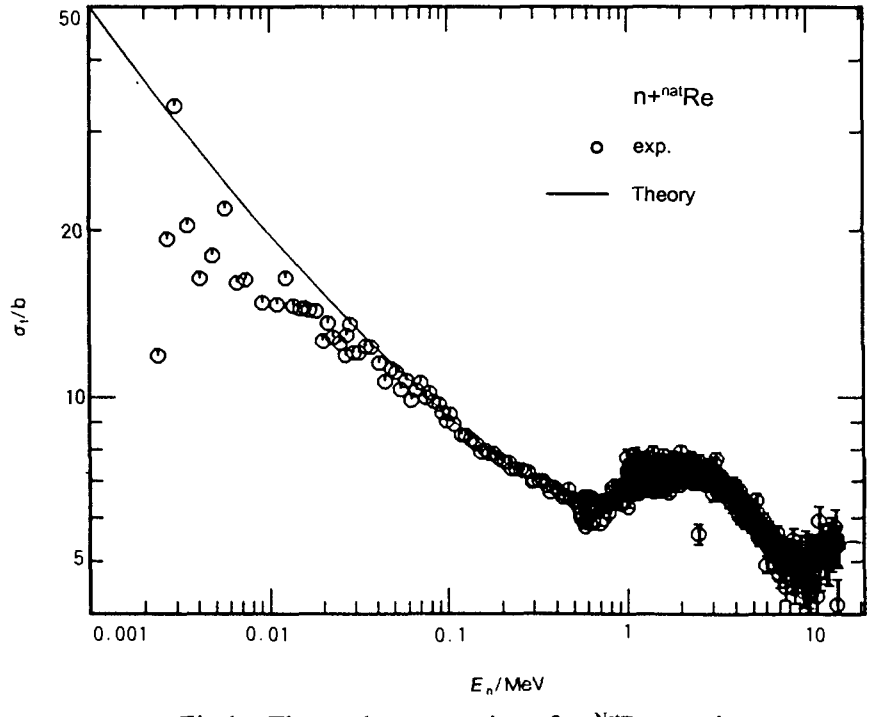

Fig.1 The total cross section of n+^{Nat}Re reaction

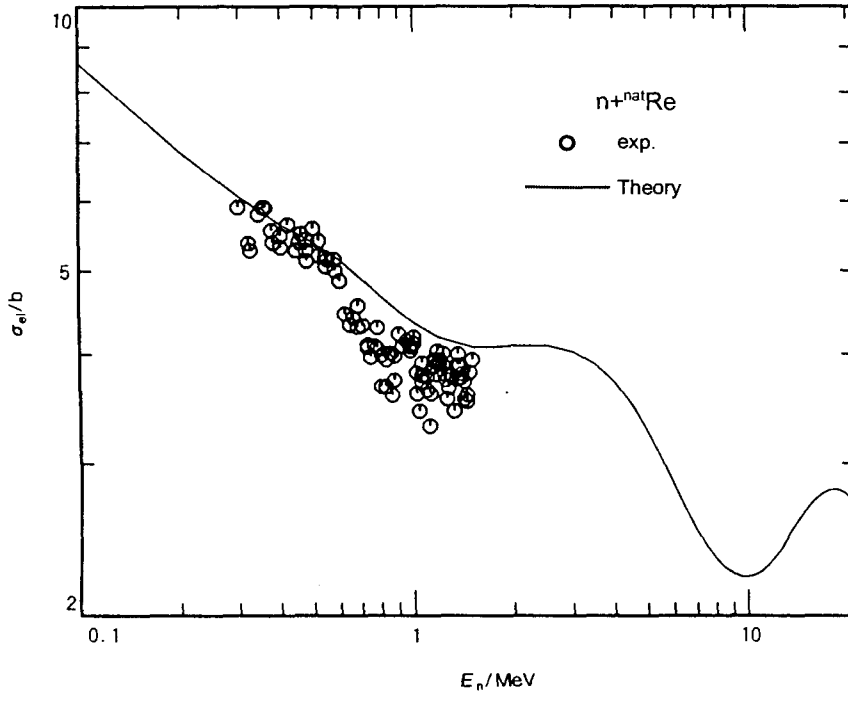

Fig.2 The elastic scattering cross section of n+^{Nat}Re reaction

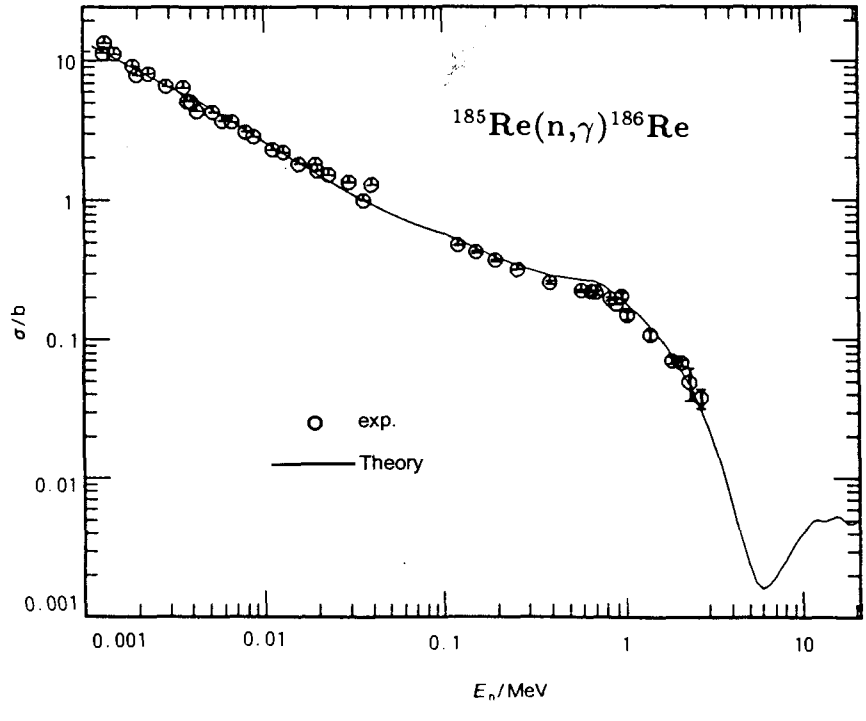

Fig.3 The cross sections of ^{185}Re(n,γ)^{186}Re reaction

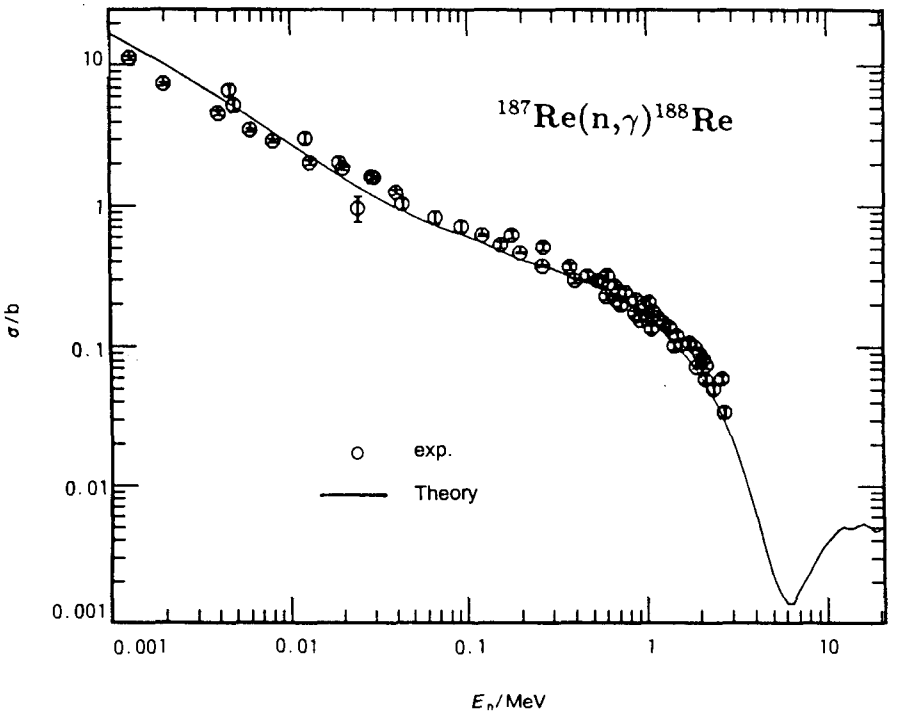

Fig.4 The cross sections of ^{187}Re(n,γ)^{188}Re reaction

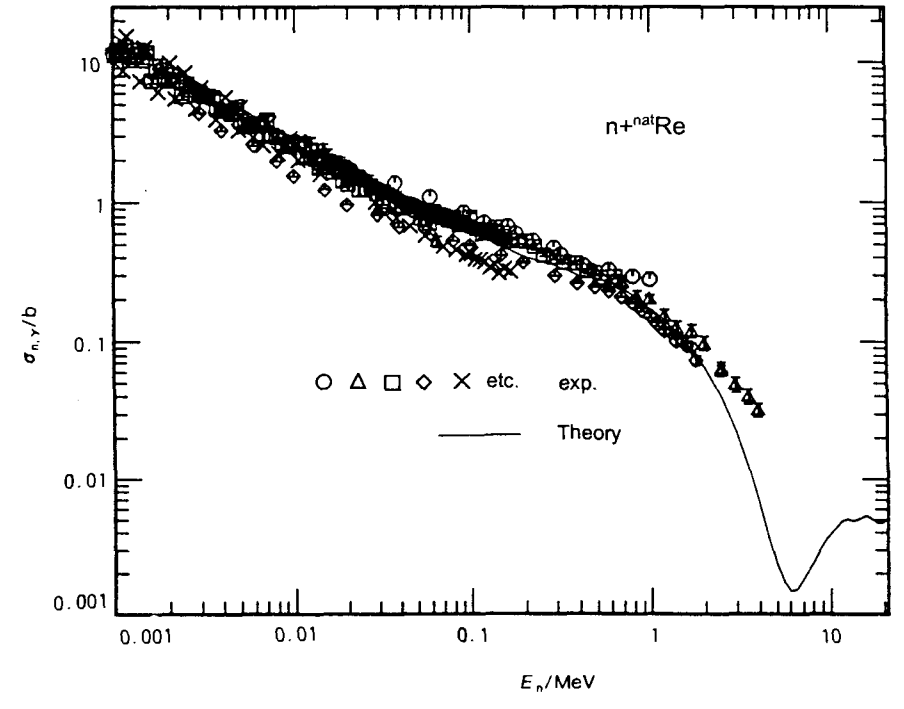

Fig.5 The cross sections of ^{Nat}Re(n,γ) reaction

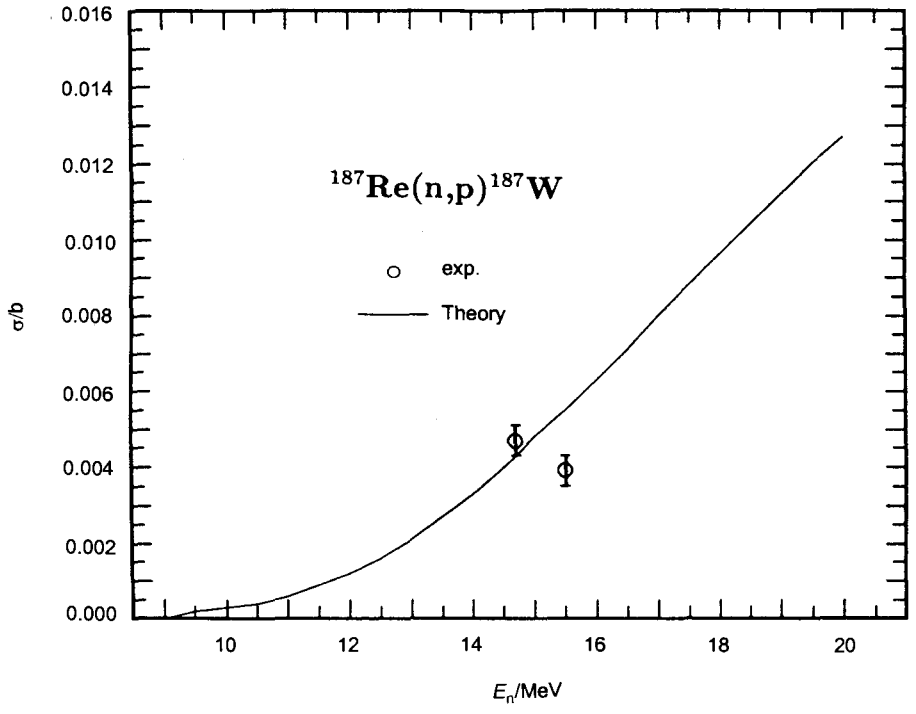

Fig.6 The cross sections of ^{187}Re(n,p)^{187}W reaction

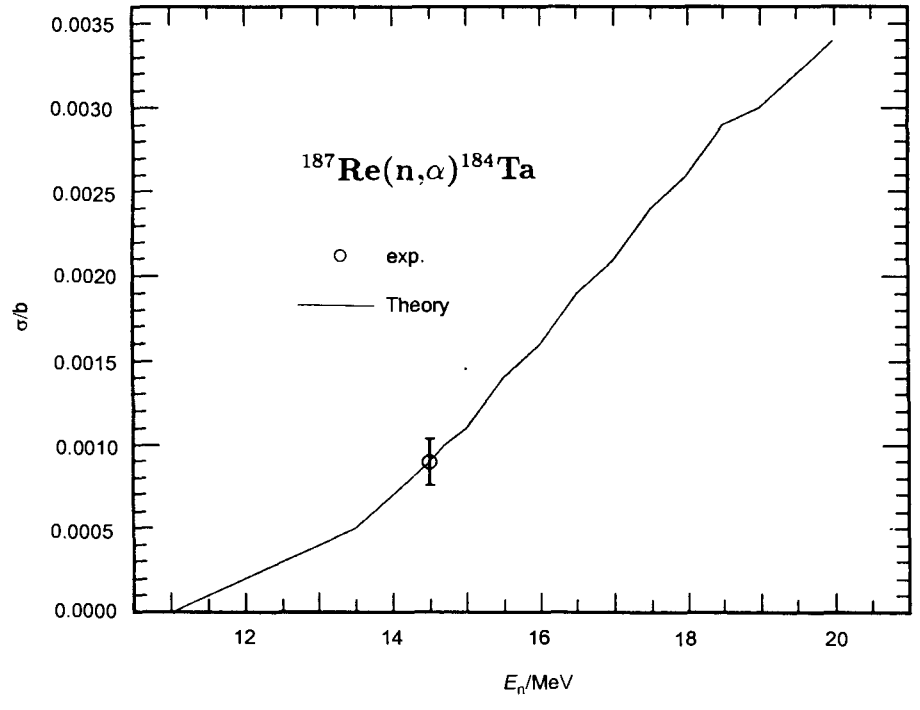

Fig.7 The cross sections of ^{187}Re(n,α)^{184}Ta reaction

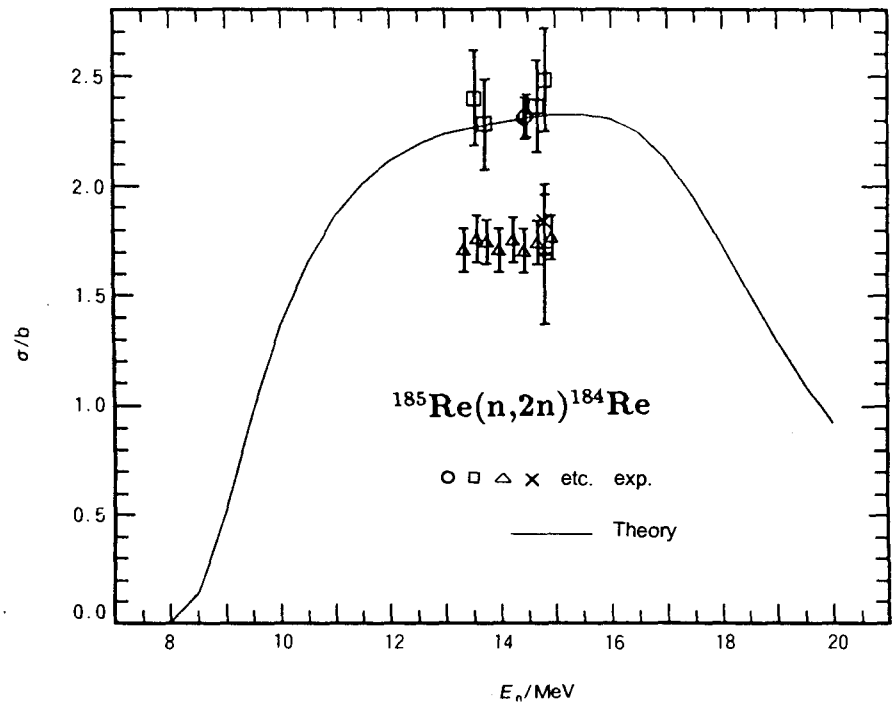

Fig.8 The cross sections of $^{185}Re(n,2n)^{184}Re$ reaction

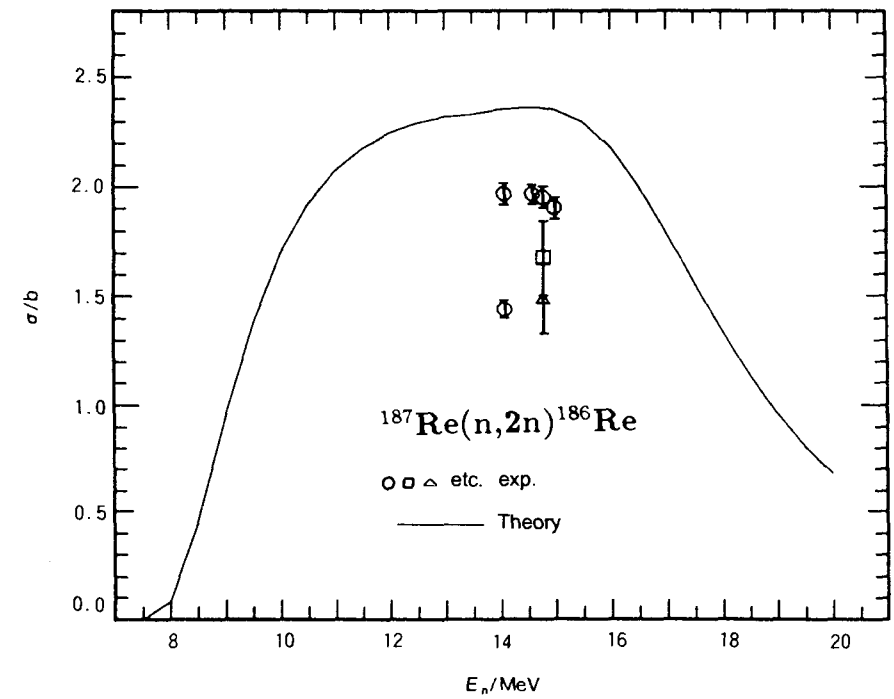

Fig.9 The cross sections of $^{187}Re(n,2n)^{186}Re$ reaction

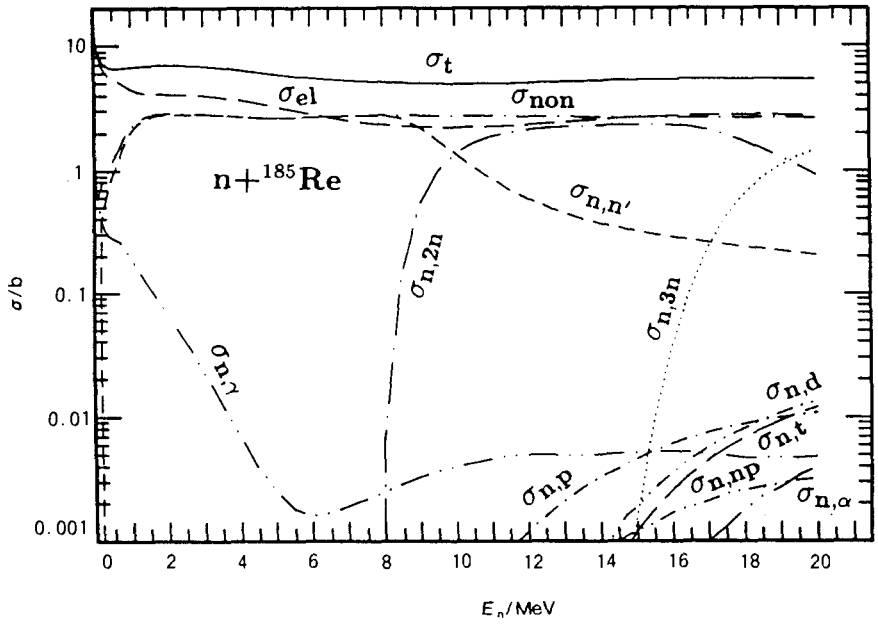

Fig.10 The cross sections of n+^{185}Re reaction

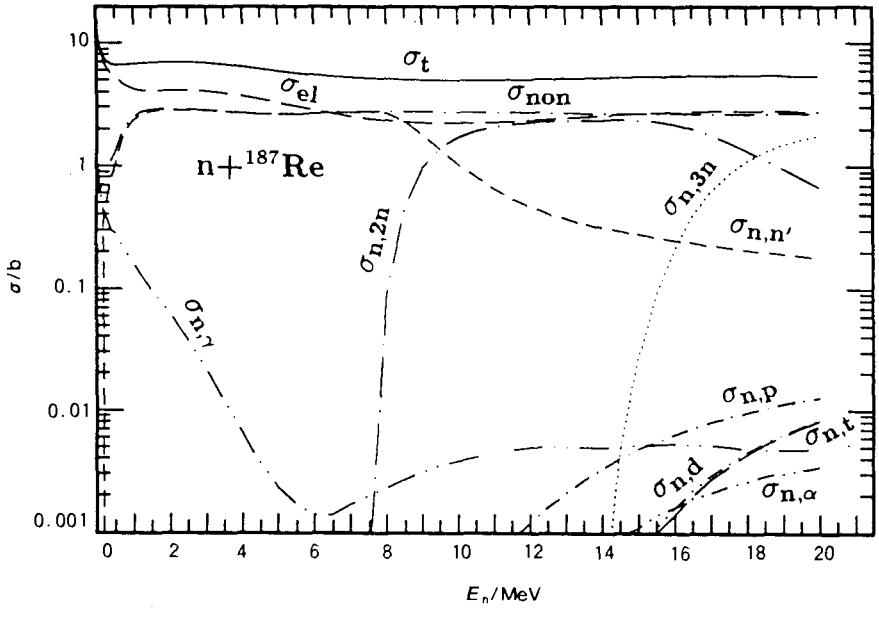

Fig.11 The cross sections of n+^{187}Re reaction

3 Summary

Based on the available experimental data of Re and neighbored nucleus W, we obtained a set of optimum optical potential parameters for $0.001 \leq E_n \leq 20$ MeV. With adjusted proton and alpha particle optical potential parameters, level density and giant dipole resonance parameters as well as K, all the cross sections of neutron induced reaction on ^{185,187,Nat}Re were obtained. Because the calculated results for many channels are in pretty agreement with existing experimental data, the predicted cross sections in energy range where there are no any experimental data are reasonable.

References

[1] Zhang Jingshang, Commu. of Nucl. Data Prog., 7, 14(1992)
[2] Shen Qingbiao, Commu. of Nucl. Data Prog., 7, 43(1992)
[3] P. D. Kunz, "Distorted Wave Code DWUCK4", University of Colorado
[4] W. Dilg, H. Vonach, EANDC(E) – 150, 40, 1972
[5] Wang Xiuyuan, Hao Fanhua, et al., EXFOR-309351, 1989
[6] Fan Tieshuan, Shi Zhaoming, et al., Chin. J. Nucl. Phys. 14, 331(1992)

CN9901231

Calculation of Cross Sections for n+^{63}Cu Reaction

Han Yinlu Yu Baosheng
(China Nuclear Data Center, CIAE)

Abstract

Based on the relevant experimental data, and optical model, evaporation model, $J\pi$-dependent exciton model, and the pick-up mechanism of cluster pre-formation, neutron induced reaction cross sections, the energy spectrum, angular distribution, double differential cross section and γ-production data were calculated for ^{63}Cu at incident neutron energies below 20 MeV. The calculated results were compared with experimental data.

Introduction

Copper is an important structure material in nuclear engineering, the neutron monitor cross sections for bombarding copper are also important. The calculation of cross section for n+^{63}Cu reaction is necessary and interesting.

In Sec.1 the theories and parameters used in the calculation are described. The calculated results and analyses are given in Sec.2. Finally, a summary is given in Sec.3.

1 Theories and Parameters

The calculation was made with the semi-classical theory code UNF[1]. This program consisted of the optical model, the unified Hauser-Feshbach and exiton model. The pre-equilibrium nuclear reaction processes were described with the $J\pi$-dependent exciton model, while the equilibrium processes were described by the Hauser-Feshbach theory with width fluctuation correction. The discrete levels in multi particle emissions for all of open channels were included. For composite particle emissions, the pick-up mechanism of cluster pre-formation was included. The preequilibrium and direct reaction mechanisms of γ emission were also included in this program. The direct inelastic scattering cross sections were obtained by the collective excitation distorted wave Born approximation.

Based on experimental data from EXFOR library and recent information, the code APOM[2], with which the best neutron optical potential parameters can be searched automatically by fitting relevant experimental total, nonelastic scattering cross sections and elastic scattering angular distributions, was used to obtain a set of optimum neutron optical potential parameters of ^{63,65,Nat}Cu as follows:

$$V = 51.4652-0.2687E-0.008952E^2-24(N-Z)/A$$
$$W\mathrm{s} = \max\{0.0,\ 16.4146-0.2305E-12(N-Z)/A\}$$
$$W\mathrm{v} = \max\{0.0,\ -0.9637+0.1994E-0.005988E^2\}$$
$$U\mathrm{so} = 6.2$$
$$r_R = 1.2428, \quad r_S = 1.3732, \quad r_V = 1.5708, \quad r_{SO} = 1.2428$$
$$a_R = 0.7419, \quad a_S = 0.3010, \quad a_V = 0.5596, \quad a_{SO} = 0.7419$$

Using this set of neutron optical potential parameters, adjusting charged particle optical potential parameters and level density parameters, all cross sections of n+^{63}Cu reactions were calculated by the code UNF. The direct inelastic scattering data were calculated by the code DWUCK4[3].

2 Calculated Results and Analyses

The calculated results of neutron total cross sections and nonelastic cross sections for n+^{63}Cu reaction are in good agreement with the experimental data of n+^{Nat}Cu reaction. Fig.1 and 2 show the comparison of the calculated elastic scattering cross sections and angular distributions with experimental data for n+^{63}Cu reaction. The calculated values are in good agreement with experimental data. Based on the above fitting, a set of neutron optical potential parameters in the energy region 0.01 ~ 20 MeV for n+^{63}Cu reactions were determined as shown in Eq.(1).

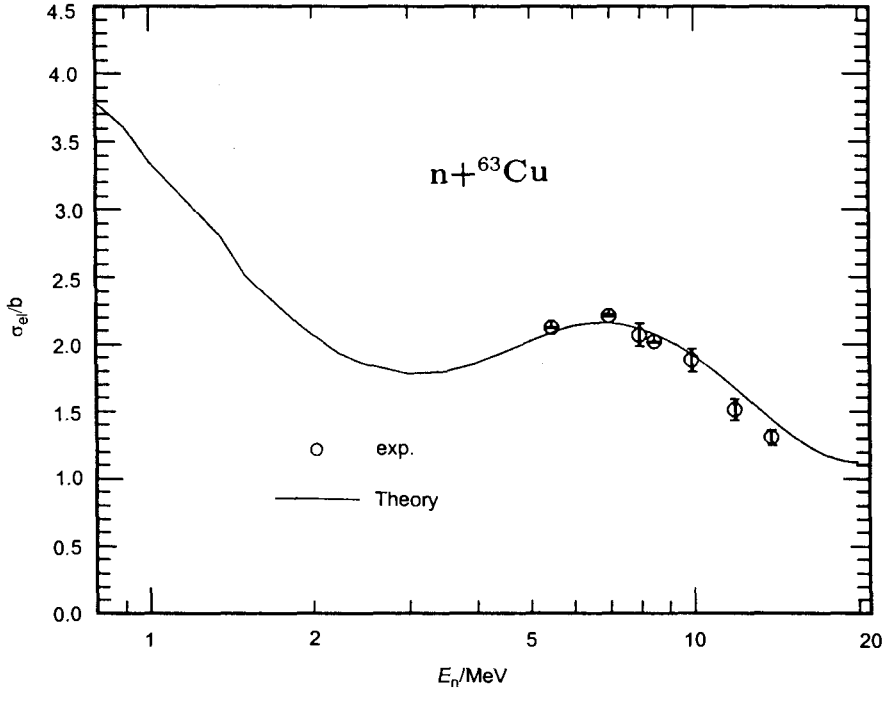

Fig. 1 The elastic scattering cross section of n+^{63}Cu reaction

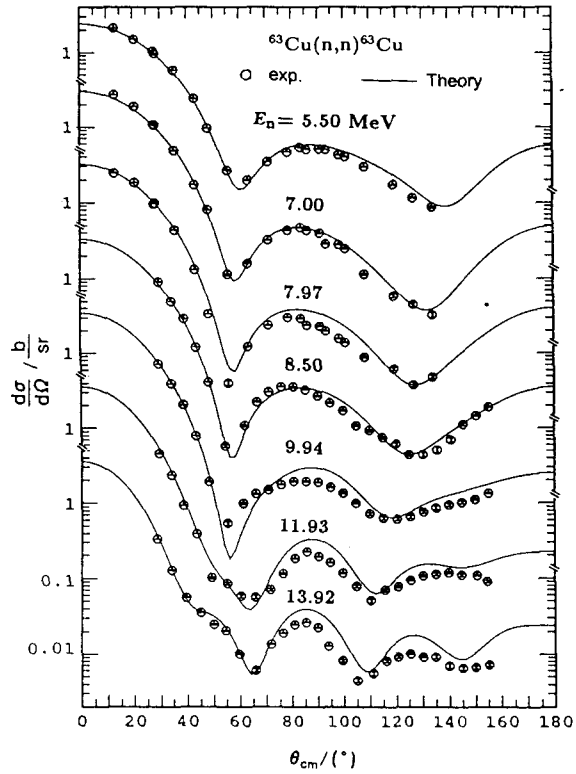

Fig. 2 The elastic scattering angular distribution of n+^{63}Cu reaction

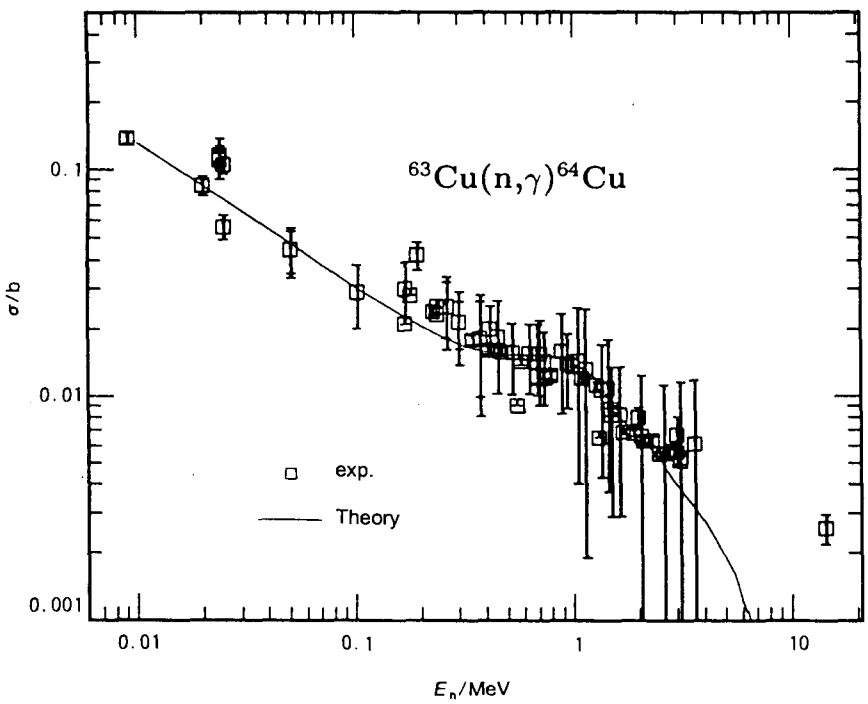

Fig. 3 The cross sections of ^{63}Cu(n,γ)^{64}Cu reaction

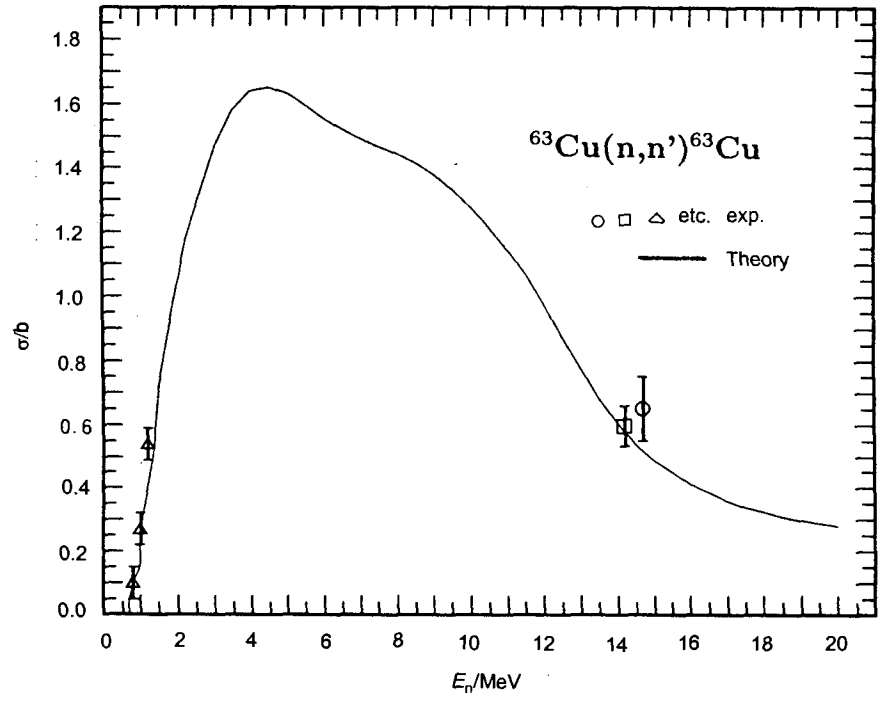

Fig. 4 The cross sections of ^{63}Cu(n,n')^{63}Cu reaction

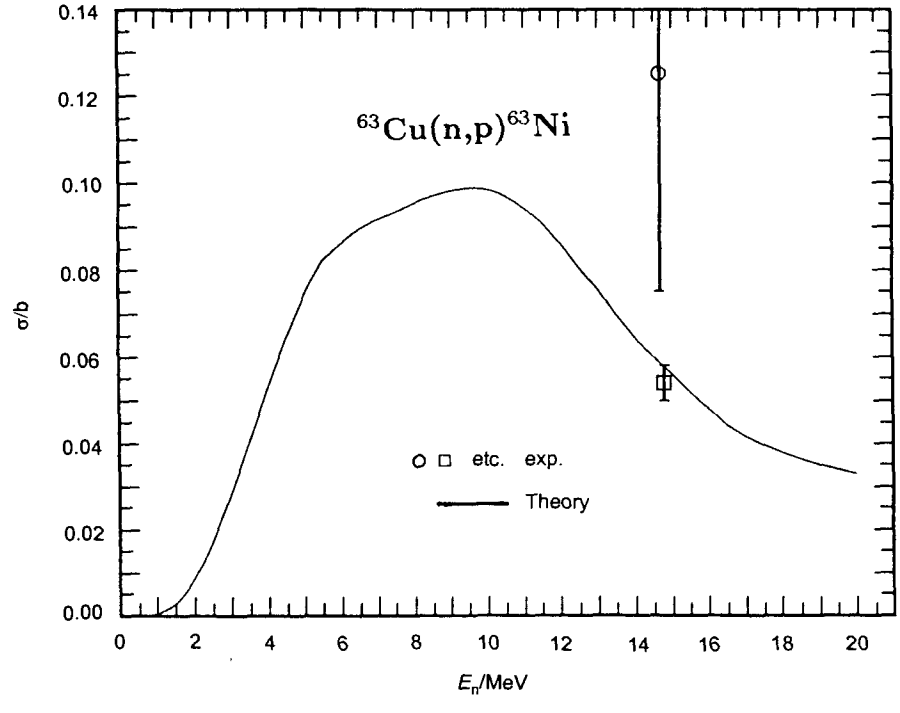

Fig. 5 The cross sections of ^{63}Cu(n,p)^{63}Ni reaction

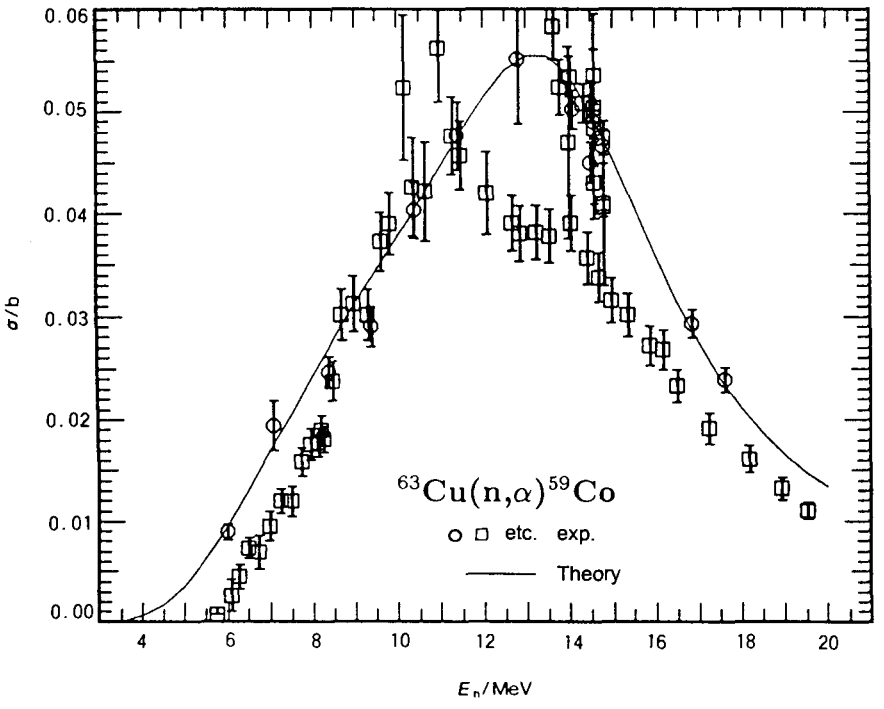

Fig. 6 The cross sections of ^{63}Cu(n,α)^{59}Co reaction

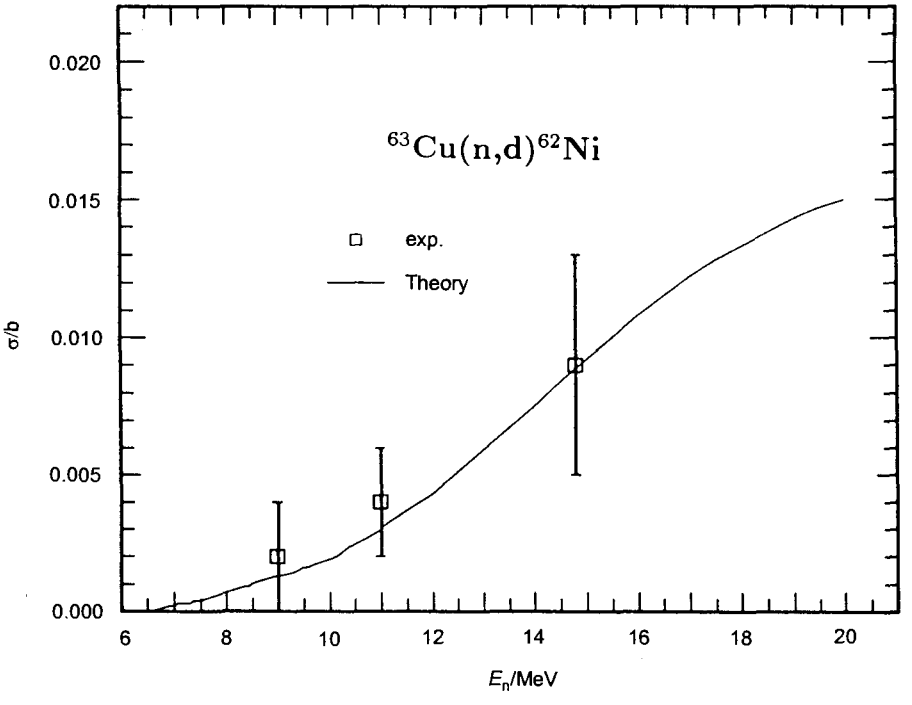

Fig. 7 The cross sections of ^{63}Cu(n,d)^{62}Ni reaction

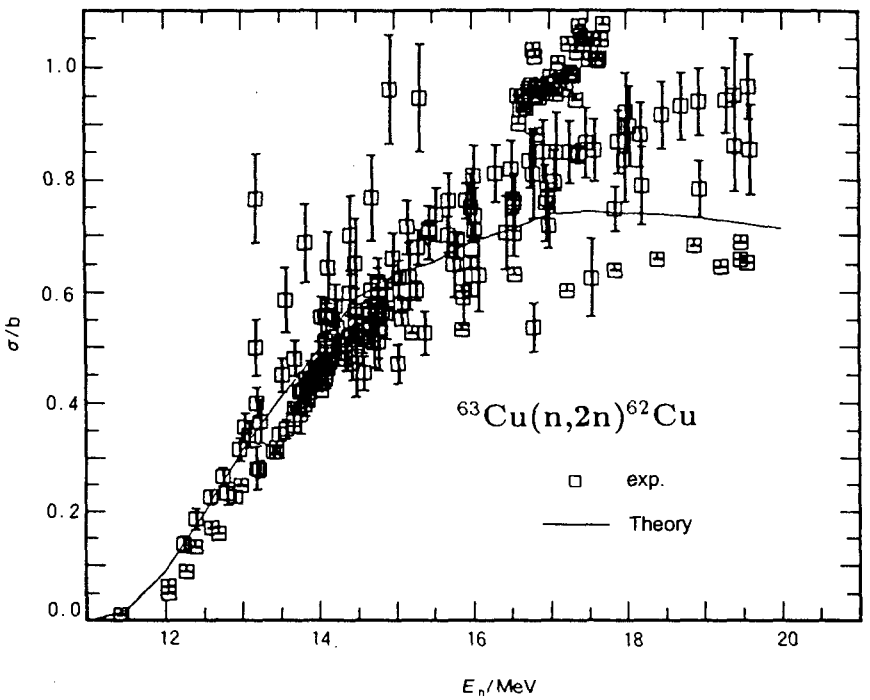

Fig. 8 The cross sections of ^{63}Cu(n,2n)^{62}Cu reaction

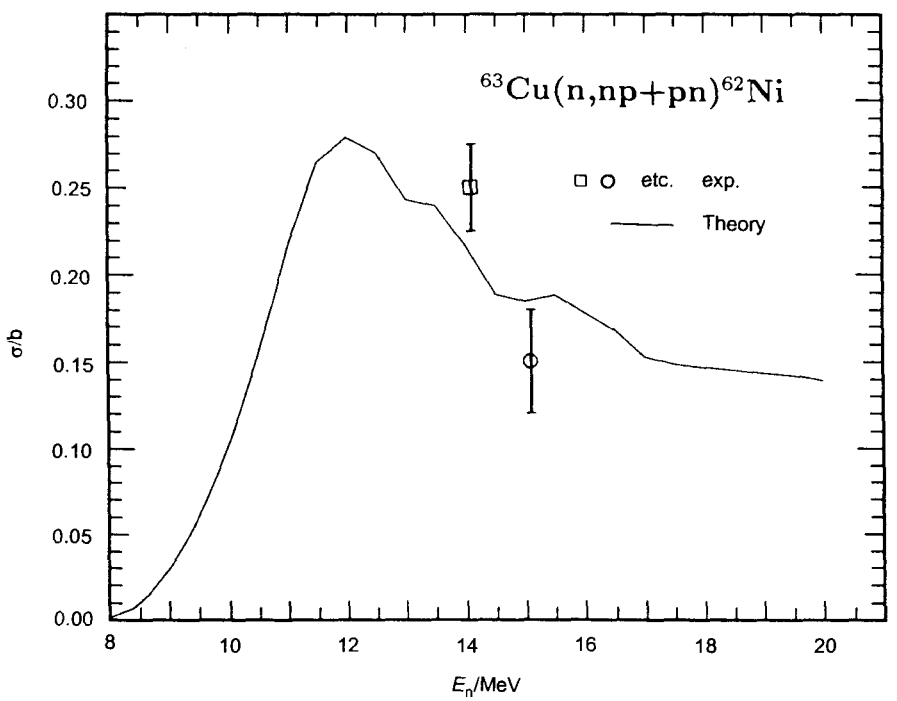

Fig. 9 The cross sections of ^{63}Cu(n,np+pn)^{62}Ni reaction

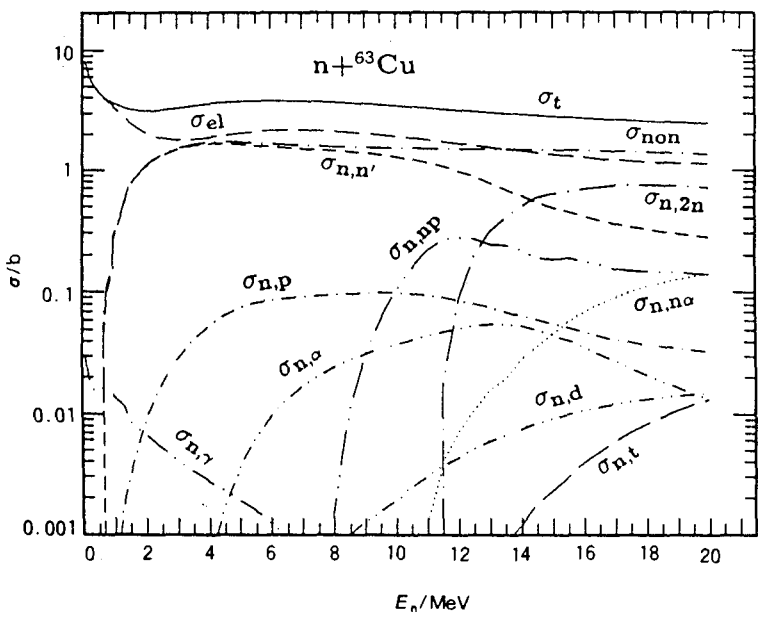

Fig. 10 The cross sections of n+^{63}Cu reaction

The comparison for calculated results and experimental data of ^{63}Cu(n,γ)^{64}Cu reaction cross sections is given in Fig.3. The calculated values are in agreement with experimental data in energy region 0.01 ~ 4 MeV, but for E_n = 14.5 MeV, the calculated value is lower than experimental data. Fig.4 and Fig.5 show the comparison of the calculated results and experimental data of ^{63}Cu(n,n')^{63}Cu[4~6] and ^{63}Cu(n,p)^{63}Ni[7,8] reaction cross sections, respectively. The calculated curves pass through the experimental data within error bars[5~7], at lower energy range and above 14 MeV, respectively. The comparison of calculated and experimental (n,α) reaction cross sections of ^{63}Cu is given in Fig.6. The calculated values fit the experimental data[9] very well. Fig.7 gives the comparison of calculated and experimental ^{63}Cu(n,d)^{62}Ni reaction cross section. The calculated curves pass through the experimental data. Figs.8 and 9 give the comparisons of calculated and experimental (n,2n) and (n,np) reaction cross sections of ^{63}Cu. The calculated results are in agreement with the experimental data. The calculated valves of (n,np) reaction is for (n,np)+(n,pn) reactions. All of the calculated results are consistent with the experimental data. Fig.10 illustrates all reaction cross sections of ^{63}Cu. The energy spectrum, angular distribution, double differential cross section and γ-production data were obtained at incident neutron energies below 20 MeV. Because the calculated results for many channels are in pretty agreement with existing experimental data, the predicted cross sections are reasonable.

3 Summary

Based on the experimental data of total and nonelastic scattering cross sections of ^{Nat}Cu reaction and the experimental data of elastic scattering cross section and angular distributions of $^{63,65,Nat}Cu$ reactions, a set of neutron optical potential parameters for $^{63,64}Cu$ was obtained. Then many nuclear data for $n+^{63}Cu$ reactions were calculated based on optical model, unified model, and the pick-up mechanism of cluster pre-formation. Because the calculated results for many channels are in pretty agreement with existed experimental data, the predicted cross sections in the energy range where there are no any experimental data are reasonable and believable.

References

[1] Zhang Jingshang, Nucl. Sci. Eng., 114, 55(1993)
[2] Shen Qingbiao, Commu. of Nucl. Data Prog., 7, 43(1992)
[3] P. D. Kunz, "Distorted Wave Code DWUCK4", University of Colorado
[4] B.Joensson, K.Nyberg, I.Bergqvist, Arkiv foer Fysik, 39, 295(1969)
[5] Shi Xiamin, Shen Ronglin, et al., Chin. J. Nucl. Phys., 4, 120(1982)
[6] N.P.Glazkov, Atommnaya Energiya, 15, 416(1963)
[7] D.L.Bowers, L.R.Greenwood, J. of Radioanalytical Chemistry, 123, 461(1988)
[8] S.M.Qaim, N.I.Molla, Nucl. Phys., A185, 614(1972)
[9] Lu Hanlin, Zhao Wenrong, et al., Chin. J. Nucl. Phys., 12, 373(1990)

CN9901232

Calculation of Neutron Induced Reactions on $^{105,108}Pd$ in Energy from 0.05 to 20 MeV

Zhang Zhengjun Sun Xiuquan Zhang Jianshu
(Depart. of Physics, Northwest University, Shanxi)

Han Yinlu Shen Qingbiao
(China Nuclear Data Center, CIAE)

Abstract

A set of neutron optical potential parameters for energy from 0.05 to 20 MeV is

obtained on the basis of available experimental data of ^{105,108,Nat}Pd and neighbor nuclei. Based on this set of optical potential parameters, all cross sections of neutron induced reaction on ^{105,108}Pd are calculated. The calculated results reproduce the experimental data well.

Introduction

The cross sections of neutron induced reactions on ^{105,108}Pd are useful for nuclear science and technology, but there are few experimental data of total cross sections, nonelastic cross sections, elastic cross sections and elastic scattering angular distributions, while there are more data on ^{Nat}Pd, with which the neutron optical potential parameters of ^{105,108}Pd can be obtained. A set of neutron optical potential parameters for ^{105,108}Pd and the calculated data of all cross sections and elastic scattering angular distributions of ^{105,108}Pd in the energy region from 0.05 to 20 MeV are presented.

1 Theories and Parameters

The code APOM94[1], DWUCK4[2] and SUNF[3] are used in our calculations. The experimental data are taken from EXFOR library. The nuclear discrete levels are taken from Ref.[4]. The parameters of nuclear levels densities and giant dipole resonance are taken from Ref.[5].

With code APOM94, the best neutron optical potential parameters were searched automatically by fitting experimental total cross sections, nonelastic cross sections and elastic scattering angular distributions. There are few experimental data of above cross sections of ^{105,108}Pd. But there are a lot of experimental data of natural nucleus of Pd. Because the neutron optical potentials are weakly dependent on the mass number, by means the data of ^{Nat}Pd a set of optimum neutron optical potential parameters of ^{105}Pd and ^{108}Pd are obtained as follows:

$$V = 56.02429 - 0.43402E - 0.0038249E^2 - 24.0(N-Z)/A,$$
$$W_S = \max\{0.0,\ 9.0538 + 0.31884E - 12.0(N-Z)/A\},$$
$$W_V = \max\{0.0,\ -1.56148 + 0.21883E - 0.074714E^2\},$$
$$U_{SO} = 6.2,$$

r_r = 1.1737, r_s = 1.38560, r_v = 1.26103, r_{so} = 1.1737,
a_r = 0.73233, a_s = 0.40000, a_v = 0.58002, a_{so} = 0.73233.

The direct inelastic scattering cross sections are calculated by code DWUCK4 on the basis of this set of neutron optical potential parameters, and the adjusted optical potential parameters of ρ, α, ^{3}He, deuteron and triton paticales, as well as level densities and giant dipole resonance parameters as the input data in SUNF code. The exciton model parameter K is taken as 600 MeV[3].

2 Calculation Results and Analyses

Fig.1 shows comparison of neutron total cross section between the calculated results of ^{105,108}Pd and experimental data of reaction on natural nucleus in the energy range from 0.01 to 20 MeV. It indicates that the theoretical values of ^{105}Pd and ^{108}Pd reproduce the experimental data very well. The comparison between calculated values and experimental data of the elastic scattering angular distributions are shown in Fig.2(a) and Fig.2(b). The theoretical values are also in good agreement with the experimental data. In the calculation a set of neutron optical potential parameters of ^{105}Pd by fitting experimental data of ^{Nat}Pd for energy from 0.05 to 20 MeV is

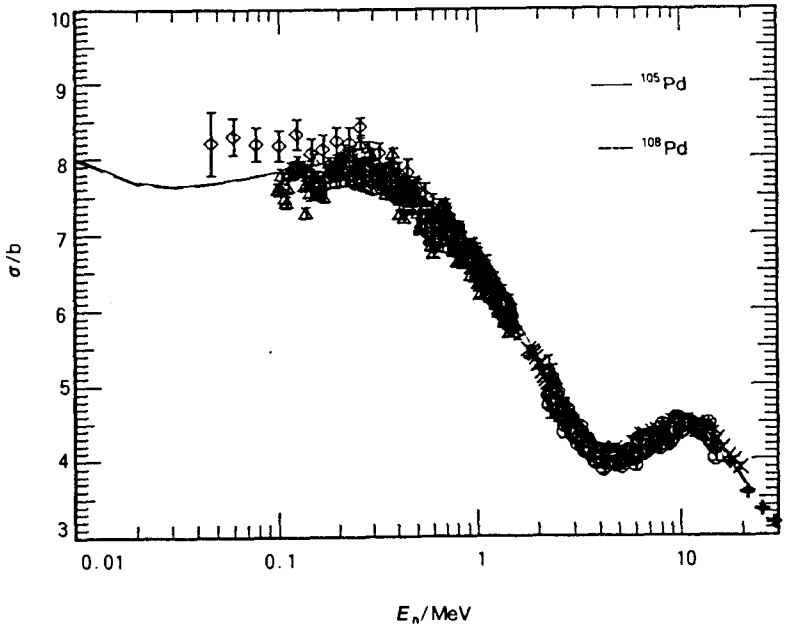

Fig.1 Comparison of neutron total cross sections between the calculated values of ^{105,108}Pd and the experimental data of ^{Nat}Pd

obtained firstly, then this set of neutron optical potential parameters were used in calculation of ^{108}Pd without any adjustment. From Fig.1, Fig.2a and Fig.2b we can see that neutron optical potential parameters are almost independent of mass number in this nuclear region and this energy range and above set of neutron optical potential parameters are reasonable for ^{105}Pd and ^{108}Pd. Fig.3 and Fig.4 show comparison of ^{105,108}Pd(n,γ) cross section between calculated results and experimental data. The calculated values of ^{105}Pd(n,γ) reproduce experimental data very well. The calculated values of ^{108}Pd(n,γ) are in good agreement with experimental data of references[6~8]. Because discrete levels of ^{108}Pd are wide, the calculated curve is not smooth. In Fig.5 and Fig.6 the calculated curves of ^{105,108}Pd(n,p) and experimental data are given. From Fig.7 we can see calculated values of ^{108}Pd(n,α) are agreement with experiment data. Lack of experimental data, in the calculation of ^{105,108}Pd(n,2n) reaction cross sections, the cross sections of ^{102,110}Pd(n,2n) reaction were referenced. Fig.8 illustrates all cross section of ^{105}Pd. Fig.9 shows all cross sections of ^{108}Pd.

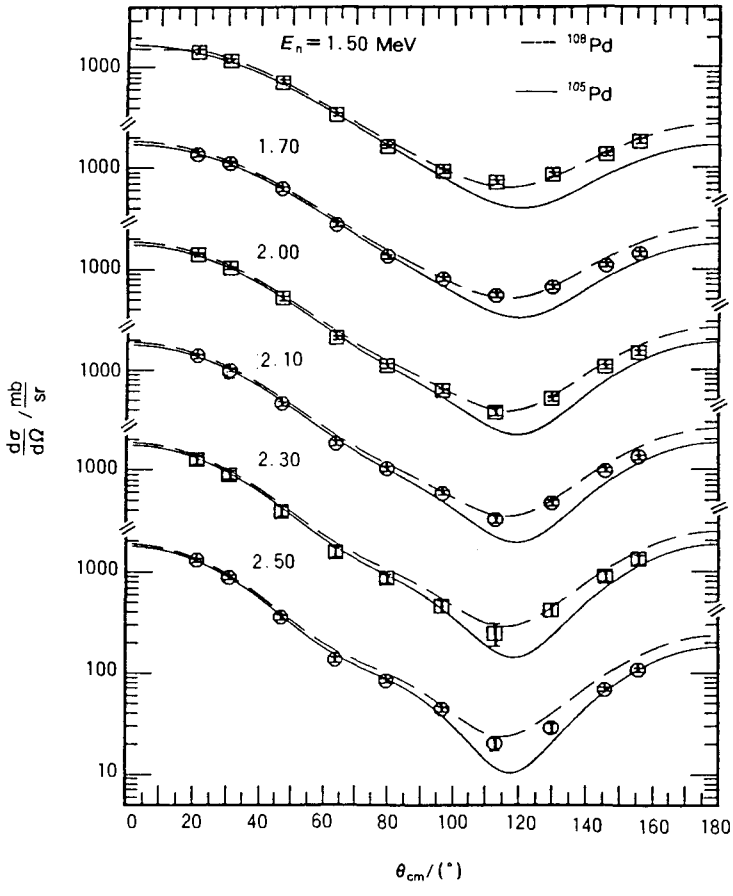

(a)

Fig.2 Comparison of neutron elastic scattering angular distribution between the calculated values and the experimental data of ^{Nat}Pd

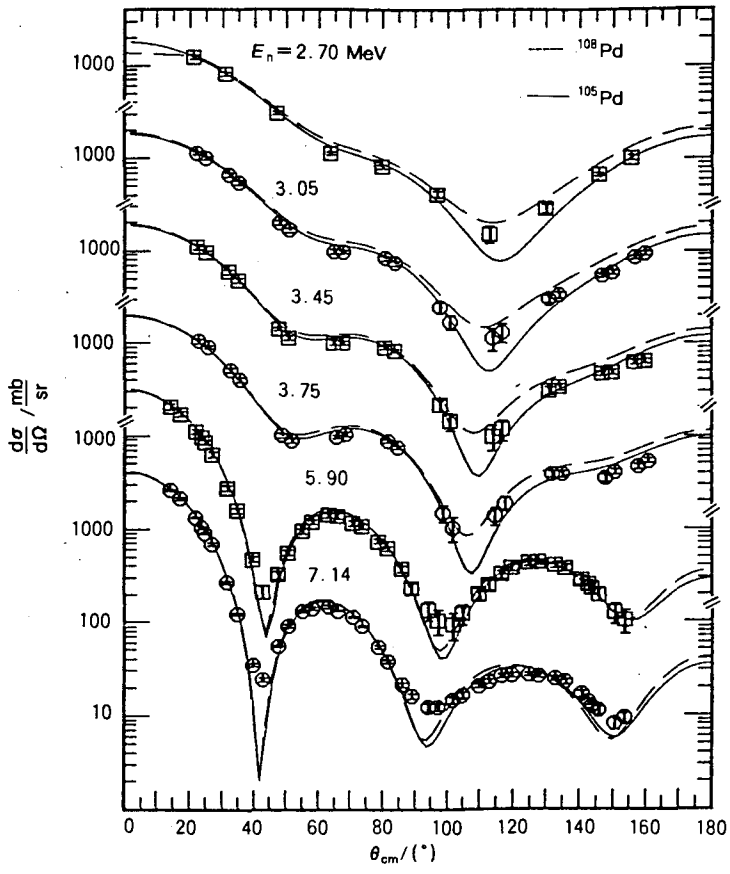

(b)

Fig.2 Comparison of neutron elastic scattering angular distribution between the calculated values and the experimental data of ^{Nat}Pd

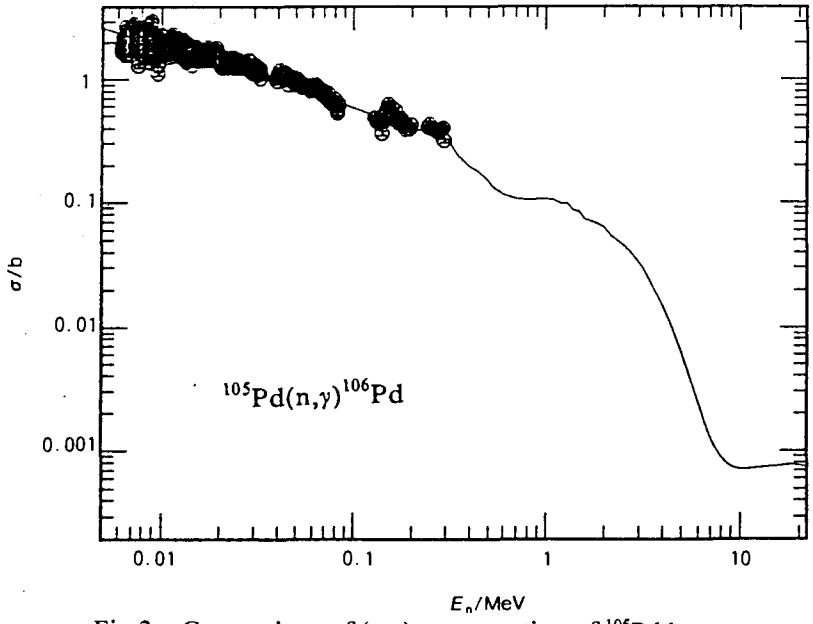

Fig.3 Comparison of (n,γ) cross section of ^{105}Pd between the calculated values and the experimental data

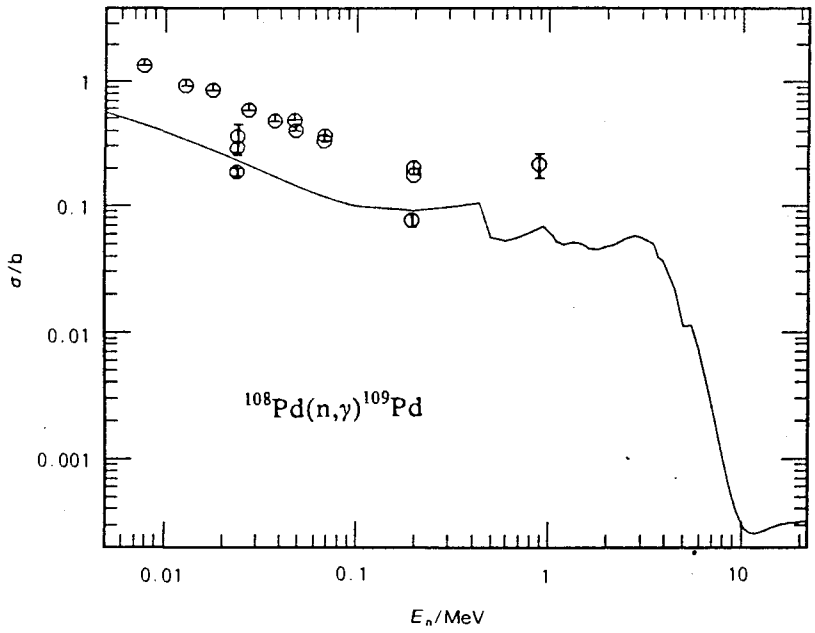

Fig.4 Comparison of (n,γ) cross section of ^{108}Pd between the calculated values and the experimental data

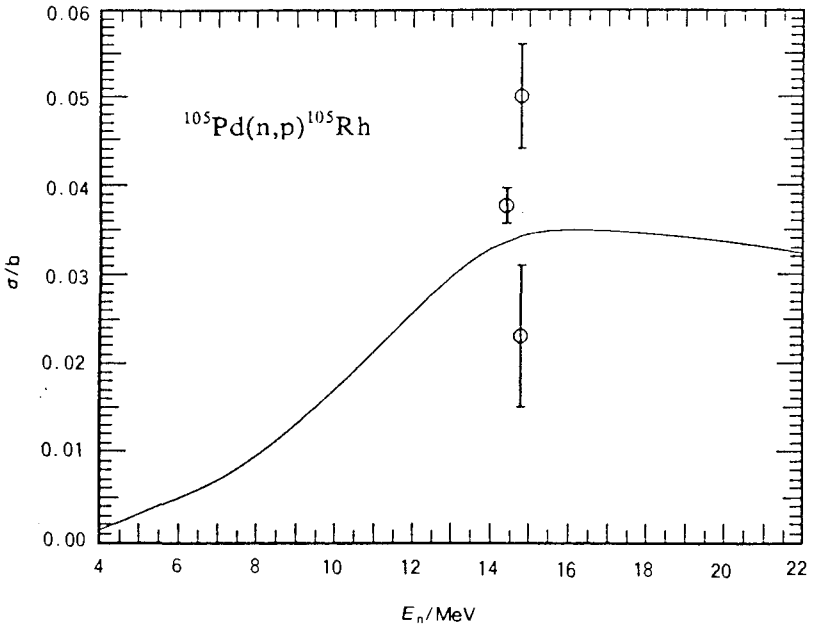

Fig.5 Comparison of (n,p) cross section of ^{105}Pd between the calculated values and the experimental data

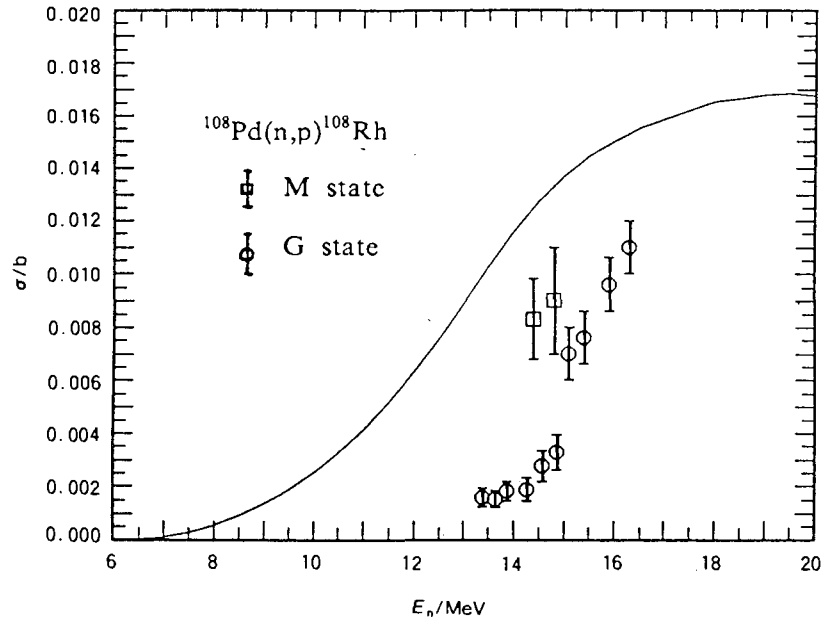

Fig.6 Comparison of (n,p) cross section of ^{108}Pd between the calculated values and the experimental data

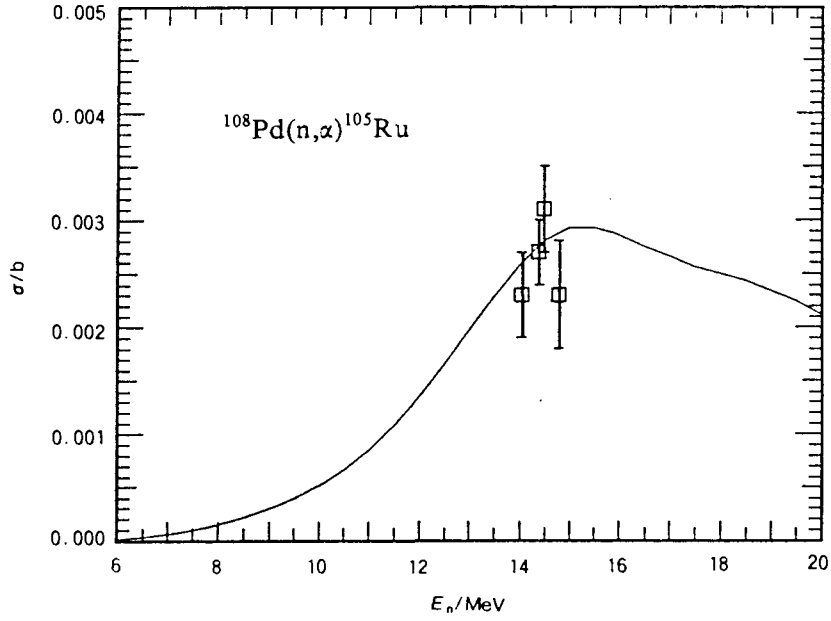

Fig.7 Comparison of (n,α) cross section of ^{108}Pd between the calculated values and the experimental data

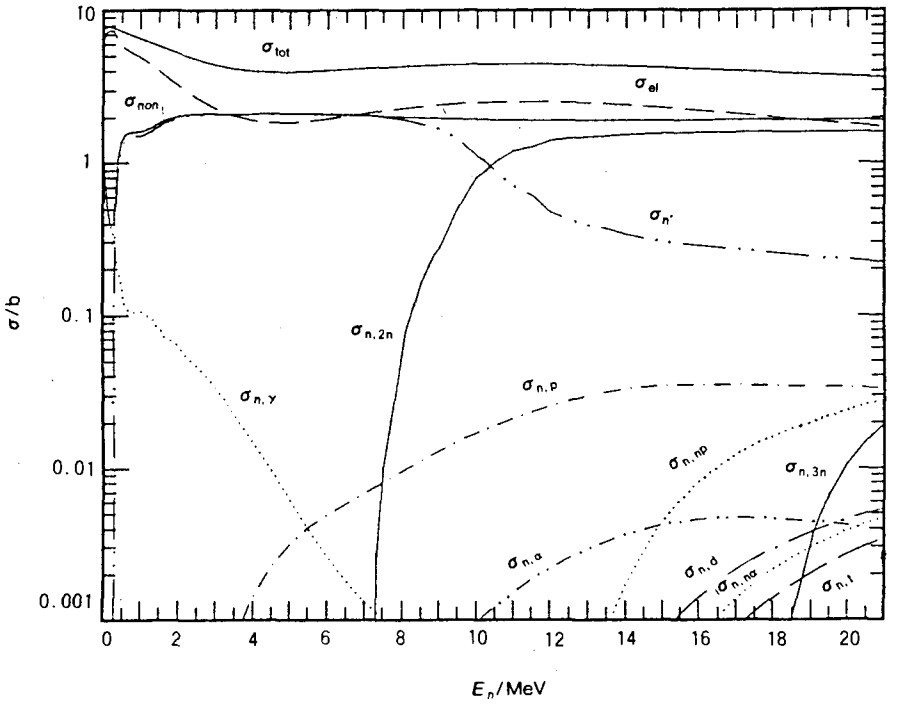

Fig.8 The calculated cross section of n+^{105}Pd reaction

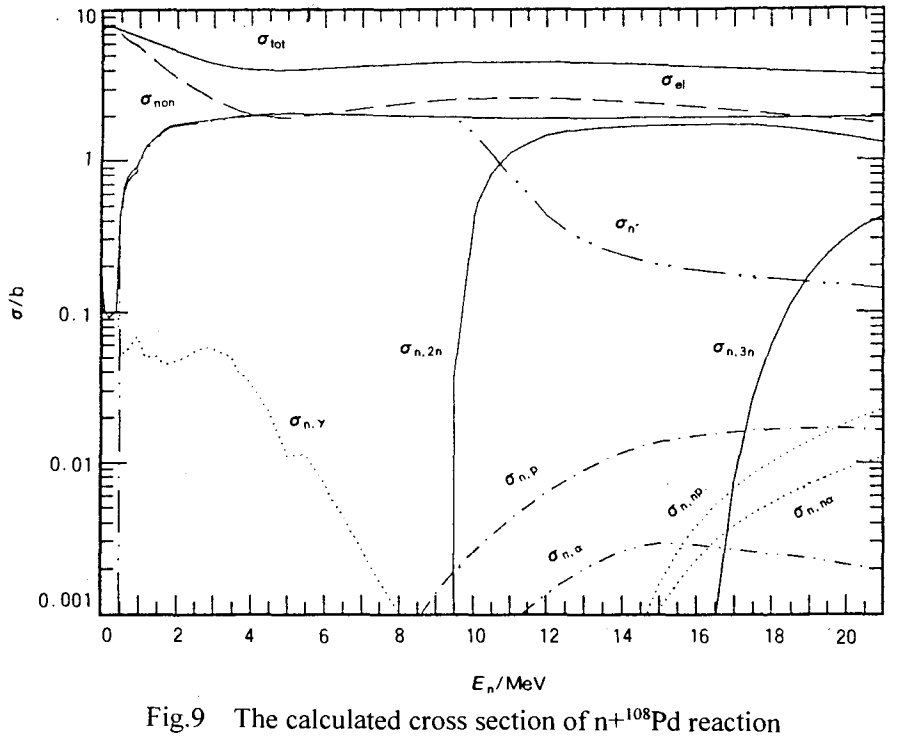

Fig.9 The calculated cross section of n+^{108}Pd reaction

3 Summary

Based on the available experimental data of ^{Nat}Pd and using the code APOM94, a set of optimum neutron optical potential parameters for ^{105}Pd and ^{108}Pd in the energy range from 0.05 to 20 MeV are obtained. Using the code DWUCK4 and SUNF and through adjusting proton, alpha, deuteron, triton charged particle optical potential parameters, level densities and giant dipole resonance parameters the various cross sections of neutron induced reactions are obtained. The calculated values basically agree with the experimental data.

References

[1] Shen Qingbiao, Commun. Nucl. Data Progress, 7, 43(1992)
[2] P. D. Kunz, "Distorted Wave Code DWUCK4", University of Colorado
[3] Zhang Jingshang, Commun. Nucl. Data Progress, 17, 18(1997)
[4] Su Zongdi et al., Commun. Nucl. Data Progress, 12, 83(1994)
[5] Su Zongdi et al., Chin. J. Nucl. Phys., 8, 149(1986); INC(CPR)-2, 1986
[6] R. L. Macklin et al., Nucl. Sci. Eng., 78, 110(1981)
[7] E. Cornelis et al., INDC(EUR)-15, p18, 1982
[8] M. Herman et al., Nucl. Phys., A35

CN9901233

III DATA EVALUATION

Evaluation of Complete Neutron Nuclear Data for ^{58,60,61,62,64,Nat}Ni

Ma Gonggui Wang Shiming
(Institute of Nuclear Science and Technology, Sichuan University, Chengdu 610064)

Introduction

Ni is a very important structure material in nuclear fusion engineering. The natural nickel consists of five stable isotopes. The neutron nuclear data were evaluated for ^{58,60,61,62,64,Nat}Ni in the energy range 10^{-5} eV to 20 MeV. The data includes total, elastic, non-elastic, total inelastic, inelastic cross sections to 33 discrete levels, inelastic continuum, (n,2n), (n,3n), (n,n'α)+(n,αn'), (n,n'p)+(n,pn'), (n,p), (n,d), (n,t), (n,α), (n,2p) and capture cross sections. The angular distributions of secondary neutron, the double differential cross sections (DDCS), the gamma-ray production data and the resonance parameters are also included. The evaluation is based on both experimental data measured up to 1995 and calculated data with program UNF. The evaluated data will be adopted into CENDL-3 in ENDF/B-6 format.

The level scheme is given in Table 1, selected from Ref.[1] new data. The binding energy of emitted the final particle are given in Table 2.

Table 1 Discrete levels of Ni isotopes (Abundance %)

^{58}Ni (68.077)		^{60}Ni (26.223)		^{61}Ni (1.14)		^{62}Ni (3.634)		^{64}Ni (0.926)	
E_l	J^π	E_l	J^π	E_l	J^π	E_l	J^π	E_l	J^π
0.0	0^+	0.0	0^+	0.0	$3/2^-$	0.0	0^+	0.0	0^+
1.4545	2^+	1.3325	2^+	0.0674	$5/2^-$	1.1729	2^+	1.3458	2^+
2.4591	4^+	2.1586	2^+	0.2830	$1/2^-$	2.0486	0^+	2.2772	2^+
2.7755	2^+	2.2849	0^+	0.6560	$1/2^-$	2.3018	2^+		
2.9018	1^+	2.5058	4^+	0.9086	$5/2^-$	2.3364	4^+		
2.9424	0^+	2.6261	3^+	1.0152	$7/2^-$	2.8912	0^+		
3.0376	2^+	3.1197	4^+	1.996	$3/2^-$	3.0585	2^+		
3.2634	2^+	3.1240	2^+			3.1580	2^+		
3.4203	3^+	3.1860	3^+						
3.5240	4^+	3.1940	1^+						

Table 2 Binding energy of emitted final particle for ^{58,60}Ni (MeV) reaction channels

	n,γ	n,n'	n,p	n,α	n,^{3}He	n,d	n,t
	n,2n	n,np	n,n α	n,pn	n,2p	n,αn	n,3n
^{58}Ni	0.0	8.9992	8.6045	6.1091	15.4849	14.9518	20.0716
	12.2030	8.1772	6.4082	8.5718	6.9525	9.2983	10.2672
^{60}Ni	0.0	7.8195	9.8606	6.4681	17.0036	15.1275	19.3301
	11.3882	9.5233	6.2948	7.4915	8.2757	7.6461	8.9992

1 Resonance Parameter

The resolved resonance parameters were given from 1.0^{-5} eV to 812 keV (to 812 keV for ^{58}Ni; to 450 keV for ^{60}Ni; to 70 keV for ^{61}Ni; to 600 keV for ^{62,64}Ni) based on ENDF/B-6 data, and supplemented by new data of Perey, Brusegan and Corvi for ^{58}Ni and ^{60}Ni, respectively.

2 Neutron Cross Section

The nuclear data of natural Ni for all reactions were obtained from summing the isotopic data weighted by the abundance. The comparison of experimental data with evaluated ones is shown in Fig.1 ~ 6. It can be seen that the present evaluation is in agreement with the experimental data.

2.1 Total Cross Section

Above the resolved resonance region, there are still some small structure in the energy range 812 keV ~ 6.0 MeV and become smooth in the energy range 6.0 ~ 20 MeV. The experimental data were taken from Larson, Perey, Smith and Koester[5~8]. In the energy range from 812 keV to 6.0 MeV, the data were mainly taken from Larson's corresponding experimental data. In the smooth energy range from 6.0 MeV to 20 MeV, they were fitted with spline function the experimental data for ^{Nat}Ni. The experimental data were taken from Perey, Budtz and Fedorov. In the energy range from 812 keV to 20 MeV for ^{58}Ni, from Harvey, Perey, Pedorov, Smith, Boschung and Stoler. In the energy range from 450 keV to 20 MeV for ^{60}Ni. Du to there are very few experimental data, total cross section of natural nickel was taken for ^{61,62,64}Ni.

2.2 Elastic Scattering Cross Section

Above the resolved resonance region, the elastic scattering cross section was obtained by subtracting the sum of cross sections of all non-elastic processes from the total cross section. In general, the agreement between the calculated cross section and the available experimental data of Li, Smith, Kinney, Guenther, Holmqvist, Korzh, Pasechnik, Ferrer, Bauer, Kazakova, Clarke, Hansen and Kammerdiener is good.

2.3 Non-Elastic Scattering Cross Section

Below 14.2 MeV, the non-elastic cross section was based on the experimental data of Beyster, Taylor, Pasechnik, MacGregor, Abromov, Machwe, Strizhak, Holmqvist and Poze for ^{Nat}Ni, most of which were measured by using sphere transmission method. Above 14.2 MeV, the model calculated result was used, and normalized to the experimental data 1.31 b at 14 MeV. A plot of these data and the evaluated data is shown in Fig.1.

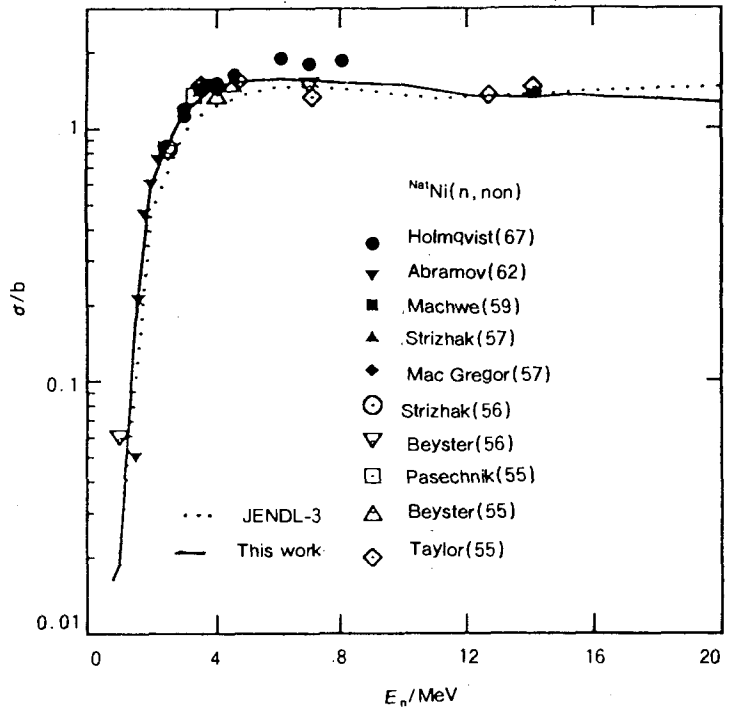

Fig.1 Non-elastic cross section for ^{Nat}Ni

2.4 Total Inelastic Cross Section

The total inelastic cross section of ^{Nat}Ni was obtained from summing the isotopic data weighted by the abundance (see Fig.2).

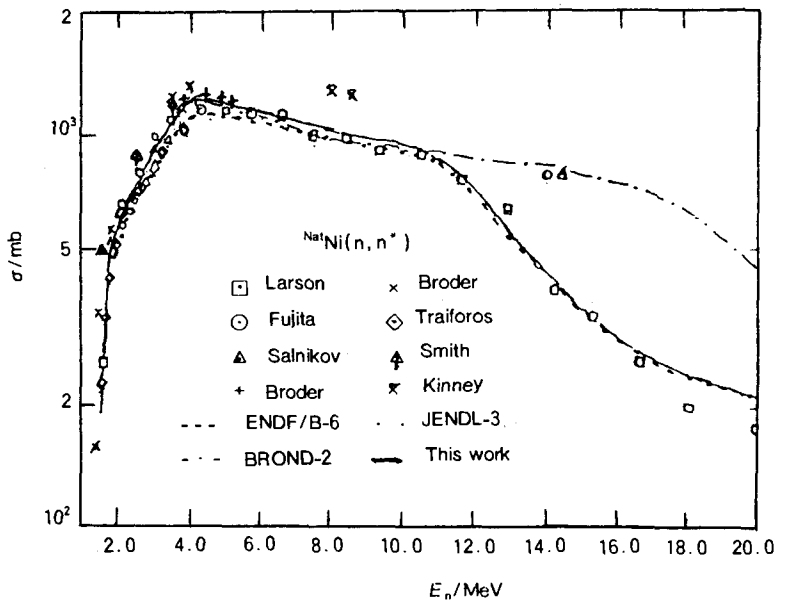

Fig.2 Total inelastic cross section for Ni

2.5 Inelastic Cross Section to the Discrete Levels and the Continuum

The inelastic scattering cross sections to 33 discrete levels were calculated by using UNF code. For 1.3325 and 1.4545 MeV levels, the data were obtained by fitting experimental data measured by Itagaki, Traiforos, Guss, Budtz, Smith, Almen, Kinney, Boschung, Rodgers, Border and Towle. For 1.1729, 2.1586, 2.2849, 2.3018, 2.4591, 2.5058, 2.6261, 2.7755, 2.9018, 2.9424, 3.0376, 3.2634 and 3.4203 MeV levels, the calculated data were normalized to the corresponding experimental value. For others, the data were taken from calculated results (see Fig.3).

The continuum part was obtained by subtracting the cross section of inelastic scattering to discrete levels from the total inelastic.

2.6 (n,2n) Cross Section

The (n,2n) cross section of ^{Nat}Ni was obtained from summing the isotopic data weighted by the abundance (Fig.4; Ref. [2]).

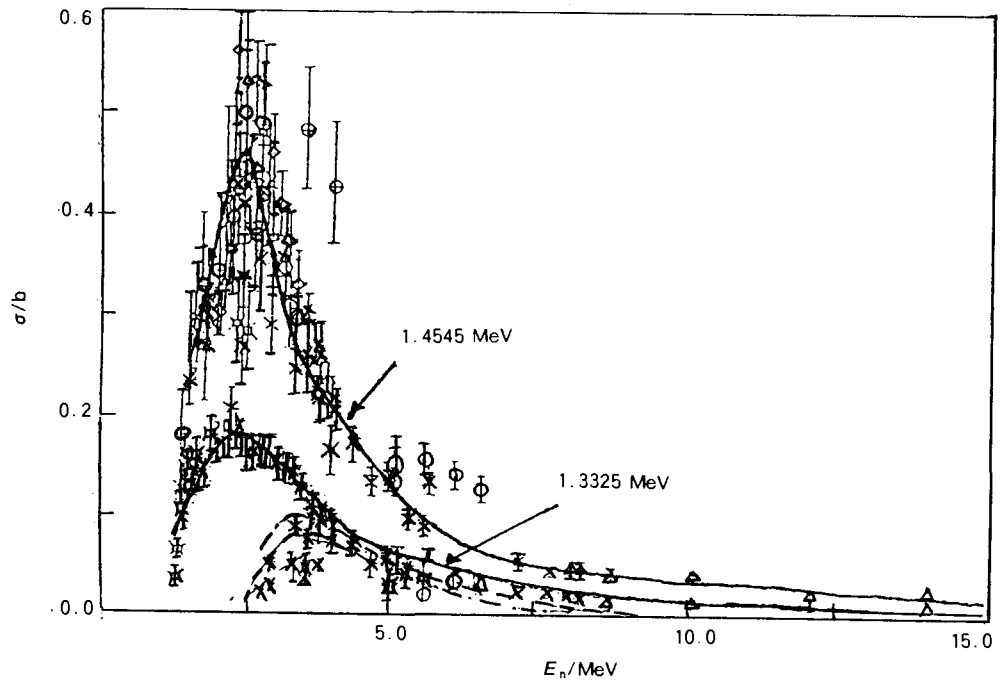

Fig.3 Inelastic cross section of Ni excited states

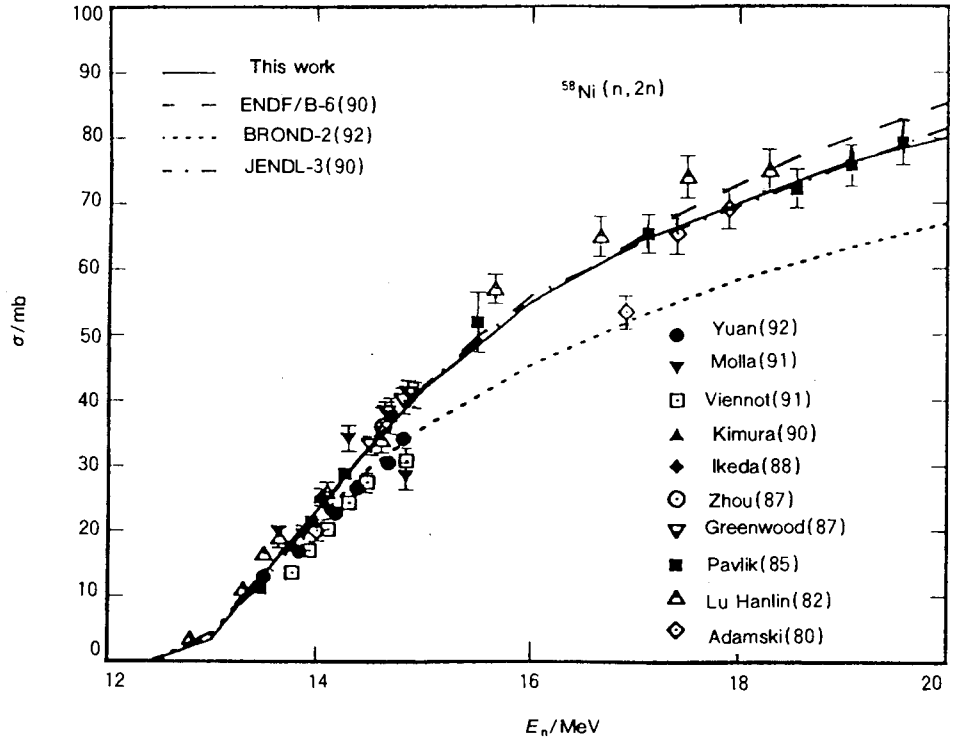

Fig.4 (n,2n) cross section for ^{58}Ni

2.7 (n,p) Cross Section

The (n,p) cross section of ^{Nat}Ni was obtained from summing the isotopic data weighted by the abundance (Fig.5 ~ 8, Ref. [3]).

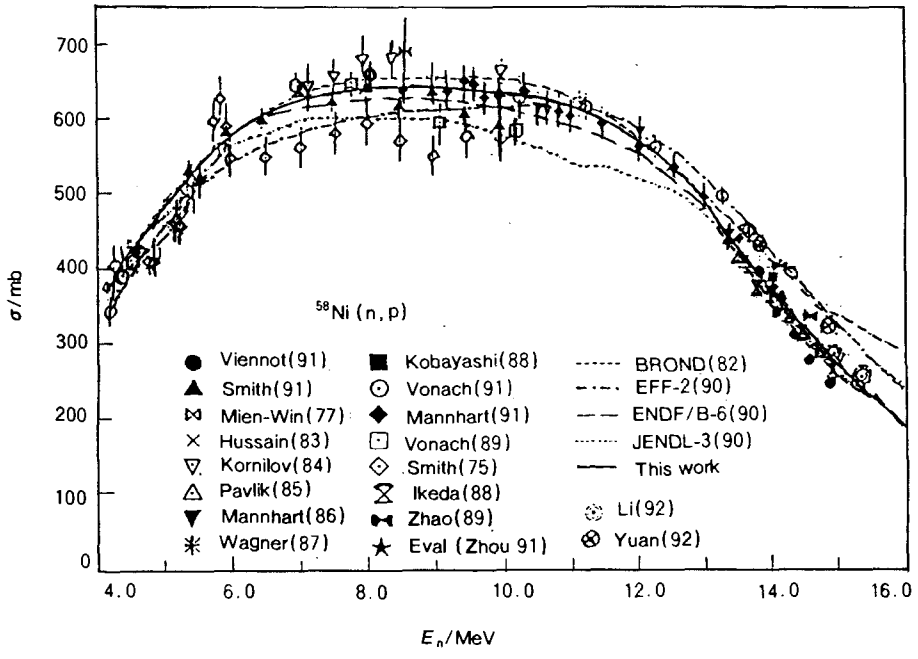

Fig.5 (n,p) cross section for ^{58}Ni

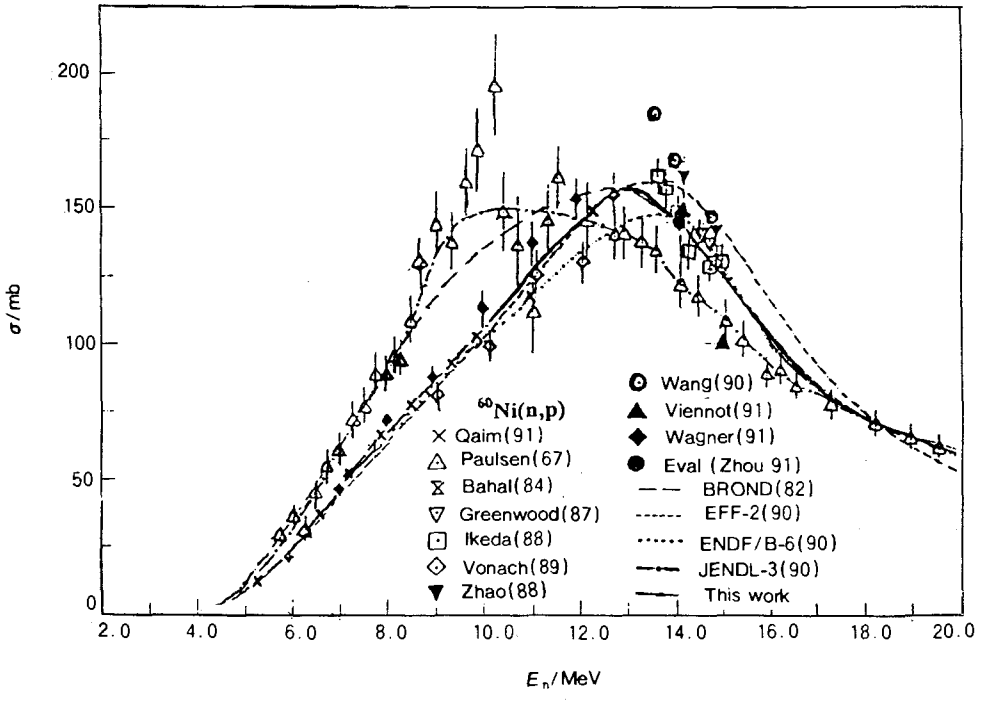

Fig.6 (n,p) cross section for ^{60}Ni

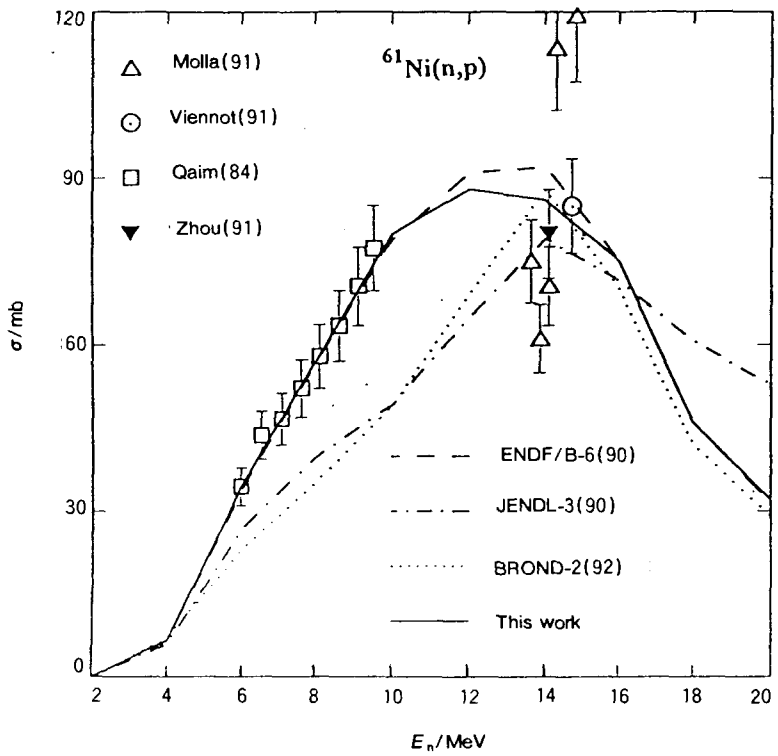

Fig.7 (n,p) cross section for ^{61}Ni

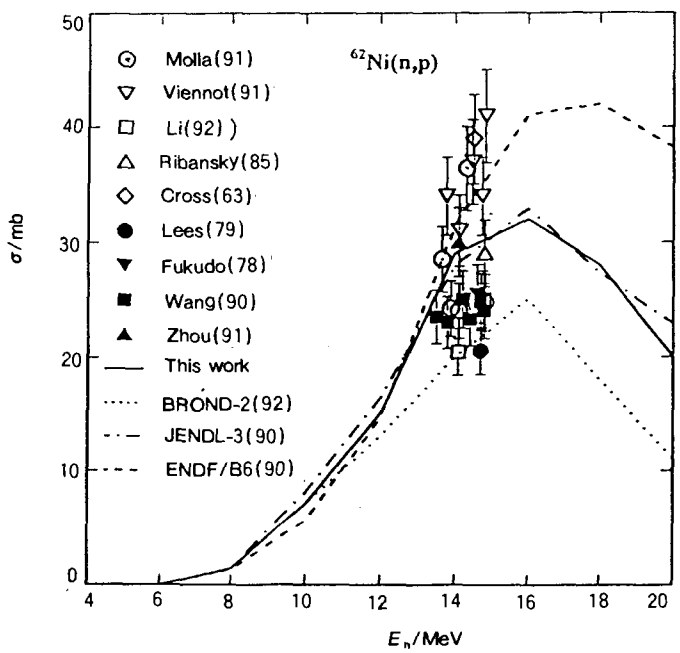

Fig.8 (n,p) cross section for ^{62}Ni

2.8 (n,α) Cross Section

The (n,α) cross section of ^{Nat}Ni was obtained from summing the isotopic data weighted by the abundance (see Fig.9, 10, Ref. [4]).

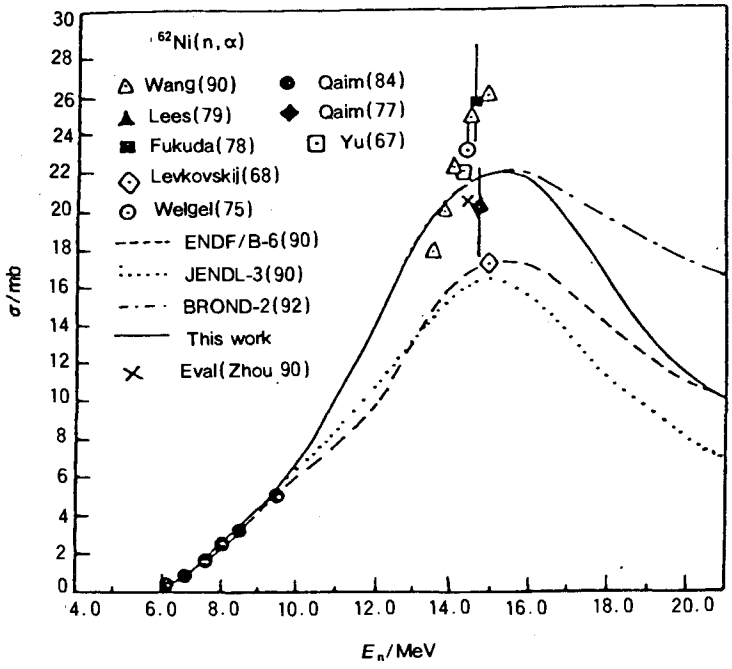

Fig.9 (n,α) cross section for ^{62}Ni

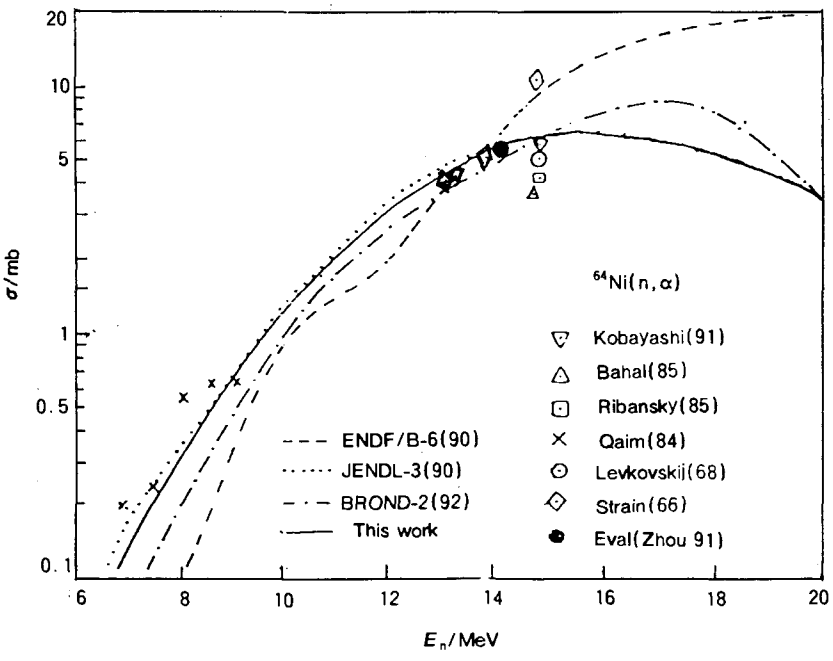

Fig.10 (n,α) cross section for ^{64}Ni

3 Secondary Neutron Angular Distributions

For elastic scattering, the experimental data measured by Qi, Hansen, Smith, Li, Kinney, Guenther, Holmgvist, Korzh, Pasechnik, Ferrer and Clarken were used to adjust the parameters in the calculations with optical model. The calculated results in good agreement with the experimental data and used for recommended data (see Fig.11, 12).

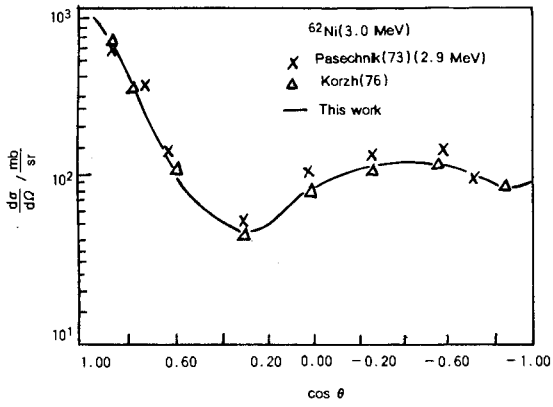

Fig.11 Elastic scatter angular distribution of 3.0 MeV for ^{62}Ni

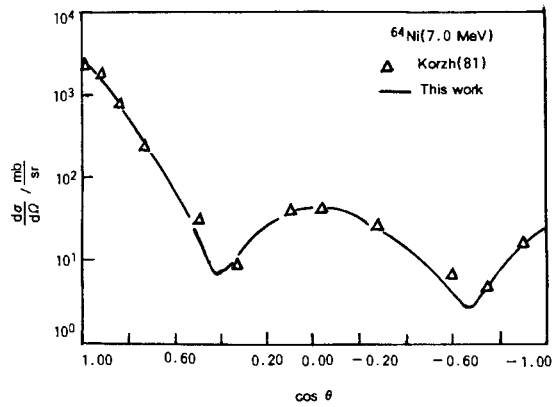

Fig.12 Elastic scatter angular distribution of 7.0 MeV for ^{64}Ni

The discrete inelastic angular distributions (MT = 51 ~ 83) were obtained from theoretical calculation results. The angular distributions for (n,2n), (n,3n), (n,n'α), (n,n'p) and continuum inelastic (MT = 16, 17, 22, 28, 91) were assumed to be isotropic.

4 The Double Differential Cross Section and γ-Ray Production Data

The double differential emission cross section (MF = 6, MT = 16, 17, 22, 28, 91, 103, 104, 105, 106, 107, 111) and γ-ray production data (MF = 12,13,14,15) were taken from the calculation results (Fig.13, 14).

5 Theoretical Calculation

An automatically adjusted optical potential code (APOM)[5] was used for searching a set of optimum neutron spherical optical potential parameters. ECIS code[6] of coupled channel was used to calculate the direct inelastic scattering for excited levels as the input data of UNF[7]. UNF code, including optical model,

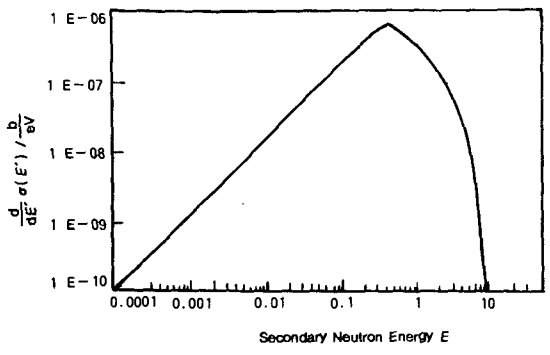

Fig.13 ^{58}Ni(n,n'p) secondary neutron spectrum at 20.0 MeV

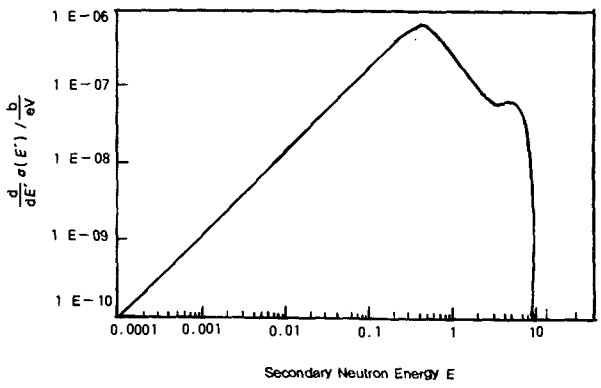

Fig.14 ^{60}Ni(n,2n) secondary neutron spectrum at 20.0 MeV

Hauser-Feshbach statistical model and exciton model, was used to calculate the data for files 3, 4, 5, 6, 12, 14, 15, which requires following input Parameters: optical potential, level density[8], giant dipole resonance and nuclear level scheme. These parameters were adjusted on the basis of experimental data in the neutron energy range from 1 keV to 20 MeV.

5.1 Optical Model, Level Density and Giant Dipole Resonance Parameters

Optical potential parameters are given in Table 3, and level density parameters and pair correction parameters are given in Table 4. The giant dipole resonance parameters are shows in Table 5, the symbols CSG, EE and GG are the peak cross section, resonance energy and full width at half maximum, respectively.

Table 3 Optical potential parameters*

	Depth / MeV		Radius / fm	Diffuses / fm
Neutron	$V_0 = 53.7339$	$W_0 = 12.3702$	$X_r = 1.1818$	$A_r = 0.7112$
	$V_1 = -0.1395$	$W_1 = -0.1642$	$X_s = 1.3200$	$A_s = 0.4340$
	$V_2 = -0.0155$	$W_2 = -1.2687$	$X_v = 1.3190$	$A_v = 0.4100$
	$V_3 = -17.5984$	$U_0 = -2.0686$	$X_{so} = 1.1764$	$A_{so} = 0.7284$
	$V_4 = 0.0$	$U_1 = 0.2659$	$X_c = 1.10$	
	$V_{so} = 3.1$	$U_2 = 0.0$		

* Note: $V_r(E) = V_0+V_1E+V_2E(2)+V_3(A-2Z)/A+V_4Z/A(1/3)$
$W_s(E) = W_0+W_1E+W_2(A-2Z)/A$
$U_v(E) = U_0+U_1E+U_2E(2)$

Table 4 Level density parameters and pair correction values of 11 excess nuclei for ^{58,60}Ni*

	n,γ	n,n'	n,p	n,α	n,^{3}He	n,d	n,t	n,2n	n,n'α	n,2p	n,3n
^{58}Ni	L 6.50	5.37	7.32	6.26	6.25	6.19	6.20	5.40	5.58	7.37	4.71
	P 1.0	2.35	−0.3	1.3	2.45	1.05	−0.1	1.2	2.5	1.1	2.4
^{60}Ni	L 6.91	6.36	7.75	7.37	7.27	7.20	7.32	6.50	6.25	7.81	5.37
	P 1.05	2.52	−0.3	1.1	2.62	1.22	−0.3	1.0	2.45	1.15	2.35

* Note: $L = [0.0088(S(z)+S(n))+Q_b]A$

$P = P(n)+P(z)$

$Q_b = 0.142$ or 0.12 (spherical or deformation)

Table 5 The 11 giant dipole resonance parameters of ^{58}Ni (twin peak)

CSG / b	2×0.034,0.026,2×0.047,0.026,0.047,0.034,2×0.047, 0.034, 3×0.05,2×0.04,0.05,0.04,0.05,2×0.04,0.05.
EE / MeV	2×16.3,16.37,2×16.62,16.37,16.62,16.3,2×16.62,16.3, 2×18.51,18.9,2×19.91,18.9,19.91,18.51,2×19.91,18.51.
GG / MeV	2×2.44,2.56,2×4.24,2.56,4.24,2.44,2×4.24,2.44, 2×6.37,7.61,2×4.16,7.61,4.16,6.37,2×4.16,6.37.

5.2 The Coupled Channel Calculation

The Legendre coefficients (L. C) of direct elastic scattering to ground state and direct inelastic scattering to excited states were calculated with coupled channel code ECIS at 23 energies.

6 Concluding Remarks

Due to the new experimental data are available in last years, the evaluated data have been considerably improved, especially cross sections of total, (n,p), (n,n'p), (n,α), (n,d), total inelastic reactions and inelastic scattering to some discrete levels.

More detail please refer to Ref. [9 ~ 12] for theoretical calculation and Ref. [13 ~ 15] for evaluation.

Acknowledgments

The authors wish to thank Prof. Liu Tingjin and Liang Qichang for their much help with this work. We also thank Prof. Chen Zhenpeng for their help in the ECIS code calculation.

References

[1] Nuclear Data Sheets, 1992, 67:195; 1992,67:271; 1992, 67:523; 1991, 64: 723; 1991, 64: 815; 1991, 62: 603; 1990, 60: 337; 1983, 39: 641
[2] Ma Gonggui, et al., CNDP, 17, 74(1997)
[3] Ma Gonggui, et al., CNDP, 15, 60(1996)
[4] Ma Gonggui, et al., CNDP, 14, 53(1995)
[5] Shen Qingbiao, et al., APOM-Acode for searching optical model parameters, CNDP, 1993, 7: 43
[6] Chen Zhenpeng, Coupled channel calculation program ECIS. Communication of Nuclear Data Progress, 1995, No.13: 33
[7] Zhang Jingshang. Nucl. Sci. Eng., 1993, 114; 55 ~ 63
[8] Zhuang Youxiang,et al., A new set of level density parameters for Fermi Gas model, Chinese Physics, 1988, 8: 721
[9] Ma Gonggui, et al., J. Sichuan Univ. (Natural Science Edition), 33, 6, 677(1996)
[10] Ma Gonggui, et al., Proc. of Tenth National Conf. of Nucl. Phys.; J. Qingdao Univ. (Natural Science Edition), Supplement, Aug., 1997
[11] Ma Gonggui, et al., Atomic Energy Science and Technology(to be published)
[12] Ma Gonggui, et al., J. Sichuan Univ. (Natural Science Edition), 33, 6, 677(1996)
[13] Ma Gonggui, et al., China Nucl. Sci. and Tech. Report, CNIC-0160, 1997
[14] Ma Gonggui, et al., Evaluation of Complete Neutron Nuclear data for $^{60\sim62,64}$Ni (internal report)
[15] Ma Gonggui, et al., China Nucl. Sci. and Tech. Report (to be published)

Some ^{235}U Reference Fission Product Yield Data Evaluation

Liu Tingjin Liang Qichang
(China Nuclear Data Center, CIAE)

Introduction

Some fission yield data are used as standards in the fission yield data measurement and evaluation, and some are used as monitor in the nuclear industry for decay heat estimation, burn-up credit study etc. All of this kind of fission yield is refered to the reference yield. Among them, the data of ^{235}U fission, especially at thermal energy, are most important ones.

The error of relatively measured fission yield data directly depends on the accuracy of the standard data used. The same situation is for the data calculated from measured ratio, R-value. Also the calculation creditability of, like, decay heat and burn-up etc. depends on the monitor fission yield data accuracy.

To satisfy the requirement of application for reference yield data, the data have been and will be continuously evaluated. Present work, in which the reference data for 20 product nuclides from ^{235}U fission were evaluated, is a part of the whole work. The work has been supported by IAEA under contract No.9504.

1 Data Collection and Evaluation

1.1 Data Collection

The all data up to now were retrieved from EXFOR master data library by using EXFOR manage system and supplementary retrieval programs for fission yield data[1]. Some data were taken from the EXFOR file, which were measured and compiled in China and haven't been merged into EXFOR master library. The data were also collected from the publications concerned. Altogether 127 entries (subentries) or papers were collected, they are listed in Table 1 and in Appendix 1 for product nuclides in detail.

1.2 Data Selection

The EXFOR BIB information and papers concerned were read carefully and analysed in physics. And then it was decided for the data to be adopted or abandoned according to the measured date, method, facility, detector, monitor, data error and discrepancy situation with others. In general, the following data were abandoned:

a. The quantity measured is not required;
b. The data were relatively measured, but their standards are not given. This is necessary especially for the evaluation of 'reference yield data', they could not be based on other standards, whose reliability are unknown.
c. Large discrepancy with others and measured method is not reliable or no information in detail;
d. Some thing is wrong in the measurements or data processing.

As a result, about half of the data were abandoned (marked by 'A' in Table 1), and 58 entries (subentries) or papers were taken (marked by 'T' in Table 1, Table 2).

Table 1 Collected experimental data
(T--Taken in the evaluation, A--Abandoned(reason))

EXFOR NO	AUTHOR	LAB.	REFERENCE	DATA	ENERGY eV	COMMENTS
10722002	R.B.STRITTMAT	1USAUI	ANS,27,862	7712	2.5-02	A(IND)
10722003	R.B.STRITTMAT	1USAUI	ANS,27,862	7712	2.5-02	A(IND)
10828002	T.C.CHAPMAN	1USALRL	PR/C,17,1089	7803	6.0+06	A(E not needed)
10864004	M.SHIMA	1CANMCM	CJP,56,1340	7810	2.5-02	T
10864010	M.SHIMA	1CANMCM	CJP,56,1340	7810	5.0-01	A(above Cd)
12729002	L.E.GLENDENIN	1USAANL	PR/C,24,2600	8112	1.7+05	A(E not needed)
12729003	L.E.GLENDENIN	1USAANL	PR/C,24,2600	8112	1.7+05	A(IND)
12895003	G.P.FORD	1USALAS	PR/C,30,195	8407	2.5-02	A(IND)
12895004	G.P.FORD	1USALAS	PR/C,30,195	8407	1.9+06	A(IND)
12895005	G.P.FORD	1USALAS	PR/C,30,195	8407	1.5+07	A(IND)
12919004	M.LINDNER	1USALRL	RCA,49,1	90	2.5-02	A(Np)
13054003	W.E.GRUMMITT	1CANCRC	CRC-470	51	2.5-02	A(^{103,106}Ru,^{137}Cs much large)
13055002	W.J.ARROL	1CANMRC	CJR/B,27,757	49	2.5-02	T(error larger)
13059002	H.B.LEVY	1USALRL	PR,124,544	61	2.5+04	A(E not needed)
13059003	H.B.LEVY	1USALRL	PR,124,544	61	2.5+04	A(E not needed)
13059004	H.B.LEVY	1USALRL	PR,124,544	61	2.5+04	A(E not needed)
13059006	H.B.LEVY	1USALRL	PR,124,544	61	2.5+04	A(E not needed)
13059007	H.B.LEVY	1USALRL	PR,124,544	61	2.5+04	A(E not needed)
13059010	H.B.LEVY	1USALRL	PR,124,544	61	2.5+04	A(E not needed)
13059013	H.B.LEVY	1USALRL	PR,124,544	61	2.5+04	A(E not needed)
13064004	H.FARRAR	1CANMCM	NP,34,367	62	2.5-02	T
13065005	H.FARRAR	1CANMCM	CJP,40,1017	62	2.5-02	T
13078002	D.R.NETHAWAY	1USALRL	PR/B,139,1505	6509	1.5+07	A(IND)
13204003	B.F.RIDER	1USAGEV	GEAP-4716	6409	2.5-02	T
13205002	B.F.RIDER	1USAGEV	GEAP-5060	6512	2.5-02	A(13204, 13206 used)
13206003	B.F.RIDER	1USAGEB	GEAP-4893	6506	2.5-02	T(not same as 13204)
13224003	H.A.STORMS	1USAMIT	CONF-65-235-1	65	2.5-02	A(IND)
13227002	R.J.MEYER	1USAANL	ANL-6900,339	68	2.5-02	T
13233005	D.J.GORMAN	1CANMCM	CJC,46,1663	6406	2.5-02	A(^{238}U)
13251003	D.R.NETHAWAY	1USALRL	PR,182,1251	6906	1.5+07	T
13259004	B.F.RIDER	1USAGEV	GEAP-5505,10	6706	6.1-01	A(above Cd)
13259005	B.F.RIDER	1USAGEV	GEAP-5505,10	6706	6.1-01	A(above Cd)
13268005	L.H.GEVAERT	1CANTOR	CJC,48,641	70	2.5-02	T
13270003	F.L.LISMAN	1USAMTR	NSE,42,191	70	2.5-02	A(^{131}Xe, data error), T(others)
13270016	F.L.LISMAN	1USAMTR	NSE,42,191	70	5.0+05	T
13270017	F.L.LISMAN	1USAMTR	NSE,42,191	70	5.0+05	T
13283002	R.M.HARBOUR	1USAORL	RCA,15,146	71	9.9+03	A(^{252}Cf)
13283003	R.M.HARBOUR	1USAORL	RCA,15,146	71	9.9+03	A(^{252}Cf)
13284003	R.C.HAWKINGS	1CANCRC	CJP,49,785	71	2.5-02	A(IND)
13286002	T.P.MC LAUGHL	1USAUSA	MC LAUGHLIN	7109	2.5-02	T
13287003	A.OKAZAKI	1CANCRC	CJP,44,237	6601	2.5-02	A(IND)
13295002	K.WOLFSBERG	1USALAS	PR/C,3,1333	7103	2.5-02	A(^{242m}Am)
13297002	P.ALEXANDER	1USAUSA	NP/A,198,228	72	1.4+07	A(IND)
13300003	B.F.RIDER	1USAGEV	GEAP-10028-35	70	1.0+06	T
13306002	B.F.RIDER	1USAGEV	GEAP-13838,(H	7206	1.0+06	A(small, disc)
13330002	R.P.LARSEN	1USAANL	LARSEN	7410	5.0+05	T
13341002	W.J.MAECK	1USAINL	ICP-1092	76	2.5-02	A
13341003	W.J.MAECK	1USAINL	ICP-1092	76	2.5-02	T
13352002	M.G.INGHRAM	1USAANL	PR,79,271	5007	2.5-02	T
13352003	M.G.INGHRAM	1USAANL	PR,79,271	5007	2.5-02	T
13365002	L.E.GLENDENIN	1USAUSA	RCS,2,793(103	51	2.5-02	A(all Y large)
13371002	S.KATCOFF	1USABNL	PR,91,1458	5309	2.5-02	A(IND)
13384004	E.A.MELAIKA	1CANMCM	CJC,33,830	55	2.5-02	T
13384005	E.A.MELAIKA	1CANMCM	CJC,33,830	55	2.5-02	T
13385002	J.A.PETRUSKA	1CANMCM	CJP,33,640	5511	2.5-02	T
13386002	J.A.PETRUSKA	1CANMCM	CJP,33,693	55	2.5-02	T

EXFOR NO	AUTHOR	LAB.	REFERENCE	DATA	ENERGY eV	COMMENTS
13386003	J.A.PETRUSKA	1CANMCM	CJP,33,693	55	2.5-02	A(^{134}Xe, disc), T(Others)
13386005	J.A.PETRUSKA	1CANMCM	CJP,33,693	55	2.5-02	T
13386006	J.A.PETRUSKA	1CANMCM	CJP,33,693	55	2.5-02	T
13395003	B.FINKLE	1USAUSA	RCS,3,1368(21	51	2.5-02	T
13406002	E.J.HOAGLAND	1USAUSA	RCS,2,1035(14	51	2.5-02	A(IND)
13419002	N.SUGARMAN	1USAUSA	RCS,2,1139(17	51	2.5-02	A(IND)
13428002	L.E.GLENDENIN	1USAANL	GLENDENIN	55	2.5-02	T
13434003	W.E.GRUMMITT	1CANCRC	JIN,5,93	57	2.5-02	A(IND)
13440003	W.J.MAECK	1USAINL	ENICO-1028	8002	7.0+05	T
13444003	G.P.FORD	1USALAS	LA-6129	7602	1.5+07	T
13457002	M.G.INGHRAM	1USAANL	PR,76,1717	4912	2.5-02	T
13464002	F.BROWN	1CANCRC	CJC,31,242	53	2.5-02	A(IND)
20768002	J.G.CUNINGHAM	2UK HAR	AERE-R-6862	7205	1.0+06	A(some much small)
20848006	T.NISHI	2JAPKTO	NISHI 22	8008	2.5-02	A(IND)
20848017	T.NISHI	2JAPKTO	NISHI 22	8008	2.5-02	A(IND)
21531004	H.THIERENS	2BLGGHT	NIM,134,299	7604	2.5-02	A(IND)
21562002	G.SIEGERT	2FR ILL	PRL,34,1034	7504	2.5-02	A(IND)
21590002	J.BLACHOT	2FR GRE	JIN,36,495	74	2.5-02	T
21605002	G.SIEGERT	2FR ILL	PR/C,14,1864	7611	2.5-02	A(IND)
21641003	S.J.BALESTRIN	2GERJLU	PR/C,20,222	7912	2.5-02	A(IND)
21689002	W.LANG	2FR ILL	NP/A,345,1,34	8008	2.5-02	A(IND)
21689004	W.LANG	2FR ILL	NP/A,345,1,34	8008	2.5-02	A(IND)
21689006	W.LANG	2FR ILL	NP/A,345,1,34	8008	2.5-02	A(IND)
21689008	W.LANG	2FR ILL	NP/A,345,1,34	8008	2.5-02	A(IND)
21689010	W.LANG	2FR ILL	NP/A,345,1,34	8008	2.5-02	A(IND)
21689012	W.LANG	2FR ILL	NP/A,345,1,34	8008	2.5-02	A(IND)
21689019	W.LANG	2FR ILL	NP/A,345,1,34	8008	2.5-02	A(IND)
21701010	H.O.DENSCHLAG	2GERMNZ	79JUELICH,2,1	7905	2.5-02	A(IND)
21701011	H.O.DENSCHLAG	2GERMNZ	79JUELICH,2,1	7905	2.5-02	A(IND)
21743002	G.MARIOLOPOUL	2FR GRE	NP/A,361,1,21	8105	2.5-02	A(IND)
21743004	G.MARIOLOPOUL	2FR GRE	NP/A,361,1,21	8105	3.0+06	A(IND)
21743005	G.MARIOLOPOUL	2FR GRE	NP/A,361,1,21	8105	3.0+06	A(IND)
21939002	H.DENSCHLAG	2FR ILL	NEANDC(E)-252	8406	2.5-02	A(IND)
22038002	P.ALEXANDER	2GERMNZ	NP/A,198,228	7212	1.4+07	A(IND)
22050009	M.ROBIN	2FR FAR	IAEA-169,(3)	74	1.5+06	T(^{143,145,146,150}Nd)
22054002	K.DEBERTIN	2GERPTB	RCA,18,(4),20	7212	2.5-02	T
22058002	R.DIERCKX	2ZZZISP	JNE,25,85	7102	2.5-02	A(^{238}U, mxw?)
22060002	J.FAHLAND	2GERMNZ	JIN,32,3149	7011	2.5-02	A(IND)
30495002	A.RAMASWAMI	3INDTRM	JIN,41,1531	7911	2.5-02	T
30947002	R.H.IYER	3INDTRM	JIN,25,465	63	2.5-02	A(^{232}Th)
30955002	E.YELLIN	3ISLSOR	IA-1190,99	6907	2.5-02	A(IND)
30955003	E.YELLIN	3ISLSOR	IA-1190,99	6907	2.5-02	A(IND)
13300002	B.F.RIDER	1USAGEV	GEAP-10028-35	70	1.0+06	T
13375004	D.R.WILES	1CANMCM	CJP,31,419	53	2.5-02	T
13382002	D.R.WILES	1USAMIT	PR,96,696	5411	2.5-02	A(Y much small,some mistake)
13383002	L.YAFFE	1CANCRC	CJC,32,1017	54	2.5-02	T
13398002	M.S.FREEDMAN	1USAUSA	RCS,3,1344(20	51	2.5-02	T
13435002	P.KAFALAS	1USAANL	JIN,4,239	57	5.0+05	T
13486002	D.C.SANTRY	1CANMCG	CJC,38,464	6003	2.5-02	T
21483002	L.CIUFFOLOTTI	2ITYMIL	EN,15,272	6804	2.5-02	T
21530002	P.FETTWEIS	2BLGMOL	ZP/A,275,359	7512	2.5-02	A(IND)
32631002	WANG YUSHENG	3CPRAEP	HFH,6,(4),229	8411	1.5+07	T
32633002	LI ZOE	3CPRAEP	HFH,2,(1),1	8002	2.5-02	T
32633003	LI ZOE	3CPRAEP	HFH,2,(1),1	8002	1.8+06	T
32635002	WANG YUSHENG	3CPRAEP	HFH,2,(3),129	8008	1.8+06	T
32635003	WANG YUSHENG	3CPRAEP	HFH,2,(3),129	8008	2.5-02	T
32635004	WANG YUSHENG	3CPRAEP	HFH,2,(3),129	8008	1.8+06	T(independent from 002)
32635005	WANG YUSHENG	3CPRAEP	HFH,2,(3),129	8008	1.8+06	T(different code)
32638003	CHEN DA	3CPRINT	78LUSHAN,,100	7808	2.5-02	T

EXFOR NO	AUTHOR	LAB.	REFERENCE	DATA	ENERGY eV	COMMENTS
13202003	J.A.MC HUGH	J 1USALRL	UCRL–10673	6302	2.5–02	A
13339002	W.H.ZIMMER	1USAARC	NT,25,289	75	5.0+05	T
13342003	L.S.KELLOGG	1USAHED	HEDL–TME–77–3	7805	5.0+05	T
13344004	E.R.EBERSOLE	1USAANL	EBERSOLE	7211	1.0+06	T
13344006	E.R.EBERSOLE	1USAANL	EBERSOLE	7211	2.5–02	T
22050004	M.ROBIN	2FR FAR	IAEA–169,(3)	74	1.5+06	T
22066002	V.M.SINCLAIR	2UK DOU	71CANT,,45	71	1.5+0	T
40363002	V.K.GORSHKOV	4CCPITE	AE,3,(7),11	5707	2.5–02	T
41084005	V.YA.GABESKIR	4CCPNIR	AE,43,59	77	1.3+06	A(no standard given)
41087004	K.A.PETRZHAK	4CCPRI	AE,42,337	7704	9.9+03	A(no useful ratio)
12771002	R.P.LARSEN	1USAANL	NSE,54,263	7407	4.0+05	A(^{99}Mo, ^{140}Ba small)
12771005	R.P.LARSEN	1USAANL	NSE,54,263	7407	2.53–02	T
	QI LINKUN	3CPRAEP	88MITO,967	8805	1.95+6	T

Table 2 Treatment of experimental data used

EXFOR	Method	Quantity (monitor)	processed
10864004	MA, REAC(mxw)	Ro(/^{105}Pd)	
13055002	RC, REAC(mxw)	Ro(/^{134}Xe)	ΔRo ~ 10%
13064004	MA, REAC(mxw)	Ro(/^{143}Nd)	ΔRo 0.3 ~ 1.5%
13065005	MA, REAC(mxw)	Ro(/^{100}Mo)	ΔRo ~2%
13204003	MA, REAC(mxw)	Ro(/^{148}Nd)	0.9928 ^{148}Nd from fission, Ro/0.9928
13206003	MA, REAC(mxw)	Ro(/^{148}Nd)	0.9928 ^{148}Nd from fission, Ro/0.9928
13227002	MA, REAC(mxw)	FY(?)	ΔFY ~ 2%
13251003	RC(γ,β), NaI, FNG(14.8)	FY(AB), σ_f 2.24b	Unit change×100, 2.24→2.06(B6)
13268005	RC(GEMUC), CCW(mxw)	FY(/^{99}Mo)	^{115}Cd, CD 336.0 0.95→0.459
13270016	MA, REAC(0.5)	FY(/^{148}Nd 1.75±0.03)	Calculate Ro
13270017	MA, REAC(0.5)	FY(AB→100%)	
13286002	RC(γ,GeLi), REAC(mxw)	FY(AB)	CD: I_γ
13300003	MA, REAC(EBR–II, 1.0)	FY(/^{148}Nd 1.75)	Calcu. Ro
13330002	MA, REAC(0.5)	FY(?)	
13341003	MA, REAC(ETR, mxw)	REL	Calcu. ^{145}Nd/^{143}Nd, ΔR→5%(disc)
13352002	MA, REAC(mxw)	FY(/^{143}Nd)	ΔR→1.5%, ^{148}Nd ΔR→5%(disc.)
13352003	MA, REAC(mxw)	FY(/^{149}Sm)	ΔR→1.5%
13384004	MA, REAC(NRX,mxw)	Ro(/^{143}Nd)	
13384005	MA, REAC(NRX,mxw)	FY(/^{149}Sm)	ΔY→2%, Calc. Ro
13385002	MA, REAC(NRX,mxw)	FY(AB?)	ΔY→3%
13386002	MA, REAC(NRX,mxw)	FY(AB?)	ΔY→3%
13386005	MA, REAC(NRX,mxw)	FY(/^{143}Nd, 5.8)	Calcu. Ro, ΔRo→1.5%
13386006	MA, REAC(NRX,mxw)	FY(/^{149}Sm, 1.13)	Calcu. Ro, ΔRo→1.5%
13395003	RC, REAC(ANL,mxw)	FY(/^{140}Ba, 6.1)	Calcu. Ro, ΔRo→4.0%
13428002	MA, REAC(mxw)	FY(?)	ΔY→2%
13440003	MA, REAC(EBR–2, 0.7)	FY(AB,100%)	
13444003	RC, CCW(14.7)	Rv(/^{99}Mo, mxw)	
13457002	MA, REAC(mxw)	Ro(/^{137}Cs)	ΔR→2%
21590002	RC(GeLi), REAC(mxw)	FY(/^{140}Ba, 6.34)	Calcu.Ro, CD: I_γ
22050009	MA, REAC(1.5)	Ro(/^{148}Nd)	ΔRo→1.5%
22054002	γ (GeLi), REAC(mxw)	FY(/^{144}Ce,5.35±0.08)	5.35→5.328±0.052(eval.)
30495002	γ(GeLi), TRD(n), REAC(mxw)	FY(AB)	CD: I_γ 529.9, 0.873; ΔY→5%
13300002	RC, REAC(EBR–2,mxw)	FY(/^{148}Nd, 1.75)	Calcu. Ro, ΔR→3%
13375004	MA, REAC(NRX,mxw)	FY(/^{133}Cs, 7.43)	Calcu. Ro, ΔR→2%
13383002	RC, REAC(NRX,mxw)	FY(/^{10}B(n,α), SIG)	eΔY→15%
13398002	RC, REAC(mxw)	FY(?)	eΔY→15%
13435002	RC(β), REAC(CP–5,0.5)	FY(AB)	eΔY~3%→10%
13486002	RC(β), REAC(NRX,mxw)	FY(/^{59}Co(n, γ), σ_f 571)	Cσ_f: 571→586.2, eΔY→10%
21483002	γ(NaI), REAC(mxw)	FY(AB)	eΔY→7%
32631002	RC, CCW(14.9)	FY(AB)	
32633002	RC(γ(NaI,GEMUC), β), REAC(mxw)	FY(AB)	

EXFOR	Method	Quantity (monitor)	processed
32633003	RC(γ,β)REAC(1.8)	FY(AB)	
32635002	RC(γ(GeLi)), REAC(1.8)	FY(AB)	CD: I_γ
32635003	RC(γ(GeLi)), REAC(mxw)	FY(AB)	CD: I_γ
32635004	RC(γ(GeLi)), REAC(1.8)	Ro(/mxw)	
32635005	RC(γ(GeLi)), REAC(1.8)	Ro(/mxw)	
32638003	γ (GeLi), REAC(1.8)	FY(/^{95}Zr, 6.45±0.06)	CY: 6.45→6.479±0.05(eval.)
13339002	MC, REAC(EBR-2, 0.5)	FY(/^{140}Ba, 6.03±0.18)	Calcu. Ro, ΔRo ~ 4%
13342003	MA, REAC(EBR-2, 0.5)	Ro(/^{137}Cs)	
13344004	MA, REAC(EBR-2, 1.0)	Ro(/^{137}Cs)	
13344006	MA, REAC(mxw)	FY(AB?)	eΔY 0.06%→1.5%
22050004	MA, REAC(1.5)	FY(AB?)	
22066002	MA(Nd), RC(others), REAC(1.5)	FY(AB)	
40363002	MA, REAC(mxw)	FY(/^{146}Nd)	Calcu. Ro, ΔRo→2%
12771005	RC(γ), REAC(2PR-3, mxw)	FY(/^{137}Cs)	ΔY~6%
QiLinkun	γ (GeLi), RC, REAC(1.95)	AB	

Notes for the table:

1. Abbreviation and symbol:

VDG	Van de Graaff accelerator
CYCLO	Cyclotron accelerator
REAC	Reactor
FNG	Fast neutron Generator
CCW	Cockcroft-Walton accelerator
RC	Radiochemistry method
γ	γ Spectrum method
MA	Mass Spectrometer method
mxw	Maxwell spectrum thermal neutron
AB(X)	Absolute measurement with method X
FY(/X)	Fission yield measured relatively to X
Ro(/X)	Ratio measured relatively to X
Rv(/X, mxw)	R value measured relatively to X at thermal energy point
Δ Y → 3%,	Designed 3% error to Y
e Δ Y → 3%,	Enlarge Y error to 3%
C	Corrected
Calcu.	Calculated
Disc	Discrepant
CHN	Chain yield
CUM	Cumulative yield
IND	Independent yield
TRD	Trace detector

2. The abbreviations not listed above are the same as EXFOR and CINDA.
3. The unit of energy is "MeV", if not specially given, but "ENERGY" column is in eV.

1.3 Measurement Error

The error given in the EXFOR data table are very different and complicated, some only for counting statistics, some only relative one, some no error, even no information, and some unreasonably small. The error of the data shows their reliability and play an important role in the data processing (determines the weight). They must be corrected for only statistical and unreasonable ones, or assigned for those not given. It is always kept in mind that they must be 'total' error. It is impossible for evaluators to give the error according to the concrete measurement conditions for each experiment, but it can be done for different measurement methods. There are some common characters and same error sources for the data

measured with same method, in general case, the error should keep at the same level. The errors are listed in Table 3 for data measured with mass spectrometer, γ energy spectrum, and radiochemistry methods. These are summarized from the collected data and based on the experience of the experimenters. In general case, if the errors given by authors are in these regions, they were not changed; if not, they were corrected or assigned. The error could be changed in the region for same method and period, depending on the value of the yield, measured energy point, date and laboratory. If there were no error given, the error were assigned according to the case, generally upper limit. It should be pointed that this is just 'general' case, in the special case the error could be out of the given region.

Table 3 The error(%) of measured fission yield data with different methods

Methods		Fission Yield		Ratio
		Before 1965	After 1965	
RC	GeLi	7~15	4~8	3~5
	NaI	8~15	6~8	3~4
	Geiger	15~25		5~6
γ Spectrum		6~10	3~6	2~3
MA		2~3	1~2	1~2

Note:

1) The error depends on fission yield value, energy point, year and laboratory measured, it can be changed in the corresponding region.
2) If the error is not given, in general case, the upper limit is taken for that.
3) The region listed in the table is just for general case, the error may be outside of the region in special case.

1.4 Standard and Correction

The data were corrected for standard yield data, γ intensity, and fission cross section.

1.4.1 Fission Yield Standard

As mentioned above, in general case, the data relatively measured were not directly taken, only the data taken ^{95}Zr, ^{99}Mo, ^{144}Ce, ^{147}Nd as standards were used, for these standard fission yield data have just been evaluated by ourself[2]. These data were corrected by using our newly evaluated data:

$$FY = FY_0 \times I_0 / I_{new} \quad (1)$$

1.4.2 γ Intensity

If the γ intensity used is given by the authors of the measurements, the data were corrected for it by using following new intensity data in order: evaluated decay data at CNDC[3], Table of Radioactive Isotopes, ENSDF computer library. If only one γ line was used in the data measurement, then it is simple

$$FY = FY_0 \times I_0 / I_{new} \tag{2}$$

If there are several γ lines were used, the correction is somewhat complicated. In this case, if the data were obtained by arithmetically averaging the data from each γ ray, then

$$FY = FY_0 \times \frac{1}{N} \sum_{i=1}^{N} I_{i0} / I_{new} \tag{3}$$

But if the data were obtained by averaging with weight, then obviously, the data from γ line with most intense intensity play a leading role (the statistical counting error and γ intensity error are small), so in this case

$$FY = FY_0 \times I_{0m} / I_{newm} \tag{4}$$

For present practical treatment, if there is a γ ray used, whose intensity is much larger than others and the energy is in the region from 100 ~ 1000 keV, the data were corrected with formula (4), if not, taken 2 or several γ rays with larger intensity and corrected by using formula (3).

1.4.3 Fission Cross Section

The data were corrected for fission cross section

$$FY = FY_0 \times \sigma_{f0} / \sigma_{fnew} \tag{5}$$

The new fission cross section was taken from ENDF/B–6.

1.5 Error Processing for Corrected Data

The error was correspondingly processed for corrected data.

1.5.1 Standard Fission Yield and Cross Section Correction

$$\Delta FY' = (FY_0'^2 + FY_{snew}'^2 - FY_{sold}'^2)^{1/2}$$

or

$$\Delta FY' = (\Delta FY'^2 + \Delta\sigma_{f'snew}'^2 - \Delta\sigma_{f'sold}')^{1/2}$$

Where $\Delta FY'$ means relative error of data FY, $\Delta FY' = \Delta FY/FY$ (the same below).

In some case, ΔFY_{sold}, the error of old standard, may not be included in the ΔFY_0, the total error of the data given by author. In this case, ΔFY_{sold} should be taken as 0.

1.5.2 γ Intensity Correction

For γ intensity correction, the FY error was not changed, due to the correction, in usual case, is not large and the γ intensity error is not given.

1.5.3 Calculating *FY* from Ratio *R*

$$\Delta FY' = (\Delta R'^2 + FY_s'^2)^{1/2}$$

1.5.4 Calculating Ratio *R* from *R*–value

$$\Delta R' = (\Delta R\nu'^2 + \Delta FY'^2 + \Delta FY_{mxw}'^2)^{1/2}$$

1.5.5 Calculating Ratio *R* from Fission Yield

As mentioned above, this evaluation is for reference fission yield data, only absolute measured data and a few data measured relatively to standards, which we have just evaluated, were used. Only the ratio was used for relatively measured data, if the standard used was given (otherwise the data were abandoned). In this case

$$\Delta R' = (\Delta FY'^2 - \Delta FY_s'^2)^{1/2}$$

If ΔFY_s is not included in the total ΔFY, given by author, then ΔFY_s is taken as 0.

The concrete processing situations of data and their errors for each subentry (paper) are listed in Table 1.

2 Data Processing

The EXFOR entries were processed with fission yield data evaluation system FYDES[1]. The data were retrieved from the EXFOR Master Library with EXFOR Library Management System according to the reactions. The data tables were standardized by means of codes FORM, FYRET or FYRETD, FYDEXCH. The corrections were made by means of codes FYCRECT or FYCRECTD. Then the data were retrieved by code FYRET1 according to product nuclides.

The data with measurements more than one were averaged with weight by using

code AVERAG. The product nuclides, for which the average has been made, are marked by 'A' and the measured data points are given by the corresponding numbers in the Table 4. It can be seen that averaging has been made for most of them.

Table 4 The evaluated ^{235}U fission yield data as reference

Z	A	*E*	FY	FY Error	Data Points	Processed		Recomm.
Sr	92	T	6.000000E+00	1.700000E-01	1			(R)
Mo	97	T	5.967447E+00	8.707969E-02	2 + 1	A	S	R
Mo	97	F	5.897125E+00	5.330354E-02	1 + 1		S	R
Mo	100	T	6.248365E+00	6.882592E-02	2 + (1)	A	S	R
Mo	100	F	6.118409E+00	5.543072E-02	1 + 1		S	R
Ru	103	T	3.040486E+00	2.950412E-02	7 + 2 + (2)	A	S S	R
Ru	103	F	3.552457E+00	5.945541E-02	3 + 2	A	S	R
Ru	103	H	3.412679E+00	1.022755E-01	1 + 1		S	R
Ru	106	T	3.913407E-01	3.429494E-03	5 + (1)	A	S S	R
Ru	106	F	6.380000E-01	4.500000E-02	1			N
Ru	106	H	1.669126E+00	6.541831E-02	1 + 1		S	R
Xe	131	T	2.999734E+00	4.678688E-02	B6+2		S	N
Xe	131	F	3.262000E+00	4.618000E-02	2	A		R
Xe	134	T	7.517494E+00	1.089694E-01	1 + (1)		S	(R)
Xe	134	F	7.694600E+00	1.082700E-01	2	A		R
Xe	135	T	6.777000E+00	1.800000E-01	1			N
Cs	133	T	6.799620E+00	4.828717E-02	3 + 1 + (3)	A	S	R
Cs	133	F	6.745700E+00	6.025500E-02	2	A		R
Cs	137	T	6.205189E+00	5.108952E-02	4 + 2	A	S	R
Cs	137	F	6.200822E+00	5.310107E-02	4 + 1 + (1)	A	S	R
Ba	140	T	6.205904E+00	6.169309E-02	9 + (2)	A	S S	R
Ba	140	F	6.151373E+00	9.871449E-02	3 + 1	A	S	R
Ba	140	H	4.596264E+00	1.161719E-01	2 + 1	A	S	R
La	140	T	6.407000E+00	1.100000E-01	1			N
Nd	143	T	5.960276E+00	4.162443E-02	3 + 3 + (2)	A	S	R
Nd	143	F	5.692010E+00	4.916045E-02	4 + 2	A	S	R
Nd	145	T	3.940305E+00	2.834605E-02	2 + 8	A	S	R
Nd	145	F	3.764107E+00	3.907484E-02	4 + 1	A	S	R
Nd	148	T	1.674706E+00	1.127934E-02	3 + 5 + (4)	A	S	R
Nd	148	F	1.697987E+00	1.122225E-02	5 + 2 + (5)	A	S	R
Sm	147	T	2.118375E+00	2.258691E-02	2 + 1	A	S	R
Sm	147	F	2.165000E+00	2.200000E-02	1			(R)
Sm	149	T	1.010102E+00	1.317217E-02	2 + (3)	A	S	R
Sm	149	F	1.045700E+00	2.279400E-02	2	A		R
Sm	151	T	4.034757E-01	4.302739E-03	2 + 1	A	S	R
Sm	151	F	4.173500E-01	9.476600E-03	2	A		R
Sm	152	T	2.531572E-01	4.408931E-03	2 + 1	A	S	R
Sm	152	F	2.952200E-01	6.660700E-03	2	A		R

Meaning in the "Data Point"

Number absolutely FY measured data sets
+ number ratio *Ro* measured sets (appear in numerator)
+(number) of ratio *Ro* measurement concerned (appear denominator)

A Average with weight

S Simultaneous evaluation

SS First simultaneous evaluation for same nuclide at different energy points, then different nuclides.
R Recommended
(R) Recommended only as reference, need to be improved
N Not recommended

The data with measurements of absolute fission yields and relative ratios were simultaneously evaluated by using code ZOTT[4]. The correlative measurements for the nuclides concerned and the treatment in the evaluation are given in Fig.1. There are two kinds of correlative measurements, one is for different energy points for the same nuclide, and the other is for different nuclides at same energy point. The first one was first processed with code ZOTT for each nuclide concerned respectively, then the second one. To avoid too complicated, the data measured at thermal energy point was divided into four groups, as shown in Fig.1, to be processed according to the actual correlation situation. The data measured at reactor spectrum were processed at same time for all nuclides concerned. The data marked 'S' in the Table 4 means that the data were simultaneously evaluated and 'SS' means the data were processed for these two kinds of correlation.

Fig.1 The correlation of measured reference fission yield data and their processing (t-thermal energy point, f-fast reactor spectrum, h-around 14 MeV)

	^{92}Sr	^{97}Mo	^{100}Mo	^{103}Mo	^{106}Ru	^{140}Ba	^{105}Pd	^{135}Xe	^{140}La	^{131}Xe	^{134}Xe	^{133}Cs	^{137}Cs	^{143}Nd	^{145}Nd	^{148}Nd	^{147}Sm	^{149}Sm	^{151}Sm	^{152}Sm
^{92}Sr																				
^{97}Mo			t																	
^{100}Mo																				
^{103}Mo				f/t h/t		t														
^{106}Ru					h/t	t														
^{140}Ba						h/t f/t														
^{105}Pd																				
^{135}Xe																				
^{140}La																				
^{131}Xe											t	t								
^{134}Xe												t								
^{133}Cs																t				
^{137}Cs												t				t				
^{143}Nd																t				
^{145}Nd														t		t				
^{148}Nd														t						
^{147}Sm																		t		
^{149}Sm																				
^{151}Sm																		t		
^{152}Sm																		t		

3 Result, Recommendation and Discussion

The evaluated results are shown in Table 4.

3.1 The Error of the Evaluated Data

It can be seen that the errors are about 1% for most of product nuclides and 2% ~ 3% for some and 7% only for one, ^{106}Ru yield at fission spectrum. The error about 1% and 2% ~ 3% of evaluated data comes from the fact that the data measured with mass spectrometer method have error 1% ~ 2% (after 1960) or 2% ~ 3% (before 1960), and multiple sets of measurements make it reduced (in the case of the data are statistical consistent). For ^{106}Ru, there is only one measured data with radio-chemistry method, so the error is larger.

3.2 Comparison with Other Evaluated Data

The evaluated data were plotted and compared with CENDL-FY, ENDF/B-6, JENDL-3 and JEF-2 (Appendix 5). It was found that the data are in good agreement among the present evaluated ones and all others for ^{100}Mo(T), ^{106}Ru(T), ^{106}Ru(H), ^{143}Nd(T), ^{143}Nd(F), ^{145}Nd(T), ^{145}Nd(F), ^{148}Nd(T), and ^{148}Nd(F), a typical example is shown in Fig.2. The present evaluated data for ^{92}Sr(T), ^{97}Mo(T), ^{97}Mo(F), ^{100}Mo(F), ^{103}Ru(T), ^{103}Ru(H), ^{131}Xe(F), ^{134}Xe(F), ^{133}Cs(F), ^{137}Cs(T), ^{137}Cs(F), ^{1}Ba(T), ^{140}Ba(F), ^{140}Ba(H), ^{147}Sm(F), ^{149}Sm(F), ^{151}Sm(F), ^{152}Sm(F), are in 'statistical agreement with the existing evaluated data, which are somewhat discrepant with each other, a typical example is shown in Fig.3. The present evaluated data for ^{103}Ru(F), Ru(F), ^{131}Xe(T), ^{134}Xe(T), ^{135}Xe(T), ^{133}Cs(T), ^{140}La(T), ^{147}Sm(T), ^{149}Sm(T), ^{151}Sm(T), ^{152}Sm(T) are outside of all existing evaluated data, although some of which are somewhat discrepant, a typical example is shown in Fig.4.

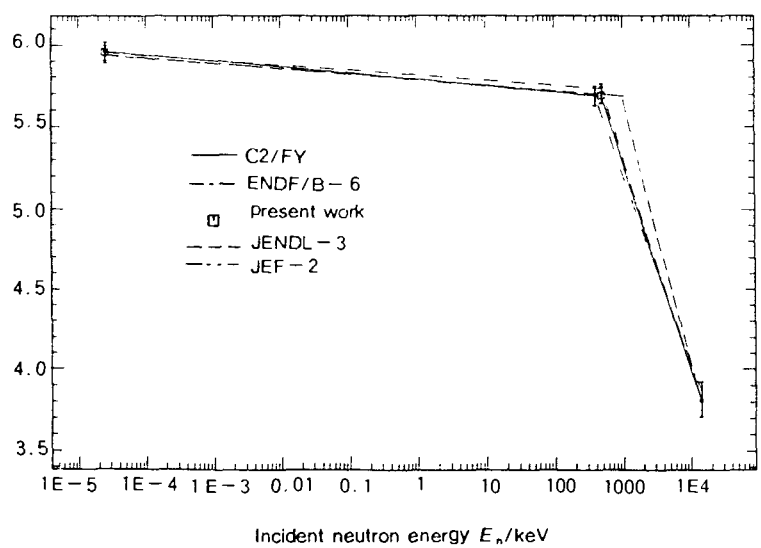

Fig.2 Intercomparison of present evaluation with others: ^{143}Nd

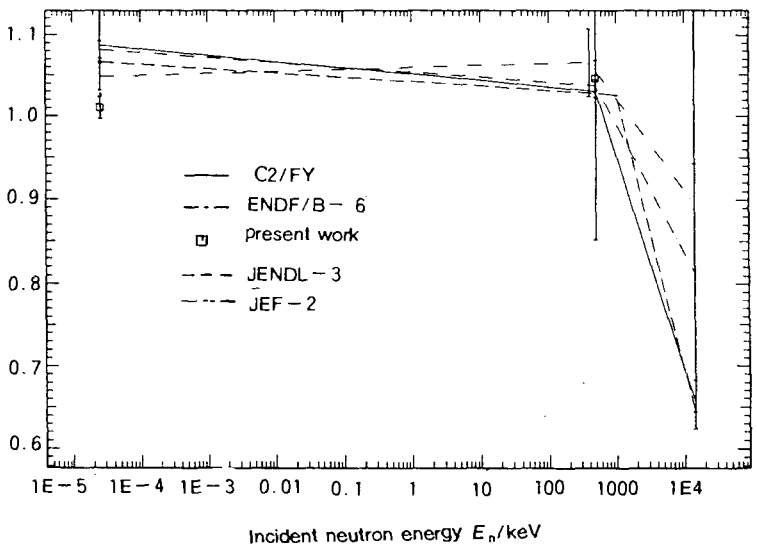

Fig.3 Intercomparison of present evaluation with others: ^{149}Sm

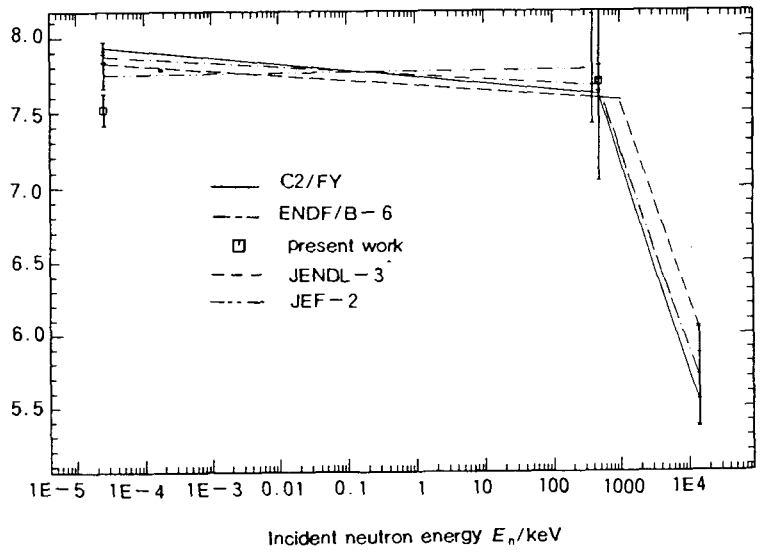

Fig.4 Intercomparison of present evaluation with others: ^{134}Xe

3.3 Recommendations

The data of ^{106}Ru(F), ^{131}Xe(T), ^{135}Xe(T), ^{140}La(T), ^{92}Sr(T) and ^{147}Sm(F) have less reliability, for there is only one measurement for them. Among them, the first four are also disagreement with other existing evaluated data, they could not be recommended as reference data to use. The data of last two only can be used as reference. For ^{134}Xe(T), there are only two measurements and the newly evaluated datum is disagreement with others, so it is also only can be used as reference.

The nuclides $^{140}_{57}$La and $^{140}_{56}$Ba are close to each other in the same mass decay chain and close to the stable nuclide $^{140}_{58}$Ce, and the independent yields of ^{140}La, ^{140}Ce are very small, so their cumulative yields should be the same and equal to the chain yield. There are more measurements for ^{140}Ba and the data are more reliable, so here the data for ^{140}Ba is also recommended for ^{140}La, instead of ^{140}La less measured data itself.

The treatment for recommendation of the data is marked in the Table 4: 'R' recommended, '(R)' taken as reference, 'N' not recommended.

3.4 Discussions

It can be seen that the data for neodymium isotope are more reliable: small error and good agreement with other, it means high accuracy and precision. The same situations are also for ^{100}Mo(T) and ^{106}Ru(T).

As pointed out above that 11 data are outside of all existing evaluated data, except for the data not recommended or only as reference for they are not reliable, the data for ^{103}Ru(F), ^{133}Cs(T), ^{147}Sm(T), ^{149}Sm(T), ^{151}Sm(T), ^{152}Sm(T) are still remained, there are more measurements for them (at least three). Among them, four for samarium isotope's yield at thermal energy point, all dada of them are based on 3 mass spectrometer measurements (1327003, F. L. Lisman, USAMTR, 1970; 13384005, E. A. Melaika, CANMCM, 1955; 13386006, J. A. Petruska, CANMCM, 1955). It should be paid attention that if there are systematical errors (they are systematically smaller) and if there will be new measurement.

4 Conclusion

The 38 cumulative fission yield, which can be used as reference yield, for 19 product nuclides were evaluated based on available experimental data up to now and processed by using average with weight code AVERAG and simultaneous evaluation code ZOTT. Only absolute yield measurements and ratios were used, in

other words, no standard yield (except for a few newly evaluated ones) was used in the evaluation. The data and their errors have been updated. Among them, 31 are recommended and 7 need to be improved. The recommended data can be used as standard in the evaluation and measurement or as monitor yield in the industry application.

The authors wish to acknowledge IAEA for their supporting this work.

References

[1] Liu Tingjin, Supplement EXFOR Retrieval Programs for Fission Product Yield, Internal Report(1996)
[2] Liu Tingjin, Commun. of Nuclear Data Progress, Vol. 18 (1997)
[3] Zhou Chunmei, Private Communication(1997)
[4] D. Muir, Nucl. Sci. & Eng., 101, 88(1989)

CN9901235

The Evaluation for Reference Fission Yield of ^{238}U Fission

Liang Qichang Liu Tingjin
(China Nuclear Data Center, CIAE)

Introduction

Some fission products are taken as internal standard nuclides in relative yield and *R*-value measurement, and some are used as monitors in the nuclear industry, these kind of fission yield (generally, cumulative yields) is refered to the reference yields.

The reference yields are not only the basis of all fission yields evaluation and measurement, but also have widely applications in the nuclear industry.

In the fission yield data evaluation and measurement, the reference yield is very important, good or poor recommended or measurement values depend upon the reference data to a great extent. The fission products to be used as internal reference nuclides in fission yield evaluation and measurement are shown in Table 1.

Table 1 Fission products whose fission yields used as reference data

nuclide	half-life	nuclide	half-life
^{83g}Kr	stable	^{85g}Kr	10.72y
^{85m}Kr	4.480h	^{86}Kr	stable
^{87}Kr	76.3m	^{88}Kr	2.84h
^{89}Sr	50.55d	^{90}Sr	28.6y
^{91g}Y	58.51d	^{95}Zr	64.02d
^{96}Zr	stable	^{95g}Nb	34.97d
^{95m}Nb	3.61d	^{95}Mo	stable
^{99}Mo	66.0h	^{100}Mo	stable
^{101}Ru	stable	^{102}Ru	stable
^{103}Ru	39.26d	^{106}Ru	371.63d
^{105g}Rh	35.36h	^{106g}Rh	29.80s
^{111g}Ag	7.45d	^{115g}Cd	53.46h
^{115m}Cd	44.6d	^{125}Sb	2.73y
^{132}Te	78.2h	^{131}I	8.04d
^{135}I	6.61h	^{131g}Xe	stable
^{131m}Xe	11.9h	^{132}Xe	stable
^{133g}Xe	5.245d	^{133m}Xe	2.188d
^{134g}Xe	stable	^{135g}Xe	9.09h
^{135m}Xe	15.29m	^{136}Xe	stable
^{137}Xe	3.818m	^{138}Xe	14.08m
^{133}Cs	stable	^{134g}Cs	2.062y
^{136}Cs	13.16d	^{137}Cs	30.17y
^{140}Ba	12.746d	^{140}La	40.272h
^{141}Ce	32.501d	^{143}Ce	33.0h
^{144}Ce	284.4d	^{141}Pr	stable
^{144g}Pr	17.28m	^{143}Nd	stable
^{144}Nd	stable	^{145}Nd	stable
^{146}Nd	stable	^{147}Nd	10.98d
^{148}Nd	stable	^{147}Pm	2.6234y
^{148g}Pm	5.370d	^{148m}Pm	41.29d
^{149}Pm	53.08h	^{151}Pm	28.40h
^{149}Sm	stable	^{151}Sm	90y
^{153}Sm	46.7h	^{153}Eu	stable
^{154g}Eu	8.8y	^{155}Eu	4.96y
^{156}Eu	15.19d	^{161}Tb	6.90d

In the application of nuclear industry, the reference yield data plays an important role, for example, in the reactor physics application, the reference yield data are widely used in the decay heat estimation, burn-up credit study, lose of reactivity per cycle, evaluation of energy release due to fission, transmutation studies, and calculation on the shielding, dosimetry, fuel handling, waste disposal, safety, as well as other nuclear physics calculation. In this field, about 60 reference yields were proposed, the product nuclides have short, medium and long half-life as shown in Table 2.

Table 2 Reference yields required for reactor physics applications

Nuclide	B. U. PWR	B. U. FBR	Monitoring	D. N.	C. E. D. H*	Radiotox
^{140}La			× × ×			
^{92}Sr			× × ×			
^{103}Ru		× × ×	× × ×		× × ×	
^{95}Zr			× × ×			
^{144}Ce			× × ×			
^{106}Ru			× × ×			
^{137}Cs			× × ×			
^{134}Cs			× × ×		× × ×	
^{154}Eu			× × ×			
^{135}Xe	× × ×					
^{103}Rh	× × ×	× × ×				
^{143}Nd	× × ×	× × ×				
^{131}Xe	× × ×	× × ×				
^{133}Cs	× × ×	× × ×				
^{149}Sm	× × ×	× × ×				
^{99}Tc	× × ×	× × ×				× × ×
^{152}Sm	× × ×					
^{147}Pm	× × ×	× × ×				
^{151}Sm	× × ×	× × ×				
^{153}Eu	× × ×	× × ×				
^{145}Nd	× × ×	× × ×				
^{155}Eu	× × ×					
^{154}Eu	× × ×					
^{109}Ag	× × ×	× × ×				
^{155}Gd	× × ×					
^{95}Mo	× × ×	× × ×				
^{147}Sm	× × ×					
^{150}Sm	× × ×					
^{101}Ru	× × ×	× × ×				
^{148m}Pm					× × ×	
^{148}Pm					× × ×	
^{156}Eu					× × ×	
^{136}Cs					× × ×	
^{79}Se						× × ×
^{93}Zr						× × ×
^{126}Sn						× × ×
^{129}I						× × ×
^{135}Cs		× × ×				× × ×
^{105}Pd		× × ×				
^{107}Pd		× × ×				
^{97}Mo		× × ×				
^{102}Ru		× × ×				
^{104}Ru		× × ×				
^{91}Zr		× × ×				
^{137}I				× × ×		
^{89}Br				× × ×		
^{94}Rb				× × ×		
^{90}Br				× × ×		
^{88}Br				× × ×		
^{85}As				× × ×		
^{138}I				× × ×		
^{98m}Y				× × ×		
^{95}Rb				× × ×		
^{139}I				× × ×		
^{97}Br				× × ×		
^{93}Rb				× × ×		
^{99}Y				× × ×		
^{91}Br				× × ×		
^{135}Sb				× × ×		

* Capture Effect on Decay Heat

From the mentioned above, a great number of reference yields are required in both fission yield measurement (or/and evaluation) and nuclear industry application, unfortunately, the accuracy of the reference fission yields from the existing libraries are not satisfied for the practical application so far, actually the discrepancy between these libraries for some reference yields is too large for the reactor physics application, it seems that much effort should be made in the evaluation and measurement of reference fission yields.

According to the CRP's requirement, the evaluation of reference fission yields have been and will be carried out in CNDC, as a part of the whole work (contract No.9504/R_0/Regular Budget Fund), the evaluation for 29 reference fission yields of 15 product nuclides from ^{238}U fission have been completed.

1 Data Analysis and Evaluation

1.1 Data Collection

All experimental data available up to now were collected, most of them were obtained from EXFOR master data library, some data were taken from the temporary EXFOR file, which were measured and compiled in China and haven't been merged into EXFOR master library. Some data were also collected from the publication concerned.

1.2 Data Selection

The EXFOR BIB information and papers concerned were read carefully and analysed in physics. The data were adopted or abandoned according to the measured date, method, facility, detector, monitor, data error and discrepancy situation with others. In general, the following data were abandoned:

a. The data measured is not required, for example, the data were measured at epithermal neutron source.

b. The data obtained by relatively measured, but their standards are not given. This is necessary especially for the evaluation of 'reference yield', the 'standard data' could not be based on the other standards, it will introduce more uncertainty.

c. Large discrepancy with others and measured method is not reliable or no information given in detail.

d. The data measured in fifties or earlier especially there are existing large discrepancy with others.

1.3 Error Estimate

The experimental error is a very important parameter in the analysis of data. Experimentalists report the errors in a variety of ways. Usually the fission yield value is reported together with the absolute accuracy that includes all of the uncertainties in the measurement, but some with a standard deviation corresponding to the precision of the measurement only, and some even no at all. So the reported errors sometimes should be adjusted to a reasonable level of the absolute accuracy.

For different measurement techniques, the different adjusting limits are set. No data are allowed to be more accurate than these limits.

For the absolute measurement, the adjusting limits are set as follows:

15% ~ 20% for Geiger-counter measurement pre-1960;

8% ~ 15% and 6% ~ 8% for NaI(Tl) measurement pre-1965 and after 1965, respectively;

4% ~ 8% for radiochemical measurement with GeLi detector;

3 % ~ 6% for Ge(Li) direct gamma-ray spectrometry measurement;

1% ~ 3% for mass spectrometry measurement.

For the ratio measurement, the adjusting limits are set as follows:

5% ~ 6% for Geiger-counter measurements;

3% ~ 5% for radiochemical measurements;

2% ~ 3% for Ge(Li) direct gamma-ray spectrometry measurements;

1% ~ 2% for mass spectrometry measurements.

1.4 Data Correction

The data were corrected for standard yield data, (intensity, fission cross section, and standard cross section used for neutron flux monitor such as Al(n,α) cross section if necessary.

1.4.1 Standard Fission Yield

As mentioned above, in general case, the fission yield obtained by relatively measured were not directly adopted, only the data taken ^{99}Mo(F,H) from ^{238}U and ^{135}Xe(F), ^{140}La(T) from ^{235}U as standards were adopted, for which the fission yield data have just been evaluated by us[1], respectively. And these relatively measured yield were corrected by using these newly standard data.

1.4.2 Gamma intensity

If the γ intensity used is given by an author, the data were corrected by using following new intensity data in order: evaluated decay data at CNDC, Table of Radioactive Isotopes, ENDSF computer library.

1.4.3 Fission Cross Section and other Standard Cross Section

If the fission cross section and standard cross section used for neutron flux monitor were given by the author of the measurement, the fission yields were corrected by using the new cross sections taken from ENDF/B-6.

2 Data Processing

After making the selection, analysis, and correction of the experimental data as mentioned above, all the adjusted experimental data were obtained, then the data processing was made. The method for data processing are the same as the fission yields evaluation of ^{235}U, the more detail please refer to the "Fission Yield Data Evaluation System-FYDES" by Liu Tingjin, here only the important content are repeated.

2.1 Data Average

If only the absolute yield are existing and there are several measurement data sets with the same incident neutron energy, target and product nuclide, the data are averaged with code AVERAG.

For a set of n measurements of value x_i and assessed standard deviation Δx_i, the following averages and the errors are calculated:

Weighted means yield

$$y_w = \frac{\sum_{i=1}^{n} \frac{1}{(\Delta x_i)^2} x_i}{\sum_{i=1}^{n} \frac{1}{(\Delta x_i)^2}}$$

The internal and external standard deviations are, respectively:

$$\sigma_1 = \sqrt{\frac{1}{\sum_{i=1}^{n} \frac{1}{(\Delta x_i)^2}}}$$

and

$$\sigma_2 = \sigma_1 \varepsilon = \sigma_1 \sqrt{\frac{\sum_{i=1}^{n} \frac{(x_i - y_w)^2}{(\Delta x_i)^2}}{n-1}}$$

A useful test of the consistency of the data is the χ^2 test:

$$\chi^2 = \sum_{i=1}^{n} \frac{(x_i - y_w)^2}{(\Delta x_i)^2} \Big/ n-1$$

The weighted mean yield was taken as the recommended value, and its error was taken to be the σ^2.

2.2 Simultaneous Evaluation

If there are several absolute fission yields and their ratio measurements for some product nuclides at the same energy and target, in order to avoid the introduction of other 'standards', the simultaneous evaluation is necessary, and is completed with the code ZOTT, taking account of measured absolute fission yields, their ratios and the measured errors as well as their correlations, making them consistent. In order to avoid too complicated, in the case of existing several absolute yields or ratio values for the same product nuclide, the data should be averaged with code AVERAG before the simultaneous evaluation, then the weighted means were used for the input data of code ZOTT. Using this code, not only the adjusted fission yields and ratios, but also their covariance matrix can be calculated.

3 Result, Comparison and Discussion

The evaluated results are as shown in Table 3.

3.1 The Errors of Evaluated Data

For the total 35 evaluated fission yield values in the Table 3, we can see that the errors are smaller than 3% for 29 values, 3.1% ~ 5% for 5, and the largest one is 5.2%.

Comparison with the main libraries, our errors are as the same level as those of ENDF/B-6. The CENDL-FY(87) and JEF-2/FY are in another same error level, and much larger than both present work and ENDF/B-6, the distribution of error for the main libraries are as shown in Table 4. No data errors were given in JENDL-3/FY.

Table 3 The results of evaluation for reference yield from ^{238}U fission

Nuclide	Energy	FY	Error	Data Sets*	Processed
^{92}Sr	F	4.4403E+00	1.0979E-01	2(2)	A S
	H	3.9440E+00	8.2076E-02	4(3)	A S
^{97}Mo	F	5.6021E+00	3.8838E-02	3(2)	A S
	H	5.4470E+00	9.7386E-02	3(1)	A S
^{103}Ru	F	6.0778E+00	5.8911E-02	8(4)	A S
	H	4.6604E+00	9.0389E-02	6(4)	A S
^{106}Ru	F	2.3922E+00	1.0967E-01	2(1)	A S
	H	2.5478E+00	1.1710E-01	2	A
^{131}I					
	H	3.8538E+00	6.7381E-02	5(2)	A S
^{133}I					
	H	5.9714E+00	9.6900E-02	6(3)	A S
^{131}Xe	F	3.2330E+00	6.9613E-02	4(2)	A S
	H	3.8143E+00	1.4630E-01	3	A
^{134}Xe					
	H	6.4616E+00	1.0870E-01	4	A S
^{135}Xe	F	6.7282E+00	1.5930E-01	6	A
	H	5.8049E+00	1.2020E-01	6	A
^{133}Cs	F	6.7631E+00	7.1388E-02	2(2)	A S
	H	6.0174E+00	1.6800E-01	2	A
^{137}Cs	F	5.9376E+00	5.0172E-02	4	A S
	H	5.1737E+00	1.8120E-01	4	A
^{140}Ba	F	5.8798E+00	3.5758E-02	12(1)	A S
	H	4.5693E+00	5.3390E-02	7	A S
^{140}La	F	5.8948E+00	8.8467E-02	3(2)	A S
	H	4.6529E+00	1.3010E-01	3	A
^{143}Nd	F	4.5338E+00	3.2080E-02	4(3)	A S
	H	4.1917E+00	1.1580E-01	4	A
^{145}Nd	F	3.7548E+00	3.2806E-02	2(1)	A S
	H	3.0894E+00	1.6000E-01	1	
^{148}Nd	F	2.1015E+00	1.8580E-02	3(1)	A S
^{147}Sm	F	2.5266E+00	3.0405E-02	2(2)	A S
	H	2.0365E+00	5.3261E-02	3	A S
^{149}Sm	F	1.5850E+00	1.9000E-02	2	A
	H	1.2038E+00	3.4174E-02	1(1)	S
^{151}Sm	F	7.8691E-01	2.4570E-02	2(2)	A S
	H	6.5409E-01	1.7017E-02	1(1)	S
^{152}Sm	F	5.2168E-01	5.7700E-03	2	A

Meaning of the symble in the table:

* Number of absolutely measured data sets, and the number of ratio measured data sets in parentheses ( )

A The average with weight

S Simultaneous evaluation

F Fission spectrum average

H High energy (around 14 MeV)

Table 4 The comparison of error distribution for main libraries

Libraries	Data Sets for Different Errors Arange							
	<1.0%	1.1%~2%	2.1%~3%	3.1%~5%	5.1%~7%	7.1%~9%	9.1%~20%	>20%
This work	7	11	11	5	1	0	0	0
ENDF/B-6	9	19	4	2	1	0	0	0
CENDL-FY(87)	1	8	4	8	3	3	1	7
JEF-2/FY	0	1	6	9	5	7	7	0

3.2 Comparison and Discussion

The present evaluated data were also compared with the ENDF/B-6, JENDL-3/FY, CENDL-FY(87), and JEF-2/FY. It was found that the present evaluated data are in good agreement with other main libraries for most nuclides within the quoted error limits. But for ^{97}Mo(H), ^{143}Nd(H), ^{149}Sm(H), and ^{151}Sm(H), the present evaluated data are obviously larger or smaller than those of other libraries. It should be emphasized that present evaluated data reflect the existing experimental data for ^{97}Mo(H)[2,3], ^{143}Nd(H)[2~5], ^{149}Sm(H)[3,6], and ^{151}Sm(H)[2,6], and these experimental data are in good agreement with each other for each product nuclide, a typical example is ^{151}Sm(H), present evaluated value is 0.6541, which is obviously smaller than the value about 0.8000 of other libraries as shown in Table 5, but there are existing two experimental data sets for ^{151}Sm(H), one absolute measurement is 0.6310[2], another ratio measurement(^{151}Sm/^{147}Sm) is 0.322[6], if taking the value for ^{147}Sm as 2.0365 of our new evaluated data (which is in good agreement with those of other libraries), then the absolute value is 0.6558 deduced from this ratio measurement, so comparing these two experimental data sets with present evaluated data, our evaluated data for ^{151}Sm(H) seems more reasonable than those of other libraries. Anyway, the fission yields for these reference product nuclides should be studied further based on more new experimental data.

4 Conclusion

The 35 cumulative fission yield for ^{238}U were evaluated based on the available experimental data up to now by using weighted average code AVERAG and simultaneous evaluation code ZOTT, only absolute yield and ratio measurements were used, i.e., no other standard yields were introduced in present evaluation. Among the 35 fission yields, 29 values are the reference fission yields required by the RCP's contract, no evaluated data for ^{152}Sm(H) was obtained due to no experimental data available, the others are needed for present simultaneous evaluation and also listed here.

Table 5 Comparison of evaluated reference fission yields for ^{238}U with other main libraries

Nuclide	Libraries	F	H
^{92}Sr	This work	4.4403±0.1098	3.9440±0.0821
	ENDF/B-6	4.3123±0.1207	3.8760±0.1085
	JENDL-3/FY	4.5092	3.9095
	CENDL-FY(87)	4.2896±0.1861	3.9739±0.2940
	JEF-2/FY	4.2263±0.0795	3.7811±0.2387
^{97}Mo	This work	5.6021±0.0388	5.4470±0.0974
	ENDF/B-6	5.5625±0.0389	5.2800±0.0739
	JENDL-3/FY	5.5746	5.3738
	CENDL-FY(87)	5.4706±0.0711	5.2373±5.2334
	JEF-2/FY	5.5235±0.5866	5.2497±0.5974
^{103}Ru	This work	6.0778±0.0589	4.6604±0.0904
	ENDF/B-6	6.2753±0.0879	4.6158±0.0923
	JENDL-3/FY	6.2096	4.6250
	CENDL-FY(87)	6.3122±0.1112	4.5116±0.1625
	JEF-2/FY	6.0728±0.2251	4.4617±0.4805
^{106}Ru	This work	2.3922±0.1097	2.5478±0.1171
	ENDF/B-6	2.4897±0.0349	2.4546±0.0687
	JENDL-3/FY	2.5311	2.4570
	CENDL-FY(87)	2.6260±0.1122	2.4274±0.2189
	JEF-2/FY	2.5491±0.2727	2.5004±0.1949
^{131}I	This work		3.8538±0.0674
	ENDF/B-6		3.9925±0.0798
	JENDL-3/FY		4.0449
	CENDL-FY(87)		3.7999±0.2027
	JEF-2/FY		3.8261±0.0997
^{133}I	This work		5.9714±0.0969
	ENDF/B-6		5.9999±0.0384
	JENDL-3/FY		6.1263
	CENDL-FY(87)		6.0199±0.1501
	JEF-2/FY5.7		440±0.3223
^{131}Xe	This work	3.2330±0.0696	3.8143±0.1463
	ENDF/B-6	3.2908±0.0329	3.9925±0.0559
	JENDL-3/FY	3.2386	4.0449
	CENDL-FY(87)	3.2035±0.0384	3.9860±0.1096
	JEF-2/FY	3.3041±0.0746	3.8257±0.0997
^{134}Xe	This work		6.4616±0.1087
	ENDF/B-6		6.4531±0.1291
	JENDL-3/FY		6.5541
	CENDL-FY(87)		6.5986±5.4260
	JEF-2/FY		6.1386±0.2162
^{135}Xe	This work	6.7282±0.1593	5.8049±0.1202
	ENDF/B-6	6.9676±0.0697	5.8393±0.1168
	JENDL-3/FY	6.8109	5.8186
	CENDL-FY(87)	6.6363±0.4964	5.9361±0.1455
	JEF-2/FY	6.5680±0.4936	5.4620±0.3320
^{133}Cs	This work	6.7631±0.0714	6.0174±0.1680
	ENDF/B-6	6.7610±0.0338	6.0172±0.0842
	JENDL-3/FY	6.6062	6.1449
	CENDL-FY(87)	6.6924±0.3416	6.1495±6.1503
	JEF-2/FY	6.7252±0.1698	5.7441±0.1200
^{137}Cs	This work	5.9376±0.0502	5.1737±0.1812
	ENDF/B-6	6.0525±0.0605	5.1460±0.1441
	JENDL-3/FY	6.0907	4.9857
	CENDL-FY(87)	5.9669±0.2089	5.0688±0.2273

Nuclide	Libraries	F	H
^{137}Cs	JEF-2/FY	6.0045±0.2499	5.6732±0.5332
^{140}Ba	This work	5.8798±0.0358	4.5693±0.0534
	ENDF/B-6	5.8152±0.0407	4.6070±0.0645
	JENDL-3/FY	5.9882	4.6523
	CENDL-FY(87)	5.9284±0.0629	4.5684±0.1022
	JEF-2/FY	5.7428±0.4118	4.7048±0.2238
^{140}La	This work	5.8948±0.0885	4.6529±0.1301
	ENDF/B-6	5.8153±0.0407	4.6112±0.0646
	JENDL-3/FY	5.9882	4.6525
	CENDL-FY(87)	6.0336±0.2173	4.8061±0.2256
	JEF-2/FY	5.7428±0.4118	4.7049±0.2237
^{143}Nd	This work	4.5338±0.0321	4.1917±0.1158
	ENDF/B-6	4.6221±0.0324	3.9087±0.0782
	JENDL-3/FY	4.5666	3.9229
	CENDL-FY(87)	4.5375±0.1803	3.9333±3.9298
	JEF-2/FY	4.8241±0.4089	3.9586±0.1140
^{145}Nd	This work	3.7548±0.0328	3.0894±0.1600
	ENDF/B-6	3.8090±0.0267	3.0038±0.1202
	JENDL-3/FY	3.7559	3.0060
	CENDL-FY(87)	3.7550±0.0352	2.9807±2.9787
	JEF-2/FY	3.8920±0.1578	2.9195±0.1954
^{148}Nd	This work	2.1015±0.0186	
	ENDF/B-6	2.1125±0.0148	
	JENDL-3/FY	2.0816	
	CENDL-FY(87)	2.0944±0.0356	
	JEF-2/FY	2.2791±0.1520	
^{147}Sm	This work	2.5266±0.0304	2.0365±0.0533
	ENDF/B-6	2.5927±0.0181	2.0912±0.0418
	JENDL-3/FY	2.5298	2.0970
	CENDL-FY(87)	2.5149±0.0387	2.0617±0.2396
	JEF-2/FY	2.6632±0.0837	2.1715±0.2190
^{149}Sm	This work	1.5850±0.0190	1.2038±0.0342
	ENDF/B-6	1.6253±0.0163	1.4582±0.0875
	JENDL-3/FY	1.6076	1.4227
	CENDL-FY(87)	1.5866±0.1083	1.4303±1.4291
	JEF-2/FY	1.6647±0.0722	1.3409±0.1068
^{151}Sm	This work	0.7869±0.0246	0.6541±0.0170
	ENDF/B-6	0.7994±0.0112	0.8015±0.0321
	JENDL-3/FY	0.8006	0.8014
	CENDL-FY(87)	0.7991±0.0136	0.8169±0.8163
	JEF-2/FY	0.8091±0.0293	0.7872±0.0757
^{152}Sm	This work	0.5217±0.0058	
	ENDF/B-6	0.5302±0.0053	
	JENDL-3/FY	0.5208	
	CENDL-FY(87)	0.5192±0.0093	
	JEF-2/FY	0.5499±0.0394	

References

[1] Liu Tingjin, Commun. of Nuclear Data Progress, Vol. 18(1997)
[2] Liu Conggui et al., Chinese Journal of Nuclear Physics, Vol. 7 No. 3, 235(1985)
[3] S. Darocyz, Atomki Kozlemenyek, 18, 317(1976)
[4] D. J. Gorman et al., Can. J. Chem., 46, 1663(1968)
[5] O. Birgul, Radiochimica Acta, 16, 104(1971)
[6] D. R. Nethaway, Journal of Inorganic and Nuclear Chemistry, 43, 889(1981)

Fission Yield Data Evaluation System FYDES

Liu Tingjin
(China Nuclear Data Center, CIAE)

Introduction

The retrieval and processing for fission yield data evaluation are quite complicated, and differ from the general complete set of neutron data evaluation in the following aspects:

1) The data in EXFOR file could be under the heading "ELEM/MASS";
2) There are more relative ratio measured data, and the data could be R-value;
3) More data need to be corrected for standard yield, gamma intensity and fission cross section and calculated from ratio or R-value;
4) For most cases, the dependence of yield on neutron energy seems linear.

Taking account of above features of fission yield data, to do the fission yield data evaluation conveniently, a fission yield data evaluation system FYDES has been developed for last two years.

1 Outline of the System

The main diagram of FYDES is shown in Fig.1.

The data are retrieved from the EXFOR Master Library with EXFOR Library Management System according to the reactions, producing EXFOR data and their index files *.EXFOR and *.INDEX, and sometimes also with code NEXFOR according to the entry (subentry) number.

The data tables with columns less than six are firstly standardized by using code FORM, producing standard data file *.FOM and then taken out with code FYRET, producing data file *.TAB. The data tables with columns more than six are firstly taken out with code FYRETD and then standardized by using code FYDEXCH. The necessary corrections are made by means of codes FYCRECT (less six columns), or FYCRECTD (more than six columns), producing data file *.CRE and FYCRECT1 (second time if needed). Then the data are retrieved by code FYRET1 according to product nuclides, producing data file *.DAT.

If there are some measurements at same energy point, they are averaged by using code AVERAG and if there are some fission yield and their ratio measurements at the same time, they are simultaneously evaluated with code ZOTT, producing data file *.PRO.

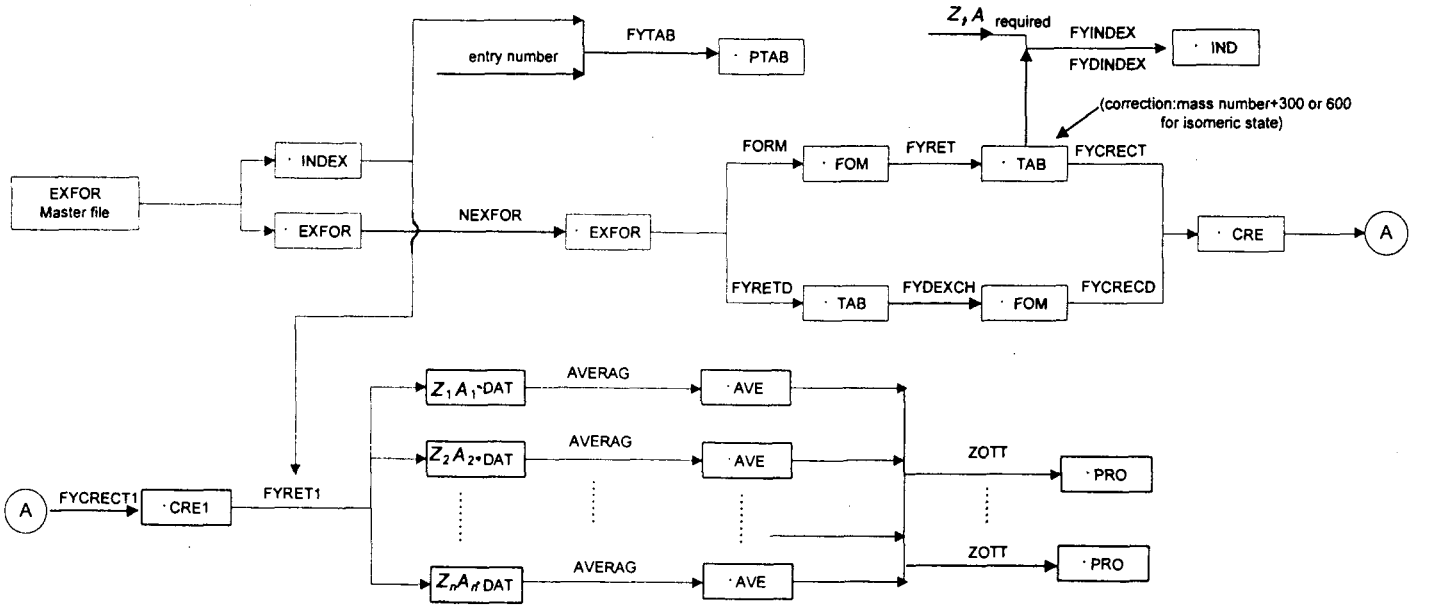

Fig.1 The main diagram of fission product yield data processing

If it is needed to give out the dependence of the yield on neutron energy, the data can be fitted by using code LIFIT with options of $y = aE+b$ or $y = y * \exp(aE)$. If the linear function could not fit the data well, then the data can be fitted with code SPF for any shape curve.

There are also some auxiliary codes FYINDEX, FYDINDEX for making index list of the product nuclides in each EXFOR subentry and FYTAB to make index table for abstract recording.

2 Data Retrieval and Data Table Standardization

The FY data can be retrieved according to the target, incident neutron energy and products by using EXFOR retrieval system. However when a product is given under the heading "ELEM/MASS", it could not be found.

To solve this problem, some supplementary programs were developed and they can be used following the retrieving by EXFOR system "RETREV", "COFFEE-CS" in the option "P" and default to the reaction field 4 (reaction product).

1) FORM[1] Exchange the column position and make the data table standardization:

Column	1	2	3	4	5	6
	Z	A	DATA	DATA-ERR		

Also make the "DATA-ERR" become absolute error.

2) FYRET Take the data table from each subentry in EXFOR data file.

3) FYRET1 Retrieve FY data according to the special Z and A, and read the reaction quantity, neutron energy, EXFOR entry number from the index file and write into the file.

If the quantities in a "HEADING" are over six (take two rows), instead of above, the following programs can be used:

4) FYRETD take out the data table.

5) FYEXC Exchange the column position and make the data table standardization.

6) FYRET1D Retrieve FY data according to Z and A.

The following should be noted, when use these codes:

(a) If the FY data are given for more than one energy point in an entry, the energy given in the retrieved data file is only maximum one.

(b) Due to there is no other function (only exchanging column position), the error in the file processed by FYRET1D may be relative or only statistical one and must be treated by following codes FYCRECT and FYCRECT1.

3 Data Correction, Codes FYCRECT and FYCRECT1

Table 1 Some examples of running code FYCRECT and FYCRECT1

13097003	11	(FY CALCULATED FROM Ro, ERR 7% GIVEN)			
ELEMENT	MASS	FY DATA	FY ERR		
NO—DIM	NO—DIM	PC/FIS	PC/FIS		
36.0	93.0	0.075	0.0I0		
36.0	94.0	1.500E—02	5.000E—03		
36.0	97.0	0.000E+00	0.000E+00		
37.0	91.0	0.930	0.050		
54.0	138.0	9.570E—01	2.000E—03		
55.0	139.0	9.880E—01	3.000E—03		
55.0	140.0	0.934	0.026		
55.0	141.0	4.245	0.297		
56.0	141.0	9.964E—01	1.700E—03		
56.0	142.0	9.810E—01	5.000E—03		
57.0	143.0	9.956E—01	3.000E—03		
13116002	6	(FY CORRECTED FOR GAMMA INTENSITY)			
ELEMENT	MASS	FY CREC	ERR CREC	FY ORIG	Irn/Ir0
NO—DIM	NO—DIM	PC/FIS	PC/FIS	PC/FIS	NO—DIM
36.0	85.0	3.989E—03	0.000E+00	3.980E—03	9.977E—01
63.0	156.0	7.247E—04	0.000E+00	5.140E—04	7.092E—01
65.0	161.0	4.932E—05	0.000E+00	4.090E—05	8.293E—01
36.0	85.0	4.009E—03	0.000E+00	4.000E—03	9.977E—01
63.0	156.0	7.543E—04	0.000E+00	5.350E—04	7.092E—01
65.0	161.0	5.282E—05	0.000E+00	4.380E—05	8.293E—01
13174002	3	(FY CORRECTED FOR GAMMA INTENSITY)			
ELEMENT	MASS	FY CREC	ERR CREC	FY ORIG	Irn/Ir0
NO—DIM	NO—DIM	PC/FIS	PC/FIS	PC/FIS	NO—DIM
36.0	85.0	3.197E—03	3.000E—05	3.190E—03	9.977E—01
63.0	156.0	2.975E—04	2.000E—06	2.110E—04	7.092E—01
65.0	161.0	2.894E—06	1.300E—07	2.400E—06	8.293E—01
13202002	3	(FY CALCULATED FROM RATIO AND STANDARD)			
ELEMENT	MASS	FY DATA	ERR CALC	REL ERR	
NO—DIM	NO—DIM	PC/FIS	PC/FIS	PER—CENT	
36.0	84.0	9.963E—0I	1.993E—02	2.00	
36.0	85.0	2.890E—01	5.780E—03	2.00	
36.0	86.0	1.948E+00	3.896E—02	2.00	
		(FY ERROR CALCULATED FROM GIVEN *c*%)			
13207002	7	(FY CALCULATED FROM RATIO AND STANDARD)			
ELEMENT	MASS	FY DATA	ERR CALC	REL ERR	
NO—DIM	NO—DIM	PC/FIS	PC/FIS	PER—CENT	
37.0	89.0	5.130E+00	7.695E—02	1.50	
37.0	90.0	4.628E+00	6.942E—02	I.50	
37.0	91.0	5.576E+00	8.364E—02	1.50	
37.0	92.0	5.075E+00	7.612E—02	1.50	
37.0	93.0	3.904E+00	5.856E—02	1.50	
37.0	94.0	1.952E+00	2.928E—02	1.50	
37.0	95.0	8.360E—0I	1.254E—02	1.50	
		(FY ERROR CALCULATED FROM GIVEN *c*%)			

The data were corrected by using codes FYCRECT and FYCRECT1, The functions and options for these codes are as follows:

1) Calculate absolute fission yield and its error from given ratio, standard and their errors;

2) Calculate ratio and its error from given *R*-value, standard fission yields and their errors at energy points to be measured and thermal;

3) Calculate ratio and its error from given fission yield, standard and their errors used;

4) Correct for standard fission yield and fission cross section;

5) Correct for gamma intensity used;

6) Calculate absolute error from given relative error;

7) Calculate absolute error from given relative error *c*% for the errors less than *c*%;

8) Calculate absolute error from given relative error in 4th column of the Table;

9) Calculate absolute total error from given absolute error1 and error2 in the Table;

10) Calculate absolute error from given absolute error1 in the data table and given additional relative error 2 (all the same).

The functions of two codes are the same, but FYCRECT1 is interfaced with FYCRECT and keeps the information written by FYCRECT.

An example of data correction is shown in Table 1, which was taken from the reference fission yield data evaluation.

4 Data Averaging, Code AVERAG

The data are averaged with code AVERAG. The mean with weight and its external error are calculated.

$$\overline{Y}_{\mathrm{w}} = \sum_{i}^{N} W_i Y_i \Big/ \sum_{i}^{N} W_i$$

$$\Delta \overline{Y}_{\mathrm{ex}} = \begin{cases} \varepsilon \Delta \overline{Y}_{\mathrm{in}} & (\varepsilon \geq 1) \\ \Delta \overline{Y}_{\mathrm{in}} & (\varepsilon < 1) \end{cases}$$

$$\varepsilon = \left(\frac{1}{N-1} \sum_{i=1}^{N} W_i (Y_i - \overline{Y}_{\mathrm{w}})^2 \right)^{\frac{1}{2}} = \left(\chi^2_{\mathrm{red}} \right)^{\frac{1}{2}}$$

$$\Delta \overline{Y}_{\mathrm{in}} = \left(\frac{1}{W} \right)^{\frac{1}{2}}$$

Where $W_i = \Delta Y_i^2$ $\qquad W = \sum_{i=1}^{N} W_i$

It can be seen that the errors given for each set of data and the discrepancy between the data sets are taken into account. In general case, the mean with weight and its external error are recommended.

The reduced χ^2 and internal error, and their arithmetical mean and its error are also calculated for reference.

An example of using AVERAG is given in Table 2.

Table 2 An example of running code AVERAG

^{235}U CUMUL FY DATA FOR FP $Z = 56$ $A = 140.0$

Input Data

(FY—Fission yield, DY(A)—Absolute error of FY, DY(%)—Relative error of FY)

	FIS Y	DY(A)	DY(%)
12771005	5.8100E+00	3.4860E−01	6.0000E+00
13383002	6.3200E+00	9.4800E−01	1.5000E+01
13398002	6.1500E+00	9.2300E−01	1.5008E+01
13486002	6.2000E+00	6.2000E−01	1.0000E+01
21483002	6.3600E+00	4.5000E−01	7.0755E+00
22054002	6.2740E+00	9.0000E−02	1.4345E+00
30495002	6.2720E+00	3.1400E−01	5.0064E+00
32635003	6.2000E+00	3.9000E−01	6.2903E+00
32638003	6.2680E+00	1.4100E−01	2.2495E+00

****

Calculated Average Fission Yield WY with Weight

(WY—Average value with weight, EY(A)—External absolute error of WY, EY(%)—External relative error of WY, EY(I), EY(%)—Internal absolute and relative error of YP)

WY	6.2525
EY(A)	0.0692
EY(%)	1.1076
EY(I)	0.0692
EY(%)	1.1076
EPS	1.00000

****

Calculated Arithmetic Average Value AY

AY	6.2060
EY(A)	0.0539
EY(%)	0.8693

5 Simultaneous Evaluation, Code ZOTT

Simultaneous evaluation is completed with code ZOTT[2], taking account of measured absolute fission yields, their ratios and the measured errors as well as their correlations, making them consistent. Using partitioned least squares method, the

Table 3 An example of running code ZOTT

1) Input Data File			
NY, NB, IPRINT, ILOG, ICOV			
7 3 0 1 1			
COMBINED Y–VECTOR FOR ^{147,149,151,152}Sm. AT THERMAL			
2.1127 1.0212 0.40428 0.24893 2.106 0.3982 0.25063			
TOTAL ERROR AND CORRELATIVE ERROR			
0.02535 0.04801 0.004852 0.087446 0.03159 0.005973			
0.002899			
0.0			
SENSITIVITY (= *R*)			
1 –1 0 0			
0 –1 1 0			
0 –1 0 1			
2) Output Result(Part)			
COMBINED Y–VECTOR FOR ^{147,149,151,152}Sm			
2.112700E+00	1.021200E+00	4.042800E–01	2.489300E–01
2.106000E+00	3.982000E–01	2.506300E–01	
(the intermediate results were omitted)			
ADJUSTED Y'			
2.118375E+00	1.010102E+00	4.034757E–01	2.531572E–01
2.097189E+00	3.994406E–01	2.506254E–01	
APPROXIMATE RELCOV(Y') BY COV LN(Y') = COV(THETA')			
S.D.(Y')			
2.258691E–02	1.317217E–02	4.302739E–03	4.408931E–03
2.577328E–02	4.908932E–03	2.897379E–03	
ADJUSTED CORRELATION MATRIX			
1.000000E+00	4.772272E–01	2.277696E–01	3.569470E–01
3.612147E–01	–3.087407E–01	–5.830039E–04	
4.772272E–01	1.000000E+00	4.772781E–01	7.479621E–01
–6.470671E–01	–6.469486E–01	–1.221651E–03	
2.277696E–01	4.772781E–01	1.000000E+00	3.569851E–01
–3.088302E–01	3.613055E–01	–5.830661E–04	
3.569470E–01	7.479621E–01	3.569851E–01	1.000000E+00
–4.839805E–01	–4.838919E–01	6.628853E–01	
3.612147E–01	–6.470671E–01	–3.088302E–01	–4.839805E–01
1.000000E+00	4.186181E–01	7.904885E–04	
–3.087407E–01	–6.469486E–01	3.613055E–01	–4.838919E–01
4.186181E–01	1.000000E+00	7.903437E–04	
–5.830039E–04	–1.221651E–03	–5.830661E–04	6.628853E–01
7.904885E–04	7.903437E–04	1.000000E+00	

"microscopic" or "elementary" and "macroscopic" or "duplicated" quantities, For example, partial and total cross section, fission yield and its ratio etc., are adjusted to get the optimum values with minimum variance derivation. Using ZOTT, not only the adjusted fission yields and ratios, but also their covariance matrix can be calculated.

The key point for using ZOTT is to construct the sensitive matrix, which describe the relationship among the quantities in the input vector. From the application point of view, it can be keep in mind that the column number of matrix is equal to the number of 'elementary' or 'microscopic' quantities (absolute fission yields at present case), and row number is equal to the number of the 'duplicated or 'macroscopic' quantities (ratios at present case). Each element is equal to 1, −1, or 0, representing the numerator, denominator, or no relation in the ratio of the corresponding 'elemental' quantities, for example, if the first ratio $R_1 = FY_2/FY_3$, the elements at the first row of the matrix are equal to 0, 1, −1 respectively, if $R_2 = FY_3 / FY_1$, the elements in the second row are −1, 0, 1 respectively.

An example of using ZOTT is given in Table 3.

6 Data Fit Programs LIFIT and SPF

The data can be fitted with linear function by using code LIFIT with options for FY = $aE+b$ or ln(FY) = $aE+b$. By means of minimum squares method, the optimum fit coefficients:

$$a = 1/c(c_{22}A_1 - c_{12}A_2)$$
$$b = 1/c(c_{11}A_2 - c_{21}A_1)$$

Were

$$c = c_{11}c_{22} - c_{12}c_{21}$$

$$c_{11} = \sum_i W_i E_i^2 \qquad c_{12} = \sum_i W_i E_i$$

$$c_{21} = c_{12} \qquad c_{22} = \sum_i W_i$$

$$A_1 = \sum_i W_i Y_i E_i \qquad A_2 = \sum_i W_i Y_i$$

For the fitting with $y = y_0 e^{aE}$, let

$$y' = \ln(y) = aE + \ln(y_0) = aE + b$$

And in this case

$$\Delta y' = \Delta y / y$$

so, the coefficients a and b can be calculated according to above formulas, and then

$$y = e^{y'}$$

The reduced χ^2 is calculated

$$\chi^2 = \frac{1}{N} - 2\sum_{i=1}^{N}(Y_i - \hat{Y})/\Delta Y_i^2$$

which express the fit merit.

An example of LIFIT is given in Table 4 and Fig.2

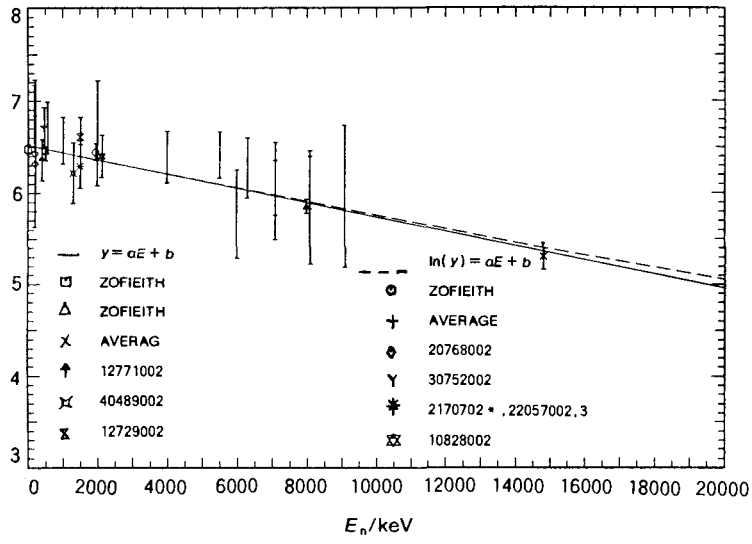

Fig.2 $^{235}U(n,f)^{95}Zr$ cumulative fission yield

Table 4 An example of running code LIFIT

1) Input File		
26	5	1
2.5300E−02	6.4791E+00	5.0450E−02
1.9500E+06	6.4431E+00	9.3610E−02
8.0000E+06	5.8503E+00	7.6130E−02
5.0000E+05	6.4301E+00	7.5500E−02
1.4800E+07	5.3062E+00	1.4480E−01
2.0000E+05	6.3200E+00	5.2000E−01
2.0000E+05	6.4300E+00	8.0000E−01
4.0000E+05	6.3600E+00	2.2430E−01
4.5000E+05	6.7100E+00	2.2000E−01
1.3000E+06	6.2170E+00	3.2800E−01
1.5000E+06	6.2900E+00	2.4000E−01
1.5000E+06	6.6100E+00	2.1000E−01
2.1300E+06	6.4000E+00	2.3000E−01
1.7000E+05	6.8100E+00	3.6000E−01
5.5000E+05	6.7100E+00	2.8000E−01
1.0000E+06	6.5700E+00	2.5000E−01
2.0000E+06	6.6500E+00	5.7000E−01

26	5	1
4.0000E+06	6.3900E+00	2.8000E−01
5.5000E+06	6.4100E+00	2.5000E−01
6.3000E+06	6.2700E+00	3.3000E−01
7.1000E+06	6.0500E+00	3.0000E−01
8.1000E+06	6.1400E+00	3.2000E−01
6.0000E+06	5.7638E+00	4.8000E−01
7.1000E+06	6.0188E+00	5.3000E−01
8.1000E+06	5.8106E+00	5.9000E−01
9.1000E+06	5.9630E+00	7.7000E−01

2.53E−02	1.95E+06	2.13+06	1.48E+07	2.00E+07

2) Output File

LN(Y)−LINEAR(E) FIT COEFFICIENTS a & b

($\ln(Y) = aE + b$ or $y = aE + \ln(y_0)$)

−1.2748E−08	1.8751E+00	6.5215E+00

****

FIT VALUES

2.5300E−02	6.5215E+00
1.9500E+06	6.3614E+00
2.1300E+06	6.3468E+00
1.4800E+07	5.4001E+00
2.0000E+07	5.0538E+00

REDUCED KSE SQARE

4.8481E−01

If the data can not be fitted well by LIFIT, for example $\chi^2 > 2.0$, the data can be fitted with code SPF[3], a general spline fitting program for multi-sets of data with knot optimization and spline order selection. It can be used for any shape curve.

An example of SPF is given in Fig.3

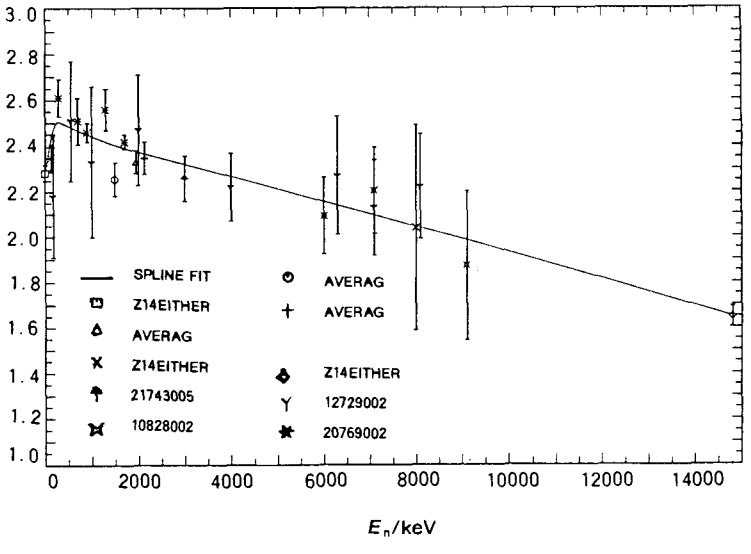

Fig.3 $^{235}U(n,f)^{147}Nd$ cumulative fission yield

References

[1] Liu Tingjin et al, Chinese Jou. of Nucl. Sci. And Eng., 1, 79(1988) (in Chinese)
[2] D. Muir, Nucl. Sci. & Eng., 101, 88(1989)
[3] Liu Tingjin, CNDP, 2, 58(1989)

CN9901237

Model Calculations for Fission Yields

Shu Nengchuan Liu Tingjin
(China Nuclear Data Center, CIAE)

Abstract

Multi-Gauss model and Zp model are used to calculate fission yields. The results are in well agreement with other data.

Introduction

The long-lived cumulative and chain yields measurements are more numerous and cover a wider range of fission system. In the mean while, they have more accurate data.

Even so, only for a limited set of fission system chain yield are well defined. The common features in this fission system is that in the valley region and at the wings of the chain distribution they have few available experiment data. It is necessary to use calculated data as a reference.

It is even worse for independent fission yields.

Here, Multi-Gauss fitting are used to fitting chain yield, and program Cyi based upon Multi-Gauss and Zp model are used to calculate cumulative and independent fission yields. The results show that most of the data are in agreement with our evaluated data[1~3] and ENDF/B-6 and experimental data.

1 Chain Yield Model and Fitting

The mass distributions of most nuclides' chain yields show some common features. It has a pair of approximately symmetrical peaks with a valley between

them (See Fig.1a and Fig.1b).

According to the empirical models, the mass distribution of chain yield can be described by[4]:

$$Y(A) = \frac{N_j}{\sqrt{2\pi\sigma_j^2}} \sum_{j=0}^{k} \exp\left(\frac{-(A - A_{0j})^2}{2\sigma_j^2} \right) \tag{1}$$

Where:

$Y(A)$ — chain yield;

A — mass of product nuclide;

k — items of Gauss;

N, σ, A_0 — the Gauss's area, width and position respectively.

In this Multi-Gauss model, it is assumed that the curve should be symmetrical at $A = A'/2$ ($A' = A_f - \nu$, A_f is the compound nuclide mass, and ν is the average number of prompt neutron). According to this, some data were fitted in reference[4], and resulted to the reduced $\chi^2 \approx 40$. χ^2 defined as follows:

$$\chi^2 = \frac{1}{n-m} \cdot \sum_{i=1}^{n} \frac{(y_i^e - y_i^c)^2}{(\Delta y_i^e)^2} \tag{2}$$

n, m are the numbers of experiment data and parameters respectively; y_i^e, y_i^c are experimental and fitted data respectively; Δy_i is the experimental data error. If the χ^2 is smaller, the result is better; when it equals to 1 or so, it shows that the fitted curve is almost through within the errors of experimental data.

Actually, the experimental data is not so symmetrical. So we do without the assumption of symmetry, and resulted $\chi^2 \approx 7$ (See Fig.1 and Fig.2)

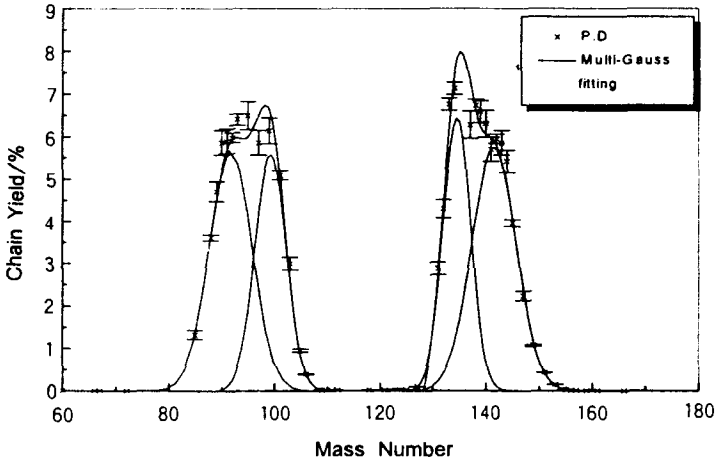

(a)

Fig.1 Multi-Gauss fitting for the chain yield of ^{235}U fission at thermal energy

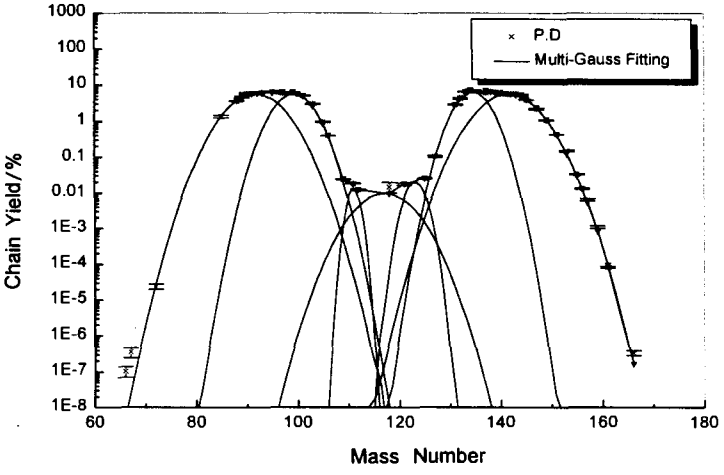

(b)

Fig.1 Multi-Gauss fitting for the chain yield of ^{235}U fission at thermal energy

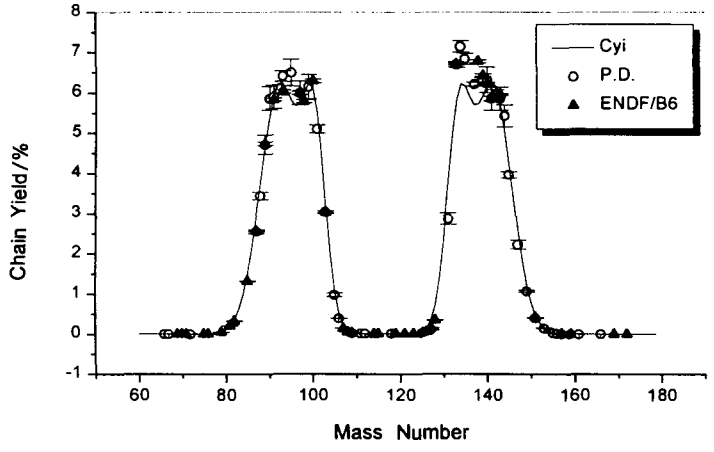

(a)

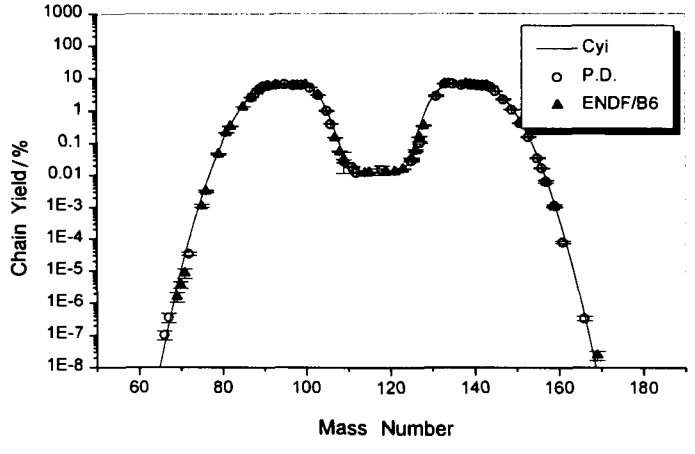

(b)

Fig.2 Cyi calculation for the chain yield of ^{235}U fission at thermal energy

2 Independent yield model

Cyi calculates the chain yield based upon Multi-Gauss model and fraction independent yield based upon *Z*p[4] model, and then calculates the cumulative yield according to the decay method of the mass chain.

*Z*p model are based upon the assumption of "unchanged charge distribution", the charge distribution of the compound nuclide has insufficient time to respond to the changes in the nuclide and thus the charge-to-mass ratio of the products of the post scission but pre-prompt neutron emission fragment of mass *A*, called *Z*p(*A*), is given by

$$Zp(A) = \frac{Z_f}{A_f} A \tag{3}$$

For a given *A*, the distribution of yield over *Z* as follows:

$$FI(A,Z) = \int_{Z-0.5}^{Z+0.5} \frac{1}{\sqrt{2\pi\sigma^2}} \exp\left(-\frac{(Z - Zp(A))^2}{2\sigma^2}\right) dZ \tag{4}$$

This Gaussian with a width σ is normalized to each mass chain.

Define:

$$\int_0^x (t) = \frac{1}{2} \mathrm{erf}\left(\frac{x}{\sqrt{2}}\right) \tag{5}$$

A. C. Whal[4] gave out a revised model:

$$FI(A,Z) = \frac{1}{2} F(A,Z) N(A) (\mathrm{erf}(V) - \mathrm{erf}(W)) \tag{6}$$

Where

$$V = \frac{Z(A) - Zp(A) + 0.5}{\sigma_Z(A)\sqrt{2}}$$
$$W = \frac{Z(A) - Zp(A) - 0.5}{\sigma_Z(A)\sqrt{2}} \tag{7}$$

F(A,Z) is the odd-even factor, *N(A)* is the factor of normalization.

Define *A'* as the fragment mass after prompt neutron emission:

$$Z_p(A_H) = A'_H \frac{Z_f}{A_f} + \Delta Z(A'_H) \tag{8}$$

Similarly:

$$Z_p(A_L) = A'_L \frac{Z_f}{A_f} + \Delta Z(A'_{Hc}) \tag{9}$$

A_H, A_L, A'_H, A'_L are the fragment masses before and after prompt neutron

emission, H and L are the indexes of heavy and low fragment masses respectively.

$A_f - A'_L = A'_{Hc}$, A_f, Z_f are the compound nuclide's mass and charge respectively.

$$A' = A - \nu(A) \tag{10}$$

$\nu(A)$ is the average of prompt neutron emission.

$\nu(A)$ and ΔZ can be resulted from experiment data analysis.

3 Calculations with Cyi[5] Program

In program Cyi, only three parameters are needed: charge Z and mass A of the compound nuclide, and the energy of the incident neutron E_n. The others have default values in a data file.

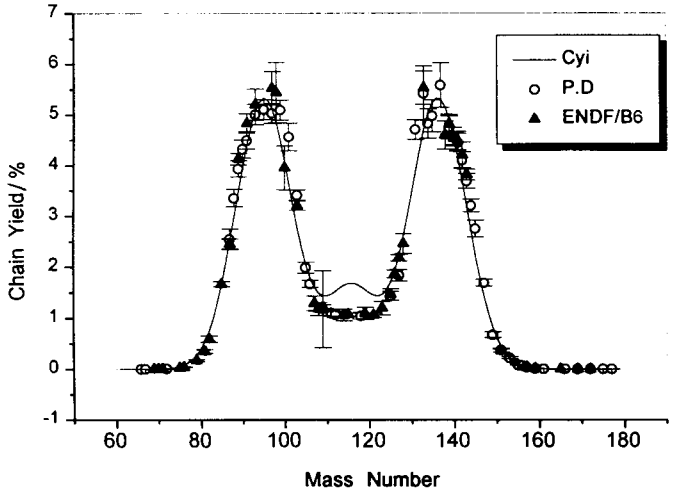

(a)

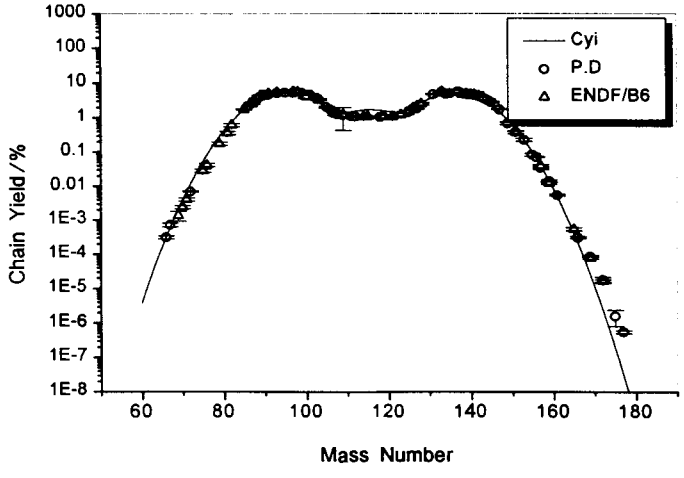

(b)

Fig.3 Cyi calculation for the chain Yield of ^{235}U fission at about 14 MeV

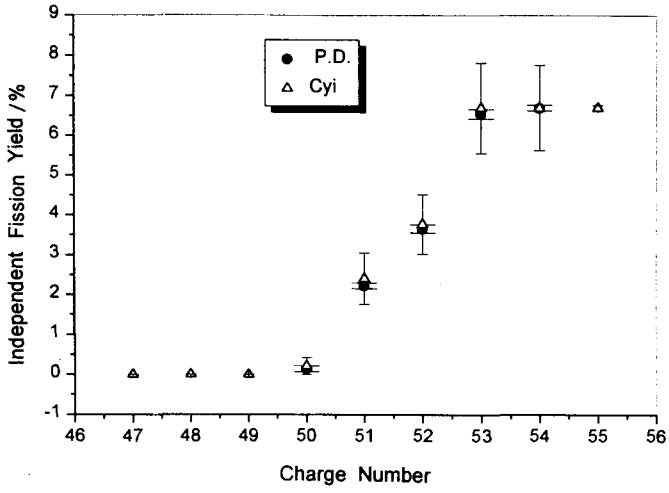

Fig.4 Cyi calculation for cumulative yield of ^{235}U fission at thermal energy (A = 133)

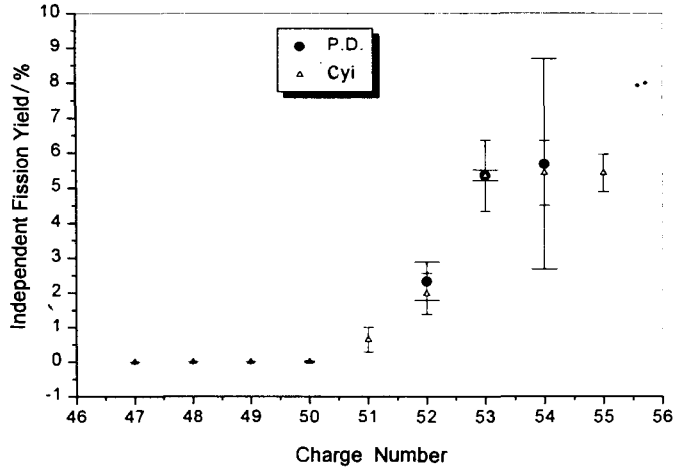

Fig.5 Cyi calculation for cumulative yield of ^{235}U fission at about 14 MeV (A = 133)

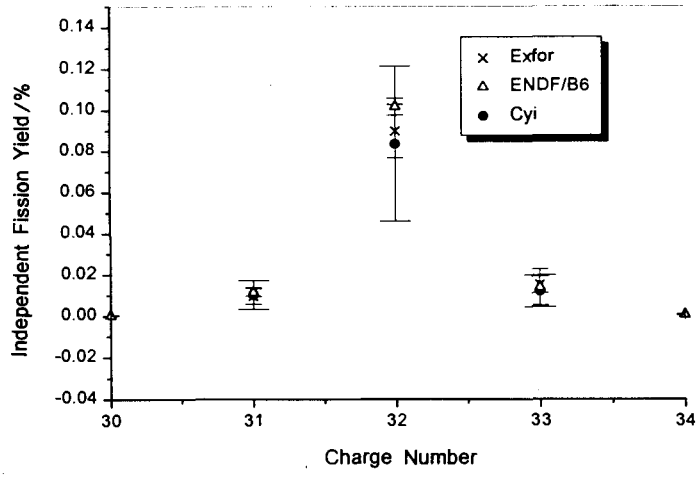

Fig.6 Cyi calculation for independent yield of ^{235}U fission at thermal energy (A = 80)

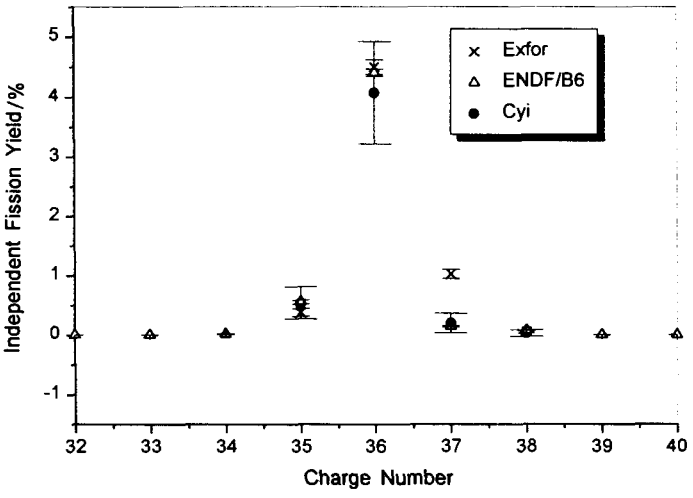

Fig.7 Cyi calculation for independent yield of ^{235}U fission at thermal energy (A = 90)

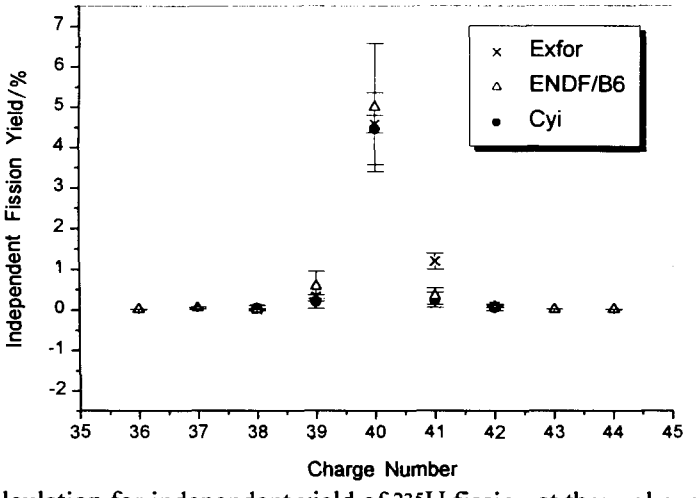

Fig.8 Cyi calculation for independent yield of ^{235}U fission at thermal energy (A = 100)

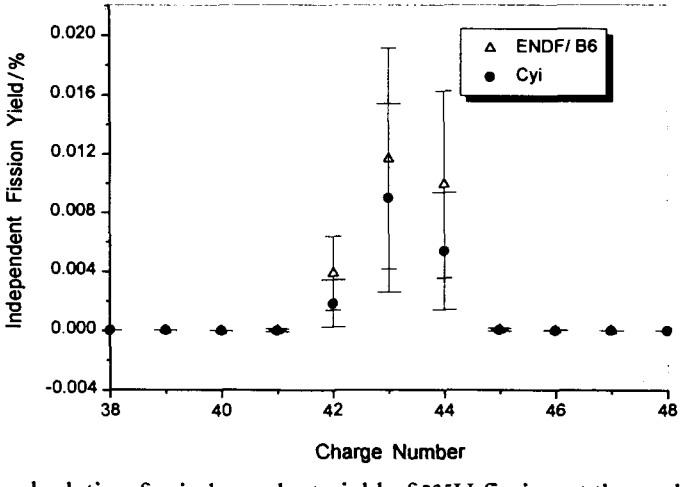

Fig.9 Cyi calculation for independent yield of ^{235}U fission at thermal energy (A = 110)

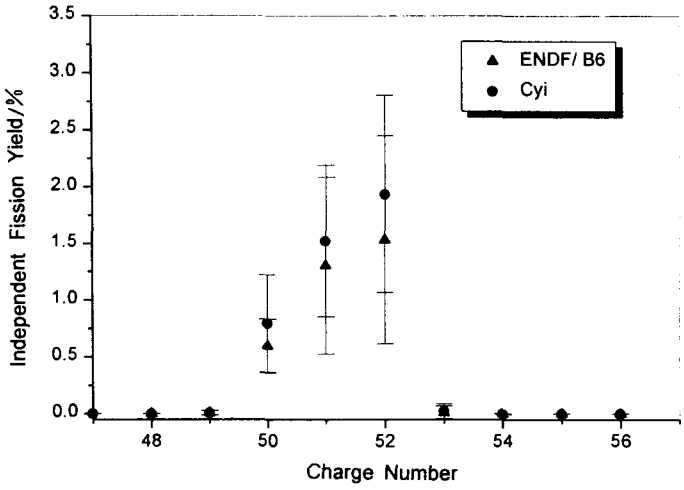

Fig.10 Cyi calculation for independent yield of ^{235}U fission at thermal energy (A = 132)

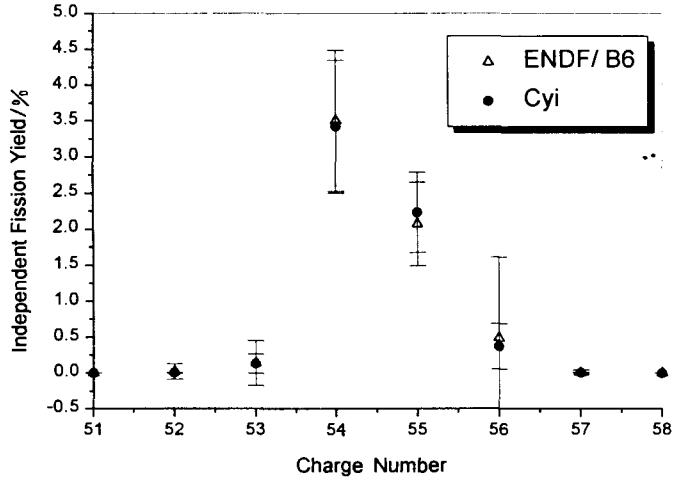

Fig.11 Cyi calculation for independent yield of ^{235}U fission at thermal energy (A = 140)

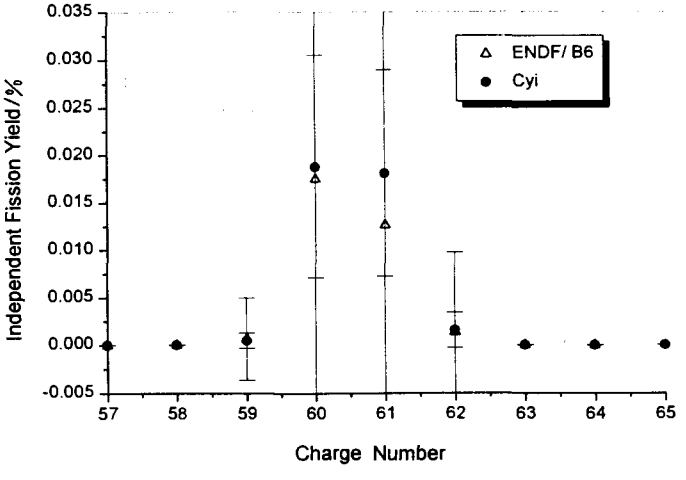

Fig.12 Cyi calculation for independent yield of ^{235}U fission at thermal energy (A = 155)

Except the fission-neutron induced fission yield data, the results of Cyi calculations give good agreement with other data (Fig.2 to Fig.12).

The symbol P.D in the figures (Fig.1 to Fig.5) refers the data recommend by Liu Tingjin[1~3] etc.

4 Conclusion

Multi-Gauss Model and Zp model are based upon semi-empirical theory, they are suited for calculation of varies of fission yields. However they should have their own parameters, which are from their experiment data.

The chain yield fitting or Cyi calculation based Multi-Gauss model, are well close to experiment data but can't describe some structures. For actual application, a spline fitting may be more suitable.

The independent and cumulative yield calculation of Cyi for thermal and 14 MeV neutrons are more reliable, the results well agreed to other data. However for the fission of fission spectrum neutron, the results need to be improved.

Acknowledgement

We appreciate Dr. A. C. Whal for providing us Cyi program and papers concerned, and Professor Liang Qicang, Cai Dunjiu, and Mr. Jin Yongli for their great help.

References

[1] Liu Tingjin etc., "Evaluation of fission yield for ^{235}U", to be published (1998.2)
[2] Liang Qicang etc., "Evaluation of fission yield for ^{238}U", to be published (1998.2)
[3] Cai Dunjiu etc., "Evaluation of fission yields for 64 nuclide of $^{239}Pu(n,F)$", to be published (1998.2)
[4] Robert William Mills, "Fission Yield evaluation". (Ph. D. Thesis, 1995)
[5] A. C. Wahl, Personal Communication (1997)

Evaluation and Calculation of Activation Cross Sections for ^{151,153}Eu(n,2n), (n,3n), (n,γ) and (n,x) Reactions below 20 MeV

Yu Baosheng Han Yinlu Gao Lan
(China Nuclear Data Center, CIAE)

Eu is a rare-earth element. Its activation cross section is important for nuclear science and technology applications. However, there are some discrepancies in several evaluated nuclear data libraries. The cross section for ^{151,153}Eu(n,2n) reactions were one of the Coordinate Research Programs of IAEA on activation cross sections for the generation of long-lived important radionuclides in fusion reactor technology. Recently, the measurements for ^{151,153}Eu(n,2n) and ^{151,153}Eu(n,γ) reactions were performed by CIAE and Peking University (PU). In this work, the activation cross sections for ^{151,153}Eu(n,2n), (n,3n), (n,γ) and some emission charged particle (n,x) reactions below 20 MeV were evaluated based on experimental and theoretical data. The results are compared with the experimental and other evaluated data from ENDF/B-6 and JENDL-3.

1 Evaluation and Analysis of Experimental Data

1.1 ^{151,153}Eu(n,2n), (n,3n) Reactions

^{153}Eu(n,2n)^{152}Eu Reaction

The cross section of ^{153}Eu(n,2n)^{152}Eu reaction is very useful for activation indicator application and waste disposal assessment of fusion reactor materials due to the half-lived of ^{152g}Eu 13.33 year. At present evaluation, much emphasis is on recommending accurate activation cross sections based on the newest measured and theoretically calculated data below 20 MeV. The new measured data were performed at CIAE and PU(Peaking University) in 1996.

The contamination from ^{151}Eu(n,γ)^{152}Eu reaction was very large if using natural sample. The measurements of ^{153}Eu(n,2n)^{152}Eu cross section are scarce. The existing measured cross sections are only for m1, m2 isomers or g state around 14 MeV, and there are large discrepancies. Therefore, the contamination from ^{151}Eu(n,γ)^{152}Eu reaction must be considered in the measurement. In the experiment of S. M. Qaim[1], the samples were oxide form of natural isotopic composition. Due to the exceptionally high ^{151}Eu(n,γ) cross sections for thermal and epitherimal neutrons, it was necessary to suppress the low-energy neutron contribution effects further. The samples were wrapped in 2 mm thick Cd foils. The neutrons up to 0.5 eV were eliminated. Furthermore, care was taken to minimize the scattering of neutrons in the

vicinity of the target. The presence of some neutrons in eV energy, however, can not be ruled out and may cause < 2% in (n,2n) cross sections. The $^{153}Eu(n,2n)^{152}Eu$ reaction to m1, m2 isomers, g state and total cross section were provided by S. M. Qaim[1] using activation method at 14.7 MeV. A. Reggoug[2] measured the cross sections to m1 and m2 isomers with Ge(Li) detector using X-ray spectroscope. The measured results seem same as S. M. Qaim[1].

Recently, the measurement for (n,2n) cross sections around 14 MeV have been performed by Lu Hanlin[3] et al. in the collaboration of CIAE, LNZ(Lanzhou University), PU by using intense neutron source from Cockrofe-Walton accelerator. The sample was made from natural oxide powder of Eu with purity better than 99%. Much emphasis were made for elimination of low-energy neutron effects and the corrections were carried out for scattered neutron, different excitation function shapes between standard reaction and reaction investigated, the interference of the gamma rays with energies close to that studied. A special experimental arrangement was made for scattered neutron correction. The measured value by S. M. Qaim[1] for $^{153}Eu(n,2n)^{152g}Eu$ reaction at 14.7 MeV was in good agreement with by Lu Hanlin[3]. Therefore, the ratio of $^{153}Eu(n,2n)^{152g}Eu$ / $^{153}Eu(n,2n)^{152}Eu$ at 14.7 MeV is reasonable.

Recently, final report[4] of IAEA CRP (Co-ordinated Research Program), edited by A. B. Pashchencko, provided the results for $^{153}Eu(n,2n)^{152g}Eu$ reaction (g state only) around 14 MeV from JAERI95, KRI 95, KRI 90 and CIAE 95. The measured results were performed by activation method with separated isotope sample in JAERI and KRI, the accurate cross sections were given. Based on these data, the cross section at 14.7 MeV for $^{153}Eu(n,2n)^{152}Eu$ reaction was reduced by using the ratio of g / tot from S. M. Qaim[1].

The evaluated experimental data at 14.7 MeV could be used to guide theoretical calculations.

$^{151}Eu(n,2n)^{150}Eu$ Reaction

The cross section were measured by S. M. Qaim[1] using activation method at 14 MeV and by J. Frehaut[5] using large Ge-loaded liquid scintillation detector from 8 to 14 MeV. Their measured data at 14 MeV were consistant with each other within errors. The data of J. Frehaut were re-normalized by using $^{238}U(n,f)$ cross section from ENDF/B-6. The evaluated data were obtained from threshold to 14 MeV. The experimental data available for $^{151,153}Eu(n,2n)$ reactions are shown in Table 1.

$^{151}Eu(n,3n)^{149}Eu$ Reaction

The data were measured by B. P. Bayhurst[6] with activation method from threshold to 25 MeV. The measured data can be used to guide theoretical calculation.

Table 1 Collected data and relevant information for ^{151,153}Eu(n,2n) reactions

Year	Author	E_n / MeV	Sample	Detector	n flux	Comments
1974	S. M. Qaim	14.7	Natural	Ge(Li)	^{27}Al(n,α)^{24}Na ^{75}As(n,2n)^{74}As	Measured ^{151}Eu(n,2n)^{150}Eu ^{153}Eu(n,2n)^{152}Eu (m1, m2, g state)
1980	J. Frehaut	8.2 ~ 14.7	Natural	STAN	^{238}U(n,f)	Measured ^{151}Eu(n,2n)^{150}Eu cross section
1990	A. A. Filatenkov	13.7 ~ 14.9	Separated Isotope	SCIN	^{27}Al(n,α)^{24}Na ^{93}Nb(n,2n)^{92m}Nb	Measured ^{152g}Eu state
1995	A. A. Filatenkov	13.52 ~ 14.9	Separated Isotope	SCIN	^{27}Al(n,α)^{24}Na ^{93}Nb(n,2n)^{92m}Nb	Measured ^{152g}Eu state
1995	Y. Ikeda	14.10 ~ 14.8	Separated Isotope	Ge(Li)	^{93}Nb(n,2n)^{92m}Nb	Measured ^{152g}Eu state
1995	Lu Hanlin	14.77	Natural	Ge(Li)	^{93}Nb(n,2n)^{92m}Nb	Measured ^{152g}Eu state

STANK (Liquid scintillator tank)
SCIN (Liquid scintillator)

1.2 ^{151,153}Eu(n,γ) Reactions

Table 2 Collected data and relevant information for ^{151,153}Eu(n,γ) reaction

Year	Author	E_n	Detector	n flux	comment
1958	N. J. Pattenden+	0.0253 eV	Crystal		Transmission Method
1960	R. B. Tattersall	0.0253 eV		B(n,ABS)	
1964	V. A. Konks	0.81 eV ~ 41.0 keV	PROPC Crystal	Pb(n,tot) Pb(n,sct)	Slowing-down-time Spectrometer
1968	V. A. Konks	0.84 eV ~ 42.0 keV	PROPC CRYSTAL		The Slowing-Down time in Lead
1971	F. Poortmans*	0.0253 eV	CRYSTAL		Deduced from thermal neutron temperature
1975	R. W. Hockenbury	6.3 ~ 297 keV	SCIN	^{10}B(n,α)	Pulse-Height and Time of Flight
1975	F. Widder	0.01 to 1.6 eV	Moxon-Rae		Time of Flight Method
1976	M. C. Moxon	10 ~ 100 keV	Moxon-Rae	^{10}B(n,α)	Averaged cross Sections. Time of flight
1977	V. N. Kononov	5 ~ 350 keV	STANK	^{197}Au(n,γ)	Time of flight
1979	M. Mizumoto	3 ~ 100 keV	STANK		Averaged Cross Sections, At Linac
1980	V. P. Vertebnyy	2.0 keV	PROPC	Pb(n,tot) Pb(n,sct)	Transmission Method, At Linac
1987	Yu. N. Trofimov*	1.0 MeV	Ge(Li)	^{197}Au(n,γ)	Activation Method
1987	D. M. Drake	3.0 ~ 2200 keV	SCIN		Averaged Cross Sections, At Linac 40.0 M
1987	V. A. Pshenichnny	1.4 MeV	Ge(Li)		^{252}Cf source
1993	Yu Weixiang	36 ~ 1120 keV	Ge(Li)	^{197}Au(n,γ)	Activation Method
1994	Xia Yijiu	22 ~ 1100 keV	HPGi(Li)	^{197}Au(n,γ)	Activation Method

STANK (Liquid scintillator Tank)
PROPC (Proportional Counter Filled with ^{3}He)
SCIN (Liquid Scintillator)
* Only Measured ^{151}Eu
\+ Only Measured ^{153}Eu

For the $^{151,153}Eu(n,\gamma)^{152,154}Eu$ reactions, there were experimental data[7~23] available at thermal energy point and in energy region from 0.01 eV to 2.20 MeV, they are shown in Table 2.

$^{153}Eu(n,\gamma)$ Reaction

The data were measured two times by V. A. Konks[9,10] using the slowing-down-time spectrometer in energy region of 0.85 eV to 41 keV in 1964 and 1968, respectively. The data were in very good agreement with R. W. Hockenbury[11] in energy region of 6.3 ~ 297 keV with liquid scintillator and M. C. Moxon[13] in 10 ~ 100 keV, as well as F. Widder[10] in 0.01 to 9.9 MeV with Moxon-Rac detector to measure the prompt γ ray for capture events. For the above measured date, the corrections were made for deadtime, background effects, monitor efficiency and multiple scattering.

From 1976 to 1980, the data were measured by V. N. Kononov[15] using STANK (liquid scintillator tank) in energy region 5 ~ 350 keV and by M. Mizumoto[16] in energy region 3 ~ 100 keV. The data using STANK were systematically higher than above ones, 7.2% at 10 keV and 12% at 100 keV. The reason may be background and multiple scattering effects. Another measured data by V. P. Vertebnyy[17] are strange lower than other one at 2.0 keV, so they are rejected in this evaluation.

In order to check the discrepancy of these measured data, after the 1980s some measurements were made by D. M. Drake[18], Yu Weixiang[19] and Xia Yixiang[20]. The data in energy region of 3 ~ 2200 keV were measured by D. M. Drake[18] with time of flight spectrometer at Linac in 1987. The cross sections were measured by Yu Weixiang[19] of the China Institute of Atomic Energy in energy region 36 ~ 1120 keV in 1993, and by Xia Yijiu[20] of Sichuan University (SCIU), cooperated with CIAE, in energy region 22 ~ 1100 keV with same method in 1994, using 4.5 MV Van de Graaff accelerator with the $T(p,n)^3He$ and Li(p,n) reaction neutron sources. The sample was made of powder europium oxide, which was pressed into tablets and packed by nylon film, each sample was sandwiched between two gold disks. The activity of the nuclide ^{154}Eu was measured in two Laboratories (CIAE, SCIU) and same standard γ-source was used to calibrate the efficiencies of HPGe(Li) spectrometers. The standards cross sections for $^{197}Au(n,\gamma)^{198}Au$ reaction were taken from ENDF/B-6. The data measured by Yu Weixiang[19] and Xia Yijiu[20] are consistent with each other. The data by D. M. Drake[18] are in good agreement with the new ones within errors. The early measured data[9~13] are also consistent with new ones within errors. Therefore, the measurements mentioned above are reliable. On

the other hand, V. N. Kononov's[15] and M. Mizunotio's[16] data are systematically higher than new one.

The thermal cross section was measured by N. J. Pattenden[7], R. B. Tattersal[8] M. Lucas[14]. The data from two laboratories[8,14] are in agreement within errors. But early data from N. J. Pattenden[7] are too higher than others. The R. B. Tattenrsa's[8] and M. Lucasl's[14] data were adopted. The averaged value is 321 ± 5 b.

In summary, the measured data by F. Widder[12], D. M. Drake[18], Yu Weixiang[19], J. Xia Yijiu[20] were adopted. Based on them, the evaluated data were obtained from 0.01 eV to 2.20 MeV. The earlier measured data were only used as reference in the theoretical calculation.

^{151}Eu(n,γ)^{152}Eu

The data were measured by same authors as ^{153}Eu(n,γ)^{154}Eu reaction. Most of experimental data were consist with each other within errors expect for the measured data by using STANK method, which are about 10% systematically higher than others in energy region 10 ~ 100 keV. Other two sets of data[22~23] were rejected in evaluation due to they are strange lower.

The measured data performed by D. M. Drake[18] in energy region of 3 ~ 2200 keV with time of flight spectrometer at Lanic in 1987 and by Yu Weixiang[19], Xia Yixiang[20] in energy region 36 ~ 1120 keV were used as base in the evaluation.

The thermal cross section was measured by R. B. Tattersal[8], F. Poortmans[21] respectively. The data from two laboratories were in agreement. The data were adopted and the averaged value is 9000±120 b.

1.3 ^{153}Eu(n,p) and (n,α) Reactions

For ^{153}Eu(n,p)^{153}Sm reaction, there are experimental data only around 14.7 MeV, measured by 4 laboratories. The early measured data were performed by R.F. Coleman[24], H. S. Qaim[25] and H. S. Pruys[26] respectively. The measured data by R. F. Colenman[24] are higher than others. The measured value with Ge(Li) detector by H. S. Pruys[26] after corrected using new reference cross section and S. M. Qaim's results[25] are consistent with measured value of A. Bari[27]. For present work, the measured values by S. M. Qaim[25], A. Bari[27] were taken as references for theoretically calculation.

For ^{153}Eu(n,α)^{150}Pm reaction, there are only 4 points experimental data, at 14.0 and 14.8 MeV, which were measured by C. S. Khurana[28,29], S. M. Qaim[25] and H. S. Pruys[26]. The cross sections measured by S. M. Qaim[25] and H. S. Pruys[26] using Ge(Li) detectors are consistent with each other within errors. The data by C. S.

Khurana[28,29] are with large error and much higher than others. The reason is effected by using mica end-window Geigermuller counter, which does not have enough particle discrimination character. The data of S. M. Qaim's and H. S. Pruys's were recommended.

For ^{151}Eu(n,α)^{148}Pm reaction, there is only one measurement by S. M. Qaim[25], 1.35±0.3 mb at 14.7 MeV.

Except for existing measured data for ^{151,153}Eu(n,α)^{148,150}Pm and ^{153}Eu(n,p)^{153}Sm reactions, there are no experimental data. For other ^{151,153}Eu(n,x) reactions, the cross sections must be calculated theoretically.

2 Theoretical Calculation and Recommendation

2.1 ^{151,153}Eu

In order to recommend the cross sections for ^{151,153}Eu(n.2n), (n,3n), (n,γ) and (n,x) reactions, the theoretical calculation were performed with UNF code[30], based on the available total cross sections of ^{Nat}Eu, nonelastic scattering cross sections were evaluated by us from (n,γ), (n,2n) etc. for ^{151,153}Eu in energy region 0.001 ~ 14 MeV. Because there are no experimental data of elastic angular distributions of Eu, the data of neighbor nucleus of Pm were used.

A set of neutron optical potential parameters of Sm was used as preliminary input data. A set of neutron optical potential parameters for ^{151,153,Nat}Eu was obtained in the energy region 0.001 ~ 20 MeV by using automatically searching code APOM[31].

$$V = 51.7941 - 0.2943E - 0.0020E^2 - 24(N-2)/A$$
$$W_S = \max\{0.0,\ 15.5141 - 0.1928E - 12.0(N-Z)/A\}$$
$$W_V = \max\{0.0,\ -2.9641 + 0.2327E - 0.0017E^2\}$$
$$W_{SO} = 6.2$$

$r_R = 1.188$	$r_R = 1.0758$	$r_V = 2.041$	$r_{SO} = 1.188$
$a_R = 0.8000$	$a_S = 0.5460$	$a_V = 0.0189$	$a_{SO} = 0.8000$

Using this set of neutron optical potential parameters and adjusted level density and giant dipole resonance parameters, the cross sections of ^{151,153}Eu(n,2n), (n,3n), (n,γ) and (n,x) reactions were calculated. The calculated data can reproduce the measured data very well.

The recommended cross sections for (n,γ) were given based on the measured and theoretically calculated data, the cross sections of resonance energy region were from JEF-2 and the energy range 0.001 ~ 2 MeV were taken from fitting values of

evaluated experimental data. The recommended activation cross sections for $^{151,153}Eu$ (n,2n), (n,γ) reactions are shown in Fig.1 ~ 5.

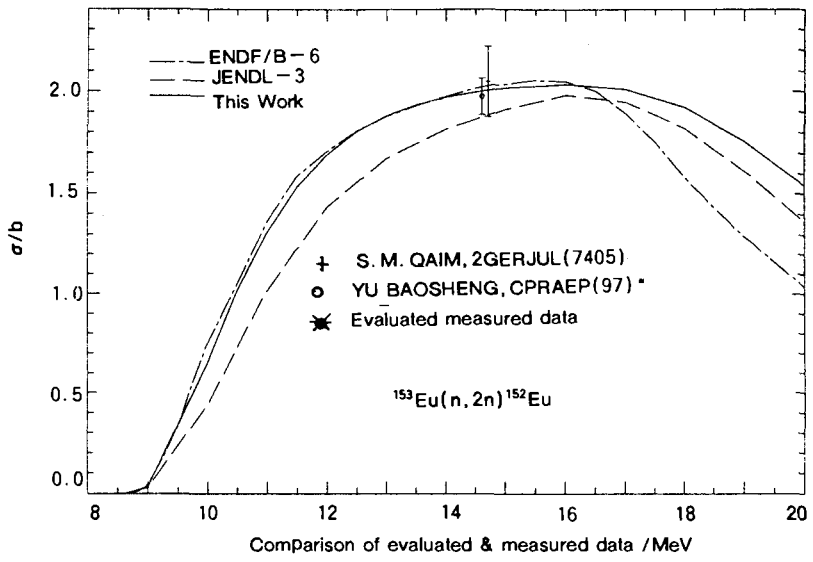

Fig.1 Comparison of evaluated & measured data $^{153}Eu(n,2n)^{152}Eu$

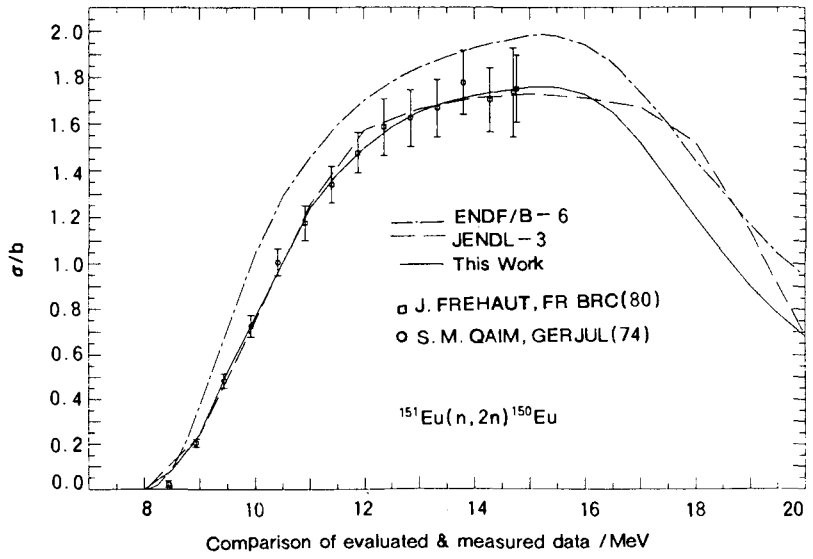

Fig.2 Comparison of evaluated & measured data $^{151}Eu(n,2n)^{150}Eu$

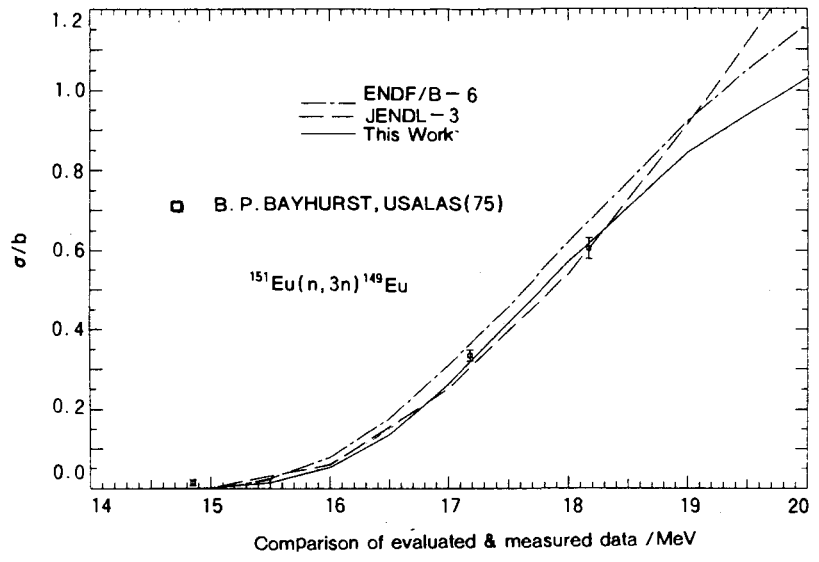

Fig.3 Comparison of evaluated & measured data $^{151}Eu(n,3n)^{149}Eu$

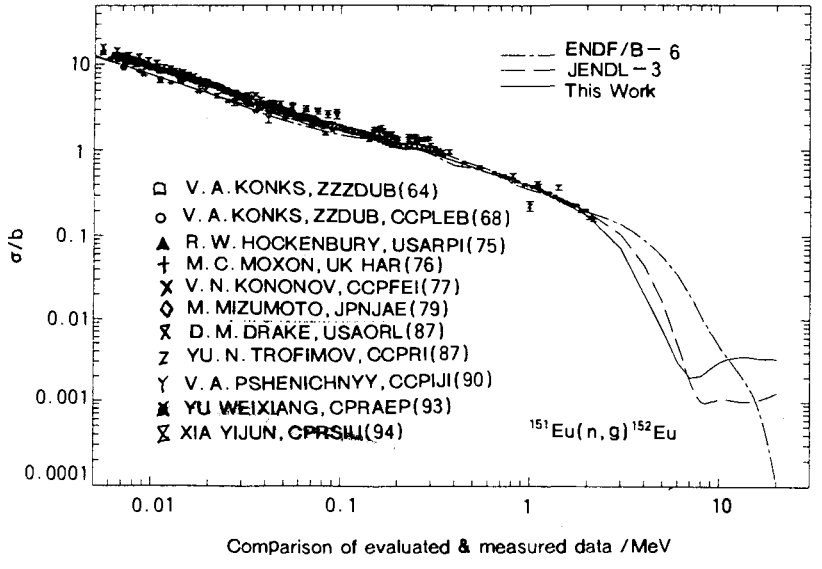

Fig.4 Comparison of evaluated & measured data $^{151}Eu(n,\gamma)^{152}Eu$

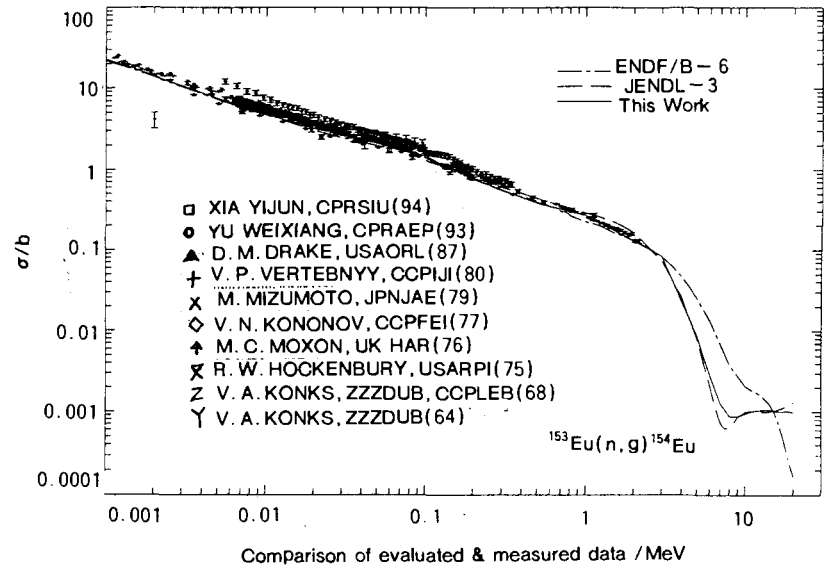

Fig.5 Comparison of evaluated & measured data $^{153}Eu(n,\gamma)^{154}Eu$

The thresholds of these (n,x) reactions are above about 8 MeV. The calculated cross sections are of the order of a few ten mb or less, generally much less. They were in agreements with existing experimental data. For the (n,α) and (n,p) reactions, the calculated curve could close or pass the data measured around 14 MeV. The calculated results for (n,x) reactions were recommended and shown in Fig.6, 7.

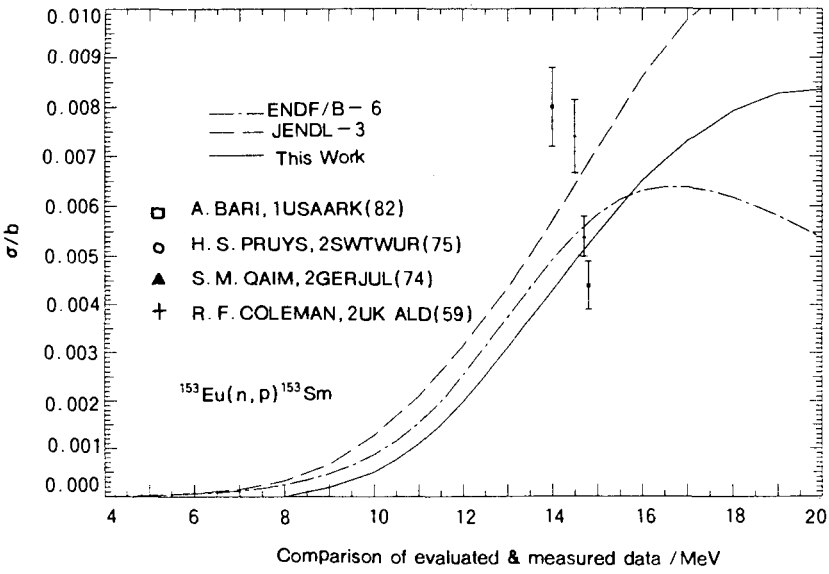

Fig.6 Comparison of evaluated & measured data $^{153}Eu(n,p)^{153}Sm$

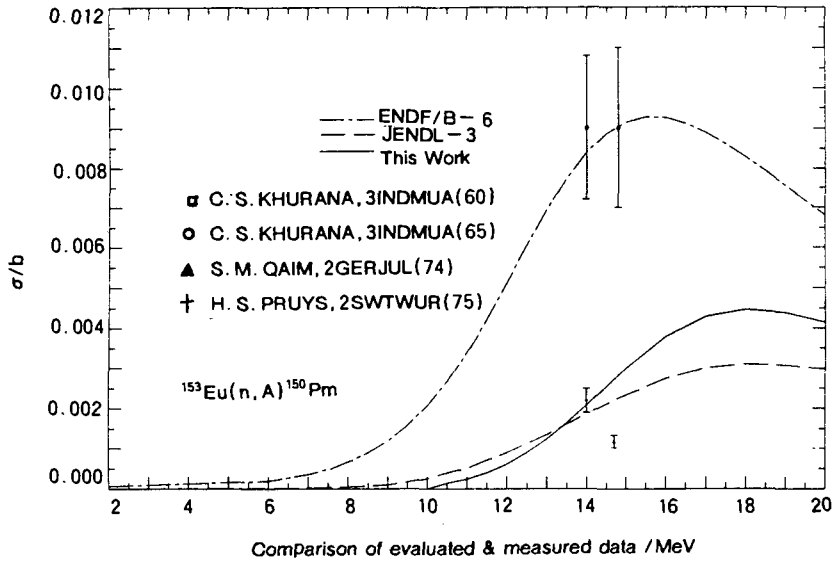

Fig.7 Comparison of evaluated & measured data $^{153}Eu(n,\alpha)^{150}Pm$

The cross sections of all reactions by neutron induced on $^{151,153}Eu$ were recommended and shown in Fig.8, 9.

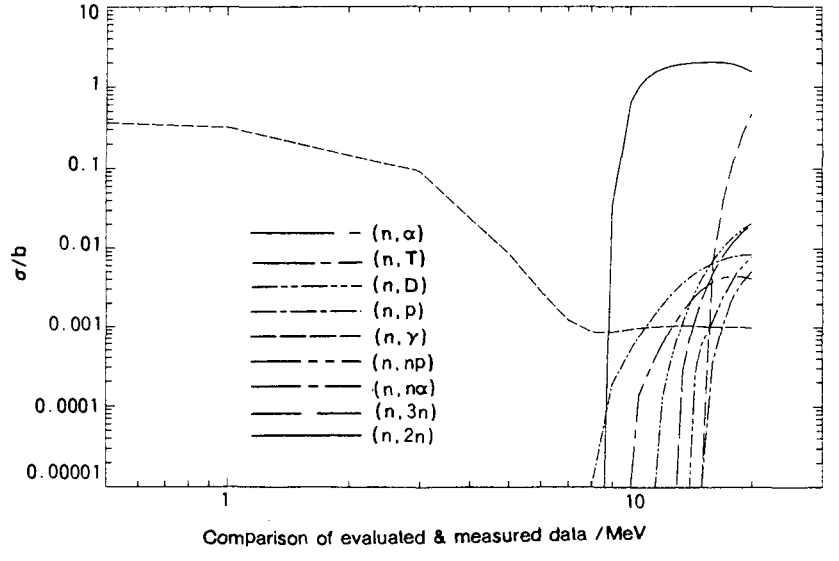

Fig.8 Evaluated cross section for n+^{153}Eu reaction

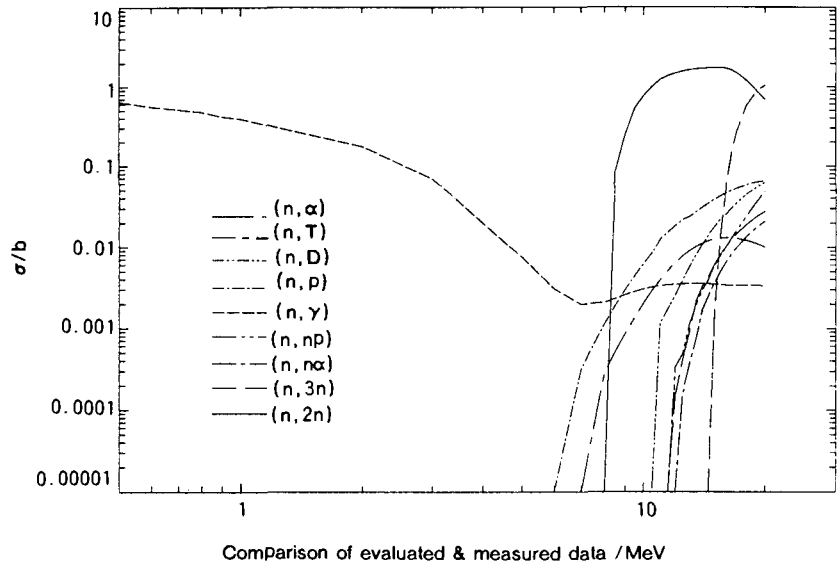

Fig.9 Evaluated cross section for n+^{151}Eu reaction

2.2 For ^{148,149,150}Eu

Because ^{148,149,150}Eu are radionuclides, there are no available measured data. The theoretical calculation were performed with UNF code[31] for ^{148,149,150}Eu(n.2n), (n,3n), (n,γ) and (n,x) reactions, cross sections. A set of neutron optical potential parameters of ^{151,153,Nat}Eu, the relevant level density and giant dipole resonance parameters of ^{148,149,150}Eu were used.

3 Summary

The evaluated cross sections for ^{151,153}Eu(n,2n)^{150,151}Eu reactions are consistent with experimental data and better than the evaluated data from other nuclear libraries.

The cross sections for ^{151,153}Eu(n,γ)^{152,154}Eu reactions were evaluated based on the new accurate measured and calculated data. The recommended cross sections are reliable.

Acknowledgments

The authors are indebted to CNNC (China National Nuclear Corporation) and CIAE for their supports, and thank Drs. Lu Hanlin, Zhao Wenrong, Shen Qingbiao and Liu Tong for their kind help and suggestions.

References

[1] S. M. Qaim et al., Nucl. Phys. /A, 224, 319(1974)
[2] A. Reggoug. et al., MOH-5, 14(1982)
[3] Lu Hanlin et al., Journal of China Nucl. Phys., 13, 203(1991)
[4] A. B. Pashchenko, INDC(NDS)-344(1997)
[5] J. Frehaut et al., EXFOR Data N0. 20416062
[6] B. P. Bayhurst et al., PR/C, 12, 451(1975)
[7] N. J. Pattenden et al., Inter. Conf. on Nuclear Data for Science and Technology P. 16, Geneva(1958)
[8] R. B. Tattersall et al., JNE/A, 12, 32(1960)
[9] V. A. Konks et al., JINR-1845, 100(1964)
[10] V. A. Konks et al., Journal YF, 7, 493(1968)
[11] R. W. Hockenbury et al., Inter. Conf. on Nuclear Data for Science and Technology Vol. 2, P. 905 Wash(1975)
[12] F.Widder et al., EIR-217(1975)
[13] Moxon et al., Ann. Nucl. Eng., 3, 339(1976)
[14] M. Lucas et al., Inter. Conf. on Nuclear Data for Science and Technology Vol., P. 431, Paris(1977)
[15] V. N. Kononoy et al., Nucl. Sci. Eng., 93, 43(1996)
[16] M. Mizumoto et al., Journal of China Nucl. Phys., 10, 233(1988)
[17] V. P. Vertebnyy et al., Journal YK, 1, 32(1980)
[18] D. M. Drake et al., Nucl. Sci. and Eng., 95, 189(1987)
[19] Yu Weixiang et al., Journal of China Nucl. Phys., 15, 71(1993)
[20] Xia Yijiu et al., Nucl. Phys. /A, 125, 57(1969)
[21] F. Poortmans et al., Nucler Physics, A, 172, 489(1971)
[22] Yu N. Trofimov et al., Conf., 87KIVE, 3, 331(1987)
[23] V. A. Pshenichnyy et al., YF, 51, 621(1990)
[24] R. F. Coleman et al., PPS, 73, 215(1959)
[25] S. M. Qaim et al., RRL, 25, 335(1976)
[26] H. S. Pryus et al., JIN, 37, 1587(1975)
[27] A. Bari et al., JRC, 75, 189(1982)
[28] C. S. Khuran et al., Inter. Conf. on Nuclear Data for Science and Technology P. 297, Waltair(1960)
[29] C. S. Khuran et al., Nucl. Phys., 69, 153(1965)
[30] Zhang Jingshang et al., Commun. of Nucl. Data Prog., 7, 43(1992)
[31] Shen Qingbiao et al., Commun. of Nucl. Data Prog., 7, 14(1992)

Evaluation of Activation Cross Sections for (n,p) and (n,n'p) Reactions on $^{63,65,Nat}Cu$

Ma Gonggui
(Institute of Nuclear Science and Technology, Sichuan Univ., Chengdu 610064)

Introduction

Copper is a very important structure material in nuclear fusion engineering. The neutron activation cross section are very useful in fusion research and other applications such as radiation safety, environmental, material damage and neutron dosimetry. More efforts are required to identify and resolve the differences and discrepancies in the existing activation cross sections from different laboratories.

The natural copper consists of two stable isotopes, i.e. ^{63}Cu, ^{65}Cu. Their abundances and threshold energys are as in Table 1.

Table 1 Isotopic abundances and their reaction threshold energyies of copper

isotope	(n,p) thresh. / MeV	(n,n'p) thresh. / MeV	abun. / %
63	1.3698	6.2228	69.17
65	0	7.5605	30.83

The cross sections of (n,p) and (n,n'p) for $^{63,65,Nat}Cu$ are recommended based on the recent experimental data and theoretically calculated results[1] from threshold up to 20 MeV. The evaluated cross sections are given in Figs.1 ~ 6 with experimental data and compared with other evaluated data.

1 $^{63}Cu(n,p)^{63}Ni$ Reaction

For (n,p) reaction, the experimental data were measured by Zhao Wenrong (97), Greenwood (89) and Qaim (69)[2-4] in the energy range from 6.0 MeV to 15.0 MeV, respectively. The evaluated data were obtained by fitting experimental data from threshold energy to 15.0 MeV. Above 15.0 MeV, the recommended data were taken from calculated result, and normalized to the fitting experimental datum of 56 mb at 15.0 MeV. The comparison of experimental data with evaluated ones is shown in Fig.1.

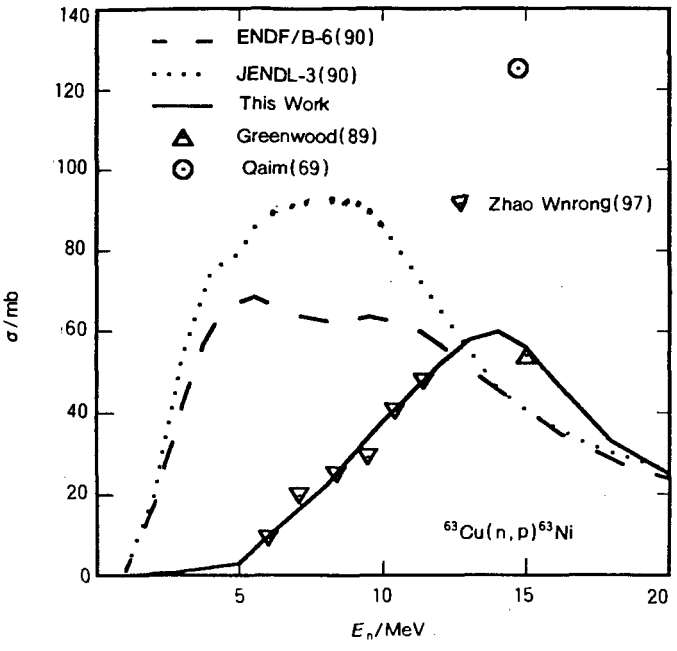

Fig. 1 (n,p) cross section for ^{63}Cu

2 ^{65}Cu (n,p)^{65}Ni Reaction

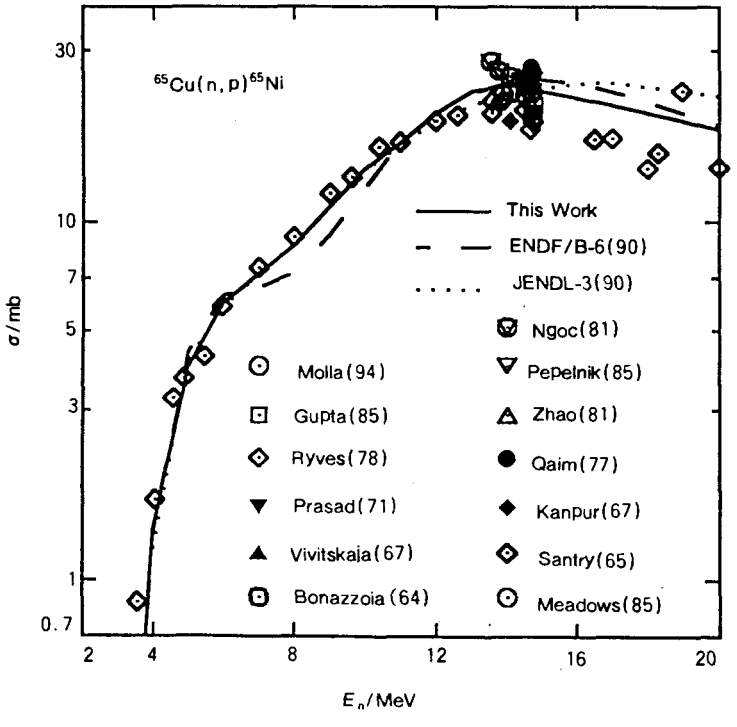

Fig. 2 (n,p) cross section for ^{65}Cu

The experimental data were measured by Molla (94), Meadows (85), Gupta (85), Ngoc (81), Zhao (81), Ryves (78), Qaim (77), Prasad (71), Kanpur (67), Vivitskaja (67), Santry (65) and Bonazzoia (64)[5~15] from 3.5 to 20.0 MeV, respectively. The evaluated data were obtained by fitting experimental data from threshold energy to 20.0 MeV. The comparison of experimental data with evaluated ones is shown in Fig.2.

3 $^{63}Cu(n,n'p)^{62}Ni$ Reaction

For (n,n'p) reaction, the experimental data were measured by Colli (59), Joensson (69) and Allan (57)[16~18] around 14.0 MeV. The recommended data were taken from calculated result, and normalized to the Colli experimental datum of 250 mb at 14.1 MeV, as shown in Fig.3.

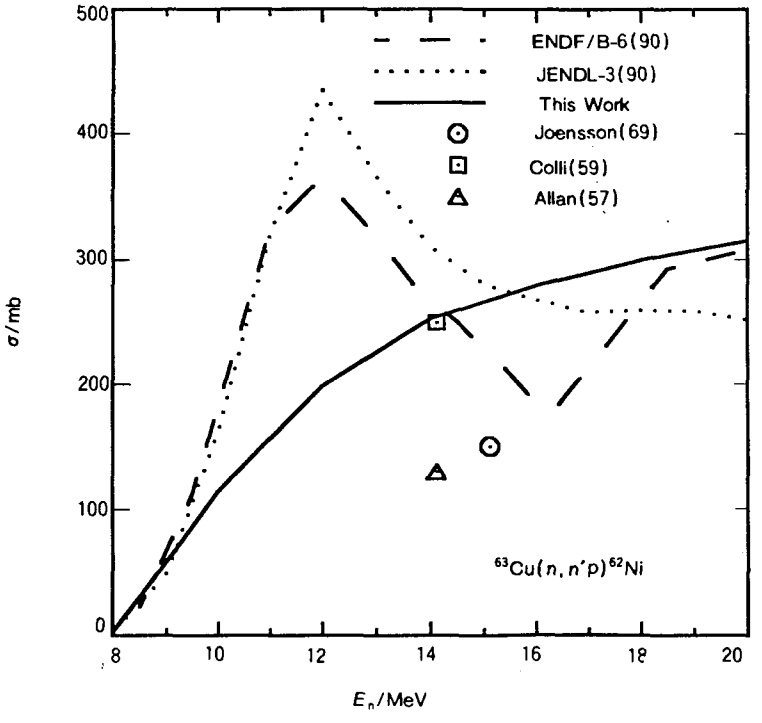

Fig. 3 (n,n'p) cross section for ^{63}Cu

4 ^{65}Cu (n,n'p)^{64}Ni Reaction

The experimental data were measured by Joensson (69) in 15.1 MeV energy point. The recommended data were taken from calculated result, and normalized to the experimental datum of 22 mb at 15.1 MeV as shown in Fig.4.

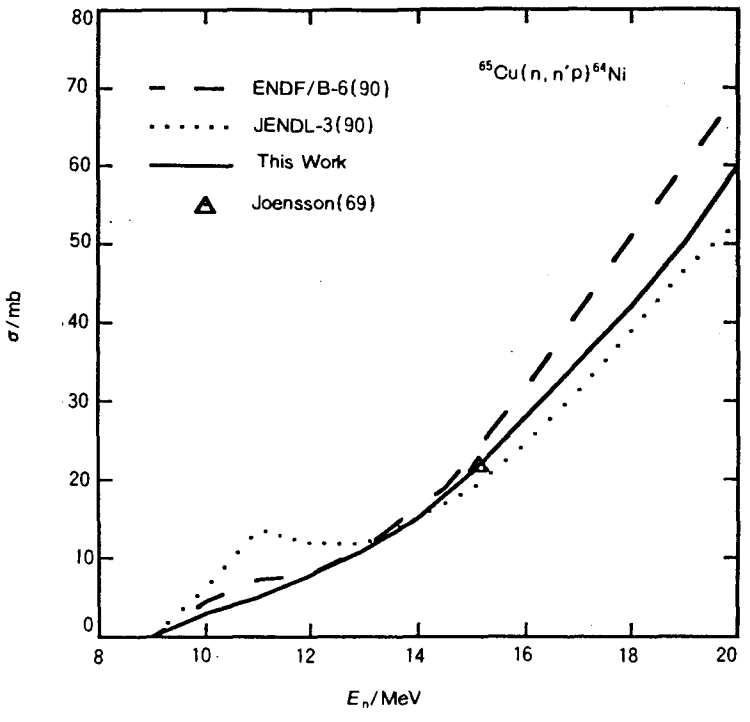

Fig. 4 (n,n'p) cross section for ^{65}Cu

5 The (n,p) and (n,n'p) Reaction for Natural Copper

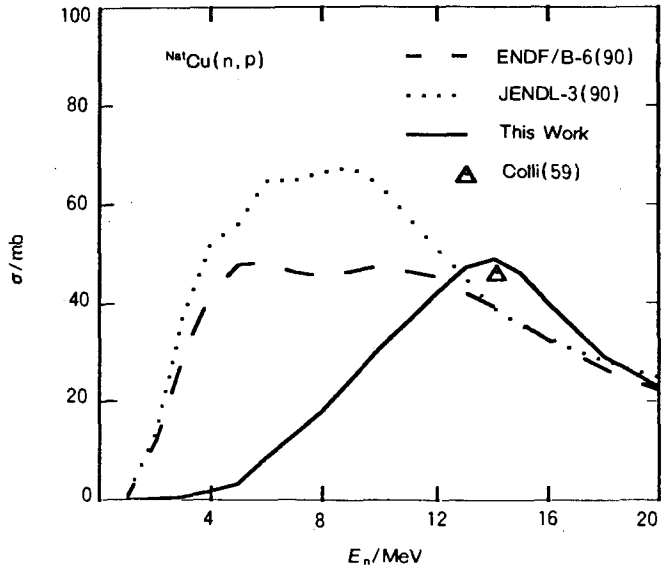

Fig. 5 (n,p) cross section for ^{Nat}Cu

For natural Cu, the experimental datum was measured by Colli (59) at 14.1 MeV energy point. The (n,p) and (n,n'p) cross sections of natural Cu were obtained from summing the isotopic data weighted by the abundance. The comparison of experimental data with evaluated ones is shown in Fig.5 and 6. It is found that the present evaluations are in agreement with the experimental data.

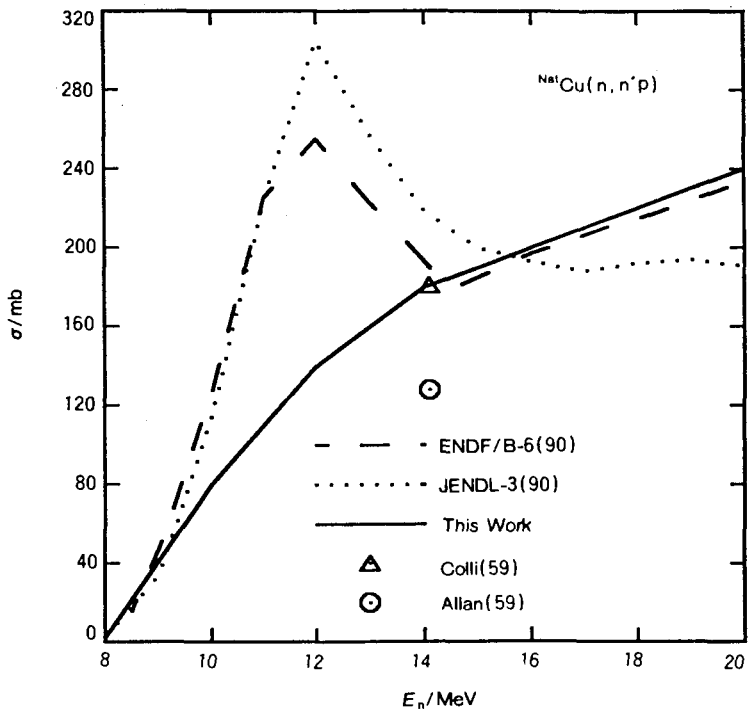

Fig. 6 (n,n'p) cross section for ^{Nat}Cu

Acknowledgement

The authors would like to thank Dr. Yu Baosheng for helpful discussion and suggestions.

References

[1] Zhang Jingshang. Nucl. Sci. Eng., 114, 55 (1993)
[2] Zhao Wenrong et al., Proc. of Tenth National Conf. of Nucl. Phys., p167(1997) Qingdao,
[3] L.R.Greenwood et al., ASTM-STP-1001, 1(1989)
[4] S. M. Qaim et al., Nuclear Physics, A283, 269(1977)
[5] N. I. Mollaetal., Proc. of Conf. on Nucl. Data for Science and Technology, 2, 938(1994) Gatlinburg, U.S.A.
[6] Meadows et al., 85SANTA 1, 123(AD01)(1985)
[7] Gupta et al., PRM 24, 637(1985)

[8] P. N. Ngoc et al., INDC(HUN)-18, 11(1981)
[9] Zhao Zhenlan et al., J. Nucl. and Radiochemistry, Beijing, 3(2), 115(1981)
[10] Ryves et al., NET 14(3), 127(1978)
[11] Prasad et al., NC, A3(3), 467(1971)
[12] B.Mitre et al., 67KANPUR, 367(1967)
[13] G. P. Vinitskaja et al., Yademaya Fizika, 5(6), 1175(67)
[14] D. C. Santry et al., Canadian Journal of Physics, 44, 1183(65)
[15] C. G. Bonazzola et al., Nucl. Physics, 51, 337(64)
[16] L. Colli et al., J. Nuovo Cimento, 13, 730(1959)
[17] B. Joensson et al., AF, 39, 295(1969)
[18] D. L. Allan et al., Proc. of Phys. Society, A70, 195(1957)

CN9901240

Calculation and Evaluation of the Activation Cross Sections for $^{187}Re(n,2n)^{186m,g}Re$ Reactions

Huang Xiaolong Lu Hanlin Zhou Chunmei
(China Institute of Atomic Energy, Beijing 102413)

The activation cross sections for $^{187}Re(n,2n)^{186m,g}Re$ reactions are calculated using UNF code. The calculations are in good agreement with the re-evaluated measured data. Finally the excitation function for $^{187}Re(n,2n)^{186m,g}Re$ reactions are evaluated and recommended based on present calculations and evaluated decay data.

Introduction

Metal rhenium is one of fusion reactor materials. Their cross section for $^{187}Re(n,2n)^{186}Re$ reaction is an important datum for the safety and environmental evaluation of fusion reactor. These cross sections are very scarce and only provided by several laboratories around 14 MeV. Among these measurements there exist large discrepancies for $^{187}Re(n,2n)^{186g}Re$ reaction and large errors for $^{187}Re(n,2n)^{186m}Re$ reaction. Therefore the theoretical calculation is necessary. On the other hand the evaluation of the activation cross sections for $^{187}Re(n,2n)^{186m,g}Re$ reactions should be done so as to meet the nuclear science and technology applications.

1 Decay Data

For the cross section value of isomeric state measured by Lu Hanlin or Y. Ikeda[1] plus ground state by Fan Tieshuan[2] at 14.8 MeV, one can easy find that the

sum is over 2400 mb. If the measurements are corrected using the newly gamma branching ratio of 137 keV γ ray, the sum will be higher. Because the new value is 8.22%[3], but Fan Tieshuan's value is 8.5%. Generally this is impossible for the cross section of (n,2n) reaction to have such higher value. Therefore the decay data used in measurement is probable wrong.

Considering this condition, the decay data of ^{186g}Re were checked and re-evaluated. It is noticed that product ^{186g}Re has two decay mode, one is the ε decay (6.9%), the other β^- decay (93.1%). In Ref.[3] the value of N is 0.822, and thus the value of gamma branching ratio of 137 keV γ ray is 8.22%. Present evaluation shows that the normalized factor N in Ref.[3] is wrong. After correcting this error the value of N is 0.883. Present N can guarantee the balance of the radiation intensities and energy. Present evaluation of γ branching ratio of 137.144 keV γ-ray is 8.83±0.26 (%).

2 Analysis of the Measurements

The measured cross sections for ^{187}Re(n,2n)^{186m}Re and ^{187}Re(n,2n)^{186g}Re reactions are summarized in Table 1 and 2, respectively.

For ^{187}Re(n,2n)^{186m}Re reaction, there are only two sets of measured data at 14.8 MeV, and in good agreement with larger errors. For the activities of ^{186g}Re product through 137 keV γ ray (I_γ = 8.22%), the gamma branching ratio of 137 keV γ ray are first corrected and renormalized using present evaluations. The recommended datum at 14.8 MeV is given based on the two corrected values, which are also listed in Table 1.

Table 1 Measured Cross Sections for ^{187}Re(n,2n)^{186m}Re Reaction

Time	Author	E_n / MeV	σ / mb	neutron flux	E_γ / keV	I_γ / %	Corrections* / mb
1997	Y. Ikeda[1]	14.80	541±189	^{93}Nb(n,2n)^{92m}Nb	137	8.22	503.6
1997	Lu Hanlin[1]	14.77	521±125	^{93}Nb(n,2n)^{92m}Nb	137	8.22	485.0
Present evaluation at 14.8 MeV : 494±114 mb							

* Renormalized for decay data only.

For ^{187}Re(n,2n)^{186g}Re reaction, all measurements can be divided into two groups. One is before 1967, another is Fan Tieshuan's in 1992 which have higher value. In Fan Tieshuan's measurement the gamma branching ratio of 137 keV γ ray is 8.5%. After correcting and renormalizing using present evaluation the data are still higher than those of the first group. The previous data were obtained before 1967 with β^- activities of residual products measured. But in Fan Tieshuan's work the measurements of the neutron fluence rate were carried out by the absolute and relative

methods, respectively, and their experimental results are in very good consistency. Considering these factors Fan Tieshuan's results seem to be more reasonable and reliable. Present recommended datum at 14.8 MeV based on Fan Tieshuan's measurements is given in Table 2.

Table 2 Measured cross sections for ^{187}Re(n,2n)^{186g}Re reaction

Time	Author	E_n / MeV	σ / mb	neutron flux	E_γ / keV	I_γ / %	Corrections / mb
1961	C. S. Khuranal[4]	14.8	1675±168	^{56}Fe(n,p)^{56}Mn			1775#
1963	R. A. Karam[5]	14.1	1440±410	^{197}Au(n,2n)^{196}Au*			1449#
1967	A. A. Druzhinin[6]	14.8	1490±160	^{27}Al(n,α)^{24}Na			1490#
1992	Fan Tieshuan[2]	14.1	1966.9±50.3	^{93}Nb(n,2n)^{92m}Nb	137	8.5	1893.4$
		14.6	1967.1±44.7				1893.6$
		14.8	1952.0±50.7				1879.0$
		15.0	1903.0±50.3				1831.9$
Present evaluation at 14.8 MeV: 1879±49 mb							

*: $T_{1/2}$ =5.3 d. #: Renormalized for reference cross sections only. $: Renormalized for decay data only.

3 Calculation and Evaluation

In order to recommend the activation cross sections for ^{187}Re(n,2n)^{186g}Re and ^{187}Re(n,2n)^{186m}Re reactions, the theoretical calculation was performed using UNF[7] program. A set of neutron optical potential parameters for ^{187}Re was first taken from those of ^{185}Re[8]. The level density and pairing correcting energy are taken from Ref. [9]. Then this set of parameters and the level density and giant dipole resonance parameters were adjusted to make the calculations be consistent with the available measurements around 14 MeV, especially with present evaluations at 14.8 MeV.

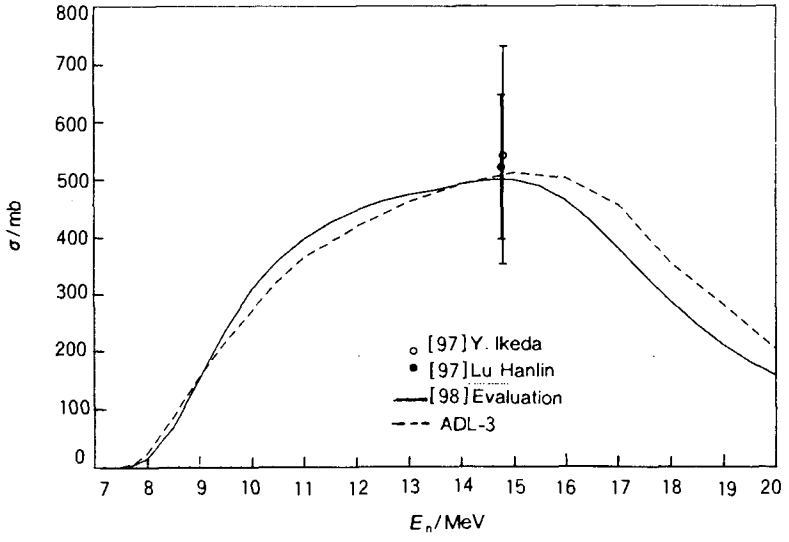

Fig.1 Cross sections for ^{187}Re(n,2n)^{186m}Re reaction

The comparison are made among the calculated measured and ADL-3 data, which shown in Fig.1 and 2. From the two Figs., one can find that present calculation is consistent with newly measurements very well, but not in good agreement with ADL-3 evaluation, especially for $^{187}Re(n,2n)^{186g}Re$ reaction.

As only measurements concentrated on 14 MeV, the evaluated activation cross sections for $^{187}Re(n,2n)^{186m}Re$ and $^{187}Re(n,2n)^{186g}Re$ reactions are taken from present theoretical calculations.

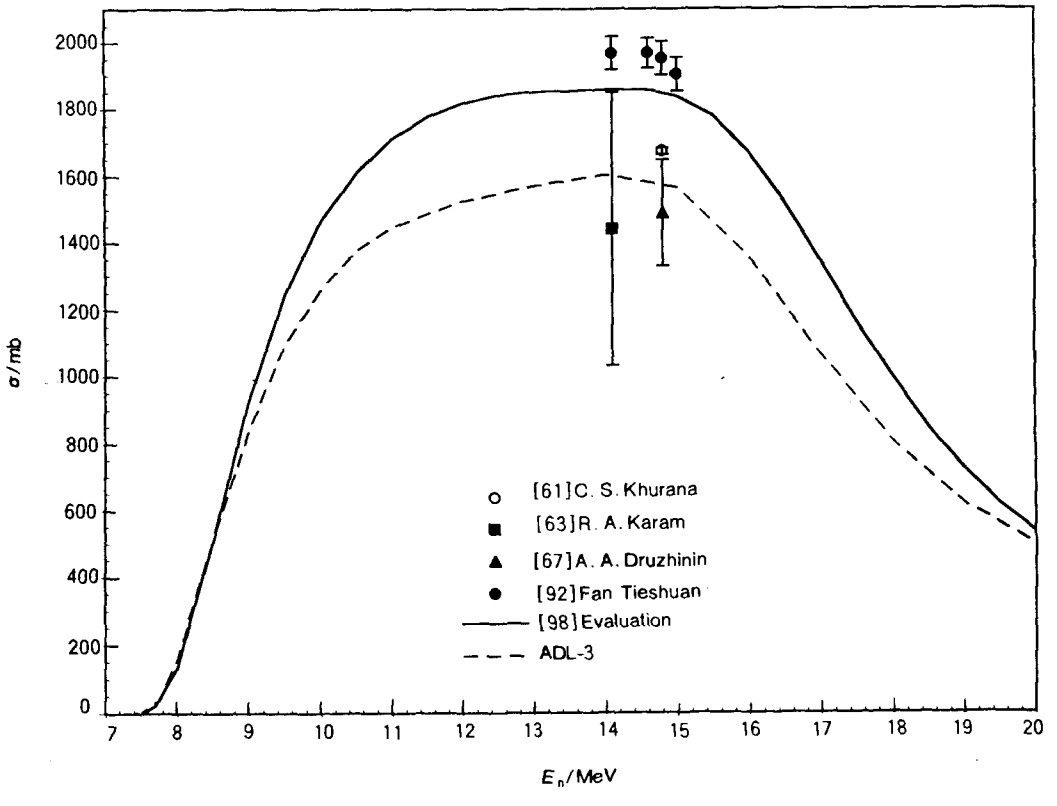

Fig.2 Cross sections for $^{187}Re(n,2n)^{186g}Re$ reaction

4 Conclusion

The cross sections for $^{187}Re(n,2n)^{186m}Re$ and $^{187}Re(n,2n)^{186g}Re$ reactions are calculated with UNF code based on the available experimental data. Their activation cross sections are taken from present calculations, and compared with measurements and other evaluations. From Figs.1 and 2, one can conclude that present calculations are consistent with the available measurements very well. The calculations should be

further checked by the measurements directly in the future because the available experimental data are very scarce and concentrated on 14 MeV.

Reference

[1] B. Pashchenko, INDC (NDS)-344, 20(1997)
[2] Fan Tieshuan et al., Chinese. J. Nucl. Phys. 14, 331(1992)
[3] R. B. Firestone et al., Table of Isotopes (8-edition), 1997
[4] C. S. Khurana et al., Nucl. Phys. 28, 560(1961)
[5] R. A. Karam et al., AD-402668, 1963
[6] A. A. Druzhinin et al., YF-5, 18(1967)
[7] Zhang Jingshang. Fast Neutron Physics, Beijing, China, 201(1991); UNF program. Chinese Nuclear Data Center, Internal file (1995)
[8] Han Yinlu, Private communication
[9] Zhuang Youxiang et al., Chinese J. Nucl. Phys. 3, 199(1986)

CN9901241

Evaluation of Cross Sections of Photonuclear Reactions for ^{180,182,183,184,186}W below 30 MeV

Yu Baosheng Han Yinlu Zhang Jingshang
(China Nuclear Data Center, CIAE)

Introduction

The photoneutron cross sections of wolfram's isotopes up to 10 MeV are very important from the view point of reactor engineering field in the context of radiation induced material damage, radiation safety, reactor incore dosimetry, etc. Meanwhile, the photonuclear reactions are usually used for performing activation analysis of minerals and other bulk material in industrial application. Therefore, the accurate photonuclear data play an important role in nuclear science and technology. In this work, the experimental data of photonuclear data for ^{180,182,183,184,186}W were evaluated, and theoretical calculations were used to supplement in the energy regions where measured photonuclear data were scarce. The recommended photonuclear data for ^{180,182,183,184,186}W were obtained based on evaluated and calculated theoretically data and compared with existing measured data.

1 Evaluation and Analysis of Experimental Data

The natural wolfram consist of five isotopes, i.e. ^{180}W (0.12 %), ^{182}W (26.498 %), ^{183}W (14.314 %), ^{184}W (30.642%) and ^{186}W (28.426 %), At present work, the photonuclear reactions, for which the cross sections were evaluated, are as follows: ^{180,182,183,184,186}W(γ,ABS), ^{180,182,183,184,186}W(γ,n)+(γ,n+p), ^{180,182,183,184,186}W(γ,2n)+(γ,2n+p), ^{180,182,183,184,186}W(γ.3n), (γ,n+p), (γ,n+α), (γ,2n), (γ,p), (γ,d), (γ,t), (γ,^{3}He), (γ,α) and the double differential cross sections of (γ,2n), (γ,3n), (γ,n+p), (γ,n+α) and (γ, n'$_{cont.}$).

The various available measured data of photonuclear reaction for wolfram's isotopes were collected and analyzed. The available experimental data[1~5] for photoneutron reaction cross sections ^{182,184,186}W are shown in Table 1. Most of the experimental data up to 1996 are included. Many data were retrieved from EXFOR master files, supplemented with new information. There are 5 sets of measured photonuclear reaction data, which cover from threshold to 30 MeV. Among 5 data sets, the data are mainly for ^{186}W with the exception of ^{182,184}W.

Table 1 Collected data of photonuclear reactions for ^{182,184,186}W

Year	Author	E_n / MeV	Sample	Detector	Reactions
1969	B. L. Berman	9.1 ~ 28.5	^{186}W	PROPC	(γ,n)+(γ,n+p)
		12.3 ~ 28.4	^{186}W	PROPC	(γ,2n)+(γ,2n+p)
		20.6 ~ 28.6	^{186}W	PROPC	(γ,3n)
1978	G. M. Gurevich	7.5 ~ 28.1	^{186}W	(γ,ABS)	
		7.4 ~ 26.9	^{184}W	(γ,ABS)	
1978	A. M. Goryachev	8.0 ~ 20.8	^{186}W	BF3	(γ,n)+(γ,n+p)+(γ,2n)
		8.0 ~ 20.8	^{184}W	BF3	(γ,n)+(γ,n+p)+(γ,2n)
		8.0 ~ 20.8	^{182}W	BF3	(γ,n)+(γ,n+p)+(γ,2n)
1980	G. M. Gurevich	7.5 ~ 19.1	^{186}W	SCIN	(γ,ABS)
		8.0 ~ 18.4	^{184}W	SCIN	(γ,ABS)
1981	G. M. Gurevich	8.7 ~ 18.9	^{186}W	NAICR	(γ,ABS)
			^{184}W	NAICR	(γ,ABS)
			^{182}W	NAICR	(γ,ABS)

1.1 ^{186}W

The measurements of photoabsorption cross sections for ^{186}W were first performed by G. M. Gurevich[2] in gamma energy region of 7.5 to 28.1 MeV in 1978. The sequence measurements were performed by G. M. Gurevich[4~5] in gamma energy region of 7.5 to 19.1 MeV in 1980 and 1981, respectively. There exist very large discrepancy among above three measured data, Gurevich's measured data[4] in 1980 are about 49 time higher than other two ones[2,5] and some resonance peaks are not appeared. In the experimental layout[4], the bremsstrahlung beam passed through the aluminum beam hardener and hit the scintillation spectrometer. The thickness of

the aluminum beam hardener and the paraffin behind the absorber are not enough, so the scattering background neutron could not be perfectly protected into the detector. The data obtained by G. M. Gurevich[5] superseded himself earlier measured results[4] below 19 MeV. The evaluated results from threshold to 20 MeV were obtained for above mentioned data.

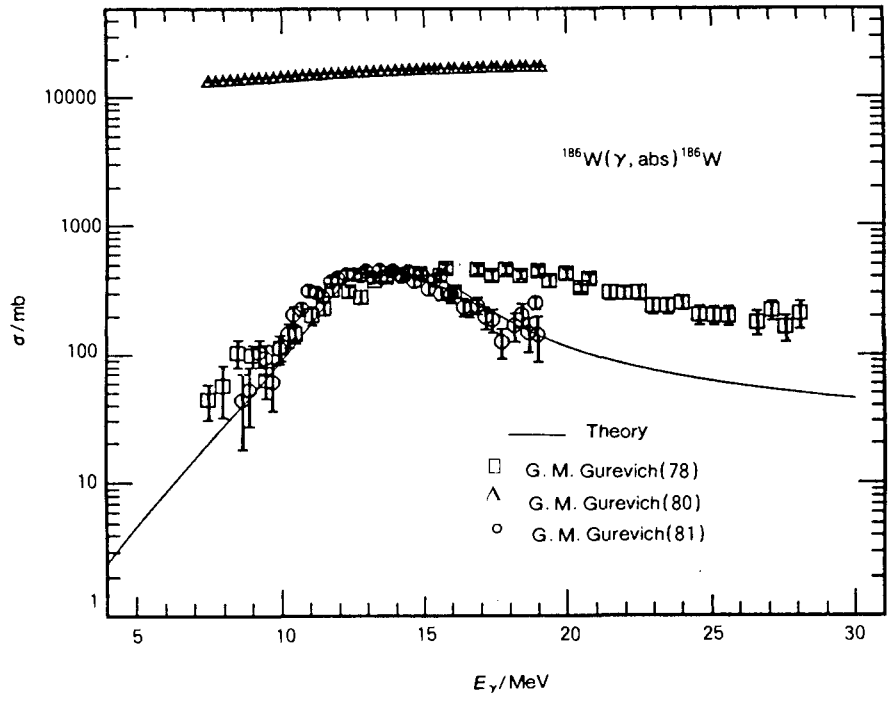

Fig.1 The comparison of calculated results with experimental data for ^{186}W(γ,abs) reaction

The photoabsorption cross section is the sum of (γ,n), (γ,n+p), (γ,2n), (γ,2n+p), (γ,3n). The photonuclear cross section were measured by B. L. Berman[1] for (γ,n)+(γ,n+p), (γ,2n)+(γ,2n+p) and (γ,3n) from 9.1(12.3,20.6) to 28.5 MeV, respectively. The cross sections for (γ,n)+(γ,n+p)+(γ,2n) were measured by A. M. Goryachev[3] from 8.0 to 20.8 MeV. The Berman's data are consistent with the Goryachev's one within errors, and both of them were consistent with the measured photoabsorption cross section by G. M. Gurevich[2,5] within error. For these data, there appear obvious peaks corresponding to (γ,n)+(γ,n+p), (γ,2n)+(γ,2n+p) and (γ,3n) reactions. For the Gurevich's data, there exist peaks corresponding to (γ,n)+(γ,n+p), (γ,2n)+(γ,2n+p) reactions consistent with the Berman's data, and the resonance energy and height are almost same. The photoabsorption cross section, especially (γ,n)+(γ,n+p)+(γ,2n) and

(γ,3n) cross sections[1], could be used to guide adjusting calculation model parameters. The data are shown in Fig.1.

1.2 ^{182,184}W

The data of photonuclear cross sections for ^{182,184}W were measured by A. M. Goryachev[3] in gamma energy region 8.0 to 20.8 MeV and by G. M. Gurevich[5] from 8.7 to 18.9 MeV. Both data, including peak position and height corresponding to ^{182,184}W(γ,n), (γ,n)+(γ,n+p), (γ,2n) reactions are in agreement with each other. The data can be used to guide adjusting model parameters.

2 Theoretical calculation and Recommendation

For ^{186}W, the theoretical calculation was used to fit the adopted experimental data[1~3,5]. The optical potential parameters were obtained from the work for calculating neutron nuclear data for W.

Adjusting some parameters concerned make the calculated various photonuclear reaction data, such as (γ,n)+(γ,n+p), (γ,2n)+(γ,2n+p) cross sections in good agreement with the experimental data.

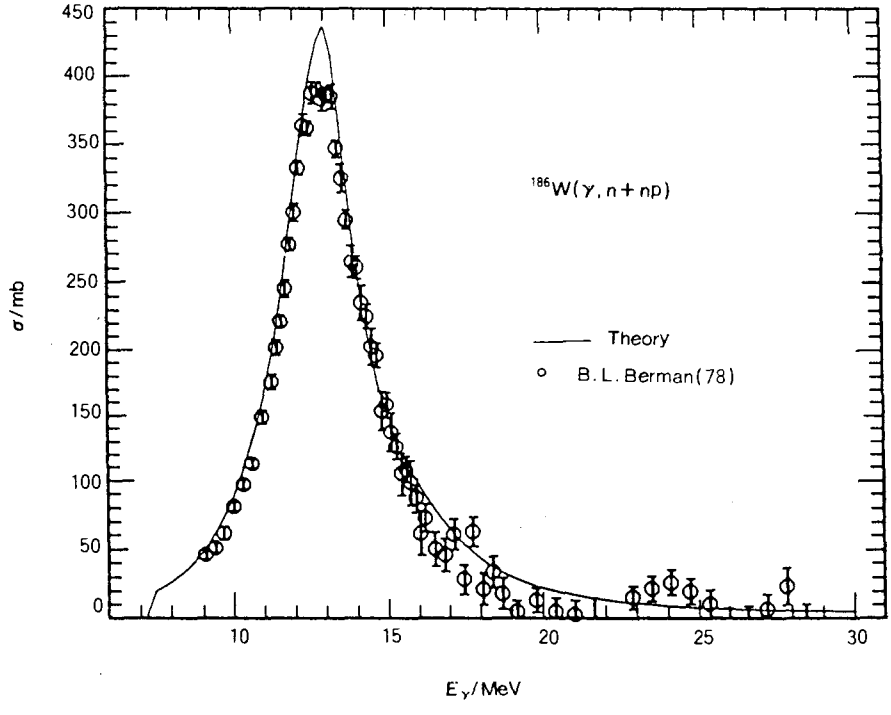

Fig.2 The comparison of calculated results with experimental data for ^{186}W(γ,n+np) reaction

The total photoneutron cross section (γ,n) are sum of the photoneutron from ground, excitation state and continuum state. The level scheme used were taken from China Nuclear Parameter Library. The continuum levels were assumed above 0.3728, 0.7617, 1.7568, 0.4870 and 0.7854 MeV for wolfram's isotopes 180, 182, 183, 184 and 186 respectively. The cross sections of photoneutron for (γ,2n) and (γ,3n) were also calculated based on the experimental data[1,3].

The cross sections were calculated from threshold to 30 MeV. The theoretically calculated values are in good agreement with the experimental data, especially they are almost overlapped in the energy region from 18 to 20 MeV. Therefore, the calculated data are reliable and are recommended, which are shown in Fig.2 ~ 4.

Based on the available experimental data of photoabsorption cross sections and photoneutron reaction cross sections for wolfram and its isotopes ^{182}W and ^{184}W, a set of optical potential parameters and photonuclear reaction parameters for ^{186}W and $^{182,184}W$ in gamma energy region threshold about 30 MeV was obtained, and the calculated results are shown in Fig.5 ~ 8.

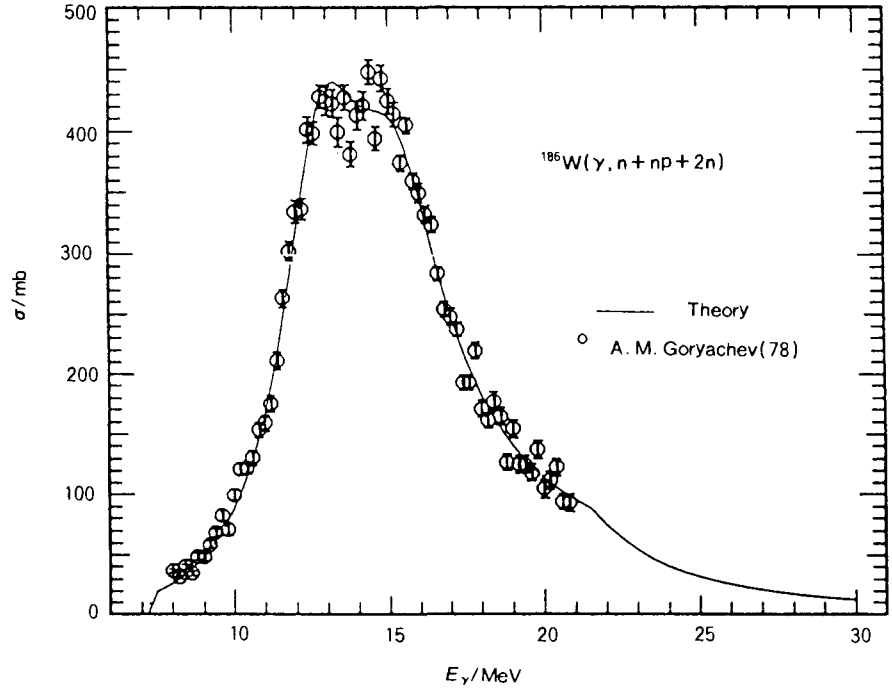

Fig.3 The comparison of calculated results with experimental data for $^{186}W(\gamma,n+np+2n)$ reaction

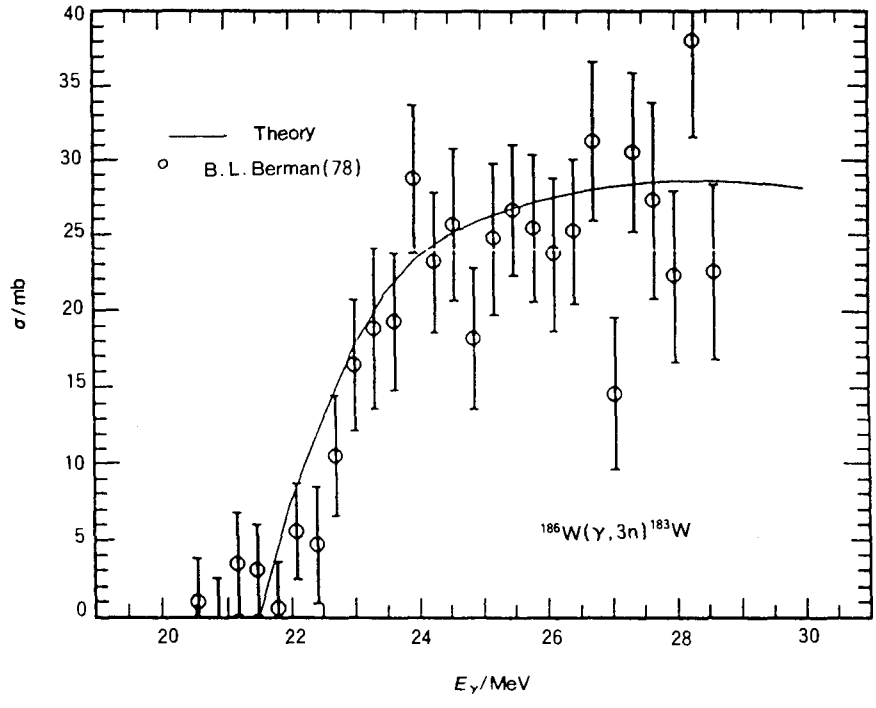

Fig.4 The comparison of calculated results with experimental data for $^{186}W(\gamma,3n)$ reaction

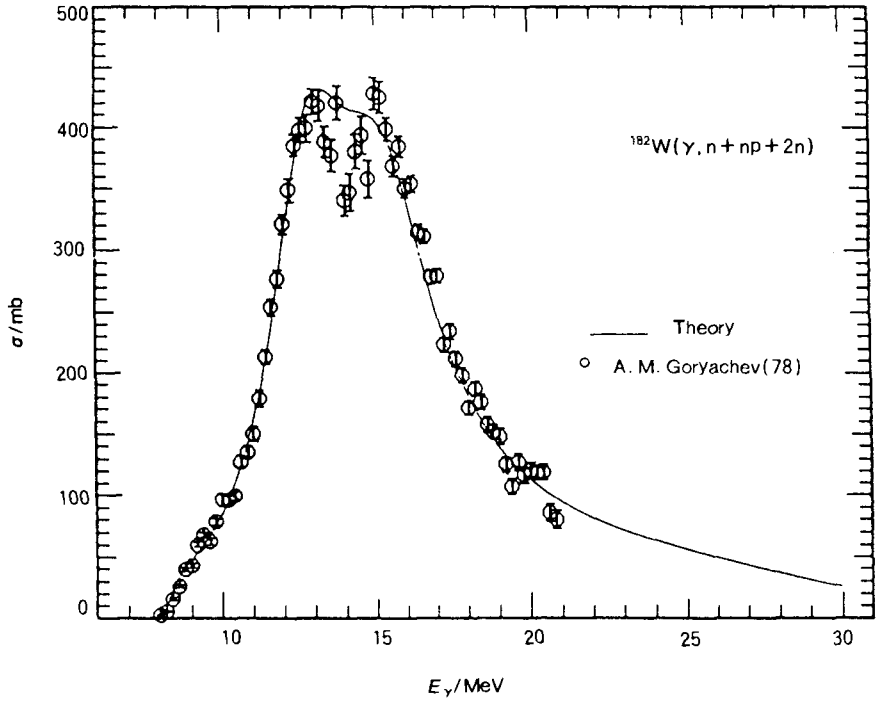

Fig.5 The comparison of calculated results with experimental data for $^{182}W(\gamma,n+np+2n)$ reaction

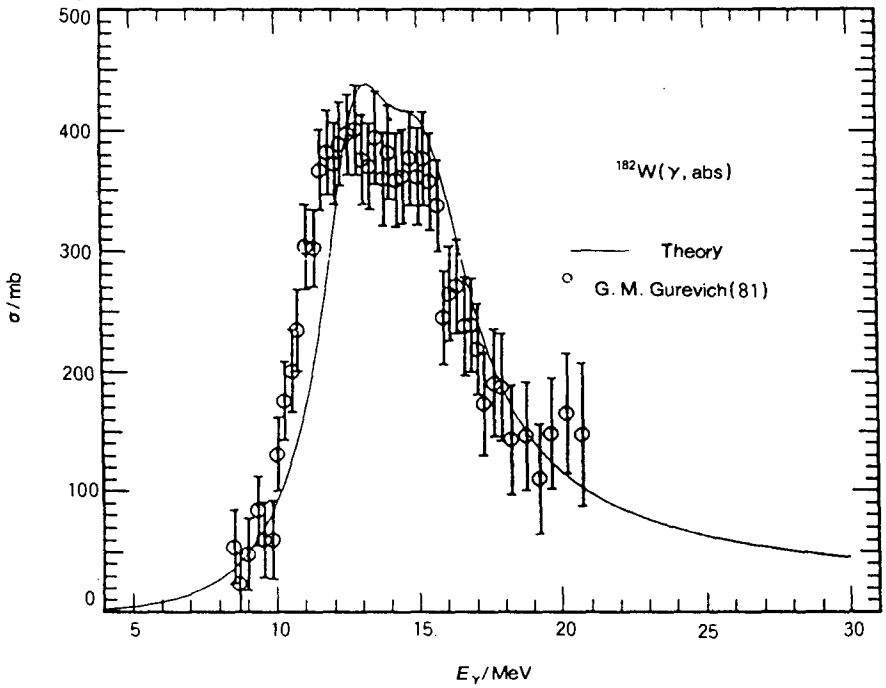

Fig.6 The comparison of calculated results with experimental data for ^{182}W(γ,abs) reaction

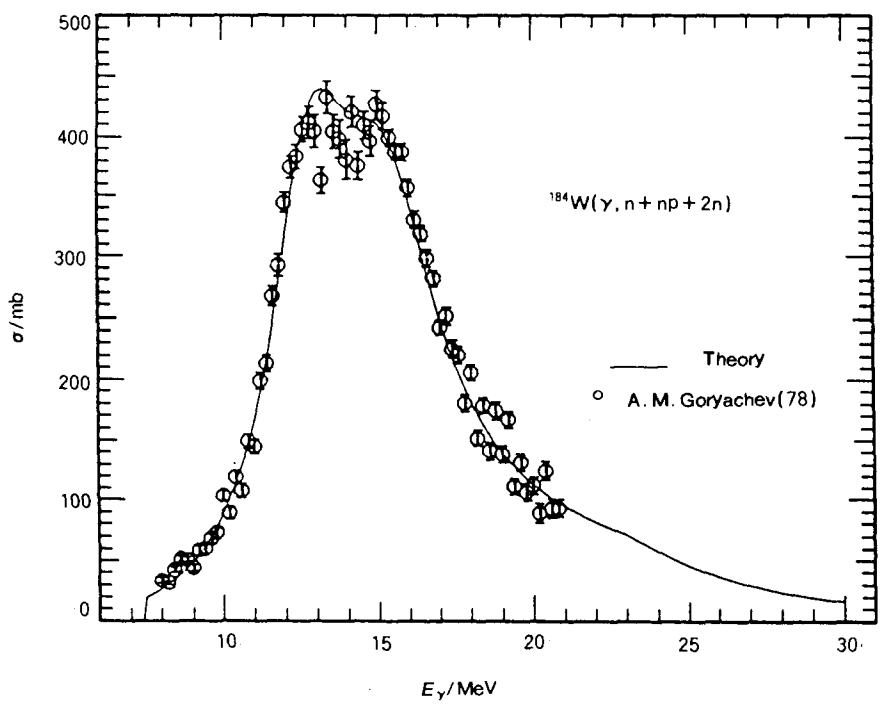

Fig.7 The comparison of calculated results with experimental data for ^{184}W(γ,n+np+2n) reaction

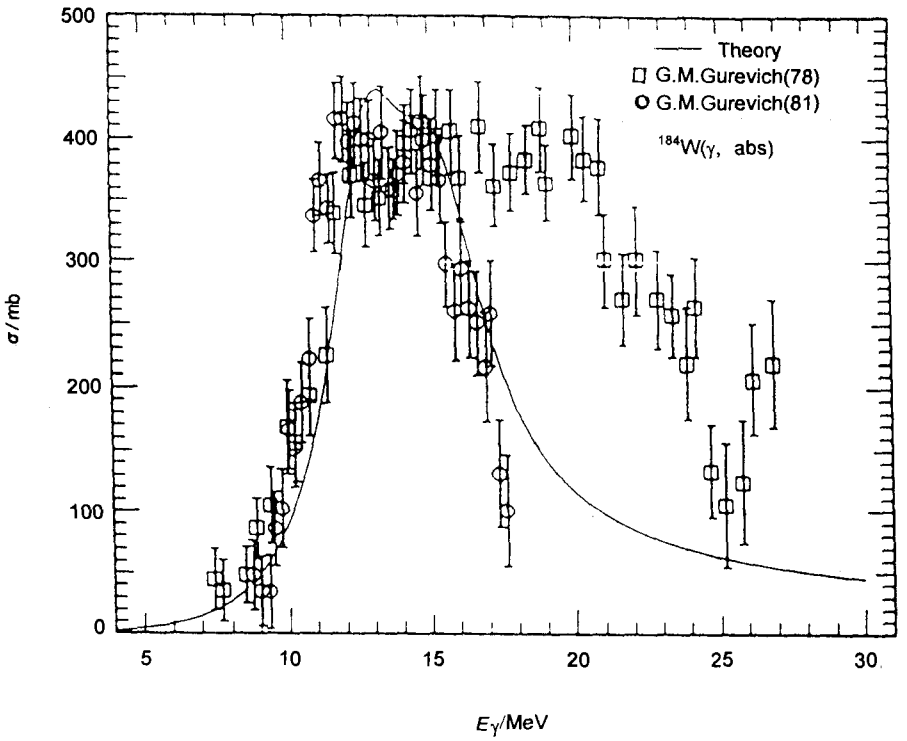

Fig.8 The comparison of calculated results with experimental data for ^{184}W(γ,abs) reaction

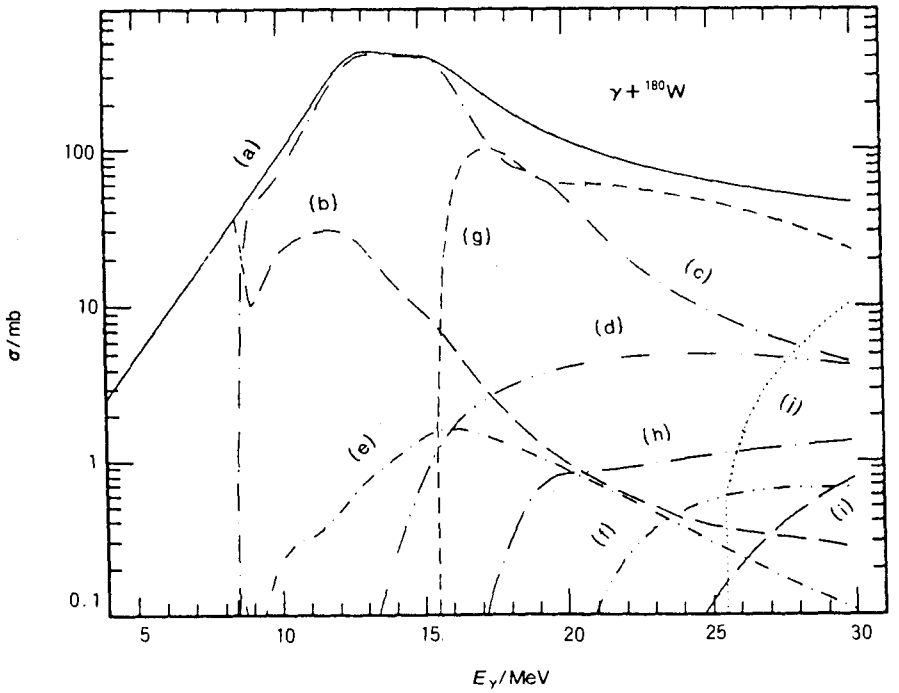

Fig.9 The recommended photonuclear reactions data for ^{180}W
(a), (b), (c), (d), (e), (f), (g), (h), (i) and (j) represent (γ,abs), (γ,γ), (γ,n), (γ,p), (γ,α), (γ,t), (γ,2n), (γ,np), (γ,nα) and (γ,3n)

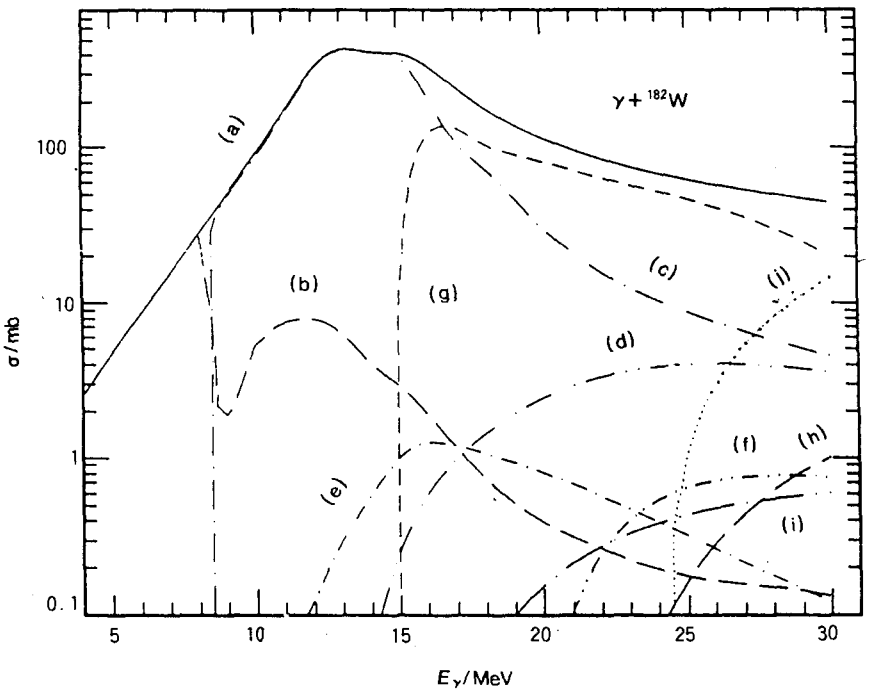

Fig.10 The recommended photonuclear reactions data for ^{182}W
(a), (b), (c), (d), (e), (f), (g), (h), (i) and (j) represent (γ,abs), (γ,γ), (γ,n), (γ,p), (γ,α), (γ,t), (γ,2n), (γ,np), (γ,nα) and (γ,3n)

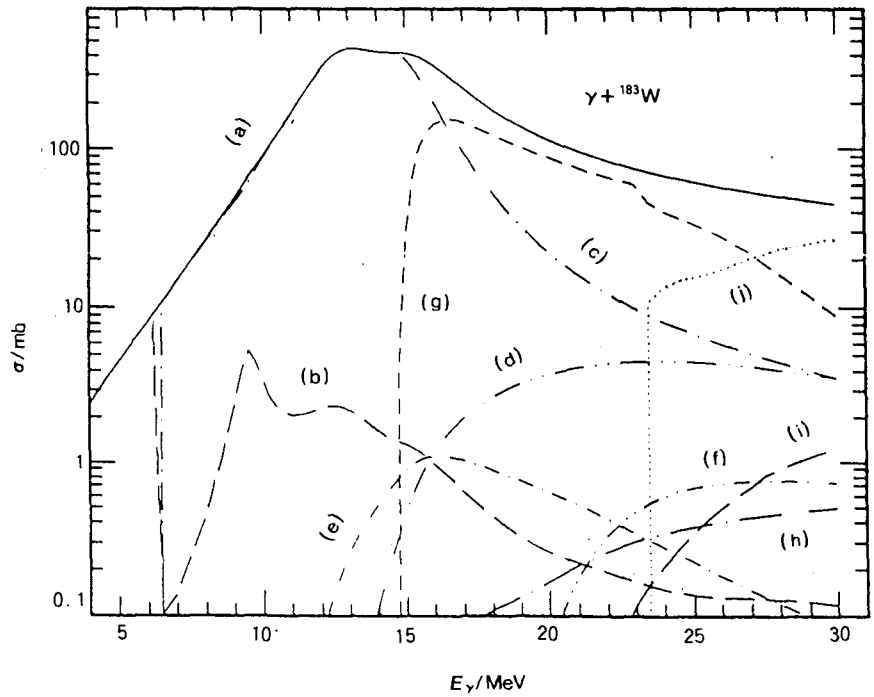

Fig.11 The recommended photonuclear reactions data for ^{183}W
(a), (b), (c), (d), (e), (f), (g), (h), (i) and (j) represent (γ,abs), (γ,γ), (γ,n), (γ,p), (γ,α), (γ,t), (γ,2n), (γ,np), (γ,nα) and (γ,3n)

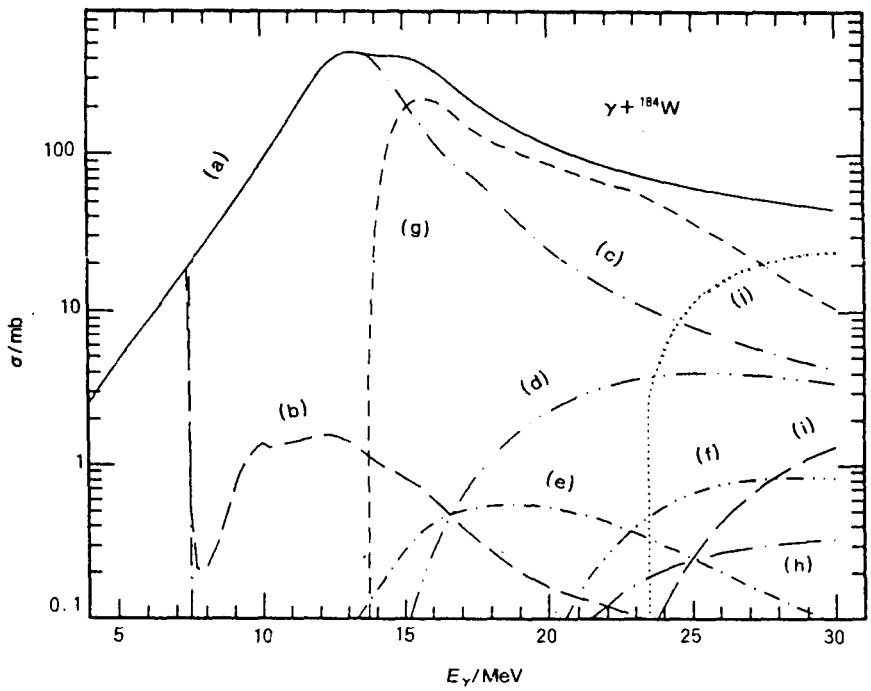

Fig.12 The recommended photonuclear reactions data for ^{184}W
(a), (b), (c), (d), (e), (f), (g), (h), (i) and (j) represent (γ,abs), (γ,γ), (γ,n), (γ,p), (γ,α), (γ,t), (γ,2n), (γ,np), (γ,nα) and (γ,3n)

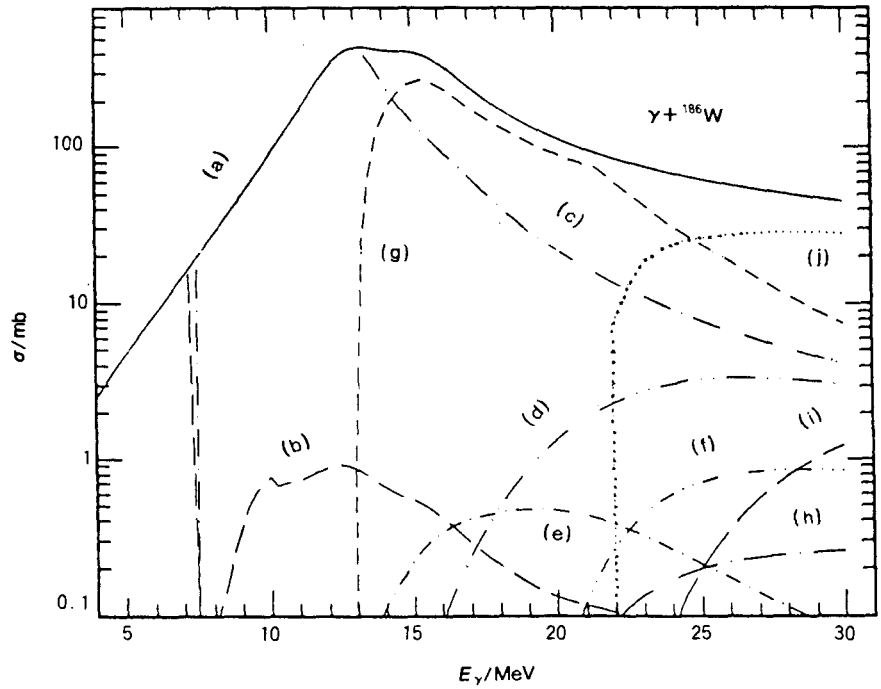

Fig.13 The recommended photonuclear reactions data for ^{186}W
(a), (b), (c), (d), (e), (f), (g), (h), (i) and (j) represent (γ,abs), (γ,γ), (γ,n), (γ,p), (γ,α), (γ,t), (γ,2n), (γ,np), (γ,nα) and (γ,3n)

For $^{180,183}W$, the used model parameters are the same as $^{182,184,186}W$. The recommended data are based on calculated data, and they are given in Fig.9 ~ 13.

For $^{180,182,183,184,186}W(\gamma,x)$ reactions, there are no experimental data. Therefore, the cross sections of emission charged particle must be calculated theoretically.

The pertinent calculations have already performed using GUNF Code[6]. At present work, the recommended cross sections for $^{180,182,183,184,186}W$ reactions from threshold to 30 MeV are given.

For the photoneutron double differential cross sections for W, the experimental data are very scarce. Therefore, the recommended data come from the theoretical calculations. The photoneutron double differential cross sections for wolfram's isotopes were obtained after testing other available experimental data, such as (γ,ABS), (γ,n), (γ,2n), (γ,2n+p), (γ,3n) etc..

Based on the optical potential parameters generated from this work for W, the double differential cross sections for emission neutron reactions, (γ,2n), (γ,3n), (γ, n+p), (γ,n+α) and ($\gamma,n_{cont.}$) with $^{180,182,183,184,186}W$ were calculated and recommended.

3 File Description for Recommended data

The data were given in ENDF/B–6 format

MF = 1 General information.

MT = 451 The general description of recommended data.

MF = 3 Photonuclear reaction cross section.

MT = 3 Photoabsorption cross section.

MT = 4 Photonuclear cross section for (γ,n) reaction.

MT = 50, 51, ..., and 91 are partial photonuclear cross section to ground, first excitation state ..., and continuum state.

MT = 16, 17 (γ,2n) and (γ,3n) reaction cross sections, respectively.

MT = 102, 103, 104, 105, 106, 107, 111 (γ,γ), (γ,p), (γ,d), (γ,t), (γ,^{3}He), (γ,α) and (γ,2p) reaction cross sections, respectively.

MF = 6 The double differential cross sections.

MT = 16 (γ,2n) reaction

MT = 17 (γ,3n) reaction

MT = 22 (γ,n+α) reaction

MT = 28 (γ,n+p) reaction

MT = 91 ($\gamma,n_{cont.}$) reaction

The check and test of the data were carried out with computer programs, including format, the consistence between the total and sum of partial cross sections,

the physics characterization and the energy balance between incident γ and emission particles.

4 Summary

The cross sections of photonuclear reactions for ^{180,182,183184,186}W have been evaluated. The characteristics of the evaluated data are as follows:

1) The present results of photonuclear reactions for ^{182,184,186}W were compared with experimental data below 30 MeV. It was shown that our results could reproduce experimental data very well.

2) The cross sections of photonuclear reactions for ^{180,182,183,184,186}W were evaluated based on the experimental data below 30 MeV and the theoretically calculated values of giant resonance in deformed nuclei. The used model parameters were determined based on experimental data. Therefore, the recommended data are reliable

Acknowledgments

The authors are indebted to IAEA (International Atomic Energy Agency), CNNC (China National Nuclear Corporation) and CIAE for their supports, and thank to Drs. Oblozinsky, T.Benson, O. Schwerer and V. V. Varlamov for their kind help and suggestions.

References

[1] B. L. Berman et al., Phys. Rev., 185, 1579(1969)
[2] G. M. Gurevich et al., J. ZEP, 28, 168(1978)
[3] A. M. Goryachev et al., J. IZK, 6, 8(1978)
[4] G. M. Gurevich et al., Nucl. Phy./A, 338, 97, (1980)
[5] G. M. Gurevich et al., Nucl. Phy./A, 351, 257(1981)
[6] Zhang Jingshang, GUNF Code, Inter Report of CEAE(1997)

CN9901242

Evaluation of Decay Data for ^{173}Lu, ^{174}Lu and ^{174m}Lu

Wu Zhendong Zhou Zhiguo Huo Junde
(Department of Physics, Jilin University, Changchun 130023)

For users' requirement we re-evaluate the decay data of ^{173}Lu, ^{174}Lu and ^{174m}Lu. In our work, we collect plenty of groups data. The recommented value was obtained by evaluating the latest data mainly and consulting the some others worthy data. The data we adopted are obtained by using precise experimental equipment and adopting good experimental method.

The half-lives,gamma-ray emission probabilities, interal conversion electron intensites of ^{173}Lu, ^{174}Lu and ^{174m}Lu are evaluated this time. The main source of references for these evaluations are also given with the recommened value.

1 Evaluation of Decay Data for ^{173}Lu

1.1 Ground State Property

a. Decay Model: Electron capture.

b. Decay Energy: $Q_\varepsilon = 670.8 \pm 1.7$ keV

c. Spin and Parity: $J^\pi = 7/2^-$

d. Produce Method ^{173}Yb(p,n), ^{175}Lu(p,3n)^{173}Hf(EC).

1.2 Half-life

We have collected five groups of experimental data.

Table 1 The half-life of ^{173}Lu

Year	Half-life / y	Ref.
1951	~1.37	[5]
1959	1.30 6	[2]
1960	1.32 8	[3]
1960	1.71 14	[1]
1960	1.37 1	[4]
	1.37 1	Weighted Mean
	1.33 2	Unweighted Mean

The data and their uncertainties are given in Table 1, in which R. G. Wilson[1] used 92.6 percent of concentrated ^{173}Yb (Including 4.31 percent of ^{174}Yb, 2.33 percent of ^{172}Yb and ^{168}Yb, ^{170}Yb, ^{171}Yb, ^{176}Yb) to produce ^{173}Lu. They followed the

track of KX-ray and gamma-ray (Such as 79 keV γ-ray). After followed 0.4 half-life he obtained the data of the half-life of ^{173}Lu. So the data of [1] are apparently higher than the data of other groups. We use the data of [2], [3] and [4] to make out weighted mean and unweighted mean, which are listed in the Table 1.

By the view of above, we choose 1.37±0.01 year as our recommended half-life of ^{173}Lu.

1.3 Data of γ-ray

a. γ energy

The data of γ energy are from [6].

b. Relative emission probability of γ-ray.

1.4 Normalizition Factor

a. $I_\varepsilon(gs) \leq 2.2$

b. From the decay scheme of ^{173}Lu[6], we know γ transition which fed ground state of daughter nucleus.

Table 2 γ energies and relative intensities of ^{173}Lu decay

E_γ/ keV	92Ad08[7]	73Se16[8]	70Ku14[9]	Recommended Value
62.17 3	0.79 4			0.79 4
78.63 3	56.0 8	60 2	61 9	56.0 8
100.724 20	24.7 4	24.0 8	24 4	24.7 4
111.109 12	0.252 10	0.33 3	0.25 5	0.252 10
122.55 3	0.079 3	0.14 7	0.086 10	0.079 3
171.393 13	13.7 5	13.6 6	13.6 13	13.7 5
179.365 11	6.49 12	6.42 20	6.3 5	6.49 21
223.163 20	0.72 3	0.73 5	0.65 6	0.72 3
223.605 12	2.61 5	2.66 5	2.6 2	2.61 5
272.105 15	100.0 15	100	100	100.0 15
285.362 6	2.88 8	2.71 4	2.7 2	2.88 8
334.321 11	0.514 20	0.503 15	0.49 5	0.514 20
350.774 18	1.42 5	1.43 5	1.50 13	1.42 5
442.08		≤0.02		≤0.02
456.79 3	0.663 22	0.60 2	0.74 9	0.663 22
557.497 25	2.45 9	2.30 8	3.0 2	2.45 9
636.11 3	6.85 22	6.7 2	8.7 6	6.85 22

c. The Calculation of normalization factor K

From $K\sum I_{\gamma i}(1+\alpha_i) + I_\varepsilon(gs) = 100\,(i = 1, 2, 3, 4, 5)$

Obtained $K = 0.212\pm0.007$.

Table 3 γ transition fed ground state of daughter nucleus

E_γ	I_γ	α
78.63	56.0 8	7.01
179.365	6.49 12	0.392
350.774	1.42 5	0.017
442.8	≤0.02	
636.11	6.85 22	0.0199

Table 4 Recommended value of γ-ray

E_γ / keV	Absolute Intensity	InternalConvertion Electron Itensity
62.17 3	0.167 10	2.25 14
78.63 3	11.9 4	83 3
100.724 20	5.24 19	2.1 7
111.109 12	0.0534 28	0.0139 7
122.55 3	0.0167 8	0.0321 15
171.393 13	2.90 14	0.249 17
179.365 11	1.38 8	0.54 3
223.163 20	0.153 8	0.289 15
223.605 12	0.553 21	0.026 7
272.105 15	21.2 8	0.538 20
285.362 6	0.61 3	0.0140 10
334.321 11	0.109 6	0.0019 8
350.774 18	0.301 15	0.0051 12
442.08	≤0.004	
456.79 3	0.141 7	0.0062 4
557.497 25	0.519 25	0.0093 5
636.11 3	1.45 7	0.0289 14

2 Evaluation of Decay Data for ^{174}Lu

2.1 Ground State Property

a. Decay Model

β^+ decay, electron capture.

b. Decay Energy

Q_ε=1376.0±1.8 keV

c. Spin and Parity

$J^\pi = 1^+$

d. Produce Method

^{174}Yb(p,n), ^{174}Yb(d,2n), ^{175}Lu(n,2n)

2.2 Half-life

We get four groups experimental data.

Table 5 The Half-life of ^{175}Lu

Year	$T_{1/2}$ / y	Ref.
1962	3.56 0.41	[10]
1964	3.56	[11]
1965	3.56	[12]
1973	3.31 0.5	[13]

2.3 Data of γ-ray

a. γ-ray energies from [14].
b. Relative emission probability of γ-ray.

Table 6 γ energies and relative intensities of ^{174}Lu decay

E_γ/ keV	87Va34[15]	74Sc15[16]	Recommended Value
76.468 2	115.3 52		115.3 52
176.653 2	0.210 10		0.21 1
1065.04 8	0.32 4	0.45 8	0.32 4
1241.847 6	100.0 21	100	100 2
1318.296 10	0.69 5	0.63 4	0.69 5

2.4 Normalization Factor

Table 7 Recommended value of γ-ray

E_γ / keV	Absolute Intensity	Internal Covertion Electron Intensity
76.468 2	5.9 3	56 3
176.653 2	0.0108 5	0.004482 21
1065.04 8	0.0164 21	
1241.847 6	5.14 13	
1318.296 10	0.035 3	

In view of that the γ-ray intensities in the data we collected all are relative intensity, no absolute intensities and Lu has electron capture decay whose intensity is difficult to be measured, so we make out the normalization factor K by using X-ray intensity. Both the internal covertion and electron capture may give out X-ray, so we have:

$$KI_{Xk} = (I_\varepsilon + KI_{cek})\omega$$

Where $\omega = 0.95$ $I_{Xk} = 1615 \pm 3$

I_{cek} = 187.0±0.8 $I_{\varepsilon} = \varepsilon_k(0^+)+\varepsilon_k(2^+) = 82$

Obtained: K = 0.0514±0.0008

3 Evaluation of Decay Data for ^{174m}Lu

3.1 Isomeric State Property

a. Decay Model

Electron capture (%I_{ε}= 0.62±0.02)

IT decay (%IT = 99.38±0.02)

b. Decay Energy

$Q_{\beta+}$(gs) = 1376.0±1.8 keV.

Q_{IT} = 170.83±0.05 keV.

c. Spin and Parity

J^{π} = 8^-

d. Produce Method

^{174}Yb(p,n), ^{174}Yb(d,2n), ^{175}Lu(n,2n)

3.2 Half-life

Table 8 The Half-life of ^{174m}Lu

Year	Half-life / d	Ref.
1960	160 10	[17]
1962	140 10	[18]
1964	150 40	[19]
1965	150 20	[20]
1967	157 5	[21]
1973	142 2	[22]
1975	141 5	[23]
	142 2	Weighted Mean
	147 7	Unweighted Mean

3.3 Data of γ-ray

Table 9 γ energy and relative intensity of ^{174m}Lu decaying to ^{174}Lu

E_{γ} / eV	87Va34[25]	Recommended Value
44.683 3	2291 50	2291 50
59.08 2		5.3* 2
67.058 3	1336 27	1336 27
111.762 7	55.0 15	55.0 15
126.2 3		2.8* 20

a. γ energy

The data of γ energy are from [24].

b. Relative emission probability of γ-ray

Table 10 γ energy and relative intensity of ^{174m}Lu Decaying to ^{174}Yb

E_γ / keV	87Va34[25]	69Gu15[26]	67Ka13[27]	Recommended Value
76.468 2	16 12			11.7 3
176.653 2	86.2 21	71	80 20	86.2 21
272.914 12	100.8 31	97	95 10	100.8 31
363.64 5	2.88 18			2.88 18
628.21 8	2.65 31			2.65 31
992.08 3	100.0 21	100	100	100.0 21
1264.98 7	3.02 23		3.0 10	3.02 23

3.4 Normalization Factor

Table 11 γ transition fed to ground state of daughter nucleus

γ transition that ^{174m}Lu fed to ground state of ^{174}Yb		
E_γ / keV	I_γ	α
76.468 2	11.7 3	9.46
γ transition that ^{174m}Lu fed to ground state of ^{174}Lu		
44.683 3	2.29E3 5	6.9 3
111.762 7	55.0 15	2.2 3

Table 12 Recommended value of γ-ray of ^{174m}Lu decaying to ^{174}Lu

E_γ / keV	Absolute Intensity	Internal Covertion Electron Intensity
44.683 3	12.5 5	86 5
59.08 2	0.0289 15	96 5
67.058 3	7.3 3	88 4
111.762 7	0.300 13	0.67 3
126.2 3	0.015 11	4 3

Table 13 Recommended Value of γ-ray of ^{174m}Lu Decaying to ^{174}Yb

E_γ / keV	Absolute Intensity	Internal Covertion Electron Intensity
76.468 2	0.064 3	0.61 3
176.653 2	0.471 19	0.195 8
272.914 12	0.550 25	0.0545 25
363.64 5	0.0157 11	0.00066 5
628.21 8	0.0145 18	
992.08 3	0.546 21	0.00263 10
1264.98 7	0.0165 14	

The data we collected are all γ-ray relative intensity, no absolute intensities were

measured. Because $I_{\varepsilon}(\mathrm{gs})+K\sum I_{\gamma}(1+\alpha_i)=100$ and I_{ε} = 0. So that $K=100/\sum I_{\gamma i}(1+\alpha_i)$, K = 0.00546±0.00018.

References

[1] R. G. Wilson et al., Phys. Rev., 117, 807(1960)
[2] J. B. Bichard et al., Phys. Rev., 116, 720(1959)
[3] E. P. Grigoev et al., Izv. Akad. Nauk SSSR, Ser. Fiz. 24, 841(1960)
[4] N. A. Bonner et al., Phys. Rev., 127, 217(1962)
[5] G. Wilkinson et al., Phys. Rev., 81, 540(1951)
[6] V. S. Shirley, Nucl. Data Sheets, 75, 377(1995)
[7] I. Adam et al., Izv. Akad. Nauk SSSR, Ser. Fiz., 56, 160(1992)
[8] V. A. Sergienko et al., Proc. 23rd Ann, Conf. Nucl. Spectrosc. Struct. At. Nuclei, Tbilisi, P103(1973)
[9] W. Kurcewie et al., Acta. Phys. Pol, A38, 123(1970)
[10] N. A. Bonner et al., Phys.Rev., 127, 217(1962)
[11] V. A. Balalaev et al., Zh. Eksperim i Teor.Fiz., 46, 1478(1964); Soviet Phys. JETP, 19, 998 (1964)
[12] L. Funke et al., Nucl. Phys., 61, 456(1965)
[13] D. Nethaway, Priv. Comm., (Febrary 1973)
[14] B. Kantele et al, Z.Physik, 204, 456(1967)
[15] V. A. Balalaev et al., Program and Theses. Proc. 19th Ann. Conf. Nucl. Spectrosc. At. Nuclei, Erevan. P124(1969)
[16] S. K. Vasilev et al., Izv. Akad. Nauk SSSR, Ser. Fiz., 51, 1898(1987)
[17] R. G. Wille et al., Phys. Rev., 118, 242(1960)
[18] N. A. Bonner et al., Phys. Rev., 127, 217(1962)
[19] V. A. Balalaev et al. Zh. Eksperim i Teor. Fiz., 46, 1478(1964); Soviet Phys. JETP, 19, 998 (1964)
[20] L. Funke et al., Nucl. Phys., 61, 456(1965)
[21] A. Gizon et al., Nucl. Phys., A96, 401(1967)
[22] D. Nethaway, Priv. Comm. (Febrary 1973)
[23] H. Kirschner et al., Z. Phys., A272, 287(1975)
[24] E. Browne, Nucl. Data Sheets, 62, 1(1991)
[25] S. K. Vasilev et al., Izv. Akad. Nauk SSSR, Ser. Fiz., 51, 1898(1987)
[26] R. Gunnink et al., UCID-15439(1969); Priv. Comm. (January 1969)
[27] J. Kantele et al., Z. Physik, 204, 456(1967)

Evaluation of Decay Data for ^{175}Hf

Zhang Wei Zhou Zhiguo Huo Junde

(Department of Physics, Jilin University, Changchun 130023)

The ^{175}Hf is an important radionuclide and its decay data are fundamental data in nuclear applications.

1 Ground State Property

a. Decay Model
Electron capture
b. Decay Energy
Q_ε = 683.3±2.9 keV
c. Spin and Parity
$J^\pi = 5/2^-$
d. Produce Method
^{174}Hf(n,γ), ^{175}Lu(p,n).

2 Half-life

We get two groups experimental data(See Table 1).

Table 1 The half-life of ^{175}Hf

Year	$T_{1/2}$ / d	Ref.
1962	70 2	[1]
1964	70 2	[2]

3 Data of γ-ray

3.1 Energy of γ-ray

The data of γ-ray are from Ref. [3] mainly.

3.2 Relative intensity of γ-ray (See Table 2)

Table 2 γ energies and relative intensities of ^{175}Hf decay

E_γ / keV	88Si22[4]	69Jo16[5]	68Ja11[6]	Recommended Value
89.36 1	2.886 22	2.6 3	2.9 5	2.86 22
113.81 2	0.352 32	0.36 4	0.35 8	0.35 3
143.9				
161.3 2		0.027 10		0.027 10
229.6 6	0.813 20	0.89 8	0.88 18	0.813 20
318.9 6		0.20 4		0.20 4
343.40 8	100	100 1	100	100 1
353.3 2	0.272 20	0.27 4		0.272 20
433.0 5	1.709 31	1.7 9	1.9 4	1.71 3

3.3 Internal Conversion Electron Intensity

The experimental internal transition data of ^{175}Hf were seen in reference[3~5, 7~9].

4 Normalization Factor

4.1 I_ε(gs) ≤ 7%

4.2 From the decay scheme of ^{175}Hf[10], the γ transition fed to ground state of daughter nucleus are given in Table 3.

Table 3 γ transition fed to ground state of daughter nucleus

E_γ / keV	I_γ	α
113.81	0.35 2	2.51
343.40	100 1	0.118
353.3	0.272 20	0.014
433.0	1.71 3	0.0663

4.3 The Calculation of Normalization Factor *K* (See Table 4)

From $K\sum I_{\gamma i}(1+\alpha_i)+I_\varepsilon(\mathrm{gs})=100$,

Obtained $K=0.81\pm0.01$

Table 4 Recommended Value of γ-ray

E_γ / keV	Absolute Intensity, P_γ	Internal Conversion Electron Intensity, P_e
89.36 1	2.32 18	12.1 9
113.81 2	0.283 25	0.71 4
143.9		
161.3 2	0.021 8	0.020 7
229.6 6	0.659 18	0.117 3
318.9 6	0.16 3	0.0235 4
343.40 8	81.0 13	9.6 15
353.3 2	0.220 16	0.00308 22
433.0 5	1.39 3	0.0921 19

References

[1] G. Wilkinson et al., Phys. Rev., 75, 696(1949)
[2] C. L. Rao et al., Can. J. Chem., 41, 2516(1963)
[3] E. N. Hatch et al., Phys. Rev., 104, 745(1956)
[4] K. Singh et al., J. Phys. Soc. Jpn., 57,3762(1988)
[5] K. H. Johansen et al., Nucl. Phys., A133, 213(1969)
[6] A. Jasinski et al., Ark. Fys., 37, 585(1968)

[7] B. Harmatz et al., Nucl. Phys., 81, 418(1966)
[8] E. Bashandy et al., Ark. Fys, 21, 49(1962)
[9] P. Erman et al., Nucl. Phys., A92, 241(1967)
[10] A. O. Macchiavelli et al., Nucl. Data Sheets, 69, 903(1993)

CN9901244

Nuclear Data Sheets Update for A= 56

Wang Zhe Li Zhihuan Huo Junde
(Department of Physics, Jilin University, Changchun 130023)

The 1992 version of Nuclear Data Sheets for A = 56 had been evaluated on the nuclear reaction and decay experiments leading to ^{56}Ti, ^{56}V, ^{56}Cr, ^{56}Mn, ^{56}Fe, ^{56}Co basis of ^{56}Ni, ^{56}Cu and ^{56}Zn since the date of last evaluation, December 1991. The nuclei of updated data are ^{56}Mn, ^{56}Fe and ^{56}Co. A new data set on ^{54}Cr(α,d)^{56}Mn E = 55 MeV was added. Nine resonances for ^{55}Mn(p,γ)^{56}Fe reaction at E_p = 1320, 1435, 1441, 1446, 1452, 1455, 1460, 1508 and 1649 keV were added. The level properties and their Gamma radiations from reaction and decay experiments are presented by means of schemes or tables. The levels and updated Gamma radiation for all nuclei are showed in the tables. The references and necessary comments are given in text.

In present paper new recommended values of half-life for ^{56}Ti, ^{56}Mn, ^{56}Co and ^{56}Ni are as follows:

^{56}Ti	$T_{1/2}$ = 0.15±0.03 s
^{56}Mn	$T_{1/2}$ = 2.5789±0.0001 h
^{56}Co	$T_{1/2}$ = 77.233±0.027 d
^{56}Ni	$T_{1/2}$ = 6.075±0.010 d

The updated version of Nuclear Data Sheets has been sent to National Nuclear Data Center, Brookhaven National Laboratory, USA, and will be published in Nuclear Data Sheets.

IV BENCHMARK TEST AND APPLICATION

Research on Amplification Multiple of Source Neutron Number for ADS

Liu Guisheng Zhao Zhixiang Zhang Baocheng Shen Qingbiao Ding Dazhao
(China Nuclear Data Center, CIAE)

Abstract

NJOY-91.91 and MILER code systems was applied to process and generate 44 group cross sections in AMPX master library format from CENDL-2 and ENDF/B-6. It is important an ADS (Accelerator-Driven System) assembly spectrum is used as the weighting spectrum for generating multi-group constants. Amplification multiples of source neutron number for several fast assemblies were calculated.

Introduction

It is effective that using an ADS assembly to transmute nuclear waste. It will be a hopeful new energy source; that is to say, the assembly will be used to produce electric power. C. Rubbia has proposed the ADS as an "energy amplifier" for producing electric power[1~3]. USA, Japan, Russia and NEA have carried out lots of research works.

A research group of "accelerator-driven clean nuclear power system" was founded at the China Institute of Atomic Energy in 1995. Up to now the research group has made great progress[4].

When a heavy target is bombarded by proton beam with about 1 GeV energy and beam current of 10 mA from an accelerator, 20 ~ 40 neutrons per proton are produced by spollation reaction. These spoliation neutrons are poured into a subcritical assembly composed of fuel element, moderator, coolant and structural material. The steady neutron fluxes with 10^{14}~10^{15} n/cm^2/s are formed through neutron multiplication.

Maybe it is not possible for China to build such accelerator with high beam intensity in a short time. So, it is important how to reduce the requirement for accelerator current. In this paper the selection of weighting spectrum generating multi-group constants and amplification nature of source neutron number for fast core of subcritical assembly will be discussed.

1 Generations of Multi-group Constants

NSLINK code system[5] was applied to process evaluated nuclear data and to generate 44-group library in AMPX master library format from CENDL-2 and ENDF/B-6. NJOY-91.91 of the NSLINK can produce infinite dilution multi-group cross sections, transfer matrices and self-shielding factors dependent on reactions, temperature and σ_0. The output data file of multi-group cross sections from module GROUPR of NJOY is called the GENDF in ENDF/B format. The another module MILER read two GENDF data files independent from and dependent on temperature, respectively. And then the two files are converted into a multi-group cross section data file with Bondarenko self-shielding factors in the AMPX master library format.

In order to test the effect of weighting spectrum used as generating multi-group constants on the calculation results of integral quantities, the both of weighting functions, i.e. standard spectrum (thermal Maxwellian $+1/E+$fission spectrum) and an energy spectrum of the calculated ADS were applied to produce two sets of 44 group libraries, respectively.

2 Transport Calculation Method

2.1 Calculation Process

Module AJAX, BONAMI, NITAWL and XSDRNPM in the SCALE–3 code system[6] were used in our calculations. The module AJAX can select the concerned multi-group data from AMPX master library to produce a new master library. The BONAMI performs a resonance self-shielding calculation based on the Bondarenko method and generates a problem-dependent master data set. The NITAWL converts the AMPX master library into an AMPX working library. The XSDRNPM is one dimensional transport code. It calculates K_{eff} and amplification multiple of source neutron number for fast subcritical assembly.

2.2 Spectrum of Spallation Neutron Source

Professor Shen Qingbiao calculated a spectrum of spallation neutron source for a lead target using Monte Carlo method. The normalized spectrum and 44-group structure are listed in Table 1.

Table 1 44-Group Energy Structure and Spallation Neutron Source Spectrum

g	ΔE / MeV	Source	g	ΔE / MeV	Source	g	ΔE / eV	Source
1	20~15	0.02206	16	1.5~1.0	0.07315	31	1000~800	0.0
2	15~12	0.05067	17	1.0~.8203	0.02673	32	800~600	0.0
3	12~10	0.04346	18	0.8203~0.5	0.04752	33	600~400	0.0
4	10~0.9	0.02565	19	0.5~0.2	0.03591	34	400~200	0.0
5	9.0~8.0	0.02935	20	0.2~0.1	0.00827	35	200~100	0.0
6	8.0~7.0	0.03654	21	0.1~0.08	8.94E-4	36	100~80	0.0
7	7.0~6.0	0.04566	22	0.08~0.06	8.94E-4	37	80~60	0.0
8	6.0~5.0	0.05229	23	0.06~0.04	8.94E-4	38	60~40	0.0
9	5.0~4.5	0.02816	24	0.04~0.02	8.94E-4	39	40~20	0.0
10	4.5~4.0	0.03266	25	0.02~0.01	8.94E-4	40	20~10	0.0
11	4.0~3.5	0.03639	26	0.01~.008	0.0	41	10~5	0.0
12	3.5~3.0	0.04059	27	0.008~.006	0.0	42	5.0~1.0	0.0
13	3.0~2.5	0.04543	28	0.006~.004	0.0	43	1.0~0.1	0.0
14	2.5~2.0	0.05325	29	0.004~.002	0.0	44	0.1~1E-5	0.0
15	2.0~1.5	0.06320	30	0.002~.001	0.0			

These spallation neutron spectrum data are used as input data running XSDRNPM to calculate the amplification multiple of source neutron number.

2.3 Calculations of Amplification Multiple of Source Neutron Number

When the source neutrons interact on fissionable nuclides, fission reactions arise and neutrons with fission spectrum energy are produced. It is also possible that other nuclear reactions occur, for example, some neutrons are absorbed by these fissionable nuclides. Especially, inelastic-scattering reactions of ^{238}U make the system spectrum soften. As these nuclear reaction processes are repeated many times, a steady energy spectrum of the assembly is formed.

Let R, μ and $\psi_g(r,\mu)$ represent outer radius, neutron direction cosine and neutron angle flux, respectively. On the surface of sphere system the number projected g group neutrons per second per cm^2 is equal to the neutron current $J_g^+(R)$. It is defined as following:

$$J_g^+(R)=\int_0^{+1}\mu\psi_g(r,\mu)\mathrm{d}\mu$$

The total neutron current is $J^+(R)=\sum_g J_g^+(R)$. The total leakage neutron

number is equal to an integral of $J^+(R)$ with respect to the outer surface of the sphere.

$$\text{Total leakage} = 4\pi R^2 J^+(R)$$

Let L and S represent the amplification multiple of source neutron number and the normalized source intensity, respectively. So,

$$L = \text{Total Leakage} / S$$

3 Weighting Spectrum Effect

A weighting function should be selected in NJOY code when multi-group constants are generated. It has been proved that the weighting function used in generating multi-group cross sections must be approximated to the spectrum of the calculated assembly spectrum as far as possible[7]. Unfortunately, the spectrum is unknown before the assembly is calculated. Therefore, a standard spectrum, i.e. thermal Maxwellian +1/*E*+ fission spectrum has usually been selected.

In order to further test the weighting spectrum effect on the calculated integral quantity results, iteration process to weighting spectrum has adopted to generate multi-group constants. Firstly, the standard spectrum is used for generating 44-group library and calculating a spectrum of the subcritical assembly including the spallation neutron source and some integral quantities. Secondly, the calculated assembly spectrum is used as weighting function to reproducing another 44-group library with the same energy structure and elements. For a subcritical sphere system of natural uranium of 20 tons with a spollation neutron source at the center such integral parameters as K_{eff}, K_∞, F_{25} (^{235}U fission rate), F_{28} (^{238}U fission rate) and C_{28} (^{238}U capture rate) have been calculated with both of the libraries of 44-groups. The results are shown in Table 2.

Table 2 Effects of Weighting Spectrum on Integral Parameters

Weighting	Group	K_{eff}	K_∞	F_{25}	F_{28}	C_{28}	Flux
System	44	0.4042	0.4304	0.0360	0.3670	2.0420	248.88
System	8			0.0359	0.3644	2.0369	248.02
Standard	44	0.3412	0.3644	0.0306	0.3003	1.8877	197.93
Standard	8			0.0307	0.3033	1.8937	198.52

With the library from the standard spectrum the calculated total flux, K_{eff}, F_{28} and C_{28} have been decreased by 20.5%, 20.7%, 18.2%, 7.6%, respectively, compared with that from the assembly spectrum. It is the reason that the spectrum of the subcritical assembly with spallation neutron source is more harder than the standard spectrum. It results in that the values of the fission cross sections weighted by the

assembly spectrum for ^{238}U at high energy region are larger than that by the standard spectrum. Consequently, the following results are calculated with the library of 44-groups reproduced by the spectrum of subcritical assembly.

4 Calculational Results

4.1 Homogeneous Sphere System Mixed ^{238}U, ^{239}Pu, ^{99}Tc and Pb

4.1.1 Amplification Multiple of Source Neutron Number Varies with K_{eff}

A fuel cycle process for a subcritical assembly of a depleted uranium sphere of 20 tons with an external source at the center of the sphere was calculated. According to these calculation results the following three models are adopted,

System 1: R = 43 cm, depleted U of 4 tons, ^{239}Pu with different weight, ^{99}Tc of 0.7 tons;

System 2: R = 49 cm, depleted U of 6 tons, ^{239}Pu with different weight, ^{99}Tc of 1.2 tons;

System 3: R = 54 cm, depleted U of 8 tons, ^{239}Pu with different weight, ^{99}Tc of 1.7 tons.

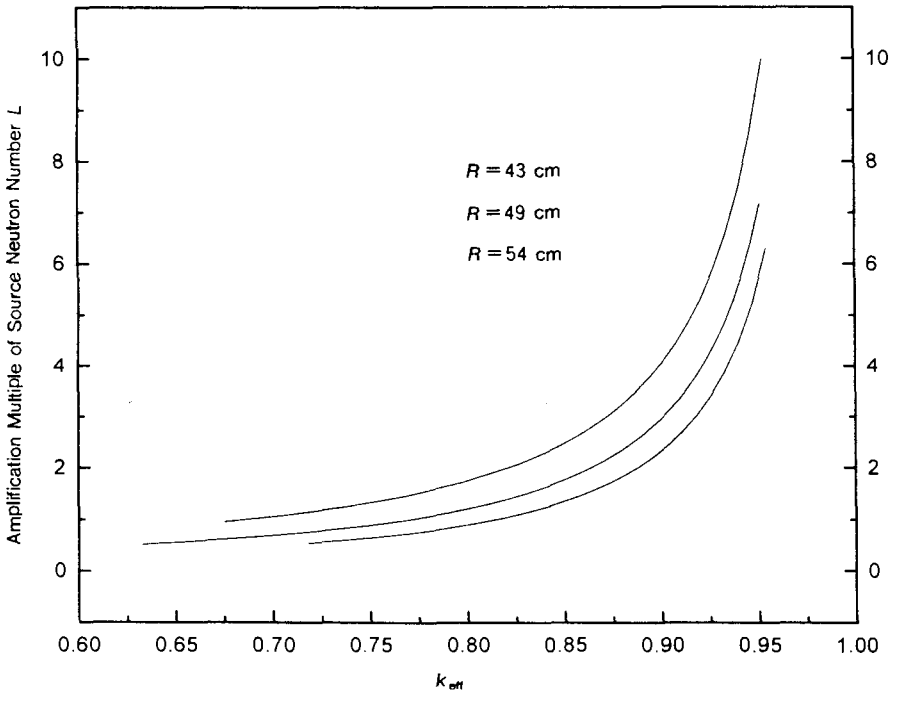

Fig.1 L varies with K_{eff} for U-Pu fuel cycle system

For System 1 the 200 kg of ^{239}Pu increased to 395 kg, so that K_{eff} and the amplification multiple L of source neutron number increased from 0.6752 and 0.9439 to 0.9523 and 9.9879, respectively. For the System 2 that 240 kg of ^{239}Pu increased to 545 kg results in that K_{eff} and L increased 0.6326 and 0.5087 to 0.9508 and 7.1818, respectively. For System 3 that 400 kg of ^{239}Pu increased to 1000 kg results in that K_{eff} and L increased from 0.7180 and 0.5355 to 0.9542 and 6.3123, respectively. All of the calculated results are shown in the Fig.1. It will be seen from the Fig.1 that the amplification multiple L of source neutron number is larger, the smaller the radius of system is.

4.1.2 Amplification Multiple of Source Neutron Number Varies with Radius of System

Three sets of calculation models, whose values of K_{eff} are equal to 0.95, 0.92, and 0.88, respectively, are selected from above the calculated System 1 (R = 43 cm). On condition that keeping the values of K_{eff} unchanged, increasing radii of systems, decreasing nuclear densities of ^{239}Pu and the values of K_{eff} selves have not been kept variations, the L values for each given system have been calculated. Three sets of the calculated results are shown in the Fig.2. It has been proved that the amplification multiple of source neutron number have been gradually decreased with increasing radius of system when all of K_{eff} values are the same. If the radii are equal, the larger value of K_{eff} is, the larger L. Keeping R = 50 cm, for example, if K_{eff} is equal to 0.88, then L is equal to 2.2; if K_{eff} = 0.95, then L = 6.9. The last value of L is more than 3 times that of the first.

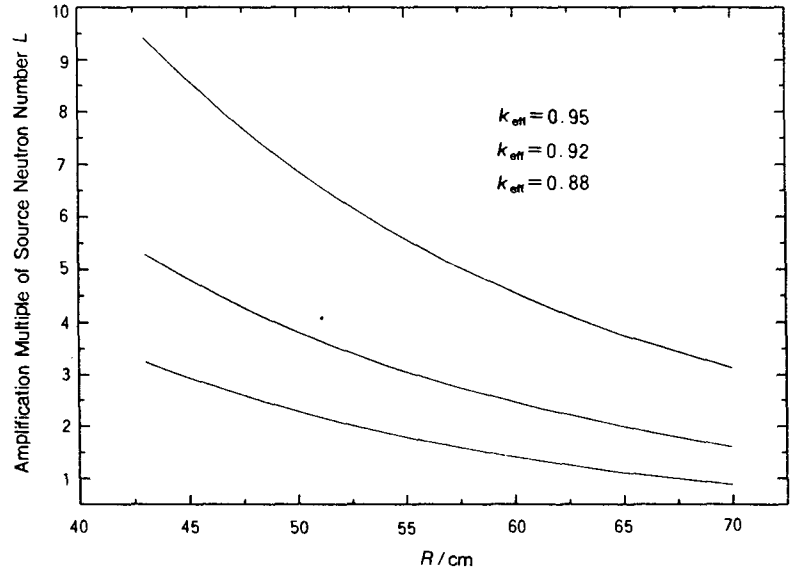

Fig.2 L varies with radius for U-Pu fuel cycle system

4.2 Homogeneous Sphere System Mixed ^{238}U, ^{239}Pu, ^{99}Tc and Pb with Graphite Reflector

For physics concept research to ADS an assumption of single direction couple was put forward by Dr. O. V. Shvedov, who is from Russia. The idea is that an U-Pu fuel cycle zone is used as the fast multiplication zone, which has small volume and 100 MWe and is mainly applied to amplification source neutron number, in order to enable the power of the thermal zone to increase to 1000 MWe. The so-called single direction couple means that a graphite reflector is added between fast and thermal zones, so that fast neutrons enter thermal zone easily and thermal neutrons enter fast zone uneasily. The single direction couple is not absolute and it can only be relative. Although capture cross section in fast energy region for graphite is 100 times larger than that of thermal energy region, thermal capture cross section of 1.0×10^{-6} b for ^{12}C is, after all, very small. What causes the single direction couple? It is the reason that the graphite is an excellent reflecting material for thermal neutrons, because elastic scattering cross section of graphite at thermal energy region is about 5 barns.

In order to make a research on the effect of graphite reflector on amplification multiple of source neutron number the following both of cores are selected,

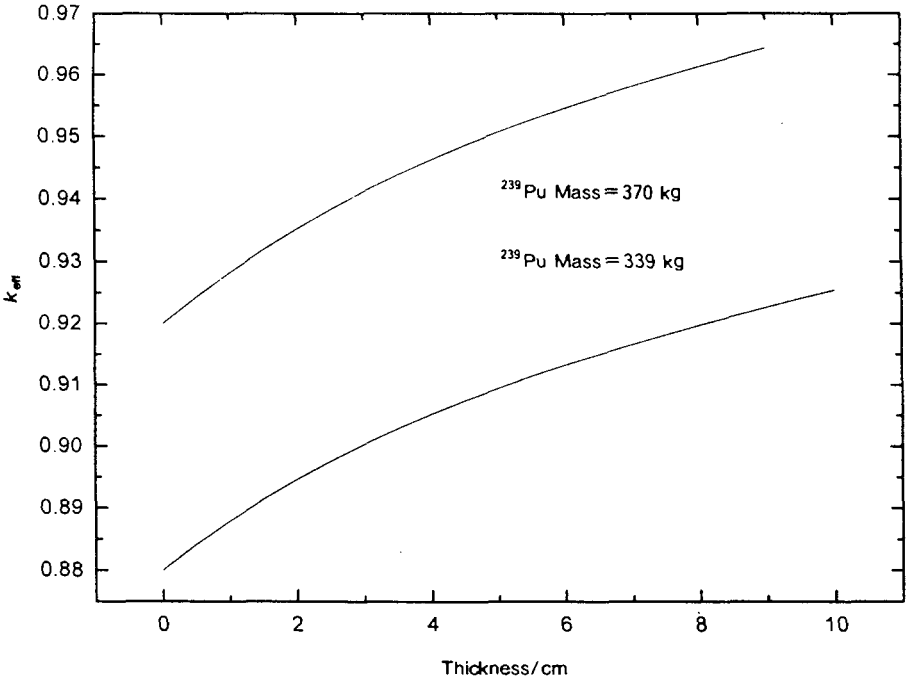

Fig.3 K_{eff} varies with graphite thickness for U-Pu fuel cycle system

K_{eff} = 0.92, R = 43 cm, 4 tons Natural Uranium, 370 kg ^{239}Pu and 700 kg ^{99}Tc;

K_{eff} = 0.88, R = 43 cm, 4 tons Natural Uranium, 339 kg ^{239}Pu and 700 kg ^{99}Tc.

And graphite is used as reflector with different thickness. It was calculated that K_{eff} and L values varied with thickness of graphite reflectors, respectively. These calculated results are presented in the Fig. 3 and 4, respectively.

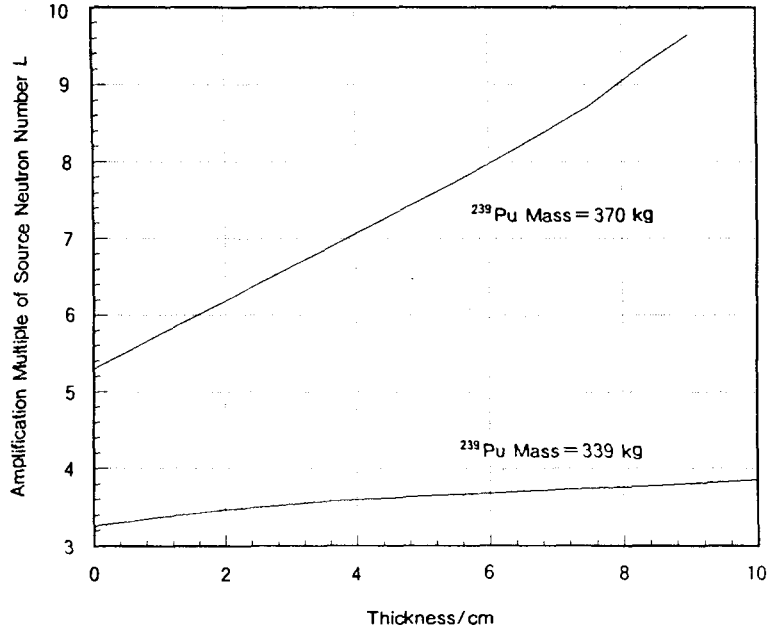

Fig.4 L varied with graphite thickness for U-Pu system

Owing to the fact that graphite is also a good reflector for fast neutrons, both of K_{eff} and L values have gradually been increased, accompanied by increasing thickness of graphite. Fig.3 shown variations in K_{eff}, two curves resemble with each other in the shape. However, they are different in Fig.4. For the curve loaded more ^{239}Pu the L value has rapidly risen with increasing the thickness of graphite reflector. When the value of thickness is from zero to 9 cm, the L value is from 3.25 to 3.80. In brief, the loaded nuclear fuel can not only be decreased appropriately but the amplification multiple of source neutron number can be increased, because the graphite reflector is added between fast and thermal zone.

5 Analyses and Conclusions

5.1 The weighting spectrum, used for generating multi-group library and applied to perform a calculation related to subcritical assembly driven by a spallation neutron source, should be the energy spectrum of the assembly. The usual standard spectrum

can not be used as weighting spectrum, otherwise the calculated amplification multiple of source neutron number will have remarkable error.

5.2 The larger $K_{eff,}$ the larger amplification multiple of source neutron number. When K_{eff} close to 1, L tends to infinity.

5.3 Increasing external radius of system and keeping the value of K_{eff} unchanged, the amplification multiple of source neutron number is decreased, because the neutrons are absorbed by the system.

5.4 It will be seen from the results calculated U-Pu fuel cycle system that if K_{eff} = 0.95, then L = 9.42, K_{eff} = 0.92, L = 5.52. It means that it is entirely possible to reduce requirement for source neutron intensity.

5.5 For a U-Pu fuel cycle system, K_{eff} is gradually increased with increasing thickness of graphite reflector. Owing to increasing value of K_{eff}, amplification multiple of source neutron number is large, too.

5.6 A fast-thermal coupled system may be a best energy amplification assembly. The target generating source neutrons is located at the center of the system. The mixed U-Pu fuel, which is close to the target, is used as a fast multiplication zone. It was surrounded with 5 cm thickness of graphite reflector. Surrounding the fast zone, there is a large thermal zone composed of Thorium or Natural Uranium with coolant heavy water. A proper fast multiplication zone can considerably increase amplification multiple of source neutron number. Graphite reflector makes it increase further. Simultaneously, the reflector has the effect on quasi-single direction couple. That is to say, fast neutron number of fast zone entering into thermal zone is much more than thermal neutron number of thermal zone entering into fast zone. It is obvious that graphite is an excellent reflecting material for thermal neutrons. Therefore, the flux level of thermal zone will be effectively raised and it is beneficial to increasing power in the thermal zone.

References

[1] F. Caminati et al., CERN / AT / 93-47(ET), 1993

[2] C. Rubbia, Proc. of Conf. on Nuclear Data for Sci. and Tec., P. 1065, Gatlinburg, May 9-13, 1994, USA

[3] C. Rubbia et al., CERN / AT / 95-44(ET), 1995
[4] Group of accelerator-driven clean nuclear energy system, "Symposium on Accelerator-Driven Clean Nuclear Energy System", China Institute of Atomic Energy in 1995
[5] P. F. A. de Leege, IRI-131-091-003, Delft University, Netherland, 1991
[6] US Nuclear Regulatory Commission Rev.3, 1984
[7] Liu Guisheng, "Homogeneous Fast Reactor Benchmark Testing of CENDL-2 and ENDF/B-6", INDC (CPR)-034 / L, June, 1995

Benchmark Testing for CENDL-2.1

Liu Ping

(China Nuclear Data Center, CIAE)

Introduction

In early 1996, the China Nuclear Data Center submitted the evaluated library CENDL-2.1 to the Nuclear Data Section of IAEA. In order to demonstrated the reliability of this library, and for wide acceptance, it was decided to subject it to benchmark testing against available integral experiments. Most of the analysts agreed that the best transport code for performing such integral tests was the continuous-energy, generalized-geometry, time-dependent, coupled neutron/photon/electron Monte Carlo code MCNP. WIMS/D4 is a general lattice cell programmer, which has been widely used in the world, is also useful for data testing, especially for thermal reactor applications.

The CENDL-2.1 library had not previously been processed into the form of an MCNP working library and WIMS library. The work was performed on the DEC AlphaServer 2100 of NDS/IAEA, using the de-facto standard, NJOY-94 nuclear data processing code system. The MCNP working library was created, a consistent WIMS library for the same materials was also created.

1 Generating of Working Library

All of CENDL-2.1 materials were processed into MCNP input working library by using NJOY94.66 on Alpha server 2100 of NDS/IAEA. Some of the key parameters are: The fractional reconstruction tolerance in RECONR is 0.002(0.2%); The fractional tolerance for thinning in BROADR is 0.002; The upper boundary of

thermal energy group is 4.0 eV. The tolerance for thinning secondary distribution in ACER is 0.05 for most materials.

All of CENDL-2.1 materials were processed into WIMS library by using NJOY94.105. Some of the key parameters are: The fractional reconstruction tolerance is 0.002; the fractional tolerance for thinning is also 0.002; A new weighting spectrum based on the spectrum from an MCNP calculation for a typical PWR fuel cell in the fast and thermal region an $1/E$ shape in the resonance region were used; the σ_0 (background cross section for self-shielding) was derived from the calculation according to normal reactor cells. Regarding the selection of resonance-group Goldstein LAMBDAS, we referenced the old WIMS library (WIMS "1981") for some materials, and selected the recommended values for some materials. The group cross sections of hydrogen bounded in water and deuterium in heavy water were calculated by using the scattering law data of ENDF/B-6.

2 Data testing Calculations and Result Analysis

Some benchmarks testing calculations have been done using MCNP-4B on RS/6000 computer and WIMS-D/4, WIMS-D/5A codes on Alpha server 2100.

2.1 Criticality Testing Calculations

The K_{eff} values of GODIVA and JEZEBEL assemblies were calculated. The calculated results of GODIVA based on CENDL-2.1, MCNP associated library and ENDF/B-6 are shown in Table 1.

Table 1 Results of K_{eff} calculations

	CENDL-2.1	MCNP LIBRARY	ENDF/B-6
K_{eff}	0.9975	1.00139	0.99782
Error / %	0.1815	0.2097	0.2134

It shows that the CENDL-2.1 gives results as good as ENDF/B-6, and better than old MCNP library. The date of ^{235}U and ^{238}U of CENDL-2.1 look satisfactory for such a benchmark.

Table 2 Results of K_{eff} calculations

	CENDL-2.1	ENDF/B-6	MCNP LIBRARY	ENDF/B-5
K_{eff}	1.00121	1.00151	0.99857	1.00228
Error /%	0.204	0.22	0.212	0.217

The calculated results of JEZEBEL are given in Table 2. It shows that the K_{eff} of MCNP recommended library is lower, CENDL-2.1 appears to give results as good as ENDF/B-6, and slightly better than ENDF/B-5.

2.2 Integral Data Testing with Fusion Neutron Source

2.2.1 Neutron Leakage Spectrum

The integral angle-dependent neutron spectrum from ^{9}Be, ^{56}Fe, lithium-oxide, liquid oxygen labs were calculated at 0.0, 12.2, 24.9, 41.8, 66.8 degrees and compared with experimental ones[1~3].

For 50.8 mm-thick beryllium slab, the spectra based on CENDL-2.1 and ENDF/B-6 are given in Table 3 and show good agreements with the experimental results as a whole energy region (50 keV ~ 15 MeV) at 0 degree. The ratio of calculation to experiment based on CENDL-2.1 is 0.9555 above 10 MeV, 1.051 from 2 ~ 10 MeV, 0.967 from 0.5 ~ 2 MeV, 0.82 from 0.1 ~ 0.5 MeV (slightly lower). At 24.9, 41.8 and 66.8 degrees, the calculated results is not in good agreements with the experiment results, especially at 66.8 degree.

Table 3 Comparison of neutron leakage spectrum for 50.8 mm-thick beryllium slab

E / MeV	Angle	Expt	CENDL-2.1	C / E	ENDF/B-6	C / E
10	0.0	3.92370	3.74912	0.9555	3.75220	0.9563
	24.9	0.25730	0.22452	0.8730	0.25114	0.976
	41.8	0.10240	0.083731	0.7595	0.09832	0.960
	66.8	0.046623	0.027967	0.6000	0.03247	0.696
2 ~ 10	0.0	0.12646	0.13286	1.051	0.11121	0.879
	24.9	0.060269	0.077879	1.292	0.05723	0.9496
	41.8	0.055711	0.071396	1.280	0.053364	0.958
	66.8	0.052344	0.060722	1.16	0.04708	0.899
0.5 ~ 2	0.0	0.091218	0.088183	0.967	0.07568	0.830
	24.9	0.052268	0.059342	1.135	0.045469	0.870
	41.8	0.051627	0.058174	1.127	0.04404	0.853
	66.8	0.048394	0.051306	1.06	0.037193	0.769
0.1 ~ 0.5	0.0	0.037633	0.030859	0.820	0.037749	1.003
	24.9	0.036902	0.027769	0.753	0.033605	0.986
	41.8	0.034073	0.027323	0.802	0.03101	0.910
	66.8	0.030698	0.022641	0.738	0.02554	0.832

For 40 cm-thick iron slab. The calculated results are given in Table 4. From 0.05 MeV to 1 MeV, CENDL-2.1 shows better agreements with the experiment than JENDL-3.2 at all degrees (0.0, 12.2, 24.9, 41.8, 66.8), but the JENDL-3.2 shows

better agreements with the experiment than CENDL-2.1 at all degrees above 1 MeV.

For lithium-oxide slab, the calculated results are given in Table 5 and Table 6 and show that the CENDL-2.1 gives reasonable results compared with the experiment results. It shows that the ^{6}Li and ^{7}Li of CENDL-2.1 look satisfactory for fusion application.

For liquid oxygen slab, the calculated results are given in Table 7. The calculated result of CENDL-2.1 is not in good agreement with the experiment at almost all degrees in the whole energy range. It should be noticed that because the double differential cross sections were not used during generating the MCNP working library for materials such as Fe etc, the results need to be further improved for the secondary neutron energy-angle distributions. The file 6 need to be added or improved for materials ^{9}Be, ^{16}O and ^{6,7}Li in CENDL-2.1.

Table 4 Comparison of integrated angular flux for 400 cm-thick Iron Slab

E / MeV	Angle	Experiment	CENDL-2.1	C/E	JENDL-3.2	C/E
	0.0	0.005213	0.0051378	0.98557	0.005573	1.0691
	12.2	0.0021269	0.0017925	0.84674	0.0018317	0.86527
>10	24.9	0.0006962	0.00067686	0.97222	0.00066086	0.94924
	41.8	0.00021809	0.0001309	0.69656	0.00019241	0.88225
	66.8	8.5131E-05	3.0923E-05	0.36325	6.5145E-05	0.76523
	0.0	0.0043863	0.0036065	0.82223	0.004417	1.0070
	12.2	0.0038303	0.0032158	0.82817	0.0039528	1.0318
1 ~ 10	24.9	0.0031395	0.0026115	0.81729	0.0032307	1.0111
	41.8	0.0024482	0.0017053	0.69656	0.0020981	0.8470
	66.8	0.001286	0.00078714	0.61209	0.000968	0.75272
	0.0	0.015683	0.014096	0.89880	0.01460	0.93101
	12.2	0.014258	0.0013628	0.95582	0.013584	0.95273
0.4 ~ 1	24.9	0.013237	0.012281	0.92775	0.011783	0.89016
	41.8	0.010699	0.009328	0.87183	0.0083752	0.78280
	66.8	0.0064569	0.0053806	0.83296	0.0043483	0.67315
	0.0	0.024540	0.023617	0.96240	0.020936	0.85314
	12.2	0.021679	0.023018	1.06177	0.020241	0.93367
0.1 ~ 0.4	24.9	0.021580	0.021436	0.99331	0.018018	0.83494
	41.8	0.019084	0.017368	0.91006	0.013480	0.70635
	66.8	0.012363	0.010295	0.83272	0.007363	0.59557
	0.0	0.003864	0.0037282	0.96486	0.003076	0.79607
	12.2	0.0030003	0.0037048	1.23481	0.0030832	1.0276
0.05 ~ 0.4	24.9	0.0030540	0.0035273	1.15498	0.0028340	0.92796
	41.8	0.0029790	0.0029897	1.00361	0.0022210	0.74555
	66.8	0.0023510	0.0020371	0.86646	0.0012858	0.54692

Table 5 Comparison of integrated angular flux for 48 mm-thick lithium-oxide assembly

E / MeV	Angle	Expt.	CENDL-2.1	C/E	JENDL-3.2	C/E
>11	0.0	5.1188	4.4905	0.87726	5.1005	0.99642
	24.9	0.18194	0.21353	1.17363	0.20352	1.1186
	41.8	0.07724	0.075671	0.97969	0.072244	0.93532
	66.8	0.027778	0.028556	1.02801	0.028855	1.0388
1 ~ 11	0.0	0.19056	0.17893	0.93899	0.19801	1.0391
	24.9	0.45563	0.044494	0.97653	0.05081	1.1152
	41.8	0.048649	0.043685	0.89795	0.048619	0.99938
	66.8	0.049517	0.044795	0.90463	0.048078	0.97094
0.1 ~ 1	0.0	0.06313	0.051099	0.80943	0.057267	0.90713
	24.9	0.011504	0.009533	0.82867	0.012668	1.1011
	41.8	0.01328	0.010877	0.81904	0.013376	1.0072
	66.8	0.011444	0.011793	1.03052	0.013983	1.2219

Table 6 Comparison of integrated angular flux for 20 cm-thick lithium-oxide assembly

E / MeV	Angle	Experiment	CENDL-2.1	C/E	JENDL-3.2	C/E
>11	0.0	0.75158	0.62439	0.83077	0.81395	1.083
	24.9	0.072925	0.070904	0.97229	0.070653	0.96884
	66.8	0.0084406	0.0073594	0.87191	0.007244	0.85823
1 ~11	0.0	0.061901	0.052408	0.84083	0.062909	1.0163
	24.9	0.04479	0.038463	0.85874	0.046206	1.0316
	66.8	0.026035	0.022231	0.85388	0.024378	0.93635
0.1 ~ 1	0.0	0.029788	0.025391	0.85238	0.029083	0.97633
	24.9	0.025094	0.023493	0.9362	0.025783	1.0275
	66.8	0.017522	0.015506	0.88493	0.016132	0.92067

Table 7 Comparison of integrated angular flux for 200 mm-thick liquid oxygen assembly

E / MeV	Angle	Experiment	CENDL-2.1	C/E	JENDL-3.2	C/E
>10	0.0	2.121	2.0669	0.97448	1.9015	0.89654
	24.9	0.073253	0.045819	0.62549	0.048821	0.75099
	41.8	0.028699	0.018299	0.63762	0.01798	0.62649
	66.8	0.013267	0.006421	0.48398	0.006886	0.51902
1 ~ 10	0.0	0.16226	0.15834	0.97584	0.13185	0.81257
	24.9	0.040638	0.042515	1.0462	0.030519	0.75099
	41.8	0.039873	0.35247	0.88398	0.027549	0.69093
	66.8	0.026942	0.01778	0.65994	0.015254	0.56616
0.1 ~ 1	0.0	0.02138	0.020505	0.95907	0.018671	0.8733
	24.9	0.011537	0.011565	1.0024	0.010183	0.8826
	41.8	0.01154	0.010476	0.9078	0.009126	0.79079
	66.8	0.0089793	0.0066881	0.74484	0.0061407	0.68387

2.3 Thermal Benchmarks Testing for the WIMS Library Based on CENDL-2.1

The WIMS-D/5A code was used for the calculations. The results with different evaluated libraries ENDF/B-6 Rev.4, CENDL-2.1, JEF-2.2, JENDL-3.2 and their comparisons of integral spectral parameters for selected benchmarks are given in the Table 8.

Table 8 Integral parameter comparisons

	Assembly	K_{eff}	Rho28	Del25	Del28	Convr
TRX-1	Exp.	1.00000(~0.30)	1.320(~1.6)	0.0987(~1.0)	0.0946(~4.3)	0.797(~1.0)
	B6	0.98853(-1.2)	1.377(+4.3)	0.0977(-1.1)	0.0974(+3.0)	0.808(+1.3)
	C2	0.99717(-0.28)	1.379(+4.5)	0.0974(-1.3)	0.0930(-1.7)	0.800(+0.34)
	J2	0.99153(-0.86)	1.370(+3.8)	0.0982(-0.54)	0.0966(+2.1)	0.809(+1.6)
	J3	0.99242(-0.77)	1.370(+3.8)	0.0972(-1.5)	0.0944(-0.18)	0.807(+1.2)
TRX-2	Exp.	1.00000(~0.10)	0.837(~1.9)	0.0614(~1.3)	0.0693(~5.1)	0.647(~0.93)
	B6	0.99113(-0.90)	0.863(+3.1)	0.0600(-2.4)	0.0690(-0.42)	0.650(+0.49)
	C2	0.99842(-0.16)	0.866(+3.5)	0.0599(-2.4)	0.0667(-3.7)	0.0644(-0.43)
	J2	0.99256(-0.75)	0.860(+2.7)	0.0603(-1.7)	0.0688(-0.79)	0.653(+0.87)
	J3	0.99474(-0.53)	0.860(+2.7)	0.0598(-2.6)	0.0674(-2.8)	0.650(+0.46)
BAPL-1	Exp.	1.00000(~0.10)	1.390(~0.72)	0.0840(~2.4)	0.0780(~5.1)	0.000
	B6	0.99431(-0.57)	1.429(+2.8)	0.0824(1.9)	0.0751(-3.7)	0.819
	C2	1.00205(+0.20)	1.435(+3.3)	0.0823(-2.1)	0.0714(-8.5)	0.812
	J2	0.99730(-0.27)	1.421(+2.2)	0.0827(-1.5)	0.0748(-4.1)	0.821
	J3	0.99880(-0.12)	1.422(+2.3)	0.0822(-2.1)	0.0734(-5.9)	0.81
BAPL-2	Exp.	1.00000(~0.10)	1.120(~0.89)	0.0680(~1.5)	0.0700(~5.7)	0.000
	B6	0.99459(-0.54)	1.188(+6.1)	0.0672(-1.2)	0.0645(-7.8)	0.746
	C2	1.00215(+0.21)	1.195(+6.7)	0.0671(-1.3)	0.0617(-12)	0.740
	J2	0.99710(-0.29)	1.183(+5.6)	0.0675(-0.69)	0.0644(-8.0)	0.748
	J3	0.99893(-0.11)	1.183(+5.6)	0.0671(-1.3)	0.0632(-9.7)	0.745
BAPL-3	Exp.	1.00000(~1.0)	0.906(~1.1)	0.0520(~1.9)	0.0570(~5.3)	0.000
	B6	0.99565(-0.44)	0.933(+3.0)	0.0516(-0.67)	0.0528(-7.3)	0.666
	C2	1.00235(+0.23)	0.939(+3.6)	0.0516(-0.67)	0.0509(-11)	0.661
	J2	0.99744(-0.26)	0.929(+2.5)	0.0519(-0.13)	0.0528(-7.4)	0.668
	J3	0.99966(-0.03)	0.929(+2.6)	0.0516(-0.75)	0.0519(-9.0)	0.665
DIMP1A	Exp.	1.00000(~0.10)	0.000	0.0000	0.0962(~3.3)	0.647(~0.46)
	B6	0.99265(-0.74)	4.045	0.2341	0.0862(-10)	0.658(+1.7)
	C2	1.00246(+0.24)	4.060	0.2340	0.0836(-13)	0.653(+0.90)
	J2	0.99782(-0.22)	4.025	0.2351	0.0852(-11)	0.658(+1.7)
	J3	0.99989(-0.01)	4.019	0.2328	0.0836(-13)	0.656(+1.4)
Average	Exp.	0.15	1.32	1.69	4.86	0.83
	B6	-0.73(~0.25)	3.85(~1.25)	-1.44(~0.62)	-4.45(~4.60)	1.16(~0.49)
	C2	0.08(~0.21)	4.30(~1.26)	-1.54(~0.63)	-8.27(~4.19)	0.27(~0.54)
	J2	-0.44(~0.26)	3.38(~1.22)	-0.92(~0.60)	-4.94(~4.57)	1.36(0.35)
	J3	-0.26(~0.28)	3.40(~1.23)	-1.66(~0.65)	-6.78(~4.35)	1.02(0.40)

Note: The meaning of the abbreviation in the Table 8 is as following:
Rho28 — epithermal / thermal capture for ^{238}U

Del25 — epiththermal / thermal fission for ^{235}U
Del28 — $^{238}U/^{235}U$ fission
Convr — ^{238}U capture/^{235}U fission

3 Results and Discussions

It can be seen that the K_{eff} values from the calculations based on CENDL-2.1 are in good agreement with experiments for all above assemblies. It also shows that the CENDL-2.1 performs with better results of K_{eff} for TRX-1.2 than other evaluated libraries, and better results of K_{eff} for BAPL-1, 2, 3 than ENDF/B-6, JEF-2.2. The JENDL-3.2 gives better results of K_{eff} for BAPL-1, 2, 3. For other integral parameters, such as Rho28, Del25, Convr, the results for CENDL-2.1 are similar to those results of other evaluated libraries, but for Del28, the result based on CENDL-2.1 is lower than others for TRX-1, 2 and BAPL-1, 2, 3.

The data of ^{235}U and ^{238}U of CENDL-2.1 looks satisfactory for the thermal reactor calculations, but underestimates the fission of ^{238}U in the resonance energy range.

Acknowledgement

The author would like to express her appreciation to NDS/IAEA and especially to Dr. D. W. Muir for the supporting the work and help with the using of Alpha Server in NDS/IAEA and the applications of MCNP4B code and Monte Carlo method.

Reference

[1] Y. Oyama, H. Maekawa: "Measurement an Analysis of an Angular Neutron Flux on a Berylium Slab Irradiated with Deuteron-Tritium Neutrons," Nucl. Sci. Eng.; 97, 220-234 (1987)
[2] Y. Oyama, S. Yamaguchi, H. Maekawa: "Experimental Results of Angular Neutron Spectrum Leaking from Slabs of Fusion Reactor Candidate Materials (I)"
[3] Y. Oyama, H. Maekawa: "Measurement of Angle-Dependent neutron spectrum from Lithium-Oxide Slab Assemblies by Time-of-Flight method," JAERI-M 83-195

Update of PHOENIX-P 42 Group Library from CENDL-2

Zhang Baocheng
(China Nuclear Data Center, CIAE)

Introduction

PHOENIX-P is a lattice physics code system, developed by the Westinghouse Electric Corporation (WEC), which was transplanted and used at Dayabay Nuclear Power Plant (DNPJVC). The associated multi-group (42-group) library was derived from the evaluated nuclear data of ENDF/B-5. Some modifications were made to the library according to the results of validation calculations. In most cases, calculations with the library can give a satisfactory results. Since the original library is from the old evaluated nuclear data, it can not meet all the requirements of reactor physics calculations of the nuclear power plant, especial the burnup calculations for fresh fuel, though the library was modified somewhere. So it is necessary to update the library with the latest version of evaluated nuclear data. To do so, based on the investigation of the old library and the information about the library[1], some programs were developed at China Nuclear Data Center (CNDC) to produce PHOENIX-P format data sets mainly from CENDL-2 and the new data were used to supersede the old ones of the PHOENIX-P library.

1 The Proceeding of Update

The generation of PHOENIX–P format data is done with the NJOY91.91 code system[2], in which the modules MODER, RECONR, BROADR, UNRESR, THERMR and GROUPR were used to produce 42-group data file GENDF from ENDF/B format evaluaed nuclear data library according to the temperatures, weighting function and so on. GENDF data file contains all necessary data, which are designated in the input file of GROUPR. Clearly GENDF is not the PHOENIX-P format data file, also some special data, like transport cross sections and resonance integral etc., can not be given directly in the GENDF file. Therefore a new module PHENR was written with the reference of the module WIMSR to convert the GENDF data into the PHOENIX–P format data and produce some additional data which are not included in the GENDF file. Besides, the structure of the PHOENIX-P 42-group library is too complicate to substitute the new data for the old ones without a proper code. JOSPH is the code, developed at CNDC, to complete the substitution.

So the code system for the update of the PHOENIX-P 42-group library was set up. The proceeding of producing and substitution of PHOENIX-P library is shown in Fig.1.

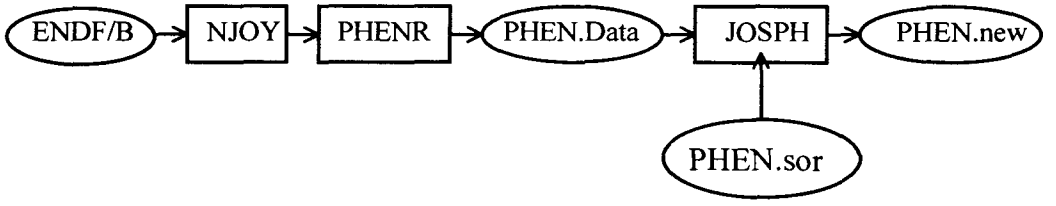

Fig.1 The update proceeding of PHOENIX-P library

Where the PHEN.sor and PHEN.new stand for the old and new PHOENIX-P library, respectively. The comparison of data among the new, old library and GENDF output file as well, shows that the code system is reliable. And that is also proved by validation calculations at Dayabay Nuclear Power Plant.

Besides substitution, the code JOSPH can be used for adding new nuclides, output of the readable list file of the library if necessary, which is easy for the user to analyze the values of cross-section.

2 PHENR Module

As mentioned above, some special data should be produced or recalculated in the PHENR module.

2.1 Resonance Integral

In the GENDF, for resonance absorber nuclide, the cross sections are given corresponding to different temperatures and σ_0s. In the PHOENIX–P library, the resonance integral tabulations are given instead, to describe the effect of self-shielding. The resonance integral can be calculated as following:

$$I_X = \int_{\Delta E} IR \frac{dE}{E} = \int_{\Delta E} \frac{\sigma_0 + \lambda \sigma_p^A}{\sigma_a^A + \lambda \sigma_p^A + \sigma_0} \sigma_X \frac{dE}{E}$$

Where λ is the Cohn-Goldstein constants, σ_0 is the parameter given through input file, σ_a^A and σ_p^A are absorption and potential scattering cross section of the absorber, respectively, σ_x is the effective cross section after self-shielding correction (the index a stands for absorption and f for fission). For the non-fissile resonance nuclide, only resonance integral of absorption is present.

2.2 Absorption and Transport Cross Section

The diffusion equation consists of three items, i.e. absorption, production and leakage item. None of them refers to the (n,2n) and (n,3n) cross sections directly. Different approximate methods are used in different codes, since the reactions are happened in the fast region (~MeV). In order to be consistent with original library, in the PHENR module, (n,2n) and (n,3n) are treated as negative and double negative capture, respectively. So the absorption cross section is corrected as follow:

$$\sigma_a^* = \sigma_a - \sigma_{n,2n} - 2\times\sigma_{n,3n}$$

Here, σ_a^* is the corrected absorption cross section. The same correction is made for the transport cross section by using σ_a^* instead of σ_a.

2.3 Scattering Matrix

PHOENIX-P 42-group library contains P_0 and P_1 scattering matrices, and the P_1 scattering matrix data is given for hydrogen, deuterium, oxygen and carbon. The scattering matrix is written in the order of destination groups. And no upscatter data is allowed above 4 eV. That means the neutron can be scattered up to 4 eV due to thermalization. Normally, the energy of thermalized incident neutron is limited by the NJOY input file, and the energy range of the destination neutron depends on the property of the nuclide, which could be over 4 eV. To meet the requirement of the PHOENIX-P data format, a special treatment of the scattering cross section should be done for the group, from which the neutron can upscatter to the group over 4 eV. If $\sigma_{i,j}$ is neutron scattering cross section from group i to group j ($E_i < E_j$ and $E_j > 4$ eV), ϕ_i is the neutron flux in the group i, the net neutron current from group j to group i is $\sigma_{j,i}\phi_j - \sigma_{i,j}\phi_i$. To keep the net neutron current consistent from high energy group j to group i, the following modification was made in the PHENR module.

$$\sigma_{j,i}^* = \sigma_{j,i} - \frac{\phi_i}{\phi_j}\sigma_{i,j}$$

Where $\sigma_{j,i}^*$ is the corrected cross section which is given in the PHOENIX-P library.

3 Generation and Substitution of Group Cross Section

For the resonance absorber, the resonance self–shielding affects not only on the absorption and fission but also on the scattering. But in the PHOENIX-P library, the

resonance integral tabulations are presented for absorption and fission only. That means the scattering cross sections do not change with the σ_0. It is very important to choose a suitable value of σ_0 to cater to the requirements of applications[3]. Therefore, σ_0 has been calculated according to the geometry and composition of typical PWR using following formula,

$$\sigma_0 = \frac{\sum_{j \neq i} N_j \sigma_j}{N_i} + \sigma_e$$

Where N_j is the concentration of nuclide j, σ_j is its total cross section, and $\sigma_e = (N_i \bar{l})^{-1}$ is the escape cross section which is introduced for heterogeneous correction ($\bar{l}$ is the mean chord length of absorption region). So the calculated value of σ_0 was given in the input file of the PHENR module. And according to σ_0 value, a self-shielding treated scattering cross section was selected in the output file of the PHOENIX-P format data.

Based on CENDL-2 and ENDF/B-6, and according to the need of DNPJVC, 42-group nuclear data sets of 9 nuclides, including ^{238}U, ^{239}Pu and ^{240}Pu etc., were updated with the code system shown in Fig.1. Here 4 isotopes of plutonium and the file of scattering law of hydrogen were derived from ENDF/B-6, and the others from CENDL-2. It should be pointed out that the Cohen-Goldstein constants of the original library and WIMS 69 library[4] were used for reference. No modification was done for the fission neutron spectrum and fission products.

4 Validation of the Updated Library

The calculations with the updated library were carried out for 4 fuel cycles of 2 units at Dayabay Nuclear Power Plant. The comparison of results among calculations with different libraries and experimental values was made.

Fig.2 to 8 show the change of critical concentration of boron with burnup. The "wec.lib results" stands for the results from the original PHOENIX-P library, and the "Framatome results" for the results calculated with Framatome code system.

From the curves of boron concentration, a significant improvement of the results, especially for the first fuel cycle, can be found due to the update of the PHOENIX-P 42-group library. Also it is notable that no adjustment was done in this work. That means these data can be used in a wide scope and its accuracy in the different calculation is stable.

The above results show the fact that the updated library is reliable and can meet the need of reactor physics calculation. Also it can be concluded that the code system, used in the generation and substitution of PHOENIX-P library, is correct.

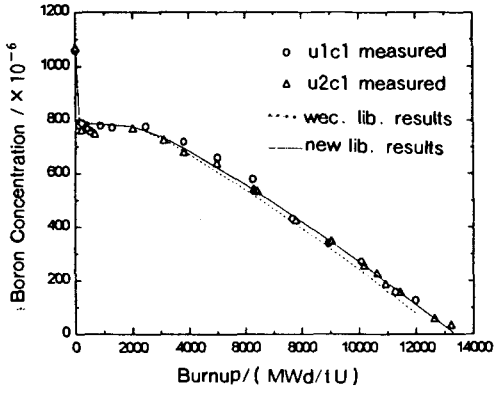

Fig.2 Boron concentration as a function of burnup for cycle 1 of units 1&2

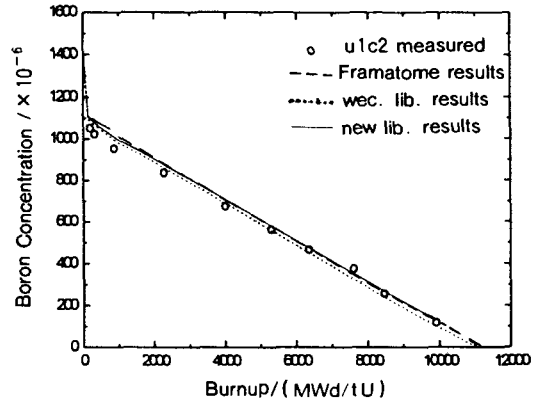

Fig.3 Boron concentration as a function of burnup for cycle 2 of unit 1

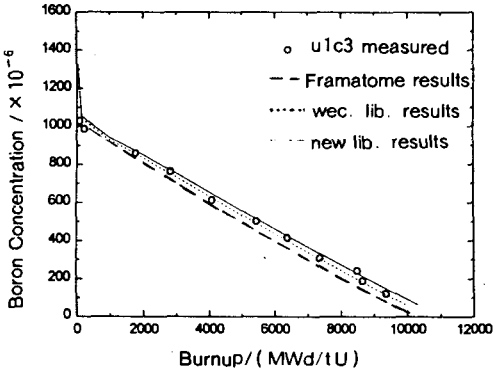

Fig.4 Boron concentration as a function of burnup for cycle 3 of unit 1

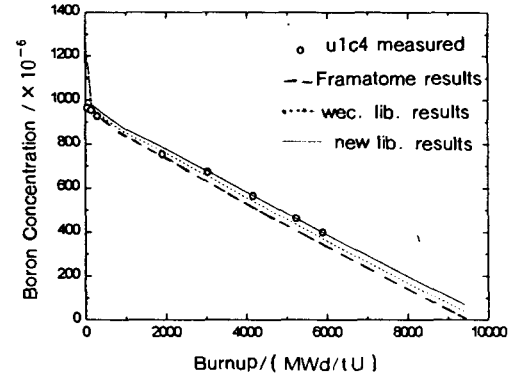

Fig.5 Boron concentration as a function of burnup for cycle 4 of unit 1

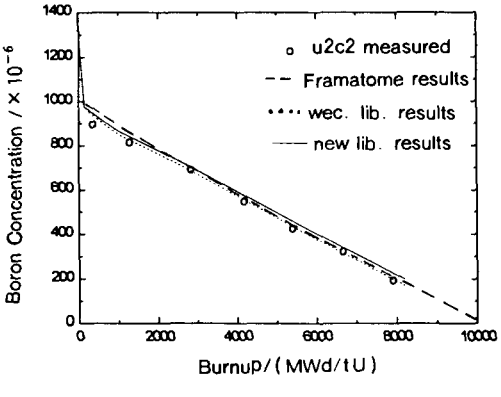

Fig.6 Boron concentration as a function of burnup for cycle 2 of unit 2

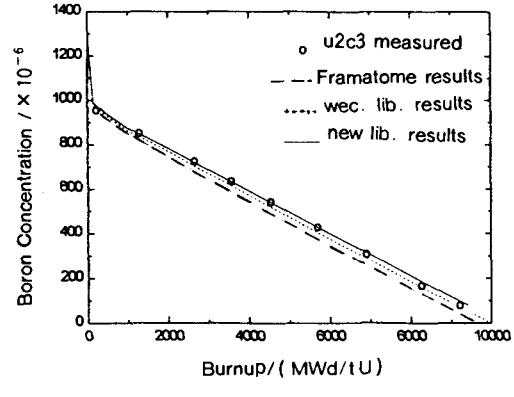

Fig.7 Boron concentration as a function of burnup for cycle 3 of unit 2

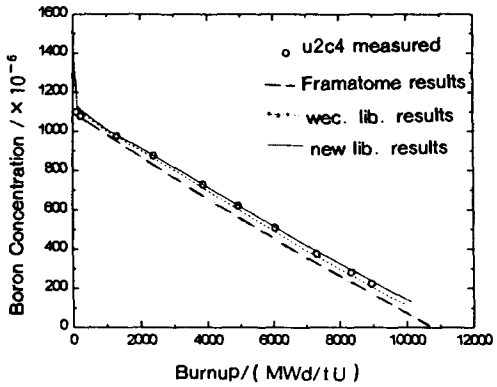

Fig.8 Boron concentration as a function of burnup for cycle 4 of unit 2

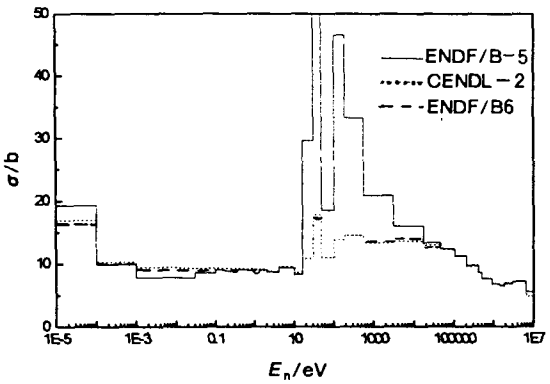

Fig.9 The comparison of ^{238}U scattering cross sections

5 Discussion and Conclusion

It is obvious that different evaluation nuclear data library is the cause of the difference of the results between old and new PHOENIX-P 42-group library. As mentioned above, the old library is based on ENDF/B-5, and the new one is based on CENDL-2 and ENDF/B-6. In general, the latter is more reliable than the former. It is well-known that ^{238}U data strongly affects on the calculated results of reactor physics parameters and their trend, due to high concentration in the uranium fuel reactors. Through comparison of group cross sections between old and new library, no obvious difference was found for fission and absorption.

The Fig.9 gives the comparison of scattering cross sections. A big difference is shown in the picture. In the resonance energy region, the value of the old library is much bigger than that of the new ones. The difference arises from the evaluation data and resonance self-shielding treatment for scattering cross sections as well. As seen in Fig.9, the bigger scattering cross section caused relative lower possibility of absorption, higher slowdown power and therefore softer neutron spectrum. All of these lead to an overestimated burnup rate of ^{235}U and overpredicted k_∞ at the beginning of fuel cycle. It also results in a lower production of ^{239}Pu and lower k_∞ at the end of fuel cycle, just like what is shown in Fig.2.

Clearly, the results could be influenced by other nuclear data. For instance, the influence of the nuclear data of plutonium would get stronger along with its

accumulation. According to the benchmark calculations for plutonium, the data of ENDF/B-6 are considered as the best one so far.

It is the first time that the Chinese evaluated nuclear data library (CENDL) is used in the nuclear power plant directly. As shown in Fig.2 to Fig.8, the calculated results from the new library, mainly deived from CENDL-2, are well consistent with the experimental results. In view of the fact that the consistency of the results, and their trend also, has been shown in every fuel cycle, it can be concluded that CENDL-2 is reliable.

As far as we know, some modifications were made in the lattice physics code PHOENIX-P at WEC and a new 70-group library has been generated for the code by WEC and Mitsubishi Heavy Industries, Ltd[5]. With the experience from this work, we can carry out the same developmental programme if necessary.

Acknowledgments

All the validation calculations were made by Dr. Yao Zenghua. The author would like to thank him for his supports and help, and thank Prof. Liu Guisheng for his helpful suggestions.

References

[1] GNPJVC, Structure of the PHOENIX-P Library. Internal file
[2] R.E. MacFarlane, NJOY91.91, A Code System for Producing Pointwise and Multigroup Neutron and Photon Cross Sections from ENDF/B Evaluated Data, PSR-171, RSIC Computer Code Collection (1993)
[3] Zhang Baocheng, Update and Benchmark Calculations of WIMS Library, Atomic Energy Science and Technology, 1998, 32(2)
[4] J. D. Macdougall, Programmes Associated with WIMS Library Tapes, AEEW-M1783, Aug. 1980
[5] H.C. Huria, Tahara Y. 8 New Multi-group for PHOENIX-P, Conf. on Nuclear Data Evaluation of IAE, ANL, 1996

V NUCLEAR DATA ACTIVITIES

Activities and Cooperation on Nuclear Data in China During 1997

Zhuang Youxiang
(China Nuclear Data Center, CIAE)

1 The Activities and Meeting in China in 1997

(1) "The Second Working Meeting on Fission Yield, Decay Data and Activation Cross Section Evaluations", June 9 ~ 12, Kunming City, Yunnan Province. Reviewed and discussed the evaluations concerned.

(2) "The Working Meeting on Neutron Data Evaluation of Fission Product nuclides", October 13 ~ 16, Taiyuan City, Shanxi Province. Reported the progress on neutron data evaluation of fission product nuclides, discussed some technical problem and arranged the further work.

2 The International Meeting and Conferences in Nuclear Data Field Attended by Staff Members of CNDC in 1997

(1) "The 21st Meeting of the International Nuclear Data Committee (INDC)", Feb. 24 ~ 27, Vienna, Austria;

(2) "The Second Co-ordination Meeting on Development of Reference Charged Particle Cross Section Database for Medical Radioisotope Production", April 7 ~ 10, Cape Town, South Africa.

(3) "The Third Workshop on Simulating Accerator Radiation Environments (SARE3)", May 7 ~ 9, Tsukuba, Japan;

(4) "The Meetings of NEA Working Party on International Cooperation Evaluation" and "Working Party on International Measurement Activity" May 14 ~ 16, Codarache, France;

(5) "The International Conference on Nuclear Data for Science and Technology (NDST-97)", May 19 ~ 24, Trieste, Italy;

(6) "The IAEA Consultants' Meeting on Technical Aspects of the Cooperation of Nuclear Reaction Data Center", May 26 ~ 28, Vienna, Austria;

(7) "The Meeting on Fission Product Yield Data for Transmutations of Minor Actinides Nuclear Waste", NOV. 5 ~ 7, Vienna, Austria;

(8) "The Workshop on Nuclear Data Online Services", Dec. 1 ~ 5, Vienna, Austria.

3 The Foreign Scientists in Nuclear Data Field Visited CNDC/ CIAE in 1997

Aug. 28: Dr. Jin Kuijper, ECN, Netherlands;

Oct. 14 ~ 16: Dr. T.V.Golashvili, Scientific Data Center, Russia,
Dr. V.Chechev, Radionuclide Data Center, Russia,
Dr. Yu Kovalev, Ministry of Atomic Energy, Russia;

Nov.4: Dr. Guinyun Kim, Pohang University of Science and Technology (POSTECH).

CINDA INDEX

Nuclide	Quantity,	Energy/ eV		Lab	Type	Documentation				Author, Comments
		Min	Max			Ref	Vol	Page	Date	
^{40}Ca	(n,α)	5.0	6.0	BJG	Expt	Jour CNDP	19	1	Jun 98	Zhang Guohui+, DOUBLE DIFF
^{45}Ti	(α,n)	4.7	26.4	SIU	Expt	Jour CNDP	19	20	Jun 98	Peng Xiufeng+, SIG
^{46}Ti	(α,2n)	4.7	26.4	SIU	Expt	Jour CNDP	19	20	Jun 98	Peng Xiufeng+, SIG
	(n,p)	6	12	AEP	Expt	Jour CNDP	19	7	Jun 98	Zhao Wenrong+, CS
^{47}Ti	(n,p)	6	12	AEP	Expt	Jour CNDP	19	7	Jun 98	Zhao Wenrong+, CS
	(d,n)	Thrsh	22	AEP	Expt	Jour CNDP	19	17	Jun 98	Zhao Wenrong+, CS
^{48}Ti	(d,2n)	Thrsh	22	AEP	Expt	Jour CNDP	19	17	Jun 98	Zhao Wenrong+, CS
	(p,n)	Thrsh	22	AEP	Expt	Jour CNDP	19	17	Jun 98	Zhao Wenrong+, CS
	(α,n)	4.7	26.4	SIU	Expt	Jour CNDP	19	20	Jun 98	Peng Xiufeng+, SIG
^{49}Ti	(p,2n)	Thrsh	22	AEP	Expt	Jour CNDP	19	17	Jun 98	Zhao Wenrong+, CS
	(α,2n)	4.7	26.4	SIU	Expt	Jour CNDP	19	20	Jun 98	Peng Xiufeng+, SIG
^{54}Fe	(n,p)	6	12	AEP	Expt	Jour CNDP	19	7	Jun 98	Zhao Wenrong+, CS
	(n,α)	6	12	AEP	Expt	Jour CNDP	19	7	Jun 98	Zhao Wenrong+, CS
^{59}Co	(n,p)	6	12	AEP	Expt	Jour CNDP	19	7	Jun 98	Zhao Wenrong+, CS
^{58}Ni	(n,,d+np+pn)	6	12	AEP	Expt	Jour CNDP	19	7	Jun 98	Zhao Wenrong+, CS
	Evalnation	10^{-5}	20	SIU	Eval	Jour CNDP	19	67	Jun 98	Ma Gonggui+, SIG, DA, DA/DE
^{60}Ni	(n,p)	6	12	AEP	Expt	Jour CNDP	19	7	Jun 98	Zhao Wenrong+, CS
	(n,α)	6	12	AEP	Expt	Jour CNDP	19	7	Jun 98	Zhao Wenrong+, CS
	Evalnation	10^{-5}	20	SIU	Eval	Jour CNDP	19	67	Jun 98	Ma Gonggui+, SIG, DA, DA/DE
^{61}Ni	Evalnation	10^{-5}	20	SIU	Eval	Jour CNDP	19	67	Jun 98	Ma Gonggui+, SIG, DA, DA/DE
^{62}Ni	Evalnation	10^{-5}	20	SIU	Eval	Jour CNDP	19	67	Jun 98	Ma Gonggui+, SIG, DA, DA/DE
^{64}Ni	Evalnation	10^{-5}	20	SIU	Eval	Jour CNDP	19	67	Jun 98	Ma Gonggui+, SIG, DA, DA/DE
^{nat}Ni	Evalnation	10^{-5}	20	SIU	Eval	Jour CNDP	19	67	Jun 98	Ma Gonggui+, SIG, DA, DA/DE
^{63}Cu	(n,α)	6	12	AEP	Expt	Jour CNDP	19	7	Jun 98	Zhao Wenrong+, CS
	Evalnation	0.001	20	AEP	Theo	Jour CNDP	19	50	Jun 98	Han YinLu+, SIG, DA, DE

Nuclide	Quantity	Energy/ eV		Lab	Type	Documentation				Author, Comments
		Min	Max			Ref	Vol	Page	Date	
^{63}Cu	(n,p)	Thrsh	20	SIU	Eval	Jour CNDP	19	134	Jun 98	Ma Gonggui+, SIG
	(n,n'p)	Thrsh	20	SIU	Eval	Jour CNDP	19	134	Jun 98	Ma Gonggui+, SIG
^{65}Cu	(n,p)	Thrsh	20	SIU	Eval	Jour CNDP	19	134	Jun 98	Ma Gonggui+, SIG
	(n,n'p)	Thrsh	20	SIU	Eval	Jour CNDP	19	134	Jun 98	Ma Gonggui+, SIG
^{nat}Cu	(n,p)	Thrsh	20	SIU	Eval	Jour CNDP	19	134	Jun 98	Ma Gonggui+, SIG
	(n,n'p)	Thrsh	20	SIU	Eval	Jour CNDP	19	134	Jun 98	Ma Gonggui+, SIG
^{71}Ga	(n,γ)	0.31	1.58	BJG	Expt	Jour CNDP	19	12	Jun 98	Shi Zhaoomin+, CS
^{85}Rb	(n,2n)	6	12	AEP	Expt	Jour CNDP	19	7	Jun 98	Zhao Wenrong+, CS
^{Nat}Zr	(n,γ)	0.01	20	ZHN	Theo	Jour CNDP	19	26	Jun 98	Liu Jianfeng+, MDL, CALC,SIG
^{93}Nb	(n,2n)	6	12	AEP	Expt	Jour CNDP	19	7	Jun 98	Zhao Wenrong+, CS
^{94}Mo	(d,n)	Thrsh	22	AEP	Expt	Jour CNDP	19	17	Jun 98	Zhao Wenrong+, CS
	(p,γ)	Thrsh	22	AEP	Expt	Jour CNDP	19	17	Jun 98	Zhao Wenrong+, CS
	(d,γ)	Thrsh	22	AEP	Expt	Jour CNDP	19	17	Jun 98	Zhao Wenrong+, CS
^{95}Mo	(d,2n)	Thrsh	22	AEP	Expt	Jour CNDP	19	17	Jun 98	Zhao Wenrong+, CS
	(p,n)	Thrsh	22	AEP	Expt	Jour CNDP	19	17	Jun 98	Zhao Wenrong+, CS
	(d,n)	Thrsh	22	AEP	Expt	Jour CNDP	19	17	Jun 98	Zhao Wenrong+, CS
	(p,γ)	Thrsh	22	AEP	Expt	Jour CNDP	19	17	Jun 98	Zhao Wenrong+, CS
^{96}Mo	(d,3n)	Thrsh	22	AEP	Expt	Jour CNDP	19	17	Jun 98	Zhao Wenrong+, CS
	(p,2n)	Thrsh	22	AEP	Expt	Jour CNDP	19	17	Jun 98	Zhao Wenrong+, CS
	(d,2n)	Thrsh	22	AEP	Expt	Jour CNDP	19	17	Jun 98	Zhao Wenrong+, CS
	(p,n)	Thrsh	22	AEP	Expt	Jour CNDP	19	17	Jun 98	Zhao Wenrong+, CS
^{97}Mo	(p,3n)	Thrsh	22	AEP	Expt	Jour CNDP	19	17	Jun 98	Zhao Wenrong+, CS
	(d,3n)	Thrsh	22	AEP	Expt	Jour CNDP	19	17	Jun 98	Zhao Wenrong+, CS
	(p,2n)	Thrsh	22	AEP	Expt	Jour CNDP	19	17	Jun 98	Zhao Wenrong+, CS
^{98}Mo	(p,3n)	Thrsh	22	AEP	Expt	Jour CNDP	19	17	Jun 98	Zhao Wenrong+, CS
	(d,p)	Thrsh	22	AEP	Expt	Jour CNDP	19	17	Jun 98	Zhao Wenrong+, CS
^{100}Mo	(d,dn)	Thrsh	22	AEP	Expt	Jour CNDP	19	17	Jun 98	Zhao Wenrong+, CS

Nuclide	Quantity	Energy/ eV		Lab	Type	Documentation				Author, Comments
		Min	Max			Ref	Vol	Page	Date	
^{100}Mo	(d,p2n)	Thrsh	22	AEP	Expt	Jour CNDP	19	17	Jun 98	Zhao Wenrong+, CS
	(p,pn)	Thrsh	22	AEP	Expt	Jour CNDP	19	17	Jun 98	Zhao Wenrong+, CS
	(p,d)	Thrsh	22	AEP	Expt	Jour CNDP	19	17	Jun 98	Zhao Wenrong+, CS
^{105}Pd	Evalnation	0.05	20	AEP	Theo	Jour CNDP	19	58	Jun 98	Zhang Zhengjun+, SIG, DA, DE
^{108}Pd	Evalnation	10^{-5}	20	AEP	Theo	Jour CNDP	19	58	Jun 98	Zhang Zhengjun+, SIG, DA, DE
^{140}Ce	(n,2n)	6	12	AEP	Expt	Jour CNDP	19	7	Jun 98	Zhao Wenrong+, CS
^{151}Eu	(n,2n)	Thrsh	20	AEP	Eval	Jour CNDP	19	122	Jun 98	Yu Baosheng+, SIG
	(n,3n)	Thrsh	20	AEP	Eval	Jour CNDP	19	122	Jun 98	Yu Baosheng+, SIG
	(n,γ)	0.001	20	AEP	Eval	Jour CNDP	19	122	Jun 98	Yu Baosheng+, SIG
	(n,p)	0.005	20	AEP	Eval	Jour CNDP	19	122	Jun 98	Yu Baosheng+, SIG
	(n, α)	Thrsh	20	AEP	Eval	Jour CNDP	19	122	Jun 98	Yu Baosheng+, SIG
^{153}Eu	(n,2n)	Thrsh	20	AEP	Eval	Jour CNDP	19	122	Jun 98	Yu Baosheng+, SIG
	(n,3n)	Thrsh	20	AEP	Eval	Jour CNDP	19	122	Jun 98	Yu Baosheng+, SIG
	(n,γ)	0.001	20	AEP	Eval	Jour CNDP	19	122	Jun 98	Yu Baosheng+, SIG
	(n,p)	0.005	20	AEP	Eval	Jour CNDP	19	122	Jun 98	Yu Baosheng+, SIG
	(n,α)	Thrsh	20	AEP	Eval	Jour CNDP	19	122	Jun 98	Yu Baosheng+, SIG
^{175}Lu	(n,2n)	10	15	AEP	Expt	Jour CNDP	19	15	Jun 98	Yu Weixiang+, CS
^{176}Hf	(n,2n)	10	18	AEP	Expt	Jour CNDP	19	10	Jun 98	Lu Hanlin+, CS
^{181}Ta	(n,2n)	6	12	AEP	Expt	Jour CNDP	19	7	Jun 98	Zhao Wenrong+, CS
^{180}W	(γ,n)	Thrsh	30	AEP	Eval	Jour CNDP	19	143	Jun 98	Yu Baosheng+, SIG, DA, DE
^{182}W	(γ,n)	Thrsh	30	AEP	Eval	Jour CNDP	19	143	Jun 98	Yu Baosheng+, SIG, DA, DE
^{183}W	(γ,n)	Thrsh	30	AEP	Eval	Jour CNDP	19	143	Jun 98	Yu Baosheng+, SIG, DA, DE
^{184}W	(γ,n)	Thrsh	30	AEP	Eval	Jour CNDP	19	143	Jun 98	Yu Baosheng+, SIG, DA, DE
^{186}W	(γ,n)	Thrsh	30	AEP	Eval	Jour CNDP	19	143	Jun 98	Yu Baosheng+, SIG, DA, DE
^{185}Re	Evalnation	0.001	20	AEP	Theo	Jour CNDP	19	42	Jun 98	Han YinLu+, SIG, DA, DE
^{187}Re	Evalnation	0.001	20	AEP	Theo	Jour CNDP	19	42	Jun 98	Han YinLu+, SIG, DA, DE
	(n,2n)	Thrsh	20	AEP	Eval	Jour CNDP	19	139	Jun 98	Huang Xiaolong+, SIG

Nuclide	Quantity	Energy/ eV		Lab	Type	Documentation				Author, Comments
		Min	Max			Ref	Vol	Page	Date	
^{Nat}Re	Evalnation	0.001	20	AEP	Theo	Jour CNDP	19	42	Jun 98	Han YinLu+, SIG, DA, DE
^{5}U	Fission Yield	10^{-5}	15	AEP	Eval	Jour CNDP	19	78	Jun 98	Liu Tingjin+, FY
^{8}U	Fission Yield	10^{-5}	15	AEP	Eval	Jour CNDP	19	92	Jun 98	Liang Qichang+, FY
^{238}Pu	Diff inelastic	0.01	20	AEP	Theo	Jour CNDP	19	38	Jun 98	Wang Shunuan+, SIG, DA
^{239}Pu	Diff inelastic	0.01	20	AEP	Theo	Jour CNDP	19	38	Jun 98	Wang Shunuan+, SIG, DA
^{240}Pu	Diff inelastic	0.01	20	AEP	Theo	Jour CNDP	19	38	Jun 98	Wang Shunuan+, SIG, DA
^{241}Pu	Diff inelastic	0.01	20	AEP	Theo	Jour CNDP	19	38	Jun 98	Wang Shunuan+, SIG, DA
^{242}Pu	Diff inelastic	0.01	20	AEP	Theo	Jour CNDP	19	38	Jun 98	Wang Shunuan+, SIG, DA

(京)新登字 077 号

图书在版编目(CIP)数据

中国核科技报告: CNIC-01266，CNDC-0022：核数据进展通讯：英文/刘廷进等著. -北京：原子能出版社，1998.6
ISBN 7-5022-1836-X

Ⅰ. 中… Ⅱ. 刘… Ⅲ. 核技术-研究报告-中国-1998-英文 Ⅳ. TL-2

中国版本图书馆 CIP 数据核字（98）第 11187 号

原子能出版社出版发行

责任编辑：孙凤春

社址：北京市海淀区阜成路 43 号 邮政编码：100037

中国核科技报告编辑部排版

核科学技术情报研究所印刷

开本：787 × 1092 1/ 16 · 印张 12 · 字数 190 千字

1998 年 6 月北京第一版 · 1998 年 6 月北京第一次印刷